Editors

Herziger, Gerd
Rheinisch-Westfälische Technische Hochschule, Aachen, Germany

Weber, Horst
Technische Universität Berlin, Optisches Institut, Berlin, Germany

Poprawe, Reinhart
Fraunhofer-Institut für Lasertechnik (ILT), Aachen, Germany

Authors

Beránek, Jaroslav
Academy of Sciences of the Czech Republic, Institute of Physics, Prague, Czech Republic

Hugenschmidt, Manfred
German-French Research Institute of Saint-Louis, Saint-Louis Cedex, France / University of Karlsruhe, Faculty of Electrical Engineering and Information Technique, Karlsruhe, Germany

Keller, Ursula
ETH Zurich, Physics Department, Institute of Quantum Electronics, Zürich, Switzerland

Marowsky, Gerd
Laser-Laboratorium Göttingen, Göttingen, Germany

Rohlena, Karel
Academy of Sciences of the Czech Republic, Institute of Physics, Prague, Czech Republic

Schulz, Wolfgang
Fraunhofer-Institut für Lasertechnik (ILT), Aachen, Germany

Seelig, Wolfgang
Technische Universität Darmstadt, Institut für angewandte Physik, Darmstadt, Germany

Simon, Peter
Laser-Laboratorium Göttingen, Göttingen, Germany

Sowada, Ulrich
Fachhochschule Kiel, Institut für Mechatronik, Kiel, Germany

Szatmári, Sándor
University of Szeged, Department of Experimental Physics, Szeged, Hungary

Uhlenbusch, Jürgen
Heinrich-Heine-Universität Düsseldorf, Institut für Laser- und Plasmaphysik, Düsseldorf, Germany

Viöl, Wolfgang
Hochschule für angewandte Wissenschaft und Kunst Fachhochschule Hildesheim/Holzminden/Göttingen, Fakultät Naturwissenschaften und Technik, Göttingen, Germany

Wester, Rolf
Fraunhofer-Institut für Lasertechnik (ILT), Aachen, Germany

Landolt-Börnstein

Editorial Office
Gagernstraße 8
D-64283 Darmstadt, Germany
fax: +49 (6151) 171760
e-mail: Redaktion.Landolt-Boernstein@springer.com

Internet
www.landolt-boernstein.com

Preface

The three volumes VIII/1A, B, C document the state of the art of "Laser Physics and Applications". Scientific trends and related technological aspects are considered by compiling results and conclusions from phenomenology, observation and experiments. Reliable data, physical fundamentals and detailed references are presented.

In the recent decades the laser source matured to an universal tool common to scientific research as well as to industrial use. Today the technical goal is the generation of optical power towards shorter wavelengths, shorter pulses, higher efficiency and higher power for applications in science and industry. Tailoring the optical energy in wavelength, space and time is a requirement for the investigation of laser-induced processes, i.e. excitation, non-linear amplification, storage of optical energy, etc. According to the actual trends in laser research and development, Vol. VIII/1 is split into three parts: Vol. VIII/1A with its two subvolumes 1A1 and 1A2 covers laser fundamentals, Vol. VIII/1B with its two subvolumes 1B1 and 1B2 deals with laser systems and Vol. VIII/1C gives an overview on laser applications.

In Vol. VIII/1B1 the following topics are treated in detail:

Part 1: Survey of laser systems

The laser principle is presented as a collection of fundamental phenomena as there are nonlinear regenerative amplification and stimulated emission by the active laser medium, as well as selection of optical modes and feedback by the resonator. The challenge is to reveal the mutual interactions of the coupled phenomena underlying the laser action, and, finally, realizing the technical optimum while approaching the physical limit. Tailoring the laser performance means to balance the fundamental phenomena involved in the laser action and actually the task is to take full advantage of the diode laser as excitation source for the laser crystal. The mechanisms of excitation, amplification and saturation in the crystal depending on spectral and spatial matching of diode pump volume to the volume of the desired laser mode dominate efficiency and beam quality.

Part 2: Short and ultrashort pulse generation

An updated review of the progress in ultrafast solid-state lasers since 1990 is given when mode-locking became a scientific topic again and the era of ultrafast dye lasers has come to its end. The advent of high-average-power diode lasers stimulated the development of femtosecond pulses in the near infrared by reaching a band width large enough to only support one to two optical cycles underneath the pulse envelope. The essential steps in scientific progress ranging from Kerr-Lens Mode-locking (KLM), self-starting passive mode-locking by Semiconductor Saturable Absorber Mirrors (SESAM) to stabilization of the Carrier-Envelope Offset (CEO) in laser oscillators with attosecond accuracy are explained, such that the expert gains a comprehensive reference and the non-expert can get an efficient starting position to enter into this field.

Part 3: Gas lasers

In seven sections, the physical and engineering aspects of different gas lasers are presented. The first gas laser was realized in 1961 half a year after T.H. Maiman had achieved the solid-state ruby laser. Solid-state crystal and liquid lasers can only be pumped by photons. Excitation by free electrons e.g. in gas discharges, fast cooling by gas dynamical effects or excitation by chemical processes is the domain of gas lasers. The different types of gases, their specific advantages and technical solutions are compiled.

September 2007 The Editors

Contents

Part 2 Short and ultrashort pulse generation

Part 2

Short and ultrashort pulse generation

2.1 Ultrafast solid-state lasers

U. Keller

2.1.1 Introduction

Since 1990 we have observed a tremendous progress in ultrashort pulse generation using solid-state lasers (Fig. 2.1.1). Until the end of the 1980's, ultrashort pulse generation was dominated by dye lasers which produced pulses as short as 27 fs with a typical average output power of about 20 mW [85Val]. Shorter pulse durations, down to 6 fs, were only achieved through additional amplification and fiber-grating pulse compression at much lower repetition rates [87For]. The tremendous success of ultrashort dye lasers in the 1970's and 1980's diverted the research interest away from solid-state lasers. In 1974 the first sub-picosecond passively mode-locked dye lasers [74Sha, 76Rud, 78Die] and in 1981 the first sub-100-femtosecond Colliding Pulse Mode-locked (CPM) dye lasers [81For] have been demonstrated. The CPM dye laser was the "work horse" all through the 1980's for ultrafast laser spectroscopy in physics and chemistry.

The development of higher average-power diode lasers in the 1980's stimulated again a strong interest in solid-state lasers. Diode laser pumping provides dramatic improvements in efficiency, lifetime, size and other important laser characteristics. For example, actively mode-locked diode-pumped Nd:YAG [89Mak1] and Nd:YLF [89Mak2, 90Kel1, 90Wei, 90Juh] lasers generated 7–12 ps pulse durations for the first time. In comparison, flashlamp-pumped Nd:YAG and Nd:YLF lasers typically produced pulse durations of ≈ 100 ps and ≈ 30 ps, respectively. Before 1990, all attempts to passively mode-lock solid-state lasers with long upper-state lifetimes (i.e. > 100 μs) resulted however in Q-switching instabilities which at best produced stable mode-locked pulses within longer Q-switched macropulses (i.e. Q-switched mode-locking) (Fig. 2.1.2). In Q-switched mode-locking, the mode-locked pico- or femtosecond pulses are inside much longer Q-switched pulse envelopes

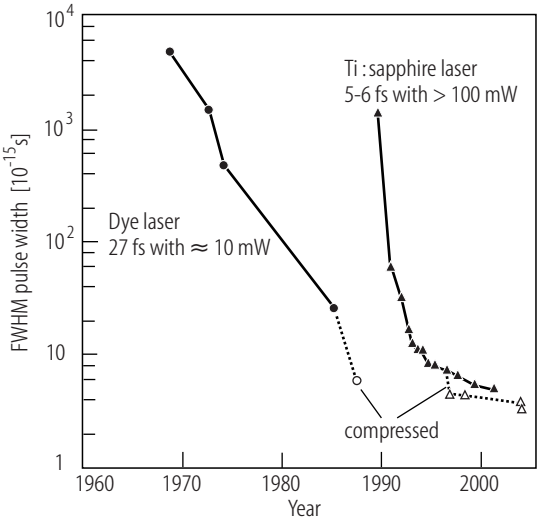

Fig. 2.1.1. Development of shortest reported pulse duration over the last three decades. Circles refer to dye-laser technology, triangles refer to Ti:sapphire laser systems. Filled symbols indicate results directly obtained from an oscillator, open symbols indicate results achieved with additional external pulse compression.

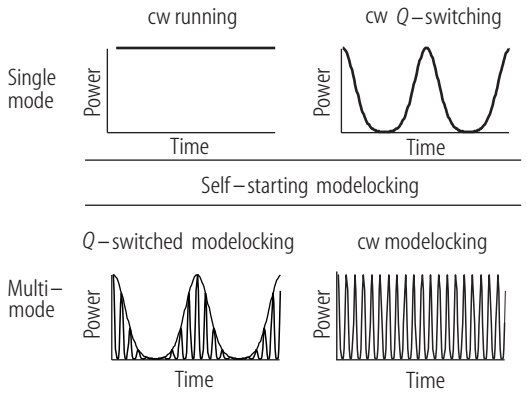

Fig. 2.1.2. Different modes of operation of a laser. cw: continuous-wave; single- and multi-mode refers to longitudinal modes.

(typically in the μs-regime) at much lower repetition rates (typically in the kHz-regime). The strong interest in an all-solid-state ultrafast laser technology was the driving force and formed the basis for many new inventions and discoveries.

Today, reliable self-starting passive mode-locking for all types of solid-state lasers is obtained with semiconductor saturable absorbers, first demonstrated in 1992 [92Kel2]. Since then, more than a decade later, the performance of compact ultrafast solid-state lasers has been improved by several orders of magnitude in pulse durations, average powers, pulse energies and pulse repetition rates, based on semiconductor saturable absorbers that are integrated into a cavity laser mirror (i.e. generally referred to as SEmiconductor Saturable Absorber Mirrors – SESAMs) [96Kel, 99Kel, 03Kel]. Diode-pumped SESAM-mode-locked solid-state lasers offer very reliable and compact ultrafast lasers with unsurpassed performance [03Pas, 04Kel]. Currently, pulse duration can range from nanosecond to a few femtoseconds depending on the different laser materials and saturable absorber parameters (Table 2.1.1 to Table 2.1.3). The average power has been increased to 60 W and 80 W directly from a mode-locked diode-pumped laser with pulse energies larger than 1 μJ [03Inn, 06Inn] and most recently even more than 10 μJ [07Maa]. The pulse repetition rate has been increased to more than 100 GHz [02Kra2].

The breakthrough of femtosecond solid-state lasers happened with the discovery of the Ti:sapphire laser [86Mou], which was the first laser that was able to support sub-10-femtosecond pulses. The existing passive mode-locking techniques, primarily developed for dye lasers, were inadequate because of the much smaller gain cross-section (i.e. in the 10^{-19} cm^2 regime) of Ti:sapphire compared to dyes (i.e. in the ns and 10^{-16} cm^2 regime). Therefore, passive pulse generation techniques had to be re-evaluated with new laser material properties in mind.

Kerr-Lens Mode-locking (KLM) [91Spe] of Ti:sapphire lasers was discovered in 1991 and is still the only successful technique to push the frontier in ultrashort pulse duration into the few-femtosecond regime with a pulse duration that only contains 1 to 2 optical cycles. For the first time in 1999 the long-lasting world record with pulse-compressed dye lasers resulting in 6-fs pulses in 1987 [87For] was passed by with KLM mode-locked Ti:sapphire lasers without any external pulse compression [99Sut, 99Mor1, 99Mor2, 00Mat]. Novel dispersion compensation methods based on chirped [94Szi] and double-chirped mirrors [97Kae] had to be developed for this result. Today, only slightly shorter pulses close to 5 fs has been obtained [01Ell]. However, the measurement of such pulses has become rather challenging and new complete pulse characterization methods (e.g. FROG [93Kan] and SPIDER [98Iac]) have been developed. KLM however has serious limitations because the mode-locking process is generally not self-starting and critical cavity alignment is required to obtain stable pulse generation. Thus, the laser cavity has to be optimized for best KLM and not necessarily for best efficiency and output power – this sets serious constraints on the cavity design, which becomes even more severe at higher average output powers and more compact monolithic cavities. Thus, passively mode-locked solid-state lasers using intracavity SESAMs have become a very attractive alternative to KLM and are more widely used today (Table 2.1.2).

Shorter pulses are only obtained with external pulse compression. Sub-4-femtosecond pulses have been demonstrated with external pulse compression [03Sch] for the first time using cascaded hollow fiber pulse compression. External pulse compression into the few optical cycle regime [99Ste] is either based on optical parametric amplification [99Shi], compression of cavity-dumped pulses in a silica fiber [97Bal], hollow fiber pulse compression [97Nis] or more recently through filamentation [04Hau1, 05Hau]. Especially the latter two allow for pulse energies of more than 100 μJ with only a few optical cycles which fulfill a central task in the generation of attosecond eXtreme UltraViolet (XUV) pulses [01Dre]. For such applications using intense few-cycle pulses in the near infrared driving extreme nonlinear processes the electric field amplitude rather than the intensity envelope becomes the important factor.

Femtosecond pulses in the near infrared reached a bandwidth large enough to only support one to two optical cycles underneath the pulse envelope. Therefore, the position of the electric field underneath the pulse envelope becomes important. This Carrier-Envelope Offset (CEO) [99Tel] can be stabilized in laser oscillators with attosecond accuracy [03Hel]. At the beginning this was a challenging task as it was not obvious how to obtain this because normally only the pulse intensity and not the electric field is detected. Also mode-locking theory fully confirms that the position of the peak electric field underneath the pulse envelope can have very large fluctuations by much more than one optical cycle. The stabilization is done in the frequency domain using the extremely stable and broadband frequency comb generated with femtosecond solid-state lasers [99Tel]. The simplest approach is based on a f-to-$2f$-interferometer [99Tel] which was first realized with a spectrally broadened Ti:sapphire laser pulse using photonic crystal fibers [00Jon, 00Apo].

The emphasis of this chapter is to give an updated review of the progress in ultrafast solid-state lasers since 1990 when mode-locking became a hot topic again and the era of ultrafast dye lasers has come to its end. The topics mentioned above will be discussed in more details. The goal is to give also to the non-expert an efficient starting position to enter into this field without providing all the detailed derivations. Relevant and useful references for further information are provided and a brief historic perspective is given throughout this chapter. A basic knowledge in lasers is required. The emphasis is on solid-state lasers because they will dominate the field in the future. More extended reviews and books have summarized the dye laser era [88Sha, 90Die]. Here, no emphasis is put on fiber and semiconductor lasers, but some useful references to recent review articles and book chapters will be provided.

2.1.2 Definition of Q-switching and mode-locking

2.1.2.1 Q-switching

The history of Q-switching goes back to 1961, when Hellwarth [61Hel] predicted that a laser could emit short pulses if the loss of an optical resonator was rapidly switched from a high to a low value. The experimental proof was produced a year later [62McC, 62Col]. The technique of Q-switching allows the generation of laser pulses of short duration (from the nanosecond to the picosecond range) and high peak power. The principle of the technique is as follows: Suppose a shutter is introduced into the laser cavity. If the shutter is closed, laser action cannot occur and the population inversion can reach a value far in excess of the threshold population that would have occurred if the shutter were not present. If the shutter is now opened suddenly, the laser will have a gain that greatly exceeds the losses, and the stored energy will be released in the form of a short and intense light pulse. Since this technique involves switching the cavity Q-factor from a low to a high value, it is known as Q-switching. Ideally Q-switched lasers operate with only one axial mode because strong intensity noise is observed in a multi-mode Q-switched laser.

In passive Q-switching the shutter is replaced by an intracavity saturable absorber. The saturable absorber starts to bleach as the intensity inside the laser continues to grow from noise due to spontaneous emission. Thus the laser intensity continues to increase which in turn results in stronger bleaching of the absorber, and so on. If the saturation intensity is comparatively small, the inversion still left in the laser medium after the absorber is bleached is essentially the same as the initial inversion. Therefore, after bleaching of the saturable absorber the laser will have a gain well in excess of the losses and if the gain cannot saturate fast enough, the intensity will continue to grow and stable Q-switching can occur. A large modulation depth of the saturable absorber then results in a high Q-switched pulse energy.

Typically the pulse repetition rate in Q-switched solid-state lasers is in the hertz to few megahertz regime, always much lower than the cavity round-trip frequency. Picosecond pulse durations can be obtained with Q-switched diode-pumped microchip lasers [89Zay, 97Zay] with pulses as short as 115 ps for active Q-switching using electro-optic light modulators [95Zay] and 37 ps for passive Q-switching using SESAMs [99Spu1, 01Spu3]. For LIDAR applications passively Q-switched Er:Yb:glass microchip lasers around 1.5 μm are particularly interesting [98Flu, 01Hae1]. The performance of Q-switched microchip lasers bridge the gap between Q-switching and mode-locking both in terms of pulse duration (nanoseconds to a few tens of picoseconds) and pulse repetition rates (kilohertz to a few tens of megahertz) (Table 2.1.3).

2.1.2.2 Mode-locking

Mode-locking is a technique to generate ultrashort pulses from lasers. In cw mode-locking the pulses are typically much shorter than the cavity round trip and the pulse repetition rate (from few tens of megahertz to a few hundreds of gigahertz) is determined by the cavity round-trip time. Typically an intracavity loss modulator (i.e. a loss modulator inside a laser cavity) is used to collect the laser light in short pulses around the minimum of the loss modulation with a period given by the cavity round-trip time $T_\mathrm{R} = 2L/v_\mathrm{g}$, where L is the laser cavity length and v_g the group velocity (i.e. the propagation velocity of the peak of the pulse intensity). Under certain conditions, the pulse repetition rate can be some integer multiple of the fundamental repetition rate (i.e. harmonic mode-locking) [72Bec]. We distinguish between active and passive mode-locking.

For active mode-locking (Fig. 2.1.3), an external signal is applied to an optical loss modulator typically using the acousto-optic or electro-optic effect. Such an electronically driven loss modulation produces a sinusoidal loss modulation with a period given by the cavity round-trip time T_R. The saturated gain at steady state then only supports net gain around the minimum of the loss modulation and therefore only supports pulses that are significantly shorter than the cavity round-trip time.

For passive mode-locking (Fig. 2.1.3), a saturable absorber is used to obtain a Self-Amplitude Modulation (SAM) of the light inside the laser cavity. Such an absorber introduces some loss to the intracavity laser radiation, which is relatively large for low intensities but significantly smaller for a short pulse with high intensity. Thus, a short pulse then produces a loss modulation because the high intensity at the peak of the pulse saturates the absorber more strongly than its low intensity wings. This results in a loss modulation with a fast initial loss saturation (i.e. reduction of the loss) determined by the pulse duration and typically a somewhat slower recovery which depends on the detailed mechanism of the absorption process in the saturable absorber. In effect, the circulating pulse saturates the laser gain to a level which is just sufficient to compensate the losses for the pulse itself, while any other circulating low-intensity light experiences more loss than gain, and thus dies out during the following cavity round trips. The obvious remaining question is – how does passive mode-locking start? Ideally from normal noise fluctuations in the laser. One noise spike is strong enough to significantly reduce its loss in the saturable absorber and thus will be more strongly amplified during the following cavity round trips, so that the stronger noise spike

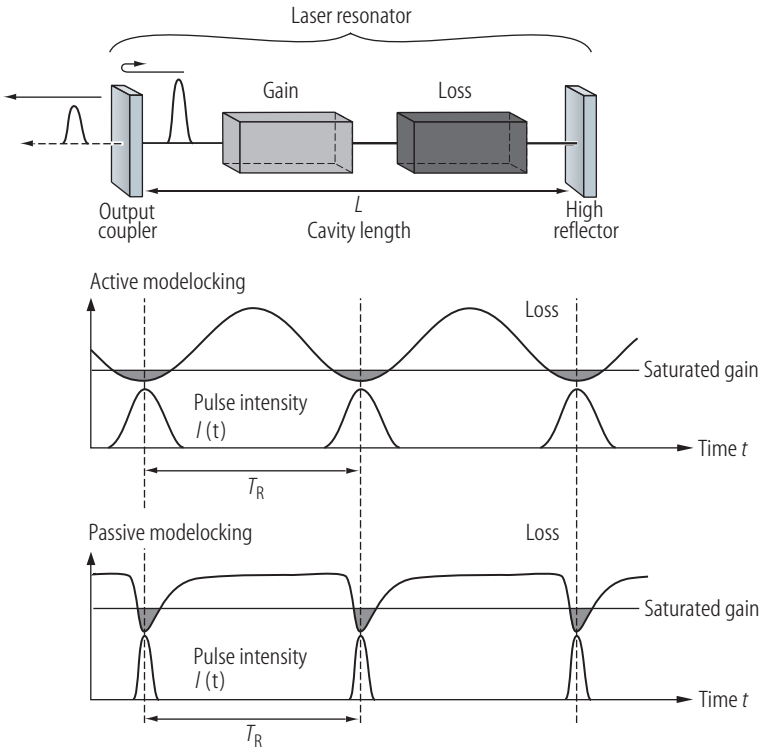

Fig. 2.1.3. Schematic laser cavity setup for active and passive mode-locking.

continues to further reduce its loss and continues its growth until reaching steady state where a stable pulse train has been formed.

Generally, we can obtain much shorter pulses with passive mode-locking using a saturable absorber, because the recovery time of the saturable absorber can be very fast, resulting in a fast loss modulation. Mode-locked pulses are much shorter than the cavity round-trip time and therefore can produce an ideal fast loss modulation inversely proportional to the pulse envelope. In comparison, any electronically driven loss modulation is significantly slower due to its sinusoidal loss modulation.

In the time domain (Fig. 2.1.4), this means that a mode-locked laser produces an equidistant pulse train, with a period defined by the round-trip time of a pulse inside the laser cavity T_R and a pulse duration τ_p. In the frequency domain (Fig. 2.1.4), this results in a phase-locked frequency comb with a constant mode spacing that is equal to the pulse repetition rate $\nu_R = 1/T_R$. The spectral width of the envelope of this frequency comb is inversely proportional to the pulse duration. Mode-locking in the frequency domain can be easily understood by the fact that a homogeneously broadened laser normally lases at one axial mode at the peak of the gain. However, the periodic loss modulation transfers additional energy phase-locked to adjacent modes separated by the modulation frequency. This modulation frequency is normally adapted to the cavity round-trip frequency. The resulting frequency comb with equidistant axial modes locked together in phase forms a short pulse in the time domain.

Mode-locking was first demonstrated in the mid-1960s using a HeNe-laser [64Har], ruby laser [65Moc] and Nd:glass laser [66DeM]. The passively mode-locked lasers were also Q-switched, which means that the mode-locked pulse train was strongly modulated (Fig. 2.1.2). This continued to be a problem for passively mode-locked solid-state lasers until the first intracavity saturable absorber was designed correctly to prevent self-Q-switching instabilities in solid-state lasers with microsecond or even millisecond upper-state lifetimes [92Kel2].

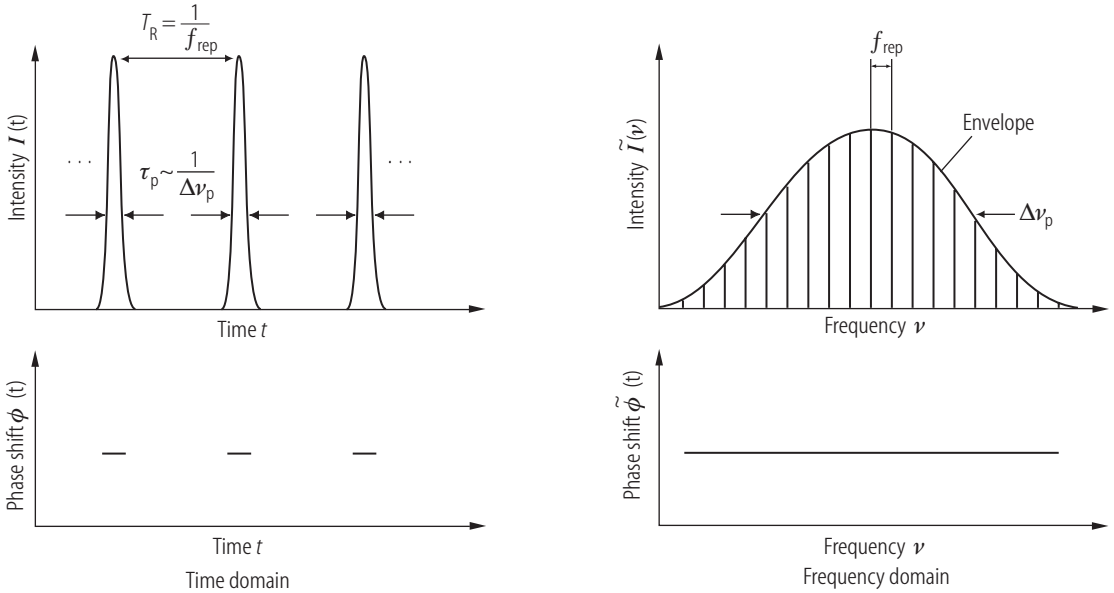

Fig. 2.1.4. Mode-locked pulses in the time and frequency domain.

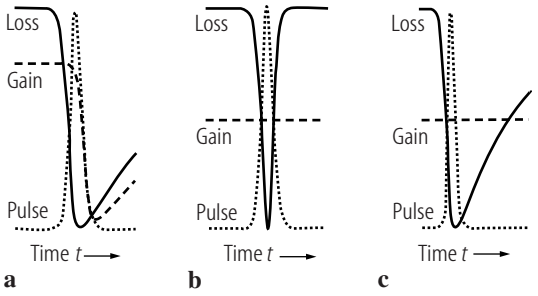

Fig. 2.1.5. Passive mode-locking mechanisms explained by three fundamental models: (**a**) slow saturable absorber mode-locking with dynamic gain saturation, (**b**) fast saturable absorber mode-locking and (**c**) slow saturable absorber mode-locking without dynamic gain saturation, which in the femtosecond regime is described by soliton mode-locking.

Q-switching instabilities are a serious issue with passively mode-locked solid-state lasers. The parameters of the saturable absorber have to be chosen such that the mode-locking is self-starting (i.e. starting from normal intensity noise of the laser) and stable, i.e. without any Q-switching instabilities (Sect. 2.1.6.8). For example, if the loss modulation becomes too large it can drive the laser unstable: The loss saturation increases the intensity inside the laser cavity. The gain then needs to saturate more strongly to compensate for the reduced loss and to keep the intensity inside the laser cavity constant. If the gain cannot respond fast enough, the intensity continues to increase as the absorber is bleached which leads to self-Q-switching instabilities or in the best case to stable Q-switched mode-locking. In the latter case, the mode-locked pulse train is strongly modulated at close to the relaxation oscillation frequency of the laser (typically in the kHz rate) (Fig. 2.1.2). A large modulation depth of the saturable absorber results in shorter pulses but an upper limit is set by the onset of Q-switching instabilities.

Passive mode-locking mechanisms are well-explained by three fundamental models: slow saturable absorber mode-locking with dynamic gain saturation [72New, 74New] (Fig. 2.1.5a), fast saturable absorber mode-locking [75Hau1, 92Hau] (Fig. 2.1.5b) and slow saturable absorber mode-locking without dynamic gain saturation in the picosecond [01Pas1] and femtosecond domain described by soliton mode-locking [95Kae1, 96Kae] (Fig. 2.1.5c). In the first two cases, a short net-gain window forms and stabilizes an ultrashort pulse. In Fig. 2.1.5a, an ultrashort net-gain window can be formed by the combined saturation of absorber and gain for which the absorber has to saturate

and recover faster than the gain, while the recovery time of the saturable absorber can be much longer than the pulse duration. Dynamic gain saturation means that the gain experiences a fast, pulse-induced saturation that then recovers again between consecutive pulses (Fig. 2.1.5a).

For solid-state lasers we cannot apply slow saturable absorber mode-locking as shown in Fig. 2.1.5a, because no significant dynamic gain saturation is taking place due to the small gain cross-section of the laser. The upper state lifetime of solid-state lasers is typically in the μs to ms regime, much longer than the pulse repetition period, which is typically in the nanosecond regime. In addition, the gain cross-section is 1000 or even more times smaller than for dye lasers. We therefore do not observe any significant dynamic gain saturation and the gain is only saturated to a constant level by the average intracavity intensity. This is not the case for dye, semiconductor and color-center lasers for which Fig. 2.1.5a describes most mode-locking processes. Therefore it was assumed that without other pulse-forming mechanisms (such as soliton pulse shaping) a fast saturable absorber is required for solid-state lasers. Kerr-lens mode-locking is nearly an ideal example for fast saturable absorber mode-locking. However, SESAM mode-locking results revealed that even a slow saturable absorber can support significantly shorter pulses even though a net gain window remains open after the short pulse (Fig. 2.1.5c). At first this seems surprising, because on the trailing edge of the pulse there is no shaping action of the absorber and even worse one would expect that the net gain after the pulse would destabilize the pulse. However, we have shown that in the picosecond regime without soliton formation, a more strongly saturated slow saturable absorber can stabilize a shorter pulse because the pulse is constantly delayed by the absorber and therefore swallows any noise growing behind himself [01Pas1]. This means that even with solid-state lasers we can work with relatively slow saturable absorbers that have approximately a recovery time in the range of 10 to 30 times the absorber recovery time. In the femtosecond regime soliton formation is actually the dominant pulse-forming mechanism and the slow saturable absorber needs only to be fast enough to stabilize this soliton – which is referred to as soliton mode-locking [95Kae1, 95Jun2, 96Kae].

2.1.3 Overview of ultrafast solid-state lasers

2.1.3.1 Overview for different solid-state laser materials

Table 2.1.1 to Table 2.1.3 give a full overview of the different results that have been achieved using different solid-state lasers. The long list as shown in Table 2.1.2 demonstrates how active the field of cw mode-locked lasers has been. The shortest pulses in the two optical cycle regime are being generated by the Ti:sapphire laser using Kerr-Lens Mode-locking (KLM). Otherwise, more recent results clearly demonstrate that the emphasis has shifted towards SESAM mode-locking because more stable and self-starting mode-locking can be achieved and the saturable absorber can be optimized independently from the cavity design. This allowed us to push the frontier in terms of pulse repetition rate and pulse energy by several orders of magnitude. Today, we can obtain a pulse repetition rate of about 160 GHz as compared to around 1 GHz in 1990. In addition, we have increased the pulse energy from the nJ-regime to more than 10 μJ from a passively mode-locked diode-pumped solid-state laser at 10–50 MHz pulse repetition rates during the last decade which is an increase of more than four orders of magnitude. More results are summarized in Table 2.1.2 and discussed below in Sect. 2.1.3.1.1 to Sect. 2.1.3.1.3. Q-switching results are restricted to microchip lasers because the pulse duration scales with the photon cavity lifetime. Thus, the shorter the laser cavity, the shorter the pulses that can be generated as discussed in Sect. 2.1.3.1.4.

In the past few years, a novel type of laser has bridged the gap between semiconductor lasers and solid-state lasers. The Vertical-External-Cavity Surface-Emitting Laser (VECSEL) [99Kuz]

combines the best of both worlds: the semiconductor gain medium allows for flexible choice of emission wavelength via bandgap engineering and offers a wealth of possibilities from the semiconductor processing world. SESAM mode-locked optically pumped VECSELs have already pulled even with solid-state lasers in the GHz pulse repetition rate regime and will be briefly reviewed in Sect. 2.1.3.1.5. For a more detailed recent review we refer to [06Kel]. Semiconductor lasers have the advantage that the SESAM can be integrated into the gain structure. This holds promise for high-volume wafer-scale fabrication of compact, ultrafast lasers. Recently, this vertical integration of ultrafast semiconductor lasers has been demonstrated for the first time and is referred to as a Mode-locked Integrated External-cavity Surface Emitting Laser (MIXSEL) [07Bel].

Ultrafast fiber lasers also demonstrate very good performances and are being briefly reviewed in Sect. 2.1.3.1.6.

2.1.3.1.1 Solid-state laser materials

Solid-state lasers can be grouped in two types: transition-metal-doped (Cr^{2+}, Cr^{3+}, Cr^{4+}, Ti^{3+}, Ni^{2+}, Co^{2+}) and rare-earth-doped (Nd^{3+}, Tm^{3+}, Ho^{3+}, Er^{3+}, Yb^{3+}) solid-state lasers (Table 2.1.1). Color-center lasers have also supported ultrashort pulse durations, but they require cryogenic cooling [87Mit, 89Isl]. A similar wavelength range can be covered with Cr:YAG lasers, for example. Table 2.1.1 to Table 2.1.3 summarize the laser parameters of these solid-state lasers and the performance that has been demonstrated with these lasers up to date with mode-locking (Table 2.1.2) and Q-switching (Table 2.1.3). Q-switching in Table 2.1.3 is restricted to microchip lasers because of the very short laser cavity that can support even picosecond pulses with Q-switching.

Several factors are important to achieve a good power efficiency: a small quantum defect, the absence of parasitic losses, and a high gain ($\sigma_L \tau_L$ product, where σ_L is the gain cross section and τ_L the upper-state lifetime of the gain medium) are desirable. The latter allows for the use of an output coupler with relatively high transmission, which makes the laser less sensitive to intracavity losses. For high-power operation, we prefer media with good thermal conductivity, a weak (or even negative) temperature dependence of the refractive index (to reduce thermal lensing), and a weak tendency for thermally induced stress fracture.

For ultrafast lasers, in addition we require a broad emission bandwidth because of large bandwidths of ultrashort pulses. More precisely, we need a large range of wavelengths in which a smoothly shaped gain spectrum is obtained for a fixed inversion level. The latter restrictions explain why the achievable mode-locked bandwidth is in some cases (e.g., some Yb^{3+}-doped media [99Hoe2]) considerably smaller than the tuning range achieved with tunable cw lasers, particularly for quasi-three-level gain media. A less obvious requirement is that the laser cross sections should be high enough. While the requirement of a reasonably small pump threshold can be satisfied even with low laser cross sections if the fluorescence lifetime is large enough, it can be very difficult to overcome Q-switching instabilities (see Sect. 2.1.6.8) in a passively mode-locked laser based on a gain material with low laser cross sections. Unfortunately, many broad-band gain media tend to have low laser cross sections, which can significantly limit their usefulness for passive mode-locking, particularly at high pulse repetition rates and in cases where a poor pump beam quality or poor thermal properties necessitate a large mode area in the gain medium.

Finally, a short pump absorption length is desirable because it permits the use of a small path length in the medium, which allows for operation with a small mode area in the gain medium and also limits the effects of dispersion and Kerr nonlinearity. The latter is particularly important for very short pulses. In addition, short pump absorption length is required for the thin-disk laser concept [94Gie] which so far supports the highest pulse energies in the 10 μJ-regime directly generated from a passively mode-locked laser [06Mar, 07Mar].

Table 2.1.1. Relevant laser materials for short and ultrashort pulse generation. λ_0: center lasing wavelength. σ_L: gain cross-section. τ_L: upper-state lifetime. $\Delta\lambda_g$: FWHM gain bandwidth. $\tau_{p,min}$: minimal pulse duration that has been demonstrated so far (coupled-cavity mode-locking schemes are not considered because of their complexity, for further information with regards to coupled-cavity mode-locking results see Table 2.1.2).

Laser material	Ref.	λ_0 [nm]	σ_L [10^{-20} cm^2]	τ_L [µs]	$\Delta\lambda_g$ [nm]	$\tau_{p,min}$	$\tau_{p,min}$ Ref.
Transition-metal-doped solid-state lasers (Cr^{2+}, Cr^{3+}, Cr^{4+}, Ti^{3+})							
Ti^{3+}:sapphire	[86Mou, 96Koe]	790	41	3.2	≈ 230	5–6 fs	[99Sut, 01Ell]
Cr^{3+}:LiSAF	[89Pay, 91Sch1, 96Koe]	850	5	67	180	9.9 fs	[03Uem]
Cr^{3+}:LiCAF	[88Pay]	758	1.23	175	115	9 fs	[02Wag]
Cr^{3+}:LiSGAF	[92Smi]	835	3.3	88	190	14 fs	[97Sor]
Cr^{3+}:LiSCAF	[92Cha]	≈ 800		80	≈ 155	90 fs	[94Wan]
Cr^{3+}:alexandrite	[79Wal, 89Sam, 96Koe]	750	0.76	260	≈ 100	3 ps	[84Pes]
Cr^{4+}:forsterite	[88Pet, 93Car, 96Koe]	1240	14.4	2.7	170	14 fs	[01Chu]
Cr^{4+}:YAG	[88Ang, 95Kue]	1378	33	4.1	≈ 250	20 fs	[02Rip1]
Cr^{2+}:ZnSe	[97Pag, 03Dru]	2500	90	7	600 (≈ 11 fs)	83 fs	[07Sor]
Cr^{2+}:ZnS	[97Pag, 03Dru]	2350	140	4.5	500		
Rare-earth-doped solid-state lasers (Nd^{3+}, Yb^{3+}, Er^{3+})							
Nd:YAG	[64Geu, 97Zay]	1064	33	230	0.6	4.5 ps	[00Lar]
Nd:YLF	[69Har, 97Zay, 96Koe]	1047	18	480	1.2	1.5 ps	[90Mal]
		1314		480		5.7 ps	[96Flu2]
Nd:YVO_4	[87Fan, 88Ris, 98For]	914	4			3 ps	[05Sch1]
	[97Zay]	1064	300	100	0.8	2.7 ps	[00Kra2, 05Lec1]
		1342	60	100		4.6 ps	[96Flu2]
Nd:$YAlO_3$		930	4.1	160	2.5	1.9 ps	[98Kel]
Nd:LSB (10 at.%)	[91Kut, 94Mey]	1064	13	118	4	1.6 ps	[96Bra2]
Nd:$GdVO_4$	[94Jen]	1064	76	90		4.4 ps	[05Agn]
Nd:(Gd,Y)VO_4	[03Qin]	1064				2.6 ps	[05Wan]
Nd:phosphate glass (LG-760)	[99Sch]	1054	4.5	323	24.3	150 fs	[95Kop1]

(continued)

Table 2.1.1 continued.

Laser material	Ref.	λ_0 [nm]	σ_L [10^{-20} cm^2]	τ_L [μs]	$\Delta\lambda_g$ [nm]	$\tau_{p,min}$	$\tau_{p,min}$ Ref.
Nd:silicate glass (LG-680)	[99Sch]	1059.7	2.54	361	35.9	68 fs	[97Aus]
Nd:fluorophosphate glass (LG-812)	[78Sch]	1054	2.6	495	26.1	60 fs	[97Aus]
Dual glass gain laser	Nd:fluorophosphate & silicate	1064				38 fs	[02Han]
Yb:YAG	[93Fan]	1030	2.0	950	6.3	340 fs	[96Kel, 99Hoe2]
		1050				136 fs	[05Uem]
Yb:YVO_4	[04Kis, 04Kra1]	1037	1.25	250		120 fs	[05Kis]
Yb:$LuVO_4$	[05Liu, 06Riv]	1020–1055	0.2–1.0	256		58 fs	[06Riv]
Yb:CAlGO	[05Pet]	1016–1050	0.75			110 fs (47 fs)	[06Zao]
Yb:KGW	[97Kul1, 97Kul2, 03Kul]	1026	2.8	≈ 250	≈ 25	100 fs	[04Pau]
Yb:KYW	[97Kul1, 97Kul2, 02Puj, 00Dem]	1025	3.0	≈ 250	≈ 25	71 fs	[01Liu]
Yb:KLuW						114 fs	[05Riv]
Yb:NGW	[06Cas]	1014–1079	≈ 2.0	380		120 fs	[06Cas]
Yb:NaYW	[07Gar]	≈ 1030	3	309		67 fs (53 fs)	[07Gar]
Yb:NLM	[05Man]	1000	3.5	285			
Yb:GdCOB	[99Mou]	1045	0.36	2600	44	90 fs	[00Dru]
Yb:BOYS	[02Dru1]	1062	0.2	1100	60	69 fs	[02Dru1]
Yb:SIS	[03Dru]	1040	0.44	820	73	70 fs	[04Dru]
Yb:CaF_2	[04Pet]					150 fs	[04Luc]
Yb:YSO	[04Jac, 95Jac]	1000–1010				122 fs	[06Thi]
Yb:LSO	[95Jac]					198 fs	[06Thi]
Yb:GSO	[06Xue]	1088	0.42	1110	70	343 fs	[07Li]
Yb:Lu_2O_3	[04Gri]	1030	1.0	820		220 fs	[04Gri]
Yb:BCBF	[96Sch]	1034	1.3	1170	24		
Yb:LSB	[05Rom]	1041	0.28	600–1200		72 fs (58 fs)	[07Riv]
Yb:YAB	[00Wan]	1040	0.8	680	25	198 fs	[02Led]
Yb:S-FAP	[94DeL]	1047	7.3	1260	4		
Yb:FAB	[94DeL]	1043	5.9	1100	4.1		
Yb:phosphate glass		1025–1060	0.049	1300	62	58 fs	[98Hoe, 99Hoe2]
Yb:silicate glass		1025–1060	0.093	1100	77	61 fs	[98Hoe, 99Hoe2]
Yb:fluoride phosphate		1025–1060	0.158	1300	81	60 fs	[98Hoe]
Er,Yb:glass	[91Lap, 96Kig, 99Lap]	1535	0.8	7900	55	255 fs	[05Spu1]

Table 2.1.2. CW mode-locked solid-state lasers using different mode-locking techniques. "Best" means in terms of pulse duration, highest average output power, highest pulse repetition rate etc. – the result for which "best" applies is in bold letters. The lasers are assumed to be diode-pumped, if not stated otherwise (except Ti:sapphire laser). ML: Mode-Locking. CCM: Coupled-Cavity Mode-locking. APM: Additive Pulse Mode-locking. RPM: Resonant Passive Mode-locking. KLM: Kerr-Lens Mode-locking. SESAM: passive mode-locking using SEmiconductor Saturable Absorber Mirrors (SESAMs). Soliton-SESAM: Soliton mode-locking with a SESAM. AOM: Acousto-Optic Modulator. EOM: Electro-Optic phase Modulator. λ_0: center lasing wavelength. τ_p: measured pulse duration. $P_{av,out}$: average output power. f_{rep}: pulse repetition rate.

Laser material	ML technique	λ_0	τ_p	$P_{av,out}$	f_{rep}	Remarks	Ref.
Ti:sapphire							
$Ti^{3+}:Al_2O_3$	active-AOM	814 nm	150 fs	600 mW	80.5 MHz		[91Cur]
		780 nm	1.3 ps	2 W	82 MHz		[92Kaf]
	CCM-APM		1.4 ps	300 mW		highly chirped 1.4 ps output pulses externally compressed down to 200 fs	[89Goo]
	CCM-RPM	860 nm	2 ps	90 mW	250 MHz		[90Kel2]
	dye sat. absorber	750 nm	140 fs			KLM started with dye saturable absorber (not understood – assumed to have a CPM Ti:sapphire laser)	[91Sar]
	KLM	880 nm	60 fs	300 mW		first demonstration of KLM (but KLM not understood)	[91Spe]
		852 nm	73 fs	240 mW	134 MHz	first experimental evidence for KLM, self-starting due to RPM	[91Kel]
						KLM, a Gaussian approximation	[91Sal1]
			47 fs	110 mW			[92Riz1]
		820 nm	39 fs	1.5 W	82 MHz		[92Kaf]
		813 nm	32 fs	320 mW	≈ 100 MHz	LaFN28-glass prisms, 2 cm Ti:sapphire crystal thickness	[92Hua1]
			33 fs			Schott F2 prisms, 8 mm Ti:sapphire crystal thickness	[92Kra1]

(continued)

Table 2.1.2 continued.

Laser material	ML technique	λ_0	τ_p	$P_{av,out}$	f_{rep}	Remarks	Ref.
		804 nm	22 fs	950 mW	100 MHz	Schott LaK31 prisms, 2 cm Ti:sapphire crystal thickness	[92Lem]
		817 nm	17 fs	500 mW	80 MHz	Schott LaKL21 prisms, 9 mm Ti:sapphire crystal thickness	[92Hua2]
		775 nm	12.3 fs			fused silica prisms, 4 mm Ti:sapphire crystal thickness	[93Cur]
		780 nm	11 fs	500 mW		fused silica prisms, 4.5 mm Ti:sapphire crystal thickness	[93Asa]
			11 fs	300 mW	100 MHz	chirped mirrors, no prisms	[94Sti]
		850 nm	8.5 fs	$\approx$ 1 mW		metal mirrors and fused silica prisms	[94Zho]
		800 nm	8.2 fs	100 mW	80 MHz	chirped mirrors only	[95Sti]
		800 nm	7.5 fs	150 mW		chirped mirrors, ring cavity	[96Xu2]
		800 nm	6.5 fs	200 mW	86 MHz	fused silica prisms and double-chirped mirrors, KLM is self-starting with SESAM	[97Jun3]
		$\approx$ 800 nm	5.8 fs	300 mW	85 MHz	fused silica prisms and double-chirped mirrors, KLM is self-starting with SESAM, pulse duration measured with SPIDER [00Mat]	[99Sut, 00Mat]
		$\approx$ 800 nm	$\approx$ 5 **fs**	200 mW	90 MHz	CaF_2 prisms, double-chirped mirrors, pulse duration measured with fit to IAC (not very accurate)	[99Mor1, 99Mor2]
		$\approx$ 800 nm	$\approx$ 5 **fs**	120 mW	65 MHz	similar to [99Mor1] but with double-Z cavity with second focus in a glass plate for additional SPM	[01Ell]
		$\approx$ 800 nm	9.5 fs	180 mW	85 MHz	KLM self-starting with novel broadband fluoride SESAM	[02Sch2]

(continued)

Table 2.1.2 continued.

Laser material	ML technique	λ_0	τ_p	$P_{av,out}$	f_{rep}	Remarks	Ref.
		780 nm	8.5 fs	1 W	75 MHz	1.5 MW peak, focused intensity 5×10^{13} W/cm^2	[98Xu]
		850 nm	13 fs	1.5 W	110 MHz	1 MW peak, 13 nJ out	[99Bed]
		800 nm	16.5 fs	170 mW	15 MHz	0.7 MW peak, 0.011 μJ	[99Cho]
		788 nm	43 fs		5.85 MHz	150 nJ, 3.5 MW peak	[03Kow]
		≈ 800 nm	26 fs 30 fs	≈ 1.5 W ≈ 2 W	11 MHz 11 MHz	130 nJ par 280 nJ, > 5 MW peak	[04Fer]
		≈ 800 nm	50 fs	1 W **2.5 W**	2 MHz 50 MHz	**0.5 μJ** 50 nJ	[05Nau]
		782 nm	23 fs	300 mW	2 GHz	ring laser, ML is self-starting due to feedback from external mirror	[99Bar]
		560–1150 nm @ −50 dBc			1 GHz	five-element ring laser	[02Bar]
	soliton-SESAM	840 nm	34 fs	140 mW	98.9 MHz	first SESAM design with a single quantum-well absorber in a Bragg reflector	[95Bro2]
			90 fs			new acronym for special SESAM design: SBR	[95Tsu]
		810 nm	13 fs	80 mW	85 MHz	shortest pulse with soliton mode-locking and no KLM	[96Kae]
		840 nm	240 fs	10 mW	**2.3 GHz**		[03Sto]
		800 nm	54 fs	3.5 W	6.23 MHz	0.56 μs pulse energy	[06Dew]
	KLM and cavity-dumped	835 nm	50 fs		≤ 950 kHz	100 nJ pulse energy	[93Ram2]
			13 fs		80 kHz	62 nJ, 5 MW peak power	[94Psh]
		800 nm	17 fs		1 kHz	212 nJ pulse energy	[96Gib]
			4.6 fs		≤ 1 MHz	2 MW peak power	[97Bal]
		780 nm	60 fs	0.36 W	0.8 MHz	**0.45 μJ** pulse energy	[06Zho]

(continued)

Table 2.1.2 continued.

Laser material	ML technique	λ_0	τ_p	$P_{av,out}$	f_{rep}	Remarks	Ref.
Cr:LiSAF							
Cr^{3+}:$LiSrAlF_6$	KLM	800–880 nm	150 fs	50 mW	82 MHz	first mode-locked femtosecond Cr:LiSAF laser, Kr-pumped	[92Mil]
		≈ 840 nm	50 fs	135 mW		Ar-ion pumped, intracavity dye absorber for starting KLM	[92Riz2]
		880–920 nm	50 fs	150 mW	85 MHz	Ar-ion pumped, regenerative AOM for starting KLM	[92Eva]
			33 fs	25 mW		Ar-ion pumped, intracavity dye absorber for starting KLM	[92Riz3]
			93 fs	5 mW		Ar-ion pumped, KLM started with intracavity SESAM	[93Riz]
			300 ps	≈ 1 mW		**first** diode-pumped mode-locked Cr:LiSAF laser, AOM or RPM for starting KLM	[93Fre]
			220 fs	≈ 10 mW		KLM started by SESAM	[94Mel]
		870 nm	90 fs	< 20 mW	90 MHz	pumped by a SHG diode-pumped actively mode-locked Nd:YLF laser, prism mode-locker to start KLM	[94Lin1]
		860 nm	97 fs	2.7 mW	80 MHz	KLM started by regen. AOM	[94Dym]
		880 nm	34 fs	42 mW	80 MHz	KLM started by regen. AOM	[95Dym]
		850 nm	55 fs	10 mW		KLM self-starting	[95Fal]
			40 fs (24 fs)	70 mW (≈ 1 mW)			[95Mel]

(continued)

Table 2.1.2 continued.

Laser material	ML technique	λ_0	τ_p	$P_{av,out}$	f_{rep}	Remarks	Ref.
		875 nm	18 fs	≈ 1 mW			[97Dym]
		880 nm	14.8 fs	70 mW	70 MHz	Kr-ion-laser pumped	[97Sor]
		850 nm	12 fs	23 mW	200 MHz	ML not self-starting	[99Uem]
		≈ 850 nm	**9.9 fs**			strong wings in IAC	[03Uem]
	soliton-SESAM	840 nm	98 fs	50 mW	120 MHz	**first** soliton mode-locking, no KLM required	[94Kop1]
		850 nm	45 fs	105 mW	176 MHz		[95Kop2, 97Kop2]
		865 nm	100 fs	11 mW	178 MHz		[95Tsu]
		842 nm	160 fs	25 mW		compact cavity design with no prisms for dispersion compensation (dispersive SESAM)	[96Kop2]
		868 nm	70 fs	100 mW		0.5 W diffraction-limited MOPA pump	[96Tsu]
		860 nm	60 fs	125 mW	176 MHz		[97Kop2]
		875 nm	50 fs	340 mW	150 MHz	low-brightness 0.9 cm wide, 15 W diode laser array	[97Kop3]
		875 nm	110 fs	**500 mW**	150 MHz	low-brightness 0.9 cm wide, 15 W diode laser array	[97Kop3]
		855 nm	57 fs	6.5 mW	150 MHz	only 72 mW pump power with 1.5 V AA batteries	[98Hop]
		848 nm	94 fs	110 mW	130 MHz	only one GTI mirror	[99Rob]
			80 fs		100 MHz	**20 fs (25 mHz ... 10 kHz) rms timing jitter**	[99Tsu]
		857 nm	146 fs	3 mW	**1 GHz**		[01Kem]
		844 nm	113 fs	20 mW	407 MHz	less than 110 mW pump	[02Hop]
		867 nm	39 fs	6.5 mW	8.6 MHz	0.75 nJ, DCM without prisms	[03Pra]
		856 nm	43 fs	5.5 mW	8.4 MHz	0.66 nJ, DCM with prisms	[03Pra]

(continued)

Table 2.1.2 continued.

Laser material	ML technique	λ_0	τ_p	$P_{av,out}$	f_{rep}	Remarks	Ref.
Cr:LiCAF							
Cr^{3+}:$LiCaAlF_6$	KLM	800 nm	170 fs	100 mW	90 MHz	Kr-pumped	[92LiK]
		793 nm	52 fs	**75 mW**	95 MHz		[98Gab]
		820 nm	20 fs	13 mW	95 MHz		[98Gab]
		≈ 850 nm	**9 fs**	220 mW	97 MHz	Ti:sapphire laser pumped, only fit to IAC measurement	[02Wag]
		≈ 850 nm	10 fs	40 mW	110 MHz	DCM and prisms, SPIDER	[03Wag]
Cr:LiSGaF							
Cr^{3+}:$LiSrGaIF_6$	KLM	830 nm	100 fs (50 fs)	35 mW	71 MHz		[95Yan]
		835 nm	64 fs			Kr-ion-laser pumped	[96Sor1]
		842 nm	44 fs	200 mW	80 MHz	Kr-ion-laser pumped, GTI	[96Sor2]
		895 nm	**14 fs**	100 mW	70 MHz	Kr-ion-laser pumped, chirped mirror	[97Sor, 98Sor]
	soliton-SESAM	839 nm	61 fs	78 mW	119 MHz		[97Loe]
			38 fs	20 mW	90 MHz		[01Dai]
Cr:LiSCAF							
Cr^{3+}:$LiSr_{0.8}Ca_{0.2}AlF_6$	KLM	860 nm	90 fs	100 mW	140 MHz	Kr-ion-laser pumped	[94Wan]
Cr:forsterite							
Cr^{4+}:Mg_2SiO_4	KLM	1.23 µm (1.21–1.27 µm)	48 fs	380 mW	81 MHz	Nd:YAG laser pumped, KLM self-starting with AOM	[93Sen]
		1.24–1.27 µm	50 fs	45 mW	82 MHz	Nd:YAG laser pumped	[93Sea]
		1.27 µm	25 fs	300 mW	80 MHz	Nd:YAG laser pumped	[93Yan]
		1.28 µm	20 fs			Nd:YVO_4 laser pumped, not self-starting	[97Zha2]

(continued)

Table 2.1.2 continued.

Laser material	ML technique	λ_0	τ_p	$P_{av,out}$	f_{rep}	Remarks	Ref.
		1.3 µm	**14 fs**	80 mW	100 MHz	double-chirped mirrors	[01Chu]
		1.3 µm	25 fs			KLM self-starting due to InAs-doped silica films [04Pra]	[02Pra]
	soliton-SESAM	1.29 µm	40 fs	60 mW		Nd:YVO_4 laser pumped	[97Zha1]
		1.29 µm	36 fs	60 mW		Nd:YVO_4 laser pumped	[97Zha2]
		1.27 µm	80 fs	68 mW	90 MHz	double-clad fiber pumped	[98Liu]
		1.26 µm	78 fs	**800 mW**	83 MHz	Nd:YAG laser pumped	[98Pet]
Cr:YAG							
Cr^{4+}:$Y_3Al_5O_{12}$	KLM	1.52 µm	120 fs	360 mW	81 MHz	Nd:YAG laser pumped, regen. AOM for starting KLM	[94Sen]
		1.51 µm	70 fs	50 mW		Nd:YAG laser pumped	[94Con]
		1.55 µm	60 fs	50 mW	235 MHz	Nd:YAG laser pumped	[94Ish]
		1.54 µm	53 fs	250 mW		Nd:YAG laser pumped	[96Ton]
		1.54 µm	43 fs	200 mW	70 MHz	Nd:YVO_4 laser pumped	[97Ton]
		1.52 µm	75 fs	280 mW	1 GHz	Nd:YVO_4 laser or Yb:fiber laser pumped	[98Mel]
		1.52 µm	55 fs		1.2 GHz	Nd:YVO_4 laser pumped	[00Tom]
		1.54 µm	115 fs	150 mW	**2.64 GHz**	Nd:YVO_4 laser pumped	[01Tom]
		1.45 µm	**20 fs**	400 mW	110 MHz	Nd:YVO_4 laser pumped	[02Rip1]
		1.52 µm	68 fs	138 mW	2.33 GHz	optimized three-element cavity	[03Tom]
		1.5 µm	26 fs 55 fs	250 mW **600 mW**	100 MHz 65 MHz	Yb-fiber laser pumped	[03Nau]
		1.569 µm	65 fs	30 mW	100 MHz	**directly diode-pumped**	[04Nau]

(continued)

Table 2.1.2 continued.

Laser material	ML technique	λ_0	τ_p	$P_{av,out}$	f_{rep}	Remarks	Ref.
	soliton-SESAM	1.541 µm	110 fs	70 mW		Nd:YVO_4 laser pumped	[96Col]
		1.5 µm	114 fs	94 mW	185 MHz	Nd:YVO_4 laser pumped	[97Spa]
		1.52 µm	200 fs	82 mW	0.9, 1.8, 2.7 GHz	Nd:YVO_4 laser pumped, 0.9 GHz fundamental, then double and triple harmonics	[97Col]
		1.52 µm	75 fs	280 mW	1 GHz	Nd:YVO_4 laser pumped	[98Mel]
		1.46 µm	400 fs	230 mW	152 MHz	Nd:YAG laser pumped, single prism for dispersion comp.	[98Cha]
		1.52 µm	44 fs	65 mW		Nd:YVO_4 laser pumped	[99Zha]
		1.5 µm	**36 fs**	300 mW		oxidized GaAs/AlAs SESAM	[02Rip2]
		1.528 µm	120 fs	95 mW	205 MHz	Yb:fiber laser pumped	[03Lag2]
		≈ 1.5 µm	57 fs	200 mW		Yb:fiber laser pumped	[03Nau]
	semiconductor-doped glass	1.510 nm	10 ps	35 mW	235 MHz	PbS-doped glass as sat. abs.	[04Lag2]
Cr^{2+}:ZnSe							
	active AOM	2.5 µm	4.4 ps	82 mW	81 MHz		[00Car]
	soliton-SESAM	2.4 µm	83 fs	80 mW	180 MHz	10 optical cycles	[07Sor]
Nd:YAG							
$Nd^{3+}:Y_3Al_5O_{12}$	active AOM	1.064 µm	25 ps			lamp-pumped: pulse shortening due to intracavity etalon	[86Ros]
	active FM	1.064 µm	12 ps	65 mW	350 MHz		[89Mak1]
	active EOM	1.32 µm	8 ps	240 mW	**1 GHz**		[91Zho]
	active AOM	1.32 µm	53 ps	1.5 W	200 MHz	lamp-pumped and harmonic mode-locked	[88Kel]

(continued)

Table 2.1.2 continued.

Laser material	ML technique	λ_0	τ_p	$P_{av,out}$	f_{rep}	Remarks	Ref.
	CCM-APM	1.064 µm	**1.7 ps**	25 mW	136 MHz		[90Goo]
			2 ps	110 mW	125 MHz		[91McC]
			6 ps	2.4 W	100 MHz	lamp-pumped	[90Liu1]
		1.32 µm	10 ps	700 mW	100 MHz	lamp-pumped	[90Liu1]
	KLM	1.064 µm	8.5 ps	1 W	100 MHz		[92Liu]
						lamp-pumped, severe instabilities	[95Chu1]
			6.7 ps	675 mW	106 MHz	Ti:sapphire laser pumped	[97Hen]
			4.5 ps	800 mW	101.5 MHz		[00Lar]
	SESAM	1.064 µm	8.7 ps	100 mW	100 MHz		[93Wei]
			6.8 ps	400 mW	217 MHz		[94Kel]
			16 ps	10.7 W	88 MHz		[99Spu3]
			19 ps	27 W	55 MHz	multiple laser heads	[00Spu]
			8.3 ps	1.59 W	130 MHz	**ceramic Nd:YAG**	[05Guo]
	polarization switching in nonlinear crystal	1.064 µm	23 ps	4 W	150 MHz	lamp-pumped, KTP crystal	[99Kub]
Nd:YLF							
Nd^{3+}:$LiYF_4$	active AOM	1.053 µm	37 ps	6.5 W	100 MHz	lamp-pumped	[87Bad]
			18 ps	12 mW	230 MHz		[89Mak2]
		1.047 µm	9 ps	150 mW	500 MHz		[90Kel1]
			7 ps	135 mW	2 GHz		[90Wei]
			6.2 ps	20 mW	1 GHz	Ti:sapphire laser pumped	[90Wal]
	active EOM	1.053 µm	13 ps	350 mW	**5.4 GHz**	Ti:sapphire laser pumped	[91Sch2]
			4 ps	400 mW	237.5 MHz		[92Wei]
			4.5 ps	400 mW	2.85 GHz		[92Wei]
		1.3 µm	8 ps	240 mW	1 GHz		[91Zho]

(continued)

Table 2.1.2 continued.

Laser material	ML technique	λ_0	τ_p	$P_{av,out}$	f_{rep}	Remarks	Ref.
	active MQW	1.047 µm	200 ps	27 mW	100 MHz	semiconductor Multiple-Quantum-Well (MQW) modulator	[95Bro3]
	active piezoelectric diffraction modulator	1.047 µm	7 ps	160 mW	160 MHz		[90Juh]
	KLM	1.047 µm	3 ps	250 mW			[94Lin2]
			2.3 ps	800 mW	82 MHz	lamp-pumped, microdot mirror	[93Ram1]
	SESAM	1.047 µm	3.3 ps	700 mW	220 MHz	Ti:sapphire laser pumped	[92Kel2]
			5.1 ps	225 mW	100 MHz		[93Wei]
			2.8 ps	460 mW	220 MHz		[94Kel]
		1.3 µm	**5.7 ps**	130 mW	98 MHz		[96Flu2]
			> 22 ps	< 20 W on-time		GaInNAs-SESAM but only quasi-cw mode-locking demonstrated	[02Sun]
			6.7 ps	580 mW	117 MHz	GaInNAs-SESAM	[04Liv]
			48 ps	630 mW	119 MHz	detailed studies about ML stability above the Q-switched mode-locking threshold	[04Sch1]
			21 ps	127 mW	**1.4 GHz**	low-loss buried resonant GaInNAs SESAM	[06Zel]
		1.053 µm	70 ps ... 4 ns	< 680 mW			[02Rot]
	CCM-APM	1.053 µm	3.7 ps	7 W	76 MHz	lamp-pumped	[90Liu2]
			1.7 ps		103 MHz		[99Jeo]
		1.047 µm	**1.5 ps**	20 mW	123 MHz		[90Mal]
			4 ps	1 W	120 MHz	pump laser for PPLN OPO	[99Lef]
	CCM-RPM	1.047 µm	3.7 ps	550 mW	250 MHz	Ti:sapphire laser pumped	[92Kel1]

(continued)

Table 2.1.2 continued.

Laser material	ML technique	λ_0	τ_p	$P_{av,out}$	f_{rep}	Remarks	Ref.
Nd:YVO$_4$							
	SESAM	1.064 µm	7 ps	4.5 W	84 MHz		[97Ruf]
			8.3 ps	198 mW	13 GHz		[99Kra1]
			6.8 ps	81 mW	29 GHz	Ti:sapphire laser pumped	[99Kra2]
			33 ps	4.4 W	235 & 440 MHz		[99Gra]
			21 ps	20 W	90 MHz		[00Bur]
			21.5 ps	**23.5 W**	**147 MHz**		[01Che1]
			4.8 ps	80 mW	39, 49, 59 GHz	Ti:sapphire laser pumped	[00Kra1]
			2.7 ps	288 mW	40 GHz		[05Lec1]
			2.7 ps	65 mW	77 GHz	Ti:sapphire laser pumped	[00Kra2]
			2.7 ps	45 mW	**157 GHz**	Ti:sapphire laser pumped	[02Kra2]
			13.7 ps	**2.1 W**	**10 GHz**		[04Lec]
			9–23 ps	< 220 mW		ion-implanted InGaAs SESAM, also see [99Led] for SESAM details	[01Led]
			31 ps	1.5 W	154 MHz	coated GaAs wafer for ML	[02She]
			6 ps			all-optical synchronization	[03Sei]
			10.6 ps	400 mW	100 MHz	detailed studies about ML stability above the Q-switched mode-locking threshold	[04Sch1]
			2.1 ps	1.28 W	96.5 MHz	output coupling (OC) SESAM, more OC-SESAM [01Spu1] and [96Sha]	[05Fan]
			13 ps	4.1 W 3.9 W 3.5 W	4.1 MHz 2.6 MHz 1.5 MHz		[03Kol]

(continued)

Table 2.1.2 continued.

Laser material	ML technique	λ_0	τ_p	$P_{av,out}$	f_{rep}	Remarks	Ref.
			16.3 ps	470 mW	**1.2 MHz**	24 kW peak	[03Pap]
			13 ps	3.5, 3.9, 4.1 W	1.5, 2.6, 4.1 MHz	with additional amplifier 50 W	[04Lut]
		1.34 µm	4.6 ps	50 mW	93 MHz		[96Flu2]
			7 ps	45 mW	5 GHz	GaInNAs SESAM	[05Spu2]
			7.3 ps	40 mW	10 GHz	4 pJ @ 10 GHz	[05Spu2]
			26 ps	850 mW	152 MHz	InAs/GaAs quantum dot SESAM	[05Su]
		914 nm	3 ps	42 mW	234 MHz	Ti:sapphire laser pumped	[05Sch1]
	nonlinear mirror ML	1.064 µm	7.9 ps	1.35 W	150 MHz		[97Agn]
		1.064 µm	29 ps	3.25 W	170 MHz	two LBO crystals used	[05Dat]
	intensity-dependent polarization rotation	1.064 µm	2.8 ps	670 mW	130 MHz		[99Cou]
Nd:LSB							
Nd:$LnM_3(BO_3)_4$	SESAM	1.062 µm	**1.6 ps**	210 mW	240 MHz	Ti:sapphire laser pumped	[96Bra2]
			2.8 ps	400 mW	177 MHz		[96Bra2]
Nd:BEL							
Nd:$La_2Be_2O_5$	active-AOM	1.070 µm	7.5 ps	230 mW	250 MHz		[91Li]
	active-FM	1.070 µm	**2.9 ps**	30 mW	238 MHz	harmonic mode-locking	[91God]
			3.9 ps	30 mW	20 GHz	harmonic mode-locking	[91God]

(continued)

Table 2.1.2 continued.

Laser material	ML technique	λ_0	τ_p	$P_{av,out}$	f_{rep}	Remarks	Ref.
Nd:YAP							
Nd:$YAlO_3$	active AOM	1.08 µm	10 ps	220 mW			[96Guy]
	SESAM	930 nm	1.9 ps	410 mW	178 MHz		[98Kel]
		1.34 µm	24 ps	7 W on-time		GaInNAs-SESAM but only quasi-cw mode-locking demonstrated	[02Sun]
	nonlinear mirror ML	1.08 µm 1.34 µm	50 ps 15 ps			$LiIO_3$ frequency doubler	[91Sta]
		1.08 µm	31 ps			pure passive ML unstable, thus used additionally AOM	[99Agn]
Nd:KGW							
Nd^{3+}:$KGd(WO_4)_2$	active-FM	1.067 µm	12 ps		200 MHz		[95Flo]
	KLM	1.067 µm	1.7 ps				[96Let]
	CCM-APM	1.067 µm	2.3 ps	850 mW	76.5 MHz		[02Maj1]
	SESAM	1.067 µm	6.3 ps	1 W	64.5 MHz		[02Maj2]
Nd:$GdVO_4$							
	SESAM	1.064 µm	9.2 ps	**5.4 W**	119 MHz		[03He]
			8 ps	600 mW	154 MHz		[03Zha]
			11.5 ps	4.9 W	140 MHz		[04Zha1]
			18.9 ps	3.46 W	0.37–3.4 GHz	GaAs wafer SESAM	[04Kon]
			12 ps	500 mW	**9.66** GHz		[04Kra2]

(continued)

Table 2.1.2 continued.

Laser material	ML technique	λ_0	τ_p	$P_{av,out}$	f_{rep}	Remarks	Ref.
			16 ps	120 mW	146 MHz	output coupling (OC) SESAM, more OC-SESAM [01Spu1] and [96Sha]	[05Zha1]
			4.4 ps	≈ 60 mW	2.5-2.7 GHz		[05Agn]
	NL mirror ML	1.064 µm	38 ps	2.65 W	121 MHz		[05Lin1]
Nd:GdYVO$_4$							
	SESAM	1.064 µm	3.8 ps	**3.9 W**	112 MHz		[04He]
			2.6 ps	2.15 W	96.4 MHz		[05Wan]
Nd:glass							
Nd:phosphate	active-AOM	1.054 µm	7 ps	20 mW		Ar-ion laser pumped	[86Yan]
		1.054 µm	≈ 10 ps	30 mW			[88Bas]
		1.054 µm	9 ps	30 mW	240 MHz		[92Hug]
		1.063 µm	310 fs	70 mW	240 MHz	Ti:sapphire laser pumped, regeneratively actively mode-locked	[94Kop2]
Nd:phosphate	active-FM	1.054 µm	9 ps	14 mW	235 MHz		[91Hug]
Nd:phosphate	CCM-APM	1.054 µm	122 fs	200 mW		Kr-ion laser pumped	[91Spi]
Nd:phosphate	soliton-SESAM	1.054 µm	150 fs	110 mW	180 MHz		[95Kop1]
		1.054 µm	120 fs	30 mW	150 MHz	single-prism for dispersion compensation	[96Kop1]
		1.057 µm	175 fs	1 W	117 MHz		[98Aus]
		1.054 µm	275 fs	**1.4 W**	74 MHz		[00Pas1]

(continued)

Table 2.1.2 continued.

Laser material	ML technique	λ_0	τ_p	$P_{av,out}$	f_{rep}	Remarks	Ref.
Nd:fluorophosphate	soliton-SESAM	1.065 μm	**60 fs**	84 mW	114 MHz		[97Aus]
Nd:silicate	soliton-SESAM	1.064 μm	130 fs	80 mW	180 MHz		[95Kop1]
	KLM	≈ 1.07 μm	64 fs	30 mW		spectral shaping required	[01Lu]
Nd: fluorophosphate and Nd:silicate	soliton-SESAM	1.064 μm	**38 fs**	40 mW		dual gain medium both at Brewster's angle	[02Han]
Yb:YAG							
Yb^{3+}:$Y_3Al_5O_{12}$	soliton-SESAM	1.03 μm	540 fs	100 mW	81 MHz	first passively mode-locked Yb:YAG laser	[95Hoe]
			340 fs	170 mW			[99Hoe2]
			2.2 ps	8.1 W	63 MHz		[99Aus]
			730 fs	16.2 W	35 MHz	first passively mode-locked thin-disk laser, 0.47 μJ pulse energy	[00Aus]
			3.3–89 ps 0.83–1.57 ps	12 W	28 MHz	tunable pulse duration	[01Bru]
			810 fs	60 W	34.3 MHz	thin-disk laser, 1.75 μJ pulse energy, 1.9 MW peak power	[03Inn]
			705 fs	**80 W**	57 MHz	thin-disk laser, 1.4 μJ pulse energy	[04Bru]
			796 fs	63 W	12.3 MHz	thin-disk laser, 5.1 μJ pulse energy, 5.6 MW peak power	[06Mar]
			791 fs	45 W	4 MHz	thin-disk laser with multi-pass cavity [64Her], **11 μJ pulse energy**	[07Mar]
		≈ 1.05 μm	**136 fs**	3.1 mW		shorter pulses only with extra spectral filtering	[05Uem]
	CCM-APM	1.03 μm	1.9 ps (4.7 ps)	2.5 W (2.7 W)	115 MHz		[03Maj]

(continued)

Table 2.1.2 continued.

Laser material	ML technique	λ_0	τ_p	$P_{av,out}$	f_{rep}	Remarks	Ref.
Yb:YVO_4							
	soliton-SESAM	1.021 μm	**120 fs**	300 mW	150 MHz		[05Kis]
Yb:$LuVO_4$							
	soliton-SESAM	1.036 μm	**58 fs**	85 mW	94 MHz		[06Riv]
Yb:CAlGO							
Yb^{3+}:$CaGdAlO_4$	soliton-SESAM	1.050 μm	110 fs	48 mW	109 MHz	strongly chirped output pulses	[06Zao]
			47 fs	38 mW	109 MHz	plus external prism pulse compressor	[06Zao]
Yb:KGW							
Yb^{3+}:$KGd(WO_4)_2$	soliton-SESAM	1.037 μm	176 fs	1.1 W	86 MHz		[00Bru]
		1.046 μm	112 fs	200 mW	86 MHz		[00Bru]
		1.028 μm	169 fs	18 mW	100 MHz		[02Maj3]
		1.037 μm	**100 fs**	126 mW		Yb:KGW and Y:KYW tested with the same cavity and SESAM	[04Pau]
		1.031 μm	296 fs	3.7 W	61 MHz		[06Maj]
		1.040 μm	433 fs	**10 W**	45 MHz	0.22 μJ pulse energy	[06Hol]
			134 fs	5.3 W	45 MHz	0.12 μJ pulse energy	[06Hol]

(continued)

Table 2.1.2 continued.

Laser material	ML technique	λ_0	τ_p	$P_{av,out}$	f_{rep}	Remarks	Ref.
Yb:KYW							
Yb^{3+}:$KY(WO_4)_2$	soliton-SESAM	1.046 μm	101 fs	100 mW	95 MHz		[02Klo]
		1.028 μm	240 fs	**22 W**	25 MHz	thin-disk laser, **0.9 μJ** pulse energy, 3.3 MW peak power	[02Bru]
		1.047 μm	123 fs	107 mW	114 MHz		[03Lag1]
		1.039 μm	**106.5 fs**	92 mW		Yb:KGW and Y:KYW tested with the same cavity and SESAM	[04Pau]
		1.029 μm	6.8 ps	90 mW	105 MHz	quantum dot SESAM under reverse bias	[05Lag]
	KLM	1.057 μm	**71 fs**	120 mW	110 MHz		[01Liu]
		1.056 μm	107 fs	126 mW	294 MHz	tunable 1042–1075 nm	[04Lag1]
	SESAM and cavity-dumping	1.040 μm	380 fs	1.35 W	1 MHz	1.35 μJ pulse energy	[05Kil1]
		1.024 μm	680 fs	3.21 W	1.06 MHz	**3 μJ** pulse energy	[07Pal]
Yb:KLuW							
Yb^{3+}:$KLu(WO_4)_2$	soliton-SESAM	1.030 μm	114 fs	31 mW	101 MHz		[05Riv]
Yb:NGW							
Yb^{3+}:$NaGd(WO_4)_2$	soliton-SESAM	1.038 μm	120 fs	360 mW	97 MHz	potential for shorter pulses	[06Cas]
Yb:NaYW							
Yb^{3+}:$NaY(WO_4)_2$	soliton-SESAM	1.030 μm	67 fs		96 MHz	Ti:sapphire laser pumped	[07Gar]
			53 fs	91 mW	96 MHz	plus external cavity SF10-prism compressor	[07Gar]

(continued)

Table 2.1.2 continued.

Laser material	ML technique	λ_0	τ_p	$P_{av,out}$	f_{rep}	Remarks	Ref.
Yb:GdCOB							
Yb^{3+}:$Ca_4GdO(BO_3)_3$	soliton-SESAM	1.045 µm	**90 fs**	40 mW	100 MHz		[00Dru, 02Dru2]
Yb:BOYS							
Yb^{3+}:$Sr_3Y(BO_3)_3$	soliton-SESAM	1.062 µm	**69 fs**	80 mW	113 MHz		[02Dru1]
Yb:SIS							
Yb^{3+}:$SrY_4(SiO_4)_3O$	soliton-SESAM	1.068 µm	94 fs	110 mW	108 MHz		[02Dru1]
		1.066 µm	**70 fs**	156 mW	98 MHz		[04Dru]
Yb:CaF_2							
	soliton-SESAM	1.049 µm	**150 fs** 230 fs	880 mW 1.74 W			[04Luc]
Yb:LSB							
Yb^{3+}:$LnM_3(BO_3)_4$	soliton-SESAM	1.053 µm	72 fs	79 mW	90 MHz	Ti:sapphire laser pumped	[07Riv]
			58 fs	73 mW	90 MHz	plus external cavity SF10-prism compressor	[07Riv]
Yb:Lu_2O_3	soliton-SESAM	1.034 µm	220 fs	266 mW	97 MHz	Ti:sapphire laser pumped	[04Gri]

(continued)

Table 2.1.2 continued.

Laser material	ML technique	λ_0	τ_p	$P_{av,out}$	f_{rep}	Remarks	Ref.
Yb:YSO							
Yb^{3+}:Y_2SiO_5	soliton-SESAM	1.041 µm	122 fs	410 mW	75 MHz		[06Thi]
Yb:LSO							
Yb^{3+}:Lu_2SiO_5	soliton-SESAM	1.044 µm	198 fs	2.61 W	75 MHz		[06Thi]
		1.059 µm	260 fs	2.6 W	75 MHz		
Yb:GSO							
Yb^{3+}:Gd_2SiO_5	soliton-SESAM	1.031 µm	1.3 ps	586 mW	101 MHz		[07Li]
		1.030 µm	343 fs	396 mW			
Yb:glass							
Yb:phosphate glass	soliton-SESAM	1.025–1.065 µm	**58 fs**	65 mW	112 MHz		[98Hoe]
Yb:silicate glass		1.03–1.082 µm	61 fs	53 mW	112 MHz		[98Hoe]
	SESAM and cavity-dumped	1.04 µm	250 fs	0.33 W	1.1 MHz	0.3 µJ pulse energy	[05Kil2]
			470 fs	0.375 W	0.5 MHz	0.75 µJ pulse energy	
Er:Yb:glass							
	active AOM	≈ 1.53 µm	90 ps	7 mW	100 MHz		[94Cer]
	active FM	1.53 µm	9.6 ps	3 mW	2.5 GHz	3^{rd}-order harmonic mode-locking	[94Lon]
		≈ 1.5 µm	9.6–30 ps	3 mW	2.5 and 5 GHz	3^{rd}-order harmonic mode-locking	[95Lap]
		1.533 µm	48 ps	1 mW	5 GHz	dual wavelength with 165 GHz separation	[98Lon]

(continued)

Table 2.1.2 continued.

Laser material	ML technique	λ_0	τ_p	$P_{av,out}$	f_{rep}	Remarks	Ref.
	SESAM	1.534 µm	2.5 ps	68 mW	114 MHz		[99Spu2]
		1.534 µm	3.8 ps	12 mW	10 GHz	nearly quantum-noise-limited timing jitter [05Sch2]	[02Kra1]
		1.535 µm	2.5 ps	50 mW	10 GHz		[02Spu]
			2.5 ps	> 5 dBm	40 GHz MUX	40 GHz multiplexed (MUX)	[02Spu]
		1.528–1.561 µm	1.9 ps	25 mW	25 GHz	gain equalized frequency comb with 36 discrete channels, tunable over C-band	[03Spu]
		1.534 µm	4.3 ps	18 mW	40 GHz		[03Zel]
		1.534 µm	1.7–1.9 ps	> 20 mW	8.8–13.3 GHz	pulse repetition rate is continuously tunable	[04Ern]
		1.533 µm	2 ps	7.5 mW	50 GHz	10 discrete channels locked to 50 GHz ITU grid	[04Zel]
		1.536 µm	3 ps	10.7 mW	**77 GHz**	optical frequency comb with > 56 dB OSNR (Optical Signal-to-Noise Ratio)	[07Zel]
		1.535 µm	20 ps	80 mW	61 MHz	first AlGaAsSb-SESAM	[04Gra]
		1.534 µm	5 ps	70 mW	61 MHz	first GaInNAs-SESAM at 1.5 µm	[05Rut]
		1.535 µm	4.7 ps	9 mW	10 GHz	AlGaAsSb-SESAM	[06Gra]
	soliton-SESAM	1.535 µm	380 fs	4 mW	100 MHz		[01Was]
		1536 µm	255 fs	58 mW	50 MHz		[05Spu1]
		1.54 µm			169 MHz	220 fs with external pulse compression, first Si/Ge-SESAM	[05Gra1]

(continued)

Table 2.1.2 continued.

Laser material	ML technique	λ_0	τ_p	$P_{av,out}$	f_{rep}	Remarks	Ref.
	soliton-CNT (Carbon NanoTube saturable absorber)	1.56 µm	100 fs	10 mW	90–200 MHz		[05Sch3]
			68 fs		85 MHz		[05Sch3]
			261 fs	63 mW	74.5 MHz	single-all CNT, nonlinear reflectivity measurements: $\Delta R_{ns} = 1.1\,\%$, $\Delta R = 0.5\,\%$, $F_{sat,A} = 57$ µJ/cm^2	[07Fon]

Table 2.1.3. Q-switched microchip lasers using different techniques. First microchip laser introduced by Zayhowski and Mooradian [89Zay]. "Best" means in terms of pulse duration, highest average output power, highest pulse repetition rate etc. – the result for which "best" applies is in bold letters. The lasers are assumed to be diode-pumped, if not stated otherwise. SESAM: passive Q-switching using SEmiconductor Saturable Absorber Mirrors (SESAMs). EOM: Electro-Optic phase Modulator. λ_0: center lasing wavelength. τ_p: measured pulse duration. E_p: pulse energy. f_{rep}: pulse repetition rate.

Laser material	ML technique	λ_0	τ_p	E_p	f_{rep}	Remarks	Ref.
Nd:YAG							
	active-EOM	1.064 μm	760 ps		4 kHz	pumped by Q-switched intracavity SHG Nd:YAG laser	[89Zay]
			270 ps	6.8 μJ	5 kHz	pulse width increases with increased f_{rep} for 5–500 kHz: 13.3 ns at 500 kHz	[92Zay]
	Cr^{4+}:YAG		337 ps	11 μJ	6 kHz		[94Zay]
			148 ps		4 kHz	optimization for max. energy [04Bur]	[03Zay]
Nd:YVO_4							
	active-EOM	1.064 μm	115 ps	**12 μJ**	1 kHz		[95Zay]
	SESAM	1.064 μm	56 ps	62 nJ	85 kHz	1.1 kW peak, 5.3 mW average	[97Bra]
			68 ps	0.37 μJ	160 kHz	5.4 kW peak, 58 mW average	[97Bra]
			143 ps	48 nJ		Output Coupling (OC) SESAM	[01Spu1]
			37 ps	53 nJ	160 kHz	1.4 kW peak, 8.5 mW average	[99Spu1, 01Spu3]
			117 ps	0.16 μJ	510 kHz	1.4 kW peak, 82 mW average	[99Spu1, 01Spu3]
			181 ps	0.28 μJ	440 kHz	1.6 kW peak, 120 mW average	[99Spu1, 01Spu3]
			2.64 ns	45 nJ	**7.8 MHz**	17 W peak, 350 mW average	[99Spu1, 01Spu3]
		1.34 μm	230 ps		53 kHz	450 kW peak	[97Flu]

(continued)

Table 2.1.3 continued.

Laser material	ML technique	λ_0	τ_p	E_p	f_{rep}	Remarks	Ref.
Nd:LSB							
	SESAM	1.062 μm	180 ps	0.1 μJ	110 kHz		[96Bra1]
	Cr^{4+}:YAG	1.063 μm	650 ps	3–4 μJ			[05Voi]
Yb:YAG							
	SESAM	1.03 μm	530 ps	**1.1 μJ**	12 kHz	1.9 kW peak	[01Spu2]
Er:Yb:glass							
	SESAM	1.535 μm	1.2 ns	45 nJ	47 kHz	2.1 mW average	[98Flu]
		≈ 1.5 μm	840 ps	**11.2 μJ**	1.4 kHz	16 mW average, 10.6 kW peak	[01Hae1]
	p-i-n modulator	1.553 μm	56 ns	470 nJ	10 kHz	previously p-i-n modulator for ML [95Bro3]	[01Han]
Cr:YAG							
		≈ 1.5 μm	42 ns		1 MHz	diode-pumped Nd:YVO_4 pumped, Q-switched ML	[01Sch]

2.1.3.1.2 Mode-locked rare-earth-doped solid-state lasers

The rare-earth-doped (e.g. Nd^{3+}, Tm^{3+}, Ho^{3+}, Er^{3+}, Yb^{3+}) solid-state lasers have favorable properties for diode-pumped high-power operation, but cannot be used in the high-power regime for femtosecond pulse generation because of their relatively small amplification bandwidth. These lasers have 4f-electrons responsible for the laser transition, which are shielded from the crystal host. Thus the gain bandwidth is normally not very large and pulse durations are limited to a few 100 fs (Table 2.1.1 and Table 2.1.2). Shorter pulses can only be obtained in inhomogeneously broadened rare-earth-doped lasers in glass hosts for example but at the expense of lower power due to the limited thermal conductivity of glasses (Table 2.1.1 and Table 2.1.2).

Typical examples are Nd^{3+}:YAG and Nd^{3+}:YVO_4. With high-power laser diodes, one or several conventional end-pumped or side-pumped laser rods and a SESAM for mode-locking, up to 27 W of average power in 19-ps pulses has been achieved with Nd^{3+}:YAG [00Spu], or 23.5 W in 22-ps pulses with Nd^{3+}:YVO_4 [01Che1]. Significantly shorter pulse durations have been achieved with Nd:YAG at lower output powers, down to 1.7 ps with 25 mW [90Goo] using the technique of Additive Pulse Mode-locking (APM). For all these Nd^{3+}-doped crystals, the relatively large laser cross sections usually make it relatively easy to achieve stable mode-locked operation without Q-switching instabilities, if the laser mode area in the gain medium is not made too large.

Phosphate or silicate glasses doped with rare-earth ions such as Nd^{3+} or Yb^{3+} have been used for pulse durations down to $\approx$ 60 fs [97Aus, 98Hoe] and output powers of a few hundred milliwatts. The relatively poor thermal properties make high-power operation challenging. Up to 1.4 W of average power in 275-fs pulses [00Pas1], or 1 W in 175-fs pulses [97Aus], have been obtained from Nd^{3+}:glass by using a specially adapted elliptical mode pumping geometry [00Pas2] initially developed for diode-pumped Cr:LiSAF lasers [97Kop1, 95Kop3]. Here, a strongly elliptical pump beam and laser mode allow the use of a fairly thin gain medium which can be efficiently cooled from both flat sides. The resulting nearly one-dimensional heat flow reduces the thermal lensing compared to cylindrical rod geometries, if the aspect ratio is large enough. A totally different route toward high peak powers is to use a cavity-dumped laser; with such a device, based on Yb^{3+}:glass, 400-nJ pulses with more than 1 MW peak power have been generated [04Kil].

Yb^{3+}:YAG has similar thermal properties as Nd^{3+}:YAG and at the same time a much larger amplification bandwidth. Another favorable property is the small quantum defect. However, challenges arise from the quasi-three-level nature of this medium and from the small laser cross sections, which favor Q-switching instabilities. High pump intensities help in both respects. An end-pumped laser based on a Yb^{3+}:YAG rod has generated 340-fs pulses with 170 mW [95Hoe]. As much as 8.1 W in 2.2-ps pulses was obtained from an elliptical-mode Yb^{3+}:YAG laser. In 2000, the first Yb^{3+}:YAG thin-disk laser has been passively mode-locked, generating 700-fs pulses with 16.2 W average power [99Aus]. The concept of the passively mode-locked thin-disk laser has been demonstrated to be power scalable, which so far lead up to 80 W in 0.7-ps pulses [06Inn].

In recent years, a few Yb^{3+}-doped crystalline gain materials have been developed which combine a relatively broad amplification bandwidth (sufficient for pulse durations of a few hundred femtoseconds) with thermal properties which are better than those of other broad-band materials, although not as good as e.g. those of YAG or sapphire. Examples are shown in Table 2.1.1 and Table 2.1.2. With an end-pumped Yb^{3+}:KGW rod, 1.1 W of average power have been achieved in 176-fs pulses [00Bru]. A Kerr-lens mode-locked Yb^{3+}:KYW laser produced pulses as short as 71 fs [01Liu], while a SESAM mode-locked Yb^{3+}:KYW produced pulses as short as 107 fs [04Pau]. Around 70-fs pulses have been obtain with SESAM mode-locked Yb^{3+}:NGW laser with 23 mW average power [06Riv], Yb^{3+}:BOYS laser with 80 mW [02Dru1], Yb^{3+}:SYS laser with 156 mW [04Dru]. However, so far the shortest pulses are still obtained with Yb:glass lasers [98Hoe]. Note that some of these media exhibit rather low emission cross sections and therefore make stable passive mode-locking difficult, while they might be very useful e.g. in regenerative amplifiers. Tungstate crystals (Yb^{3+}:KGW, Yb^{3+}:KYW) have been rather useful for passive mode-locking since they have relatively high cross sections. Yb^{3+}:KYW has been applied in a thin-disk laser, generating

22 W in 240-fs pulses [02Bru]. With improved crystal quality, significant performance enhancements appear to be feasible. Another new class of materials with particular importance are the Yb^{3+}-doped sesquioxides such as Y_2O_3, Sc_2O_3 and Lu_2O_3, which appear to be very suitable for high-power operation with short pulses.

Up to a few years ago, the repetition rate of passively mode-locked solid-state lasers was limited to a few gigahertz. *Q*-switching instabilities have limited the highest pulse repetition rates (Sect. 2.1.6.8). In recent years, the consequent exploitation of the flexibility of SESAMs supported passively mode-locked lasers with multi-GHz pulse repetition rates, very good pulse quality, comparatively high output powers, and wavelength tunability in the areas of interest (for example the ITU-specified C-band from approximately 1525 nm to 1565 nm, ITU stands for International Telecommunication Union). Passive mode-locking means that the pulses are achieved without using any expensive multi-gigahertz electronics. In addition, the pulses originate from fundamental mode-locking. Thus, every output pulse is a copy of the same single pulse, which travels back and forth in the cavity. Therefore, pulse-to-pulse variations are minimized and the phase of the pulses is constant. For the first time, pulse repetition rates above 10 GHz from passively mode-locked ion-doped solid-state lasers have been generated with Nd:YVO_4 lasers at a center wavelength around 1 μm [99Kra1]. This laser has a large gain cross section and therefore *Q*-switching instabilities are more strongly suppressed. Shortly afterwards the frontier was pushed up to 77 GHz [00Kra2] and 160 GHz [02Kra2]. The average power has been optimized at a 10 GHz pulse repetition rate to as high as 2.1 W [04Lec]. The peak power was sufficient for efficient nonlinear frequency conversion. For example, a synchronously pumped Optical Parametric Oscillator (OPO) was demonstrated producing picosecond pulses broadly tunable around 1.55 μm with up to 350 mW average output power [04Lec, 02Lec]. Such all-solid-state synch-pumped OPOs can reach the S-, C- and L-band in telecommunication. With an additional Yb-doped fiber amplifier the repetition rate was pushed up to 80 GHz [05Lec2]. Particularly in the telecom wavelength ranges (around 1.3 μm and 1.55 μm), where only few solid-state gain media are available, multi-GHz pulse repetition rates initially were not directly possible [97Col, 95Lap]. However, with improved SESAM designs [05Spu3] and an improved understanding of the *Q*-switching instabilities [04Sch1, 05Gra2] full C-band tuning [03Spu] and up to 77 GHz pulse repetition rate [07Zel] has been demonstrated with a diode-pumped Er:Yb:glass laser. At 1.3 μm both Nd:YLF [06Zel] and Nd:YVO_4 [05Spu2] have been passively mode-locked at GHz repetition rates. In addition, the timing jitter of diode-pumped solid-state lasers is very close to the quantum noise limit [05Sch2].

2.1.3.1.3 Mode-locked transition-metal-doped solid-state laser

Transition-metal-doped (e.g. Cr^{2+}, Cr^{3+}, Cr^{4+}, Ti^{3+}, Ni^{2+}, Co^{2+}) solid-state lasers are characterized by a much broader amplification bandwidth, typically allowing for pulse durations well below 0.5 ps, but also usually by significantly poorer thermal properties and lower laser cross sections. Ti^{3+}:sapphire is a notable exception, combining nearly all desired properties for powerful ultrafast lasers, except that the short pump wavelength excludes the use of high-power diode pump lasers, and that the quantum defect is large. These lasers have 3d-electrons responsible for the laser transition, which are not very well shielded from the host material. Thus these lasers are strongly phonon-broadened and can support much shorter pulses than the rare-earth-doped crystal. Presently, the shortest pulses generated from a laser are based on Ti:sapphire using KLM (Table 2.1.1).

Using a frequency-doubled solid-state laser as a pump source, Ti^{3+}:sapphire lasers have been demonstrated to generate pulses with durations below 6 fs and a few hundred milliwatts of average power [99Sut, 01Ell]. For these pulse durations, KLM is required, and self-starting may be achieved with a SESAM in addition [99Sut, 00Sut]. With a SESAM alone, 13-fs pulses with 80 mW have been demonstrated [96Kae]. If significantly longer pulse durations are acceptable, several watts of average power can be generated with a commercially available Ti^{3+}:sapphire laser, usually pumped

with a frequency-doubled diode-pumped solid-state laser at ≈ 1 μm. Another option is to achieve rather high pulse energies and peak powers by using a very long laser cavity and limiting the peak intensities by the use of longer and chirped pulses in the cavity, which may be compressed externally. Such a laser has been demonstrated to produce 130-nJ pulses with < 30 fs pulse duration and > 5 MW peak power [04Fer]. And more recently with a 2-MHz cavity pulse energies as high as 0.5 μJ have been demonstrated still maintaining < 40-fs pulses [05Nau].

Diode-pumped femtosecond lasers can be build with crystals like Cr^{3+}:LiSAF, Cr^{3+}:LiSGaF, Cr^{3+}:LiSCAF etc. (see Table 2.1.2) which can be pumped at longer wavelengths than Ti^{3+}:sapphire. However, these media have much poorer thermal properties and thus can not compete with Ti^{3+}:sapphire in terms of output power; the achievable optical bandwidth is also lower. Cr^{3+}:LiSAF lasers have generated pulses as short as 12 fs [99Uem], but only with 23 mW of output power, using KLM without self-starting ability. This has been more recently further reduced to 9.9 fs [03Uem]. The highest achieved mode-locked power was 0.5 W in 110-fs pulses [97Kop3] using SESAM mode-locking. More recently, compact Cr^{3+}:LiSAF lasers with very low pump threshold have been developed, delivering e.g. 136-fs pulses with 20 mW average power for < 100 mW optical pump power using again SESAM mode-locking in order to optimize the laser cavity design independently of the saturable absorber [02Aga].

Cr^{4+}:forsterite emits around 1.3 μm and is suitable for pulse durations down to 14 fs with 80 mW using KLM [01Chu], or for 800 mW in 78-fs pulses using SESAM [98Pet]. Normally, a Nd^{3+}-doped laser (which may be diode-pumped) is used for pumping of Cr^{4+}:forsterite. The same holds for Cr^{4+}:YAG, which emits around 1.4–1.5 μm and has allowed to generate pulses with 20 fs, 400 mW [02Rip1].

Cr^{2+}-doped II–VI materials have become interesting for ultrafast solid-state lasers in the mid-infrared regime [04Sor, 05Sor]. In recent years, Cr^{2+}:ZnSe has been identified as another very interesting gain material which is in various ways similar to Ti^{3+}:sapphire, but emits at mid-infrared wavelengths around 2.2–2.8 μm. This very broad bandwidth should allow for pulse durations below 20 fs, although until recently the shortest achieved pulse duration is much longer, ≈ 4 ps [00Car]. The large Kerr nonlinearity of this medium is causing significant problems for short-pulse generation. However, the main obstruction for femtosecond pulses turned out to be the water absorption lines in the resonator around 2.5 μm [07Sor]. Water absorption lines have been identified as a problem for SESAM mode-locking before [96Flu2]. Removing the water absorption in the Cr:ZnSe laser resulted in 80 fs pulses at a center wavelength of 2.5 μm. These are only about 10 optical cycles [07Sor].

2.1.3.1.4 *Q*-switched ion-doped solid-state microchip lasers

Q-switching results are restricted to microchip lasers because the pulse duration scales with the photon cavity lifetime. Thus, the shorter the laser cavity, the shorter the pulses that can be generated. Microchip lasers [89Zay] are single axial frequency lasers using a miniature, monolithic, flat-flat, solid-state cavity whose mode spacing is greater than the medium-gain bandwidth. They rely on gain guiding, temperature effects and/or other nonlinear optical effects to define the transverse dimension of the lasing mode. The microchip lasers are longitudinal-pumped with a diode laser. Table 2.1.3 summarizes the results obtained with actively and passively *Q*-switched microchip lasers. The shortest pulses of only 37 ps were obtained with Nd:YVO_4 passively *Q*-switched with a SESAM attached to the microchip laser (Fig. 2.1.6) [99Spu1, 01Spu3]. Using different laser crystal thicknesses ranging from 185 μm to 440 μm the pulse duration could be changed from 37 ps to 2.6 ns and the pulse repetition rate from 160 kHz to 7.8 MHz. Such a laser therefore can be easily adapted to different application requirements. Active *Q*-switched microchip lasers generated pulses as short as 115 ps [95Zay]. These results also demonstrate that passively *Q*-switched microchip lasers can bridge the gap in terms of pulse durations between mode-locking and *Q*-switching. Generally the pulse energies in actively *Q*-switched microchip lasers tend to be higher (e.g. 12 μJ in [95Zay]),

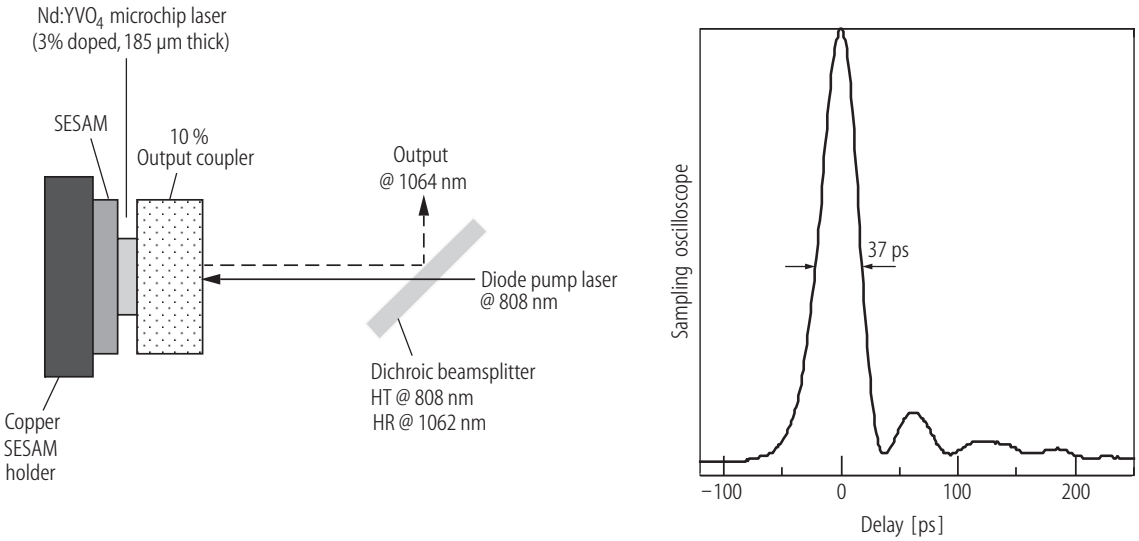

Fig. 2.1.6. Passively Q-switched Nd:YVO_4 microchip laser producing pulses as short as 37 ps with 53 nJ pulse energy, 160 kHz pulse repetition rate, and an average power of 8.5 mW. The SESAM design is based on an A-FPSA with 35 InGaAs/GaAs multiple-quantum-well saturable absorbers and a 50 % top reflector resulting in a modulation depth of 13 %.

however a passively Q-switched Yb:YAG microchip laser using a SESAM resulted in 1.1 µJ pulse energy [01Spu2]. More results are summarized in Table 2.1.3.

2.1.3.1.5 Ultrafast semiconductor lasers

Diode-pumped Vertical-External-Cavity Surface-Emitting Lasers (VECSELs) [99Kuz] combine the world of diode-pumped solid-state lasers and semiconductor lasers: The semiconductor gain medium allows for flexible choice of emission wavelength via bandgap engineering. The combination of the mature optical pumping technology extensively used for diode-pumped solid-state lasers with efficient heat removal of solid-state thin-disk lasers resulted in performance of VECSELs that surpasses anything possible to date with conventional semiconductor lasers. Continuous-wave output powers of up to 30 W with an M^2 of 3 have been reported from such optically pumped VECSELs [04Chi], and electrically pumped devices have reached 0.5 W single-mode output power [03McI]. A more detailed review of passively mode-locked VECSELs has been given recently [06Kel].

Concerning high-performance passive mode-locking, a domain where diode-pumped solid-state lasers have been dominant for years using SEmiconductor Saturable Absorber Mirrors (SESAMs) (Table 2.1.2), the VECSEL possesses the advantage of a large gain cross-section which suppresses Q-switching instabilities. Thus, VECSELs are ideally suited for high-repetition-rate mode-locking in combination with high average output powers. After the first demonstration of a passively mode-locked VECSEL in 2000 [00Hoo], pulse width and output power have improved continuously to 486-fs pulses at 10 GHz with 30 mW [05Hoo] and 4.7-ps pulses at 4 GHz with 2.1 W average output power [05Asc1]. More results are summarized in Table 2.1.4.

Novel SESAMs based on Quantum-Dot SEmiconductor Saturable Absorber Mirrors (QD-SESAMs) were developed to move towards an even more ambitious goal: the integration of the absorber into the VECSEL gain structure [04Lor]. In a first step passive mode-locking with the same mode area in the gain and the absorber had to be demonstrated for the full wafer-scale integration. We refer to this as "1:1 mode-locking" which was successfully demonstrated using these new QD-SESAMs and therefore the viability of the integrated-absorber VECSEL concept

Table 2.1.4. Passively mode-locked Vertical External Cavity Surface Emitting semiconductor Lasers (VECSELs) using different mode-locking techniques. "Best" means in terms of pulse duration, highest average output power, highest pulse repetition rate etc. – the result for which "best" applies is in bold letters. The VECSELs are either electrically pumped (EP-VECSELs) or optically pumped using diode lasers (OP-VECSELs). ML: Mode-Locking. QW: Quantum Well. λ_0: center lasing wavelength. τ_p: measured pulse duration. $P_{av,out}$: average output power. f_{rep}: pulse repetition rate.

Laser material	ML	λ_0	τ_p	$P_{av,out}$	f_{rep}	Remarks	Ref.
ML OP-VECSEL							
GaAs-based							
GaAs/AlGaAs QWs	active	850 nm	100 ps			acousto-optic modulator	[99Hol]
InGaAs-based							
12 InGaAs/GaAs QWs	SESAM	1030 nm	22 ps	20 mW	4.4 GHz	**first passively ML VECSEL**	[00Hoo]
9 InGaAs/GaAs QWs		950 nm	3.2 ps	213 mW	2 GHz		[01Hae2]
7 InGaAs/GaAs QWs		1040 nm	15 ps	< 100 mW	2.1 GHz	harmonic mode-locking	[07Saa]
6 InGaAs/GaAsP QWs		1030 nm	13.2 ps	16 mW	328 MHz		[01Gar]
		1040 nm	**477 fs**	100 mW	1.21 GHz	strain-balanced InGaAs QW	[02Gar]
6 InGaAs/GaAs QWs		1034 nm	**486 fs**	30 mW	**10 GHz**		[05Hoo]
5 InGaAs/GaAs QWs		950 nm	15 ps 3.9 ps	950 mW 530 mW	6 GHz	soliton-like pulse shaping in the positive GVD regime [02Pas]	[02Hae]
7 InGaAs/GaAsP QWs		980 nm 960 nm	9.7 ps 4.7 ps	55 mW 25 mW	21 GHz 30 GHz	low saturation QD-SESAM 1:1 ML for the first time towards wafer scale integration	[04Lor]
		957 nm	4.7 ps	**2.1 W**	4 GHz		[05Asc1]
		960 nm	6.1 ps	**1.4 W**	**10 GHz**		[05Asc2]
		960 nm	3 ps	100 mW	**50 GHz**		[06Lor]
13 InGaAs/AlGaAsP + intracavity LBO		975 nm 489 nm	3.8 ps 3.9 ps	83 mW 6 mW	1.88 GHz 1.88 GHz		[05Cas]

(continued)

Table 2.1.4 continued.

Laser material	ML	λ_0	τ_p	$P_{av,out}$	f_{rep}	Remarks	Ref.
InGaAsP-based							
7 InGaAsP QWs		1.5 μm	6.5 ps	13.5 mW	1.34 GHz		[03Hoo]
20 InGaAsP/InGaAsP QWs		1.554 μm	3.2 ps	120 mW	2.97 GHz		[05Lin2]
ML EP-VECSEL							
InGaAs-based							
GaAs/AlGaAs QWs	active	830 nm	81 ps	4 mW	960 MHz	quasi-cw, liquid N_2 cryostat cooling	[93Jia]
7 InGaAs/GaAs QWs	SESAM	980 nm	57 ps	40 mW	1.1 GHz	first electrically pumped passively ML VECSEL	[03Jas]
			14.8 ps	≈ 10 mW	15 GHz	novel compact linear cavity	[04Jas]
			50 ps	30 mW	6 GHz	SA dynamics [05Zha2]	[04Zha2]

has been demonstrated [04Lor]. With the QD-SESAM we can resolve the saturation issue for higher pulse repetition rates (i.e. shorter cavities) with nearly equal laser beam sizes in the gain and the absorber to obtain a stable cavity design. This requires a lower saturation fluence. With QD-SESAMs we can obtain both a low saturation fluence and a sufficiently low modulation depth with the optimization of the dot density and the design of the structure (i.e. moving from a antiresonant to a resonant design) [07Maa]. This is not possible with quantum-well absorbers. With an optimized QD-SESAM consisting of only one single self-assembled InAs quantum-dot layer at low growth temperatures we succeeded to push the repetition rate of passively modelocked VECSELs up to 50 GHz [06Lor]. In addition, these QD-SESAMs allowed for the first demonstration of passively modelocked VECSEL with an integrated saturable absorber layer in the gain structure [07Bel, 07Maa]. This will ultimately offer the potential for wafer-scale fabrication and operation at even higher repetition rates. We refer to this device as the Modelocked Integrated eXternal-cavity Surface Emitting Laser (MIXSEL). Such lasers could become an enabling technology basis for ultra-compact high-repetition-rate laser devices suitable for cost-efficient high-volume fabrication.

The ultimate goal is to extend the excellent results with optically pumped VECSELs to electrical pumping. However, this is not just a simple extension even though very promising results have been achieved in the cw regime with 500 mW average output power [03McI]. Initial mode-locking results reported however only very moderate average output power well below 100 mW [04Zha2].

For comparison, it is also instructive to consider briefly the performance of pulsed edge-emitting semiconductor diode lasers, which can exhibit the highest pulse repetition rates of any optical source. The obvious advantages of compactness, efficiency of pumping, and ease of manufacture and integration make these sources primary candidates for applications such as optical time-domain multiplexing, microwave carrier generation and optical clock recovery. The efficiency of direct modulation of the diode current falls off exponentially with increasing frequency above the diode relaxation resonance, which lies typically in the range 1–10 GHz: Thus the highest repetition frequencies are achieved using mode-locking of monolithic diode lasers, with gain, saturable absorption and/or external modulation all built into a single chip. Mode-locked edge-emitting diodes are immensely versatile in repetition frequency, from individual gain-switched pulses, through the microwave region of the spectrum and up to THz. The various schemes developed to realize lasers of this type have been reviewed by Avrutin et al. [00Avr]. Passive mode-locking, with a reverse-biased saturable absorber section included in the monolithic cavity, is particularly well-adapted to the generation of ultrashort pulses at high repetition rate because it does not require electrical modulation, which imposes a bandwidth limitation on repetition rate, and also impresses phase structure on the pulses. The first demonstration of such a monolithic device was reported by Vasil'ev et al. [89Vas], who reported a 100-GHz train of 2.5-ps pulses from an AlGaAs/GaAs injection laser, corresponding to fundamental mode-locking of the 380-μm long cavity. The highest output power to date is 250 mW at 4.3 GHz [06Pla]. Unfortunately, such high average power cannot be extended to pulse repetition rates well above 10 GHz because gain guiding at higher current densities gives rise to higher-order transverse modes. In addition, edge-emitting semiconductor lasers have strongly asymmetric beam profiles, which often need to be corrected with precisely mounted lenses. Typically, the same epitaxial layer forms both the gain (with a forward-biased section) and the saturable absorber (with a reverse-biased section) – and can therefore not be optimized independently. The long interaction length in the device introduces significant dispersion and nonlinearities. It is also challenging to fabricate an edge-emitting laser cavity length with a very precise pulse repetition rate and have this laser synchronized to an external reference clock. A more extensive recent review of ultrashort pulse generation with edge-emitting semiconductor lasers is given in [95Jia, 95Vai, 03Del, 00Avr].

Higher output power can be achieved from Semiconductor Optical Amplifiers (SOAs) [92Del, 95Del]; it is outside the scope of this review. However, mode-locking of SOAs in external cavities currently attracts considerable interest. It involves extreme pulse chirping, so that the amplifier is re-pumped during the passage of the pulse. Stretching and external recompression of these pulses is accomplished using chirped fiber Bragg gratings, with dispersion $> 1600\ \mathrm{ps\,nm^{-1}}$. A system of

this type has recently been reported by the Delfyett group achieving 590-fs pulses with 1.4 kW of peak power [05Kim].

2.1.3.1.6 Ultrafast fiber lasers

Mode-locked and Q-switched ion-doped fiber lasers also showed a lot of progress during the last ten years. More recent reviews on mode-locked fiber lasers are given in book chapters and review articles by I.N. Duling et al. [95Dul], by M.E. Fermann [94Fer, 95Fer, 97Fer, 03Fer] and by H.A. Haus [95Hau1, 95Hau2]. Generally, mode-locked fiber lasers generate significantly lower pulse energies and longer pulse durations than bulk lasers. However, recent progress in mode-locked fiber lasers resulted in Er/Yb-doped fiber lasers that generate 2.7-nJ pulses at 32 MHz with 100 fs pulse duration [96Nel]. Much shorter pulses but also at much lower pulse energies have been obtained in Nd-doped fiber lasers with pulse durations as short as 38 fs [92Hof] and in erbium fiber lasers with pulses as short as 84 fs [93Fer] and 63 fs [95Tam]. Fiber lasers require somewhat different saturable absorber parameters than bulk lasers. However, as has been demonstrated early on, the SESAM parameters can be adjusted for stable cw mode-locking of fiber lasers [91Zir, 93Obe]. Thus, the interested readers are referred to the review articles given above.

Impressive results have been obtained with fiber amplifiers and we refer interested readers to a more recent review given by A. Galvanauskas [03Gal]. A. Tünnermann's group achieved new world record results with 400-fs pulses at 75 MHz and an average power of 76 W based on Yb-doped double-clad fiber-based Chirped Pulse Amplification (CPA) system [03Lim]. This system is based on a SESAM mode-locked Nd:glass laser, a fiber stretcher, one Yb-doped preamplifier, one Yb-doped power amplifier and a transmission grating pulse compressor. This result has been further improved using an Yb-doped photonic-crystal-fiber-based CPA system producing 220-fs pulses at 73 MHz and an average power of 131 W [05Ros]. This corresponds to a pulse energy of 1.8 μJ and a peak power as high as 8.2 MW. In this case the seed laser is a SESAM mode-locked Yb:KGW laser followed by a bulk grating stretcher.

2.1.3.2 Design guidelines of diode-pumped solid-state lasers

An all-solid-state ultrafast laser technology is based on diode-pumped solid-state lasers. These lasers have to be optimized to support stable pulse generation. The discussion in the following sections will show that a small saturation energy of the laser medium results in a lower tendency of self-Q-switching instabilities. The saturation fluence of a four-level laser system is

$$F_{\mathrm{sat,L}} = \frac{h\nu}{m\sigma_{\mathrm{L}}} \tag{2.1.1}$$

and for a three-level system

$$F_{\mathrm{sat,L}} = \frac{h\nu}{m\left(\sigma_{\mathrm{L}} + \sigma_{\mathrm{L}}^{\mathrm{abs}}\right)} \ , \tag{2.1.2}$$

where $h\nu$ is the lasing photon energy, σ_{L} is the gain cross section, $\sigma_{\mathrm{L}}^{\mathrm{abs}}$ is the absorption cross section of the three-level gain medium and m is the number of passes through the gain medium per cavity round trip. In case of a standing-wave laser cavity this factor is $m = 2$, in a unidirectional ring laser cavity it is $m = 1$. A small saturation energy, low pump threshold and good beam quality is obtained with a small pump and cavity mode volume while maintaining good spatial overlap of the pump laser and laser mode. This can be easily obtained when a diffraction-limited pump laser is used, as for example in a Ti:sapphire laser. The lower limit of the pump volume is then set

by diffraction, and ultimately pump-induced damage to the crystal. However, diode laser arrays or bars do not generate diffraction-limited pump beams, which makes the situation a bit more complicated and is therefore explained next.

The propagation of diffraction-limited Gaussian laser beams is extensively described in many text books, as for example in [91Sal2] and [86Sie]. A beam quality factor M^2 was introduced to describe the propagation of non-diffraction-limited beams [89Sas]. The objective was to provide propagation equations for non-diffraction-limited beams that retain the simplicity of the fundamental Gaussian mode beam equations. The M^2-factor is given by

$$M^2 \equiv \frac{\theta}{\theta_\mathrm{G}} \quad \text{with} \quad \theta_\mathrm{G} \equiv \frac{\lambda}{\pi W_{0,\mathrm{G}}} \,, \tag{2.1.3}$$

where θ is the actual far-field divergence angle of any beam with any mixtures of modes, θ_G the far-field Gaussian beam divergence angle, $W_{0,\mathrm{G}}$ the beam waist of a Gaussian beam which is set equal to the beam waist of the non-diffraction-limited beam. The quantity M^2 is then a numerical expression of (inverse) beam quality with 1 being a perfect Gaussian beam and higher values indicating "poorer" quality. This is entirely equivalent to the "number of times diffraction limit" quantity introduced by Siegman [86Sie]. The beam quality does not give any information about the details of higher-order mode content in the beam. The propagation of laser beams with M^2 larger than 1, can be reduced to standard Gaussian beam propagation after substituting the wavelength λ_n with a new "effective wavelength" λ_eff given by

$$\lambda_\mathrm{eff} = M^2 \cdot \lambda_n \,, \tag{2.1.4}$$

where λ_n is the wavelength in the dispersive medium (i.e. $\lambda_n = \lambda/n$) in which the beam is propagating. Physically, this means that non-diffraction-limited beams propagate like an ideal diffraction-limited Gaussian beam but with the new, longer "effective wavelength". Beams with larger M^2 have larger "effective wavelengths", and therefore a smaller depth of focus for a given beam waist.

The output beam of a laser diode array or broad-stripe diode suffers from poor beam quality. In the so-called "fast" axis, perpendicular to the pn-junction of the diode laser, the light diverges with a large angle (25 ° to 40 ° typically) from a narrow aperture of $\approx$ 1 μm. However, in this direction the light is nearly diffraction-limited with $M^2_\mathrm{fast} \approx 1$. Thus, even though the light in the fast axis is highly divergent, it can be efficiently collected with a "fast" high-numerical aperture lens and tightly focused due to its diffraction-limited nature. In the "slow" axis, parallel to the pn-junction of the diode laser, the beam typically has a divergence of $\approx$ 10 °. For single-stripe diodes, the emitting aperture is $\approx$ 3 μm, resulting in a beam close to diffraction-limited. For higher-power "arrays" of such apertures, the divergence is also $\approx$ 10 °, but the total aperture has increased to typically 50 μm to more than 200 μm, or in case of "arrays of arrays" (i.e. bars) to a width of approximately 1 cm. The diode laser light in the slow axis is therefore many times worse than diffraction-limited. High-brightness diode arrays with $\approx$ 1 W output power and $\approx$ 100 μm stripe width typically have $M^2_\mathrm{slow} \approx 10$, whereas low brightness bars with $\approx$ 20 W and $\approx$ 1 cm stripe width have $M^2_\mathrm{slow} > 1000$. The slow axis ultimately limits the spot size of focused pump due to the requirements of mode matching to the laser mode.

With such pump lasers, the lowest pump threshold can be achieved with the following Optimized-Mode-Matching (OMM) design guidelines applied to both fast and slow axis of the diode pump laser [90Fan, 97Kop3]:

1. Determine M^2 for the pump beam (2.1.3) where $2W_{0,\mathrm{G}}$ is set equal to the width of the pump source D_p. The width of the pump source is approximately given by the stripe width of a diode array or bar or more accurately by the second-order intensity moment.
2. Determine the "effective wavelength" λ_eff (2.1.4).
3. Set the depth of focus or confocal parameter b of the pump beam approximately equal to the absorption length L_a of the pump beam in the laser medium, i.e. $b \approx L_\mathrm{a}$.

4. Determine the smallest pump beam waist $W_{0,\mathrm{opt}}$ for which a good mode overlap over the absorption length of the pump and the cavity mode can be obtained. This is the minimum pump spot size in the gain medium that still guarantees good laser beam quality and therefore determines the lowest pump threshold: Calculate optimum beam waist radius $W_{0,\mathrm{opt}}$ using Rayleigh range formula for an ideal Gaussian beam (i.e. $b = 2z_0$, where z_0 is the Rayleigh range of a Gaussian beam) with the "effective wavelength" given in (2.1.4) and a confocal parameter b given in 3. of this enumeration:

$$W_{0,\mathrm{opt}} = \sqrt{\frac{\lambda_{\mathrm{eff}} b}{2\pi}} = \sqrt{\frac{M^2 \lambda_n L_\mathrm{a}}{2\pi}} \,. \tag{2.1.5}$$

From (2.1.5) it becomes clear that for a small spot size the absorption length L_a in the gain medium should be as short as possible. The absorption length, however, limits the maximum pump power at which some thermal effects will start to degrade the laser's performance. This will be more severe for "thermally challenged" lasers which exhibit a low thermal heat conductivity and/or upper-state lifetime quenching. Low thermal conductivity results in large thermal lenses and distortions, which limit the maximum pump power. Such a thermally challenged laser material is Cr:LiSAF which is interesting for an all-solid-state femtosecond laser. Upper-state lifetime quenching as observed in Cr:LiSAF results in the following: As the temperature in the laser medium increases, the upper-state lifetime of the laser drops, and the pump threshold increases. Beyond a critical temperature, the laser actually switches off. If the absorption length is too short for these materials, this critical temperature occurs at relatively low pump powers. There is an optimum doping level for best mode matching to the available pump diodes and for minimizing pump-induced upper-state lifetime quenching.

In standard diode pumping, we use high-brightness diode arrays (i.e. brightness as high as possible) and apply OMM, (2.1.1)–(2.1.5), only in the slow axis of the diodes and weaker focusing in the fast axis. This results in an approximately circular pump beam that becomes slightly elliptical when the laser crystal is pumped at a Brewster angle. The standard diode pumping is explained in more detail by the example of a diode-pumped Cr:LiSAF laser [94Kop1]. With this standard pumping approach, the average output power was limited by the mentioned thermal problems to 230 mW cw and 125 mW mode-locked with 60-fs pulses [97Kop2]. Standard diode pumping has also been successfully used with most other solid-state lasers such as Nd:YAG. Such lasers are not "thermally challenged", and much higher average output power has been achieved with this approach.

Significantly more output power can be obtained with a diode-pumped Cr:LiSAF laser for which OMM, (2.1.1)–(2.1.5), is applied in both axes in combination with a long absorption length and efficient cooling [97Kop1, 95Kop3]. Optimized mode matching in both axes results in a highly elliptical laser mode in the crystal, because the pump beam can be focused to a much smaller beam radius in the diffraction-limited fast axis compared to the slow axis. Additionally, we can extract the heat very efficiently with a thin crystal of ≈ 1 mm height and obtain approximately a one-dimensional heat flow. With cylindrical cavity mirror we still obtained nearly ideal TEM_{00} output beams. Using a 15 W, 0.9 cm wide diode pump array with $M^2_{\mathrm{slow}} = 1200$ and $M^2_{\mathrm{fast}} = 1$ [95Ski], the average output power of such a diode-pumped Cr:LiSAF laser was 1.4 W cw, 500 mW mode-locked with 110-fs pulses, and 340 mW mode-locked with 50-fs pulses [97Kop2]. Combined with a relatively long absorption length, we pumped a thin sheet volume with a width of approximately 1 mm, a length of $L_\mathrm{a} \approx 4$ mm and a thickness of ≈ 80 µm in the laser crystal. This approach has been also applied to a diode-pumped Nd:glass laser, resulting in an average output power of about 2 W cw and 1 W mode-locked with pulses as short as 175 fs [98Aus] and more recently 1.4 W with pulses as short as 275 fs [00Pas1]. In addition, a diode-pumped Yb:YAG laser with the same approach produced 3.5 W average power with 1-ps pulses and 8.1 W with 2.2-ps pulses [99Aus].

2.1.3.3 Laser cavity designs

2.1.3.3.1 Typical picosecond lasers

The setups of picosecond lasers typically do not differ very much from those of lasers for continuous-wave operation. Some mode-locker is installed, which might be either an Acousto-Optic Modulator (AOM) for active mode-locking (Sect. 2.1.4.1) or e.g. a SESAM (Sect. 2.1.4.2 and Sect. 2.1.4.3) for passive mode-locking. Also, the cavity design needs to fulfill a few additional demands. As an example, we refer to Fig. 2.1.7a, which shows the setup of a high-power Nd^{3+}:YAG laser [00Spu], passively mode-locked with a SESAM. The cavity design must provide appropriate beam radii both in the laser head (where the fundamental Gaussian mode should just fill the usable area) and on the SESAM to obtain an appropriate degree of saturation. This depends on a number of factors: the output power, the output coupler transmission, the cavity length, and the saturation fluence of the SESAM. Obviously the cavity length must be chosen to obtain the desired repetition rate. The equations given in Sect. 2.1.6.8 can be used to ensure that the chosen design will not suffer from Q-switching instabilities. The laser head is side-pumped in the mentioned example, but end-pumped laser heads can also be used, where the pump light is typically injected through a folding mirror which is highly reflective for the laser light.

The SESAM should typically be used as an end mirror, not as a folding mirror. Otherwise a tendency for the generation of multiple pulses, which would meet on the SESAM, might be induced. Similar setups can be used for actively mode-locked lasers, where the SESAM is replaced by an AOM. The AOM should be placed close to an end mirror, for similar reasons as discussed above for the SESAM.

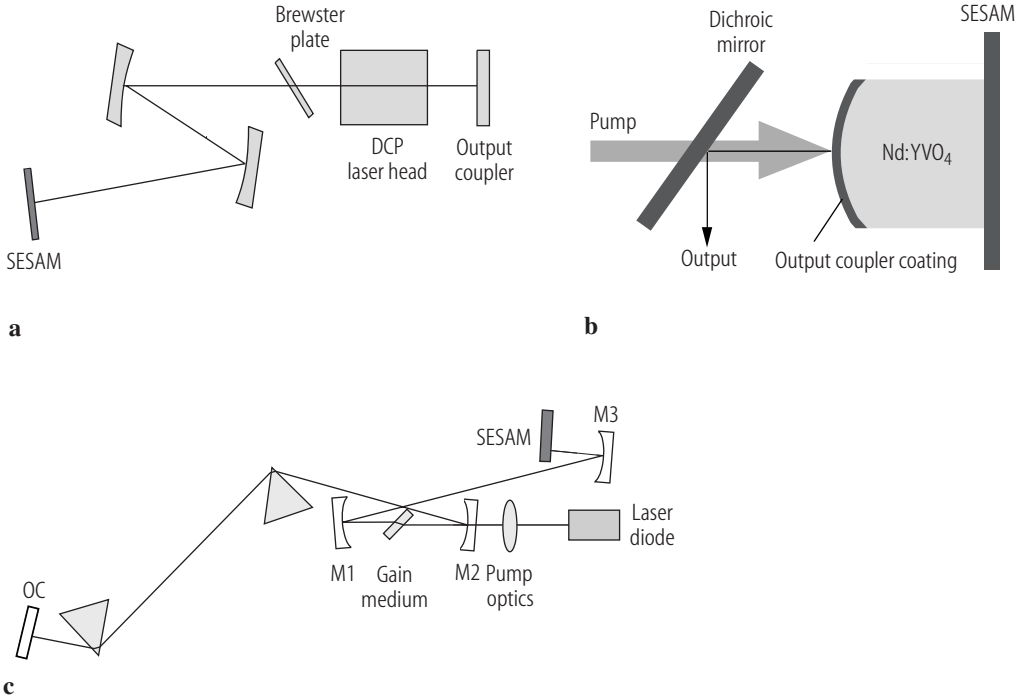

Fig. 2.1.7. (**a**) Setup of a passively mode-locked high-power Nd^{3+}:YAG laser, containing a Direct-Coupled Pump (DCP) laser head, two curved mirrors, a SESAM, and an Output Coupler mirror (OC) with 7 % transmission. (**b**) Quasi-monolithic setup as used for passively mode-locked Nd^{3+}:YVO_4 lasers with repetition rates above 20 GHz. (**c**) Typical setup of a femtosecond laser. The gain medium is pumped with a laser diode. A prism pair is used for dispersion compensation, and a SESAM as mode-locker.

For high pulse repetition rate an even simpler cavity design has been used. In the 1-μm spectral region, Nd:YVO_4 has been found to be a particularly suitable gain medium for very high repetition rates, as already discussed in Sect. 2.1.3.1. For repetition rates of 40 GHz and above, a quasi-monolithic design [99Kra2] is useful, where the output-coupler mirror is a dielectric coating directly fabricated on a curved and polished side of the laser crystal, while the SESAM is attached to the other side of the crystal (see Fig. 2.1.7b). The crystal may be anti-reflection-coated on the flat side, or just uncoated. Note that with a reflecting coating on this side, there is a cavity effect: Depending on the exact size of the air gap between crystal and SESAM, the optical field can more or less penetrate the SESAM structure, and accordingly the effective modulation depth and saturation fluence of the SESAM are modified. In this case for optimum performance, one has to manipulate the width of the air gap. A quasi-monolithic cavity design has also been used for Q-switched microchip lasers (Fig. 2.1.6) and described in more detail in Sect. 2.1.3.1.

Counterpropagating waves overlap in the crystal, leading to the phenomenon of spatial hole burning, which can have significant influence on the mode-locking behavior [95Bra2, 95Kae3, 01Pas2]. In particular, it allows for shorter pulses, although often with some amount of chirp, because gain narrowing is effectively eliminated: even without a mode-locker, such lasers tend to run with a significant emission bandwidth, and the mode-locker more or less only has to lock the phases of the running cavity modes.

2.1.3.3.2 Typical femtosecond lasers

Most femtosecond lasers are based on an end-pumped laser setup, with a broad-band laser medium such as Ti^{3+}:sapphire, Cr^{3+}:LiSAF, Nd:glass or Yb^{3+}:glass (see Sect. 2.1.3.1 for an overview). In the case of Ti^{3+}:sapphire, the pump source can be either an Ar ion laser or a frequency-doubled solid-state laser. In any case, one typically uses a few watts of pump power in a beam with good transverse beam quality, because the mode radius in the Ti^{3+}:sapphire rod is usually rather small. Other gain media like Cr^{3+}:LiSAF, Nd:glass or Yb^{3+}:glass are typically pumped with high-brightness diode lasers, delivering a few watts with beam-quality factor M^2 in the order of 10 in one direction and < 5 in the other direction, which allows for diffraction-limited laser output with typically a few hundred milliwatts.

The typical laser cavities (see Fig. 2.1.7c as an example) contain two curved mirrors in a distance of a few centimeters on both sides of the gain medium. The pump power is usually injected through one or both of these mirrors, which also focus the intracavity laser beam to an appropriate beam waist. One of the two "arms" of the cavity ends with the output coupler mirror, while the other one may be used for a SESAM as a passive mode-locker. One arm typically contains a prism pair (Sect. 2.1.5.2.3), GTI (Sect. 2.1.5.2.1) or chirped mirrors (Sect. 2.1.5.2.4) for dispersion compensation, which is necessary for femtosecond pulse generation. In most cases, femtosecond lasers operate in the regime of negative overall intracavity dispersion so that soliton-like pulses are formed.

Instead of a SESAM, or in addition to it, the Kerr lens in the gain medium can be used for mode-locking (Sect. 2.1.4.4). In most cases, soft-aperture KLM is used. Here, the cavity design is made so that the Kerr lens reduces the mode area for high intensities and thus improves the overlap with the (strongly focused) pump beam. This is achieved by operating the laser cavity near one of the stability limits of the cavity, which are found by varying the distance between the above mentioned curved folding mirrors, or some other distance in the cavity.

For the shortest pulse durations around 5–6 fs, the strong action of KLM as an effective fast saturable absorber is definitely required. Also double-chirped mirrors (Sect. 2.1.5.2.4) are required for precise dispersion compensation over a very broad bandwidth. Typically, several dispersive mirrors are used in the laser cavity, and additional mirrors may be used for further external compression. A broadband SESAM allows for self-starting mode-locking.

Higher pulse energies and peak powers have been generated by using laser setups with reduced repetition rates of only a few MHz. The long cavity length required for such repetition rates is achieved by inserting a multi-pass cell [64Her]. However, the limiting factor to the pulse energy is ultimately not the practically achievable cavity length but rather the nonlinearity of the gain crystal – at least in the sub-30-femtosecond domain: If self-phase modulation becomes too strong, this destabilizes the mode-locking process.

2.1.3.3.3 High-power thin-disk laser

The by far highest average powers in the sub-picosecond domain can be obtained from thin-disk Yb^{3+}:YAG lasers, passively mode-locked with a SESAM. The first result, with 16.2 W in 700-fs pulses [00Aus], received a lot of attention for its unusually high output power. More importantly, this new approach introduced the first power-scalable technology for sub-picosecond lasers. For this reason, further big improvements became possible, first to 60 W average power [03Inn] and later even to 80 W [04Bru], in both cases with pulse durations near 700 fs. Recently, pulse energies well above 1 μs have been generated directly from the passively mode-locked thin-disk laser first with 5.1 μs [06Mar] and then even with 11 μs [07Mar] pulse energies. These lasers are operated in the soliton mode-locked regime (Sect. 2.1.6.7). For thermal reasons negative dispersion was obtained with GTI dispersive mirrors (Sect. 2.1.5.2.1), which however also have to be carefully optimized.

The power scalability of the passively mode-locked thin-disk laser is important. First of all, the thin-disk laser head [94Gie] itself is power-scalable because of the nearly one-dimensional heat flow in the beam direction: Thermal effects (like thermal lensing) do not become more severe if the mode area is scaled up proportional to the power level. A possible problem is only the effect of stress, which has to be limited with refined techniques for mounting the crystal on the heat sink. The SESAM also has the geometry of a thin disk and thus does not limit the power: More power on an accordingly larger area does not significantly increase the temperature excursion, nor the optical intensities in the device. Finally, the tendency for Q-switching instabilities does not become stronger if e.g. the pump power and the mode areas in the disk and the absorber are all doubled while leaving pump intensity and cavity length unchanged. Thus the whole concept of the passively mode-locked thin-disk laser is power-scalable in the sense that the output power can be increased without making the following key challenges more severe: heating in the disk, heating or non-thermal damage of the SESAM, and Q-switching instabilities. Of course, further power increases can introduce other challenges which are no issue at lower powers, such as the difficulty to do dispersion compensation with optical elements that can stand the very high intracavity powers.

For a longer period the maximum pulse energy obtained directly from a passively mode-locked thin-disk laser had been 1.75 μJ [03Inn]. A further increase of the pulse energy was limited by strong nonlinearities of initially unknown origin. We then discovered that the Kerr nonlinearity of the air inside the cavity was large enough to add a significant amount of nonlinear phase shift per cavity roundtrip. Numerical estimations using the nonlinear refractive index of air show good agreement with the missing nonlinearity in [03Inn]. To avoid contributions of the air to the nonlinear phase shift, we thus covered the laser cavity with a box that was then flooded with helium, which has a negligible nonlinearity compared to air. This resulted in pulse energies of 5.1 μJ and then even 11 μJ with transform-limited soliton pulses of about 790 fs duration. These are the highest pulse energies ever obtained directly from a cw modelocked laser without any further amplification.

We believe that in the near future we can scale cw mode-locked thin-disk lasers to average powers of around 500 W and to pulse energies well above 100 μJ. In comparison low-repetition-rate Ti:sapphire lasers will not scale as well and are currently limited to the sub-1- μJ regime, even with cavity dumping (Table 2.1.2) Simple pulse compression of the high-energy ultrafast Yb:YAG thin-disk laser resulted in 33-fs pulses with a peak power of 12 MW [03Sue]. Further improvements resulted in pulses as short as 24 fs and peak intensity around 1014 W/cm^2. Such a source even makes high-field physics experiments possible but at a much higher pulse repetition rate than the

typical 1-kHz rate. This greatly increases the signal-to-noise ratio in measurements [07Mar] and reduces space-charge effects that tend to hide the underlying interesting physical processes with current sources at 1 kHz.

2.1.4 Loss modulation

2.1.4.1 Optical modulators: acousto-optic and electro-optic modulators

Many textbooks, for example [86Sie, 84Yar, 98Sve], have reviewed optical modulators for pulse generation. Today the most important optical modulators for short pulse generation are the acousto-optic and electro-optic modulators. The acousto-optic modulators have the advantage of low optical insertion loss and can readily be driven at high repetition rates. They are typically used for cw mode-locking. However, for Q-switching their loss modulation is limited and the switching time is rather slow. Therefore, acousto-optic modulators are primarily used for repetitive Q-switching of cw-pumped lasers (e.g. Nd:YAG) and electro-optic modulators are used for Q-switching in general.

For mode-locking the acousto-optic modulator typically consists of an acousto-optic substrate (typically fused quartz) and a transducer that launches an acoustic wave into the substrate. An acoustic resonator is formed when opposite to the transducer the crystal substrate is air backed. Then the acoustic wave is reflected and an acoustic standing wave is formed which produces a light modulator at twice the microwave drive frequency. At higher frequencies (a few hundreds of megahertz to a few gigahertz) the loss modulation is strongly reduced by the acoustic attenuation in the substrate. Thus, at higher modulation frequencies a sapphire [90Kel1, 90Wei] or a GaP [90Wal] substrate has been used successfully.

2.1.4.2 Saturable absorber: self-amplitude modulation (SAM)

Saturable absorbers have been used to passively Q-switch and mode-lock many lasers. Different saturable absorbers, such as organic dyes, color filter glasses, dye-doped solids, ion-doped crystals and semiconductors have been used. Independent of the specific saturable absorber material, we can define a few macroscopic absorber parameters that will determine the pulse generation process.

The relevant macroscopic properties of a saturable absorber are the modulation depth, the nonsaturable loss, the saturation fluence, the saturation intensity and the impulse response or recovery times (Table 2.1.5). These parameters determine the operation of a passively mode-locked or Q-switched laser. In our notation we assume that the saturable absorber is integrated within a mirror structure thus we are interested in the nonlinear reflectivity change $R(t)$ as a function of time and $R(F_{\mathrm{p,A}})$ as a function of the incident pulse energy fluence on the saturable absorber. If the saturable absorber is used in transmission, we simply characterize the absorber by nonlinear transmission measurements, i.e. $T(t)$ and $T(F_{\mathrm{p,A}})$. Both the saturation fluence $F_{\mathrm{sat,A}}$ and the absorber recovery time τ_{A} are determined experimentally without any needs to determine the microscopic properties of the nonlinearities. The saturation fluence of the absorber does not only depend on material properties but also on the specific device structure in which the absorber is integrated, which gives significantly more design freedom.

Standard pump-probe techniques determine the impulse response $R(t)$ and therefore τ_{A}. In the picosecond regime we typically only have to consider one picosecond recovery time, because much faster femtosecond nonlinearities in the saturable absorber give negligible modulation depth. This is shown with a semiconductor saturable absorber in Fig. 2.1.8, where the differential impulse

Table 2.1.5. Saturable absorber quantities, their defining equations and units.

Quantity	Symbol	Defining equation or measurement	Unit
Saturation fluence	$F_{\mathrm{sat,A}}$	measurement $R(F_{\mathrm{p,A}})$ or $T(F_{\mathrm{p,A}})$, (Fig. 2.1.9)	J/cm^2
Recovery time	τ_{A}	measurement $R(t)$ or $T(t)$, (Fig. 2.1.8)	s
Incident beam area	A_{A}	measurement	cm^2
Saturation energy	$E_{\mathrm{sat,A}}$	$E_{\mathrm{sat,A}} = A_{\mathrm{A}} F_{\mathrm{sat,A}}$	J
Saturation intensity	$I_{\mathrm{sat,A}}$	$I_{\mathrm{sat,A}} = F_{\mathrm{sat,A}}/\tau_{\mathrm{A}}$	W/cm^2
Modulation depth	ΔR or ΔT	measurement $R(F_{\mathrm{p,A}})$ or $T(F_{\mathrm{p,A}})$, (Fig. 2.1.9)	
Nonsaturable loss	ΔR_{ns} or ΔT_{ns}	measurement $R(F_{\mathrm{p,A}})$ or $T(F_{\mathrm{p,A}})$, (Fig. 2.1.9)	
Incident pulse energy	E_{p}	measurement	J
Incident pulse fluence	$F_{\mathrm{p,A}}$	$F_{\mathrm{p,A}} = E_{\mathrm{p}}/A_{\mathrm{A}}$	J/cm^2
Incident intensity	$I_{\mathrm{A}}(t)$	$F_{\mathrm{p,A}} = \int I_{\mathrm{A}}(t)\,\mathrm{d}t$	W/cm^2

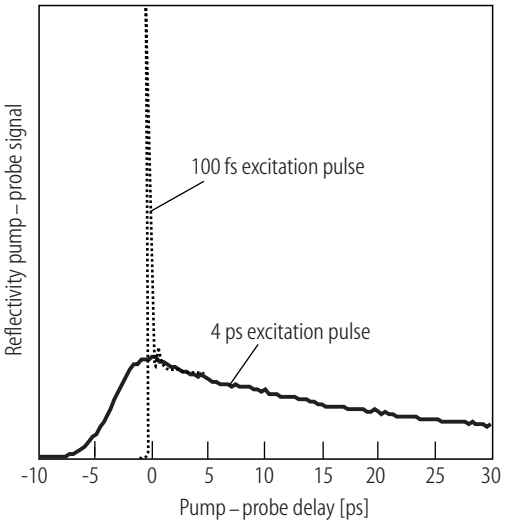

Fig. 2.1.8. Typical measured impulse response of a SESAM measured with standard degenerate pump-probe measurements using two different excitation pulse durations. The saturable was grown at low temperature, which reduced the recovery time to about 20 ps. The short intraband thermalization recovery time results in negligible modulation depth with a 4 ps excitation pulse. Thus, only the slower recovery time due to carrier trapping is important in the picosecond regime.

response $DR(t)$ was measured for two different excitation pulse durations using a semiconductor saturable absorber. For excitation with a picosecond pulse the pump-probe trace clearly shows no significant modulation depth with a fast time constant. In the femtosecond pulse regime we normally have to consider more than one absorber recovery time. In this case the slow component normally helps to start the initial pulse formation process. The modulation depth of the fast component then determines the pulse duration at steady state. Further improvements of the saturable absorber normally require some better understanding of the underlying physics of the nonlinearities which can be very interesting and rather complex. A more detailed review about the microscopic properties of ultrafast semiconductor nonlinearities for saturable absorber applications is given in a recent book chapter [00Sie]. Ultrafast semiconductor dynamics in general are discussed in much more detail by [99Sha]. However, the basic knowledge of the macroscopic properties of the absorber and how to measure [04Hai] and adjust them to a certain value is normally sufficient for stable pulse generation.

The saturation fluence $F_{\mathrm{sat,A}}$ is determined and defined by the measurement of the nonlinear change in reflectivity $R(F_{\mathrm{p,A}})$ as a function of increased incident pulse fluence (Fig. 2.1.9). The traveling-wave rate equations [89Agr] in the slow absorber approximation give normally a very

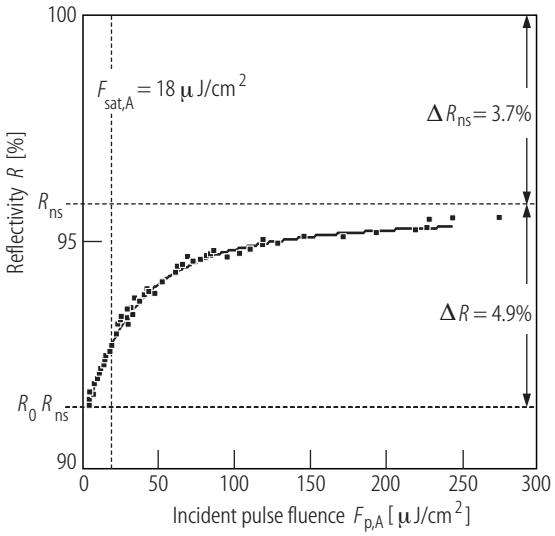

Fig. 2.1.9. Measured nonlinear reflectivity as a function of incident pulse fluence on a typical SESAM. Theoretical fit determines the macroscopic saturable absorber parameters: saturation fluence $F_{\mathrm{sat,A}}$, modulation depth ΔR and nonsaturable loss ΔR_{ns}.

good fit and determine the saturation fluence $F_{\mathrm{sat,A}}$, modulation depth ΔR and nonsaturable losses ΔR_{ns} of the absorber [95Bro1, 04Hai].

The modulation depth is typically small (i.e. a few percent to a fraction of a percent!) to prevent Q-switching instabilities in passively mode-locked solid-state lasers [99Hoe1]. Thus it is reasonable to make the following approximation:

$$\Delta R = 1 - \mathrm{e}^{-2q_0} \approx 2q_0 \;, \quad q_0 \ll 1 \;, \tag{2.1.6}$$

where q_0 is the unsaturated amplitude loss coefficient.

The saturation of an absorber can be described with the following differential equation [89Agr]:

$$\frac{\mathrm{d}q\,(t)}{\mathrm{d}t} = -\frac{q\,(t) - q_0}{\tau_{\mathrm{A}}} - \frac{q\,(t)\,P\,(t)}{E_{\mathrm{sat,A}}} \;, \tag{2.1.7}$$

where $q\,(t)$ is the saturable amplitude loss coefficient that does not include any nonsaturable losses and $P\,(t)$ is the time-dependent power incident on the absorber. Note that (2.1.7) may not be precise for high excitations where inverse saturable absorption can start to become important: For example, high excitation many times above the saturation fluence can result in additional effects such as two-photon absorptions, free carrier absorption, thermal and even various damage effects [99Tho], [05Gra2]. Two-photon absorption only starts to become significant in the femtosecond pulse width regime and results in an earlier roll-off of the nonlinear reflectivity at high incident pulse fluences. This is a well-known effect and has been used in power-limiting devices before [86Wal]. In this regime, however, the absorber is operated more closely to the damage threshold which needs to be evaluated separately. Our experience is that damage in semiconductor saturable absorbers typically occurs at around 100 times the saturation fluence of the absorber with long-term degradation observed close to below this damage threshold. Therefore, we normally operate the device a least an order of magnitude below this damage threshold, ideally at an incident pulse fluence of 3 to 5 times the saturation fluence of the absorber. We therefore neglect these very high-fluence effects in the following discussion. They, however, will become important again for suppressing Q-switching instabilities and will be discussed in more detail in Sect. 2.1.6.8.

At any time t the reflected (or transmitted) intensity $I_{\mathrm{out}}\,(t)$ from the saturable absorber is given by

$$I_{\mathrm{out}}\,(t) = R\,(t)\,I_{\mathrm{in}}\,(t) = \mathrm{e}^{-2q(t)} I_{\mathrm{in}}\,(t) \tag{2.1.8}$$

for a given input pulse $I_{\mathrm{in}}(t)$. Then the total net reflectivity is given by

$$R_{\mathrm{tot}} = \frac{F_{\mathrm{out}}}{F_{\mathrm{in}}} = \frac{\int I_{\mathrm{out}}(t)\,\mathrm{d}t}{\int I_{\mathrm{in}}(t)\,\mathrm{d}t} = 1 - \frac{2}{F_{\mathrm{in}}}\int q(t)\,I_{\mathrm{in}}(t)\,\mathrm{d}t\ . \tag{2.1.9}$$

This determines the total absorber loss coefficient q_{p}, which results from the fact that part of the excitation pulse needs to be absorbed to saturate the absorber:

$$R_{\mathrm{tot}} = \mathrm{e}^{-2q_{\mathrm{p}}} \approx 1 - 2q_p\ . \tag{2.1.10}$$

From (2.1.9) and (2.1.10) it then follows

$$q_{\mathrm{p}} = \frac{1}{F_{\mathrm{in}}}\int q(t)\,I_{\mathrm{in}}(t)\,\mathrm{d}t = \int q(t)\,f(t)\,\mathrm{d}t\ , \tag{2.1.11}$$

where

$$f(t) \equiv \frac{I_{\mathrm{in}}(t)}{F_{\mathrm{in}}} = \frac{P_{\mathrm{in}}(t)}{E_{\mathrm{p,in}}} \quad \text{with} \quad \int f(t)\,\mathrm{d}t = \frac{1}{F_{\mathrm{in}}}\int I_{\mathrm{in}}(t)\,\mathrm{d}t = 1\ . \tag{2.1.12}$$

We then distinguish between two typical cases: a slow and a fast saturable absorber.

2.1.4.2.1 Slow saturable absorber

In the case of a slow saturable absorber, we assume that the excitation pulse duration is much shorter than the recovery time of the absorber (i.e. $\tau_{\mathrm{p}} \ll \tau_{\mathrm{A}}$). Thus, we can neglect the recovery of the absorber during pulse excitation and (2.1.7) reduces to:

$$\frac{\mathrm{d}q(t)}{\mathrm{d}t} \approx -\frac{q(t)\,P(t)}{E_{\mathrm{sat,A}}}\ . \tag{2.1.13}$$

This differential equation can be solved and we obtain for the Self-Amplitude Modulation (SAM):

$$q(t) = q_0 \exp\left[-\frac{E_{\mathrm{p}}}{E_{\mathrm{sat,A}}}\int_0^t f(t')\,\mathrm{d}t'\right]\ . \tag{2.1.14}$$

Equation (2.1.11) then determines the total absorber loss coefficient for a given incident pulse fluence $F_{\mathrm{p,A}}$:

$$q_{\mathrm{p}}(F_{\mathrm{p,A}}) = \int q(t)\,f(t)\,\mathrm{d}t = q_0\frac{F_{\mathrm{sat,A}}}{F_{\mathrm{p,A}}}\left(1 - \mathrm{e}^{-F_{\mathrm{p,A}}/F_{\mathrm{sat,A}}}\right)\ . \tag{2.1.15}$$

It is not surprising that q_{p} does not depend on any specific pulse form because $\tau_{\mathrm{p}} \ll \tau_{\mathrm{A}}$. It is useful to introduce a saturation parameter $S \equiv F_{\mathrm{p,A}}/F_{\mathrm{sat,A}}$. For strong saturation ($S > 3$), we have $q_{\mathrm{p}}(F_{\mathrm{p,A}}) \approx q_0/S$ (2.1.15) and the absorbed pulse fluence is about $F_{\mathrm{sat,A}}\,\Delta R$.

2.1.4.2.2 Fast saturable absorber

In the case of a fast saturable absorber, the absorber recovery time is much faster than the pulse duration (i.e. $\tau_{\mathrm{p}} \gg \tau_{\mathrm{A}}$). Thus, we can assume that the absorption instantaneously follows the absorption of a certain power $P(t)$ and (2.1.7) reduces to

$$0 = -\frac{q(t) - q_0}{\tau_{\mathrm{A}}} - \frac{q(t)\,P(t)}{E_{\mathrm{sat,A}}}\ . \tag{2.1.16}$$

The saturation of the fast absorber then follows directly from (2.1.16):

$$q(t) = \frac{q_0}{1 + \dfrac{I_\mathrm{A}(t)}{I_\mathrm{sat,A}}} , \tag{2.1.17}$$

where we used the fact that $P_\mathrm{sat,A} = E_\mathrm{sat,A}/\tau_\mathrm{A}$ and $P(t)/P_\mathrm{sat,A} = I_\mathrm{A}(t)/I_\mathrm{sat,A}$. In the linear regime we can make the following approximation in (2.1.17):

$$q(t) \approx q_0 - \gamma_\mathrm{A} P(t) \quad \text{with} \quad \gamma_\mathrm{A} \equiv \frac{q_0}{I_\mathrm{sat,A} A_\mathrm{A}} . \tag{2.1.18}$$

The total absorber loss coefficient q_p, (2.1.10)–(2.1.11), now depends on the pulse form and for a sech^2-pulse shape we obtain for an incident pulse fluence $F_\mathrm{p,A}$ and the linear approximation of $q(t)$ for weak absorber saturation (2.1.18):

$$q_\mathrm{p}(F_\mathrm{p,A}) = \frac{1}{F_\mathrm{p,A}} \int q(t)\, I_\mathrm{A}(t)\, \mathrm{d}t = q_0 \left(1 - \frac{1}{3}\, \frac{F_\mathrm{p,A}}{\tau\, I_\mathrm{sat,A}}\right) . \tag{2.1.19}$$

We will later see that we only obtain an analytic solution for fast saturable absorber mode-locking, if we assume an ideal fast absorber that saturates linearly with pulse intensity (2.1.18) – which in principle only applies for weak absorber saturation in a real absorber. For a maximum modulation depth, we then can assume that $q_0 = \gamma_\mathrm{A} P_0$ (assuming an ideal fast absorber over the full modulation depth). We then obtain with (2.1.19) a residual saturable absorber loss of $q_0/3$, which the pulse experiences to fully saturate the ideal fast saturable absorber.

2.1.4.3 Semiconductor saturable absorbers

2.1.4.3.1 Semiconductor dynamics

Semiconductors are well suited absorber materials for ultrashort pulse generation. In contrast to saturable absorber mechanisms based on the Kerr effect, ultrafast semiconductor nonlinearities can be independently optimized from the laser cavity design. In addition, ultrafast semiconductor spectroscopy techniques [99Sha] provide the basis for many improvements of ultrashort pulse generation with semiconductor saturable absorbers.

The semiconductor electronic structure gives rise to strong interaction among optical excitations on ultrafast time scales and very complex dynamics. Despite the complexity of the dynamics, different time regimes can be distinguished in the evolution of optical excitations in semiconductors. These different time regimes are schematically illustrated in Fig. 2.1.10, which shows the energy dispersion diagram of a 2-band bulk semiconductor which is typical for a III–V semiconductor material. Optical excitation with an ultrafast laser pulse prepares the semiconductor in the coherent regime (time regime I in Fig. 2.1.10). In this regime, a well-defined phase relation exists between the optical excitations and the electric field of the laser pulse and among the optical excitations themselves. The coherence among the excitations in the semiconductor gives rise to a macroscopic polarization (dipole moment density). Since the macroscopic polarization enters as a source term in Maxwell's equations, it leads to an electric field which is experimentally accessible. The magnitude and decay of the polarization provide information on the properties of the semiconductor in the coherent regime. The irreversible decay of the polarization is due to scattering processes (i.e. electron–electron and electron–phonon scattering) and is usually described by the so-called dephasing or transversal relaxation time. For a mathematical definition of this time constant the reader is referred to [99Sha, 90Goe, 75All].

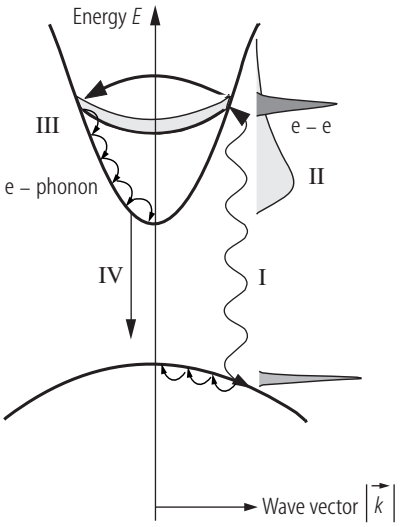

Fig. 2.1.10. Schematic dispersion diagram of a 2-band bulk semiconductor showing the time regimes I–IV after optical excitation, see text for more details. e–e: electron–electron scattering. e–phonon: electron–phonon scattering.

After the loss of coherence, ultrafast spectroscopy of semiconductors is solely concerned with the dynamics of the population, i.e., electron and hole distributions. In this incoherent regime, the time regimes II–IV in Fig. 2.1.10 can be distinguished, as described as follows. The initial electron and hole distributions are non-thermal in most cases, i.e., they cannot be described by Fermi–Dirac statistics with a well-defined temperature [85Oud, 86Kno, 87Sch]. Scattering among charge carriers is mainly responsible for the redistribution of energy within the carrier distributions and for the formation of thermal distributions. This thermalization is shown as time regime II in Fig. 2.1.10, for the example of a thermalizing electron distribution where thermalization occurs through scattering among the electrons. For excitation of the continuum, thermalization usually occurs on a time scale of 100 fs under most experimental conditions. The exact thermalization time strongly depends on the carrier density, the excess photon energy with respect to the band edge and the type of carrier [99Sha].

In general, the carriers have a temperature different from the lattice temperature after thermalization has been completed. In Fig. 2.1.10 it is assumed that the carriers have a higher temperature than the lattice. For this case, Fig. 2.1.10 schematically shows the cooling of carriers by the emission of phonons, i.e., energy transfer to the lattice. Cooling defines the time regime III. Typical time constants are in the picosecond and tens of picosecond range.

Finally, the optically excited semiconductor returns to thermodynamic equilibrium by the recombination of electron–hole pairs. Recombination is shown as time regime IV in Fig. 2.1.10. In a perfect semiconductor crystal, recombination proceeds via the emission of photons or Auger processes at high carrier densities. These recombination processes in a good quality semiconductor (i.e. with a low level of defect states) take place on time scales of hundreds of picoseconds and longer.

Another ultrafast process is encountered if large densities of deep-level traps are incorporated in a semiconductor. Trapping of carriers into deep levels can proceed on sub-picosecond time scales (not shown in Fig. 2.1.10). Since carrier trapping is important in many saturable absorber applications, it is discussed in more details in Sect. 2.1.4.3.2.

We note that the different time regimes temporally overlap. For example, a scattering process may destroy the coherence and contribute to thermalization. Nevertheless, it is very useful to distinguish between the different time regimes because they are a convenient means for the description of the complex semiconductor dynamics. The schematic picture of the different time regimes also demonstrates that two or more time constants are usually required to describe the temporal response of a semiconductor absorber. For example, we recall that thermalization typically takes place on the 100-fs time scale while carrier trapping proceeds on time scales from a few hundreds

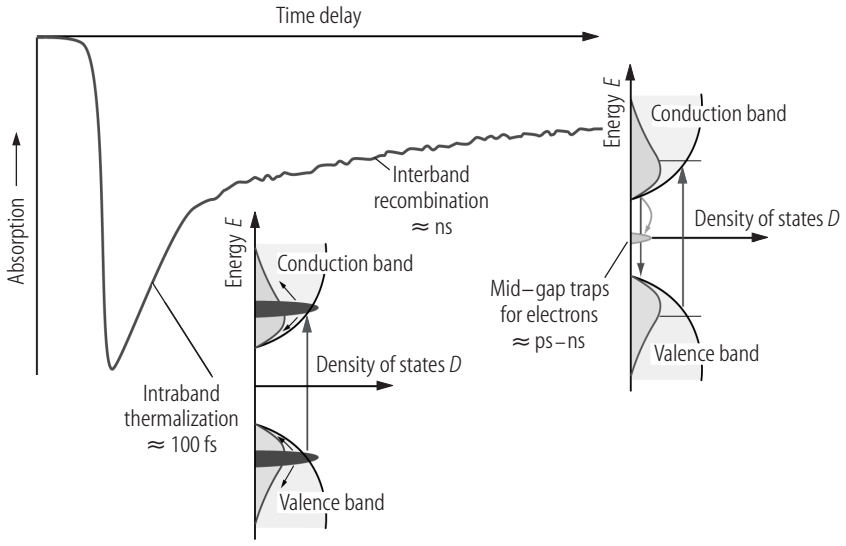

Fig. 2.1.11. Typical Self-Amplitude Modulation (SAM) observed in a semiconductor saturable absorber: A semiconductor can absorb light if the photon energy is sufficient to excite carriers from the valence band to the conduction band. Under conditions of strong excitation, the absorption is saturated because possible initial states of the pump transition are depleted while the final states are partially occupied. Within typically 60–300 fs after the excitation, the carriers in each band thermalize, and this already leads to a partial recovery of the absorption. On a longer time scale – typically between a few ps and a few ns depending on defect engineering – they will be removed by recombination and trapping. Both processes can be used for mode-locking of lasers.

of femtoseconds to tens of picoseconds. This results in the measured Self-Amplitude Modulation (SAM) of a semiconductor saturable absorber as shown in Fig. 2.1.11. This corresponds to the loss modulation used for passive mode-locking in Fig. 2.1.3.

2.1.4.3.2 Typical self-amplitude modulation (SAM) from semiconductor saturable absorbers

Figure 2.1.11 shows a typical Self-Amplitude Modulation (SAM) observed in semiconductor saturable absorbers and their different relaxation processes as discussed in Sect. 2.1.4.3.1. Semiconductor saturable absorber applications in ultrashort pulse generation often require picosecond or sub-picosecond absorber recovery times [01Pas1]. The simplest way to obtain such short absorber recovery times would be to remove the optically excited carriers from the bands a few hundreds of femtoseconds to a few tens of picosecond after they have been created. However, intrinsic recombination processes are usually too slow to deplete the band states of a semiconductor on picosecond or sub-picosecond time scales. Therefore, one generates defect states in the band gap which give rise to fast carrier trapping to deplete the bands. The trapping time is determined by the density and the type of the traps. Higher trap densities give rise to faster trapping.

Standard methods for the controlled incorporation of defect and trap states are ion implantation [89Zie] and Low-Temperature (LT) molecular beam epitaxy [88Smi]. More uncontrolled incorporation of defects occurs close to surfaces. In ion-implanted semiconductors, the trap density and the type of defect are determined by the implantation dose. The growth temperature controls the defect density in LT semiconductors where larger defect densities are incorporated at lower temperatures [94Liu, 93Wit]. Semiconductor saturable absorbers can be produced either with Molecular

Beam Epitaxy (MBE) or with Metal-Organic chemical Vapor deposition (MOVPE). MBE gives us the additional flexibility to grow semiconductors at lower temperatures, down to ≈ 200 °C, while MOVPE usually requires growth temperatures of ≈ 600 °C to break up the incident molecules on the wafer surface during the growth. Lower growth temperatures lead to microscopic structural defects which act as traps for excited carriers and thus reduce the recovery time, which is beneficial for the use in ultrafast lasers. Optimized materials combine an ultrafast recovery time with low saturation fluence, high modulation and small nonsaturable losses. This material optimization issue has been addressed for ion-implanted [99Led] and LT-grown [96Sie, 99Hai1, 99Hai2] semiconductor saturable absorbers.

2.1.4.3.3 Semiconductor saturable absorber materials

Semiconductor materials offer a wide flexibility in choosing the emission wavelength of the lasers. It ranges from ≈ 400 nm in the UV using GaN-based materials to ≈ 2.5 μm in the mid-infrared using GaInAsSb-based materials. More standard high-performance semiconductor material systems which can be grown today cover the infrared wavelength range from 800 nm up to 1.5 μm. Semiconductor compounds used for these wavelengths are AlGaAs (800 nm to 870 nm), InGaAs (870 nm to about 1150 nm), GaInNAs (1.1 μm to 1.5 μm), or InGaAsP (1.5-μm range). A larger wavelength range for a given material composition may only be obtained at the expense of increased defect concentrations because of an increased lattice mismatch to a given substrate material. Generally, bulk quantum-well and quantum-dot semiconductor saturable absorbers have been used. Especially, the quantum-dot saturable absorbers turned out to be advantageous for the integration into the VECSEL structure [04Lor, 07Maa].

2.1.4.3.3.1 InGaAs/GaAs/AlGaAs semiconductor material system

This material is best-suited for the 800 nm–1.1 μm wavelength range because of the near-perfect lattice match between GaAs and AlGaAs. InGaAs saturable absorbers have been grown on AlAs/GaAs Bragg mirrors and have been the material of choice for SESAMs at an operation wavelength of ≈ 1 μm. However, thicker InGaAs saturable absorbers above the critical thickness had surface striations that introduced too much scattering losses to be used inside a laser [94Kel]. Low-temperature MBE growth (see more details in Sect. 2.1.4.3.2) resulted in strain-relaxed structures with surfaces that were optically flat, but with strongly increased defect densities. For SESAM applications this is actually advantageous, and has been exploited to optimize the dynamic response of the SESAM. InGaAs saturable absorbers on AlAs/GaAs Bragg mirrors have even been used at an operation wavelength of 1.3 μm [96Flu2, 97Flu] and 1.55 μm [03Spu, 04Zel]. However, these highly strained layers with high indium content exceed the critical thickness, and show significant nonsaturable losses due to strain and defect formation. Optimized low-temperature MBE growth, however, (Sect. 2.1.4.3.2) allowed improved InGaAs SESAMs to support stable mode-locking and Q-switching in diode-pumped solid-state lasers.

2.1.4.3.3.2 GaInAsP/InP semiconductor material system

This material system can be lattice-matched on the InP substrate but suffers from low refractive-index contrast and poor temperature characteristics. Due to the low refractive-index contrast, a high number of InP/GaInAsP mirror pairs are required to form Distributed Bragg Reflectors (DBRs). This demands very precise control of the growth to achieve DBRs with uniform and accurate layer thickness.

2.1.4.3.3.3 GaInNAs semiconductor material

Recently, dilute nitrides (i.e. GaInNAs) have attracted strong attention for laser devices in the telecommunication wavelength range between 1.3 μm and 1.55 μm that can use high-contrast GaAs/AlGaAs DBR mirrors [02Har, 02Rie]. Adding a few percent of nitrogen to InGaAs has two advantages: a redshift of the absorption wavelength and a reduction of the lattice mismatch to GaAs. The drawback is that the nitrogen incorporation decreases the crystalline quality, which is a big challenge for the fabrication of active devices. However, SESAMs are passive devices relying on fast defect-induced nonradiative carrier recombination to allow for short-pulse generation. GaInNAs saturable absorber on GaAs/AlsAs Bragg mirrors operating at 1.3 μm have been demonstrated for solid-state laser mode-locking. The first GaInNAs SESAM was reported to mode-lock a quasi-cw pumped Nd:YLF and Nd:YALO laser at 1.3 μm [02Sun]. Self-starting stable passive cw mode-locking of a solid-state laser with a GaInNAs SESAM was demonstrated more recently [04Liv]. A detailed study of the absorber properties and the mode-locking behavior revealed that GaInNAs SESAMs provide low saturation fluences and possess extremely low losses [04Liv, 04Sch2, 05Gra3]. These SESAMs supported mode-locking at repetition rates of 5 GHz and 10 GHz [05Spu2]. In 2003, GaInNAs SESAMs at 1.5 μm were shown to mode-lock Er-doped fiber lasers but had too much loss for solid-state lasers [03Okh]. Just recently for the first time successful mode-locking of a solid-state laser at 1.54 μm using a GaInNAs SESAM has been demonstrated [05Rut].

2.1.4.3.3.4 AlGaAsSb semiconductor material

Another interesting long-wavelength semiconductor saturable absorber material is based on antimonide. The quaternary alloy AlGaAsSb has a wide band-gap tunability (1.55 μm to 0.54 μm) and intrinsically low modulation depth [03Saa, 04Ost]. Similar to InGaAsP, AlGaAsSb is lattice-matched to InP, but its absorption edge is not as steep as the one of InGaAsP [87Ada]. Therefore, operating the absorber in the bandtail results in a sufficiently small modulation depth (i.e. usually below 0.5 %) suitable for high-repetition-rate lasers. An Sb-based SESAM can be grown by MOVPE with AlGaAsSb/InP DBRs [06Ost]. Compared to InGaAsP, AlGaAsSb forms a high refractive-index contrast with InP (0.4) allowing for a lower number of Bragg periods. The first antimonide SESAM self-started and mode-locked a 61-MHz Er:Yb:glass laser [04Gra]. More recently, this was extended to an Er:Yb:glass laser at 10 GHz, 1535 nm and with 4.7 ps pulse duration [06Gra].

2.1.4.3.3.5 GaAs wafer for ≈ 1 μm

Simple GaAs wafers have been used as saturable absorbers to mode-lock [04Kon] and Q-switch [00Li, 01Che1] solid-state lasers at a wavelength of ≈ 1 μm. Photo electrons in the conduction band are generated from mid-gap defect states (i.e. EL2) present in GaAs wafers. These EL2-defects have similar properties as the arsenic antiside point defects in LT-grown materials (Sect. 2.1.4.3.2). This transition, however, has a very high saturation fluence in the range of 1 mJ/cm^2 [06Li] which is typically about 100 times higher than the standard valence-to-conduction band transition generally used for SESAMs. This strongly increases the tendency for Q-switching instabilities (Sect. 2.1.6.8).

2.1.4.3.3.6 Semiconductor-doped dielectric films

Saturable absorbers based on semiconductor-doped dielectric films have been demonstrated [99Bil]. In this case, InAs-doped thin-film rf-sputtering technology was used which offers similar advantages as SESAMs, i.e. the integration of the absorber into a mirror structure. At this point, however,

the saturation fluence of ≈ 10 mJ/cm^2 is still rather high for stable solid-state laser mode-locking. In comparison, epitaxially grown SESAMs typically have a saturation fluence in the range of 10 μJ/cm^2 depending on the specific device structure.

2.1.4.3.4 Historical perspective and SESAM structure

Semiconductor saturable absorbers have been used as early as 1974 in CO_2 lasers [74Gib] and 1980 for semiconductor diode lasers [80Ipp]. A color-center laser was the first solid-state laser that was cw mode-locked with an intracavity semiconductor saturable absorber [89Isl]. However, for both the diode and color-center laser, dynamic gain saturation supported pulse formation and the recovery time of the slow saturable absorber was not relevant for pulse generation (Fig. 2.1.5a). In addition, because of the large gain cross section (i.e. approximately 10^{-14} cm^2 for diode lasers and 10^{-16} cm^2 for color-center lasers) Q-switching instabilities were not a problem. This is not the case for most other solid-state lasers, such as ion-doped solid-state lasers, which have typically 1000 or even more times smaller gain cross sections. Thus, the semiconductor saturable absorber parameters (Fig. 2.1.8 and Fig. 2.1.9) have to be chosen much more carefully for stable cw mode-locking.

We typically integrate the semiconductor saturable absorber into a mirror structure, which results in a device whose reflectivity increases as the incident optical intensity increases. This general class of devices is called SEmiconductor Saturable Absorber Mirrors (SESAMs) [92Kel2, 96Kel, 03Kel]. A detailed description and guideline how to design a SESAM for either passive mode-locking or Q-switching for different laser parameters is given in recent book chapters [99Kel, 03Pas]. SESAMs are well-established as a useful device for passive mode-locking and Q-switching of many kinds of solid-state lasers. The main reason for this device's utility is that both the linear and nonlinear optical properties can be engineered over a wide range, allowing for more freedom in the specific laser cavity design. In addition, semiconductor saturable absorbers are ideally suited for passive mode-locking solid-state lasers because the large absorber cross section (in the range of 10^{-14} cm^2) and therefore small saturation fluence is ideally suited for suppressing Q-switching instabilities [99Hoe1].

Initially, SESAMs for solid-state lasers were used in coupled cavities [90Kel2, 92Kel1], because these early SESAM designs introduced too much loss for the laser cavity (Fig. 2.1.12b). In 1992, this work resulted in a new type of intracavity saturable absorber mirror, the Antiresonant Fabry–Perot Saturable Absorber (A-FPSA) [92Kel2, 94Kel] where the absorber was integrated inside a Fabry–Perot structure of which the bottom reflector was a high reflector (i.e. approximately 100 %) (Fig. 2.1.12c). This was the first intracavity saturable absorber design that allowed for passive mode-locking of diode-pumped solid-state lasers without Q-switching instabilities. The Fabry–Perot was operated at antiresonance to obtain broad bandwidth and low loss. The A-FPSA mirror was mainly based on absorber layers sandwiched between the lower semiconductor and the higher SiO_2/TiO_2 dielectric Bragg mirrors. The top reflector of the A-FPSA provides an adjustable parameter that determines the intensity entering the semiconductor saturable absorber and therefore the saturation fluence of the saturable absorber device. Therefore, this design allowed for a large variation of absorber parameters by simply changing absorber thickness and top reflectors [95Bro1, 95Jun1]. This resulted in an even simpler SESAM design with a single quantum well absorber layer integrated into a Bragg mirror [95Bro2] (Fig. 2.1.12d) – this was later referred to as Saturable Bragg Reflectors (SBRs) [95Tsu].

In the 10-fs regime with Ti:sapphire lasers we have typically replaced the lower semiconductor Bragg mirror with a metal mirror to support the required large reflection bandwidth [96Flu1, 97Jun1]. No post-growth processing is required with an ultrabroadband monolithically grown fluoride semiconductor saturable absorber mirror that covers nearly the entire gain spectrum of the Ti:sapphire laser. Using this SESAM inside a Ti:sapphire laser resulted in 9.5-fs pulses [02Sch2]. The reflection bandwidth was achieved with a $AlGaAs/CaF_2$ semiconductor Bragg mirror [00Sch]. More recently a broadband SESAM was fabricated by increasing the reflection bandwidth

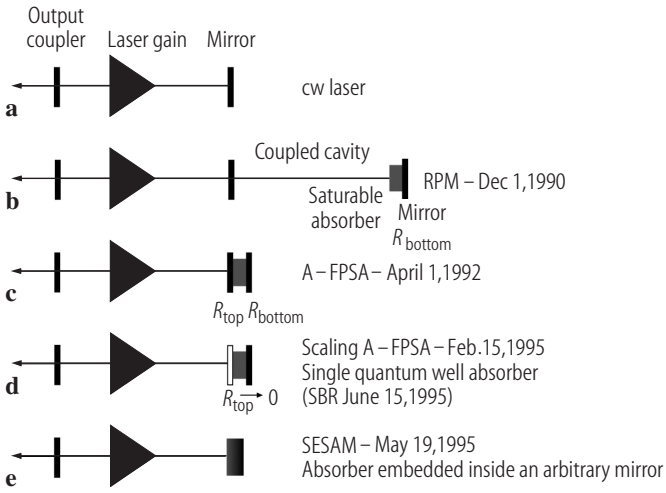

Fig. 2.1.12. Historical evolution of different SESAM designs: (**a**) Ordinary cw laser. (**b**) Initially the semiconductor saturable absorber was used inside a nonlinear coupled cavity, termed Resonant Passive Mode-locking (RPM) [90Kel2]. (**c**) First intracavity saturable absorber to passively mode-lock diode-pumped solid-state lasers without Q-switching instabilities: Antiresonant Fabry–Perot Saturable Absorber (A-FPSA) [92Kel2]. (**d**) Scaling of the A-FPSA resulted in a single quantum well saturable absorber integrated into a Bragg mirror [95Bro2] – later also referred to as Saturable Bragg Reflector (SBR) [95Tsu]. (**e**) General concept of SEmiconductor Saturable Absorber Mirror (SESAM) without any restrictions on the mirror design [95Kel, 96Kel].

of an AlGaAs/AlAs or InGaAlP/AlAs Bragg mirror using wet oxidation of AlAs which creates low-index Al_xO_y layers [04Tan].

In 1995 [95Kel] it was further realized that the intracavity saturable absorber can be integrated in a more general mirror structure that allows for both saturable absorption and negative dispersion control, which is now generally referred to as a SEmiconductor Saturable Absorber Mirror (SESAM) (Fig. 2.1.12e). In a general sense we then can reduce the design problem of a SESAM to the analysis of multilayered interference filters for a given desired nonlinear reflectivity response for both the amplitude and phase. The A-FPSA [92Kel2], the Saturable Bragg Reflector (SBR) [95Bro2, 95Tsu, 95Kno] and the Dispersive Saturable Absorber Mirror (D-SAM) [96Kop2] are then special examples of SESAM designs. In this more general class of design we do not restrict ourselves to Bragg mirror structures, which are defined by a stack of quarter-wave layers with alternating high and low refractive indices (e.g. [95Kno]). For example, we have demonstrated with many examples that non-quarter-wave layers in mirrors give more design freedom for integrating the absorber layers into the mirror structure. Furthermore, double-chirped semiconductor mirror structures can provide very broadband negative dispersion [99Pas1].

One important parameter of a SESAM device is its saturation fluence, which has typical values in the range of 10–100 $\mu J/cm^2$. Lower saturation fluence is particularly relevant for fundamentally mode-locked solid-state lasers with GHz pulse repetition rates and high average power [05Spu3]. Novel design structures allowed to substantially lower the saturation fluence of SESAMs into the 1 $\mu J/cm^2$ regime [05Spu3]. New terms "LOw-Field-Enhancement Resonant-like SESAM device" (LOFERS) [03Wei1] and "Enhanced SESAM device" (E-SESAM) [03Wei2] were introduced. A LOFERS can be used to further reduce saturation fluence without the detrimental effects of strongly resonant structures such as bistability and narrow bandwidth. Such a design has a low-finesse resonant structure such that the field strength is substantially higher in the spacer layer containing the absorber and therefore reducing the saturation fluence further.

So far the SESAM is mostly used as an end mirror of a standing-wave cavity. Very compact cavity designs have been achieved for example in passively Q-switched microchip lasers (Fig. 2.1.6)

and passively mode-locked miniature lasers (Fig. 2.1.7b) where a short laser crystal defines a simple monolithic cavity. The SESAM attached directly to the laser crystal then formed one end-mirror of this laser cavity. As the laser cannot be pumped through the SESAM, the laser output needs to be separated from the collinear pump by a dichroic mirror. These examples suggest that there is need for a device that combines the nonlinear properties of the SESAM with an output coupler. This has been demonstrated before for a passively mode-locked fiber laser [96Sha] and later also for solid-state lasers [01Spu1].

2.1.4.4 Effective saturable absorbers using the Kerr effect

2.1.4.4.1 Transverse and longitudinal Kerr effect

The extremely rapid response and the broad bandwidth of the Kerr nonlinearity are very attractive for a mode-locking process. For high intensities, the polarization inside a dielectric medium does not proportionally follow the electric field anymore. This gives rise to an index change proportional to intensity. Off-resonance, this nonlinear optical effect is extremely fast, with estimated response times in the few-femtosecond range. The transverse and longitudinal effects resulting from the intensity dependence are shown schematically in Fig. 2.1.13. The transverse Kerr effect retards the central and most intense part of a plane wave front and thus acts as a focusing lens, referred to as the Kerr lens. Along the axis of propagation, the longitudinal Kerr effect retards the center of an optical pulse, producing a red shift of the leading part of the pulse, and a blue shift in the trailing part. Consequently, the longitudinal Kerr effect has been named Self-Phase Modulation (SPM).

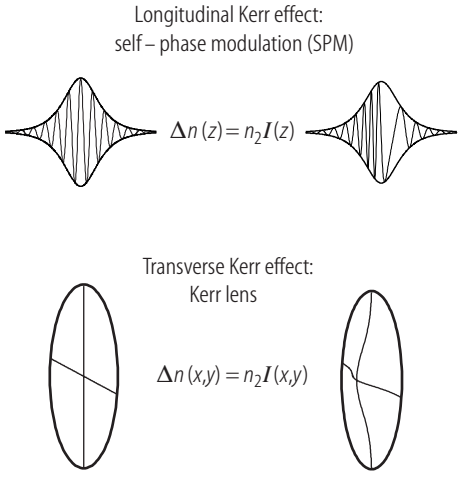

Fig. 2.1.13. The Kerr effect gives rise to an increase of the refractive index with intensity, causing a retardation of the most intense parts of a pulse (i.e. for $n_2 > 0$). In its longitudinal form, the Kerr effect causes Self-Phase Modulation (SPM) and in its transverse form, a nonlinear lens is formed in the central part of the beam profiles (i.e. Kerr lens).

2.1.4.4.2 Nonlinear coupled cavity

The longitudinal Kerr effect can also be used to produce the same effect as a fast saturable absorber. To do this, the phase nonlinearity provided by the longitudinal Kerr effect has to be converted into an effective amplitude nonlinearity. The earliest mode-locking schemes based only on SPM used a coupled cavity to convert SPM into SAM. In the soliton laser [84Mol], pulses compressed by SPM and anomalous dispersion in the coupled cavity are directly coupled back into the main laser cavity. This provides more gain for the center of the pulse. Pulses as short as 19 fs have been

demonstrated with color-center lasers [87Mit]. Later, the SPM-to-SAM conversion with a coupled cavity was demonstrated even when the pulses inside the coupled cavity were broadened due to positive group velocity dispersion [89Kea]. In this case, no compressed pulse was fed back into the main cavity. An effective SAM was obtained because SPM inside the coupled cavity generates a phase modulation on the pulse that adds constructively at the peak of the pulse in the main cavity and destructively in the wings, thus shortening the pulse duration inside the main cavity. This was also later referred to as Additive Pulse Mode-locking (APM) [89Ipp]. Although very powerful in principle, these coupled-cavity schemes have the severe disadvantage that the auxiliary cavity has to be stabilized interferometrically. An alternative method for converting the reactive Kerr nonlinearity into an effective saturable absorber was discovered in 1991: Kerr-Lens Mode-locking (KLM) [91Spe].

2.1.4.4.3 Kerr lens

The discovery of Kerr-lens mode-locking has been a breakthrough in ultrashort pulse generation [91Spe]. Initially the mode-locking mechanism was not understood and was somewhat of a mystery. But within a short time after the initial discovery it became clear that the transverse Kerr effect provides a fast saturable absorber. In KLM, the transverse Kerr effect produces a Kerr lens (Fig. 2.1.13) that focuses the high-intensity part of the beam more strongly than the low-intensity part. Thus, combined with an intracavity aperture the Kerr lens produces less loss for high intensity and forms an effective fast saturable absorber [91Kel, 91Sal1, 91Neg] (Fig. 2.1.14). A similar mode-locking effect can be obtained without a hard aperture when the Kerr lens produces an increased

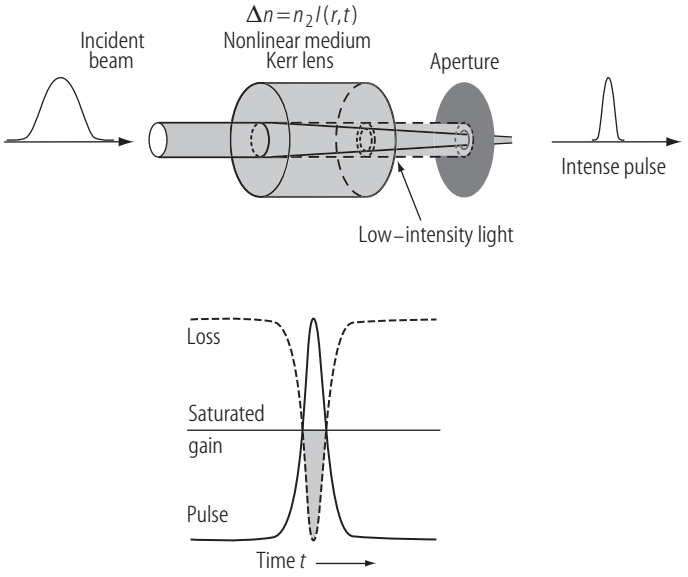

Fig. 2.1.14. Kerr-Lens Mode-locking (KLM) is obtained due to the Kerr lens at an intracavity focus in the gain medium or in another material, where the refractive index is increased with increased intensity $\Delta n = n_2 I(r,t)$, where n_2 is the nonlinear refractive index and $I(r,t)$ the radial- and time-dependent intensity of a short-pulsed laser beam. In combination with a hard aperture inside the cavity, the cavity design is made such that the Kerr lens reduces the laser mode area for high intensities at the aperture and therefore forms an effective fast saturable absorber. In most cases, however, soft-aperture KLM is used where the reduced mode area in the gain medium improves for a short time the overlap with the (strongly focused) pump beam and therefore the effective gain. A significant change in mode size is only achieved by operating the laser cavity near one of the stability limits of the cavity.

overlap of the laser mode with the pump profile in the gain medium [93Pic]. The Kerr lens provides the strongest advantage for the pulsed operation when the cavity is operated close to the stability limit. Optimization guidelines for SAM produced by the Kerr lens in different cavities can be found in [95Mag]. Unfortunately, the transverse Kerr effect couples the mode-locking process with the laser cavity mode. In contrast, the use of only the longitudinal Kerr effect in mode-locking totally decouples the mode-locking process from the laser mode. This allows optimum cavity design for scaling the laser to higher powers and to higher pulse repetition rates without being constrained by the Kerr lens.

2.1.4.4.4 Nonlinear polarization rotation

In fiber lasers a different Kerr-effect-based effective saturable absorber has been used to generate pulses as short as 38 fs [92Hof] – the shortest pulses generated directly from a fiber laser so far. An effective fast saturable absorber is obtained with a Kerr-induced nonlinear polarization rotation in a weakly birefringent fiber combined with a polarization-dependent loss. Previously, a similar idea has been used to "clean up" high-intensity pulses by reducing the low-intensity pulse pedestals [92Tap, 92Bea].

2.1.4.5 Nonlinear mirror based on second-harmonic generation

The second-order nonlinear susceptibility $\chi^{(2)}$ nonlinearities can also be used to construct effective saturable absorbers [88Sta]. A nonlinear mirror based on this principle consists of a frequency-doubling crystal and a dichroic mirror. For short pulses, a part of the incident laser light is converted to the second harmonic, for which the mirror is highly reflective, and converted back to the fundamental wave, if an appropriate relative phase shift for fundamental and second-harmonic light is applied. On the other hand, unconverted fundamental light experiences a significant loss at the mirror. Thus the device has a higher reflectivity at higher intensities. This has been used for mode-locking e.g. with up to 1.35 W of average output power in 7.9-ps pulses from a Nd^{3+}:YVO_4 laser [97Agn]. The achievable pulse duration is often limited by group-velocity mismatch between fundamental and second-harmonic light.

2.1.5 Pulse propagation in dispersive media

2.1.5.1 Dispersive pulse broadening

Dispersion compensation is important in ultrashort pulse generation. When a pulse travels through a medium, it acquires a frequency-dependent phase shift $\phi(\omega) = k\, n(\omega) L$, where k is the wave number, $n(\omega)$ the refractive index and L the medium length. A phase shift which varies linearly with the frequency corresponds to a time delay, without any change of the temporal shape of the pulse. Higher-order phase shifts, however, tend to modify the pulse shape and are thus of relevance for the formation of short pulses.

The phase shift can be expanded in a Taylor series around the center angular frequency ω_0 of the pulse:

$$\phi(\omega) = \phi_0 + \frac{\partial \phi}{\partial \omega}(\omega - \omega_0) + \frac{1}{2}\frac{\partial^2 \phi}{\partial \omega^2}(\omega - \omega_0)^2 + \frac{1}{6}\frac{\partial^3 \phi}{\partial \omega^3}(\omega - \omega_0)^3 + \ldots$$

Table 2.1.6. Sellmeier equations for different materials. The wavelength λ is given in units of μm.

Material	Defining Sellmeier equation	Constants
Fused quartz	$n^2 = 1 + \frac{A\lambda^2}{\lambda^2 - \lambda_1^2} + \frac{B\lambda^2}{\lambda^2 - \lambda_2^2} + \frac{C\lambda^2}{\lambda^2 - \lambda_3^2}$	$A = 0.6961663$ $\lambda_1 = 0.0684043$ $B = 0.4079426$ $\lambda_2 = 0.1162414$ $C = 0.8974794$ $\lambda_3 = 9.896161$
SF10 glass	$n^2 = a_0 + a_1\lambda^2 + \frac{a_2}{\lambda^2} + \frac{a_3}{\lambda^4} + \frac{a_4}{\lambda^6} + \frac{a_5}{\lambda^8}$	$a_0 = 2.8784725$ $a_1 = -0.010565453$ $a_2 = 3.327942 \times 10^{-2}$ $a_3 = 2.0551378 \times 10^{-3}$ $a_4 = -1.1396226 \times 10^{-4}$ $a_5 = 1.6340021 \times 10^{-5}$
Sapphire	$n^2 = 1 + \frac{a_1\lambda^2}{\lambda^2 - b_1} + \frac{a_2\lambda^2}{\lambda^2 - b_2} + \frac{a_3\lambda^2}{\lambda^2 - b_3}$	$a_1 = 1.023798$ $a_2 = 1.058264$ $a_3 = 5.280792$ $b_1 = 0.00377588$ $b_2 = 0.0122544$ $b_3 = 321.3616$

Here, the derivatives are evaluated at ω_0. $\partial\phi/\partial\omega$ is the group delay T_g, $\partial^2\phi/\partial\omega^2$ the Group Delay Dispersion (GDD), $\partial^3\phi/\partial\omega^3$ the Third-Order Dispersion (TOD). The GDD describes a linear frequency dependence of the group delay and thus tends to separate the frequency components of a pulse: For positive GDD, e.g., the components with higher frequencies are delayed with respect to those with lower frequencies, which results in a positive "chirp" ("up-chirp") of the pulse. Higher orders of dispersion generate more complicated distortions. Material dispersion is normally described with Sellmeier equations for the refractive index as a function of the wavelength, i.e. $n(\lambda)$. With the Sellmeier equations (Table 2.1.6) all the necessary dispersive quantities can be calculated (Table 2.1.7). An example is given in Table 2.1.8.

The broader the bandwidth of the pulse (i.e., the shorter the pulse duration), the more terms of this expansion are significant. GDD which acts on an initially unchirped Gaussian pulse with Full-Width-at-Half-Maximum (FWHM) pulse duration τ_0, increases the pulse duration according to [86Sie]

$$\frac{\tau_p(z)}{\tau_0} = \sqrt{1 + \left(\frac{4\ln 2\, d^2\phi/d\omega^2}{\tau_0^2}\right)^2}\,, \tag{2.1.20}$$

where it is assumed that the incident pulse is transform-limited, i.e. the time–bandwidth product of the Gaussian pulse is $\tau_0 \Delta\nu_p = 0.4413$, where $\Delta\nu_p$ is the Full-Width-at-Half-Maximum (FWHM) spectral width of the pulse intensity (Fig. 2.1.15). Only second-order dispersion (i.e. $\partial^2\phi/\partial\omega^2$) and higher orders are broadening the pulse. The first-order dispersion gives the group delay, i.e. the delay of the peak of the pulse envelope. It is apparent that the effect of GDD becomes strong if GDD $> \tau_0^2$. Similarly, TOD becomes important if TOD $> \tau_0^3$. It is important to note that for dispersive pulse broadening (which is in the linear pulse propagation regime) the spectrum of the pulse remains unchanged, only the spectral content of the pulse is redistributed in time. With positive dispersion the long-wavelength part of the spectrum is in the leading edge of the pulse and the short-wavelength part in the trailing edge of the pulse, i.e. "red is faster than blue" (Fig. 2.1.15). In the regime of strong pulse broadening, i.e. $d^2\phi/d\omega^2 \gg \tau_0^2$, we can reduce (2.1.20)

Table 2.1.7. Dispersion quantities, their defining equations and units. k_n: wave vector in the dispersive media, i.e. $k_n = k\,n = n\,2\,\pi/\lambda$, where λ is the vacuum wavelength. z: a certain propagation distance. c: vacuum light velocity. ω: frequency in radians/second.

Quantity	Symbol	Defining equation	Defining equation using $n\,(\lambda)$
Phase velocity	v_p	$\dfrac{\omega}{k_n}$	$\dfrac{c}{n}$
Group velocity	v_g	$\dfrac{\mathrm{d}\omega}{\mathrm{d}k_n}$	$\dfrac{c}{n}\dfrac{1}{1-\dfrac{\mathrm{d}n}{\mathrm{d}\lambda}\dfrac{\lambda}{n}}$
Group delay	T_g	$T_\mathrm{g} = \dfrac{z}{v_\mathrm{g}} = \dfrac{\mathrm{d}\phi}{\mathrm{d}\omega}\,,\ \ \phi \equiv k_n z$	$\dfrac{nz}{c}\left(1-\dfrac{\mathrm{d}n}{\mathrm{d}\lambda}\dfrac{\lambda}{n}\right)$
Dispersion: 1st order		$\dfrac{\mathrm{d}\phi}{\mathrm{d}\omega}$	$\dfrac{nz}{c}\left(1-\dfrac{\mathrm{d}n}{\mathrm{d}\lambda}\dfrac{\lambda}{n}\right)$
Dispersion: 2nd order		$\dfrac{\mathrm{d}^2\phi}{\mathrm{d}\omega^2}$	$\dfrac{\lambda^3 z}{2\,\pi\,c^2}\dfrac{\mathrm{d}^2 n}{\mathrm{d}\lambda^2}$
Dispersion: 3rd order		$\dfrac{\mathrm{d}^3\phi}{\mathrm{d}\omega^3}$	$\dfrac{-\lambda^4 z}{4\,\pi^2 c^3}\left(3\dfrac{\mathrm{d}^2 n}{\mathrm{d}\lambda^2}+\lambda\dfrac{\mathrm{d}^3 n}{\mathrm{d}\lambda^3}\right)$

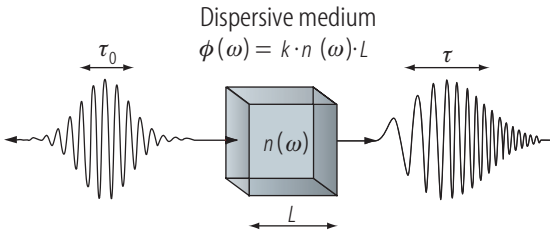

Fig. 2.1.15. Dispersive pulse broadening through a material with positive dispersion.

to

$$\tau_\mathrm{p}\,(z) \approx \frac{\mathrm{d}^2\phi}{\mathrm{d}\,\omega^2}\,\Delta\,\omega_\mathrm{p}\,, \tag{2.1.21}$$

where $\Delta\,\omega_\mathrm{p} = 2\pi\,\Delta\,\nu_\mathrm{p}$ is the FWHM spectral width (in radians/second) of the pulse intensity.

2.1.5.2 Dispersion compensation

Without any dispersion compensation the net GDD for one cavity round trip is usually positive, mainly because of the dispersion in the gain medium. Other components like mirrors may also contribute to this. However, in lasers with > 10 ps pulse duration the dispersion effects can often be ignored, as the total GDD in the laser cavity is typically at most a few thousand fs^2, much less than the pulse duration squared (2.1.20). For shorter pulse durations, the GDD has to be considered, and pulse durations well below 30 fs usually require the compensation of Third-Order Dispersion (TOD) or even higher orders of dispersion depending on the thickness of the gain material. In most cases, the desired total GDD is not zero but negative, so that soliton formation

Table 2.1.8. Examples of material dispersions calculated from the Sellmeier equations given in Table 2.1.6 and the equations given in Table 2.1.7.

Material	Refractive index n at a center wavelength of 800 nm	Propagation constant k_n at a center wavelength of 800 nm
Fused quartz	$n\,(0.8\ \mu\text{m}) = 1.45332$	
	$\left.\frac{\partial n}{\partial \lambda}\right\|_{800\ \text{nm}} = -0.017\ \frac{1}{\mu\text{m}}$	$\left.\frac{\partial k_n}{\partial \omega}\right\|_{800\ \text{nm}} = 4.84 \times 10^{-9}\ \frac{\text{s}}{\text{m}} = 4.84\ \frac{\text{ns}}{\text{m}}$
	$\left.\frac{\partial^2 n}{\partial \lambda^2}\right\|_{800\ \text{nm}} = 0.04\ \frac{1}{\mu\text{m}^2}$	$\left.\frac{\partial^2 k_n}{\partial \omega^2}\right\|_{800\ \text{nm}} = 3.61 \times 10^{-26}\ \frac{\text{s}^2}{\text{m}} = 36.1\ \frac{\text{fs}^2}{\text{mm}}$
	$\left.\frac{\partial^3 n}{\partial \lambda^3}\right\|_{800\ \text{nm}} = -0.24\ \frac{1}{\mu\text{m}^3}$	$\left.\frac{\partial^3 k_n}{\partial \omega^3}\right\|_{800\ \text{nm}} = 2.74 \times 10^{-41}\ \frac{\text{s}^3}{\text{m}} = 27.4\ \frac{\text{fs}^3}{\text{mm}}$
SF10 glass	$n\,(0.8\ \mu\text{m}) = 1.71125$	
	$\left.\frac{\partial n}{\partial \lambda}\right\|_{800\ \text{nm}} = -0.0496\ \frac{1}{\mu\text{m}}$	$\left.\frac{\partial k_n}{\partial \omega}\right\|_{800\ \text{nm}} = 5.70 \times 10^{-9}\ \frac{\text{s}}{\text{m}} = 5.70\ \frac{\text{ns}}{\text{m}}$
	$\left.\frac{\partial^2 n}{\partial \lambda^2}\right\|_{800\ \text{nm}} = 0.176\ \frac{1}{\mu\text{m}^2}$	$\left.\frac{\partial^2 k_n}{\partial \omega^2}\right\|_{800\ \text{nm}} = 1.59 \times 10^{-25}\ \frac{\text{s}^2}{\text{m}} = 159\ \frac{\text{fs}^2}{\text{mm}}$
	$\left.\frac{\partial^3 n}{\partial \lambda^3}\right\|_{800\ \text{nm}} = -0.997\ \frac{1}{\mu\text{m}^3}$	$\left.\frac{\partial^3 k_n}{\partial \omega^3}\right\|_{800\ \text{nm}} = 1.04 \times 10^{-40}\ \frac{\text{s}^3}{\text{m}} = 104\ \frac{\text{fs}^3}{\text{mm}}$
Sapphire	$n\,(0.8\ \mu\text{m}) = 1.76019$	
	$\left.\frac{\partial n}{\partial \lambda}\right\|_{800\ \text{nm}} = -0.0268\ \frac{1}{\mu\text{m}}$	$\left.\frac{\partial k_n}{\partial \omega}\right\|_{800\ \text{nm}} = 5.87 \times 10^{-9}\ \frac{\text{s}}{\text{m}} = 5.87\ \frac{\text{ns}}{\text{m}}$
	$\left.\frac{\partial^2 n}{\partial \lambda^2}\right\|_{800\ \text{nm}} = 0.064\ \frac{1}{\mu\text{m}^2}$	$\left.\frac{\partial^2 k_n}{\partial \omega^2}\right\|_{800\ \text{nm}} = 5.80 \times 10^{-26}\ \frac{\text{s}^2}{\text{m}} = 58\ \frac{\text{fs}^2}{\text{mm}}$
	$\left.\frac{\partial^3 n}{\partial \lambda^3}\right\|_{800\ \text{nm}} = -0.377\ \frac{1}{\mu\text{m}^3}$	$\left.\frac{\partial^3 k_n}{\partial \omega^3}\right\|_{800\ \text{nm}} = 4.21 \times 10^{-41}\ \frac{\text{s}^3}{\text{m}} = 42.1\ \frac{\text{fs}^3}{\text{mm}}$

can be exploited. Usually, one requires sources of negative GDD, and in addition appropriate higher-order dispersion for shorter pulses. The most important techniques for dispersion compensation are discussed in the following subsections. Different optical elements that introduce wavelength-dependent refraction (i.e. prism pairs, Sect. 2.1.5.2.3) or wavelength-dependent diffraction (i.e. grating pairs, Sect. 2.1.5.2.2) can be used to introduce an additional wavelength dependence to the round-trip phase and thus contribute to the overall dispersion. A wavelength-dependent round-trip phase can also be introduced with GTIs (Sect. 2.1.5.2.1) and chirped mirrors (Sect. 2.1.5.2.4).

The challenge in ultrashort pulse generation is dispersion compensation over a large bandwidth to compensate for the dispersive pulse broadening that is occurring in the gain material and other elements inside the laser cavity. Dispersion compensation is important because for example, a 10-fs (1-fs) Gaussian pulse at the center wavelength of 800 nm is broadened to 100 fs (1 ps) after only 1 cm of fused quartz due to second-order dispersion. This follows from (2.1.21) for the regime of strong pulse broadening and Tables 2.1.6–2.1.8. In addition, in femtosecond lasers the pulses are ideally soliton pulses for which a constant negative dispersion over the full spectral width of the pulse balances the chirp of the self-phase modulation. The necessary negative dispersion required for a certain pulse duration follows from (2.1.74). It is required that all higher-order dispersion terms are negligibly small.

For optimum soliton formation of a sub-10-fs pulse inside the laser, only a very small amount of a constant negative total intracavity dispersion is necessary to form a stable soliton pulse (2.1.74). For example, we estimated the necessary dispersion to be only -10 fs^2 for a Ti:sapphire laser producing 6.5-fs pulses [97Jun3, 98Sut]. Here we assumed an estimated self-phase modulation coefficient of about 0.07/MW, an average output power of 200 mW using a 3 % output coupler and a pulse repetition rate of 86 MHz. This results in an intracavity pulse energy of 77.5 nJ. With (2.1.74) then follows an estimated negative group delay dispersion of -10 fs^2 in a cavity round trip.

There are different methods for dispersion compensation, such as the Gires–Tournois Interferometer (GTI), grating pairs, prism pairs and chirped mirrors. The dispersion compensation is summarized in Table 2.1.9 with the symbols defined in Fig. 2.1.16.

2.1.5.2.1 Gires–Tournois interferometer (GTI)

A Gires–Tournois Interferometer (GTI) [64Gir, 92Kaf] is a very compact dispersion-compensation element, which basically replaces one flat laser cavity mirror. The negative dispersion is obtained due to the Fabry–Perot interferometer, operated in reflection (Fig. 2.1.16a). Normally, in a GTI the rear mirror is highly reflective over the whole wavelength range (i.e. ideally 100 %) whereas the front mirror has a relatively low reflectivity, typically a few percent. The spacer layer in the Fabry–Perot should contain a non-absorbing material and is very often air, such that the thickness can be easily changed. The phase shift varies nonlinearly by 2π for each free spectral range, calculated as $\Delta\nu = c/2nd$, where n and d are the refractive index and the thickness of the spacer material, respectively. Within each free spectral range, the GDD oscillates between two extremes the magnitude of which is proportional to d^2 and also depends on the front-mirror reflectivity. Ideally, the GTI is operated near a minimum of the GDD, and the usable bandwidth is some fraction (e.g. one tenth) of the free spectral range, which is proportional to d^{-1}:

$$\frac{\mathrm{d}^2\phi}{\mathrm{d}\omega^2} \propto d^2 \;, \quad \left\{\text{Bandwidth of } \frac{\mathrm{d}^2\phi}{\mathrm{d}\omega^2}\right\} \propto \frac{1}{d} \;. \tag{2.1.22}$$

In Table 2.1.9 the material dispersion in the GTI spacer layer was neglected. The bandwidth compared to the other techniques is limited, thus a GTI is typically used for pulse durations above 100 fs. There is a trade-off: A broader bandwidth is obtained with a smaller Fabry–Perot thickness but then the amount of negative dispersion is strongly reduced. For example, an air-spaced GTI with 80 μm thickness and a top reflectivity of 4 % produces a negative dispersion of about -0.13 ps^2 at a wavelength of 799 nm. In comparison a 2.25 μm thick air space results in about -100 fs^2 at a wavelength of 870 nm.

Tunable GDD can be achieved if the spacer material is a variable air gap, which however must be carefully stabilized to avoid unwanted drifts. More stable but not tunable GDD can be generated with monolithic designs, based e.g. on thin films of dielectric media like TiO_2 and SiO_2, particularly for the use in femtosecond lasers. The main drawbacks of GTI are the fundamentally limited bandwidth (for a given amount of GDD) and the limited amount of control of higher-order dispersion.

2.1.5.2.2 Grating pairs

Grating pairs [69Tre] produce negative dispersion due to the wavelength-dependent diffraction (Fig. 2.1.16b). To obtain a spatially coherent beam two paths through the grating pair are required. Compared to prism pairs (Sect. 2.1.5.2.3), pairs of diffraction gratings can generate higher dispersion in a compact setup. However, because of the limited diffraction efficiency of gratings, the losses of a grating pair are typically higher than acceptable for use in a laser cavity, except in

Table 2.1.9. Dispersion compensation, its defining equations and figures. c: light velocity in vacuum, λ: wavelength in vacuum, λ_0: center wavelength of pulse spectrum, ω: frequency in radians/second.

Quantity	Defining equation
Gires–Tournois Interferometer (GTI) (Fig. 2.1.16a)	d: thickness of Fabry–Perot n: refractive index of material inside Fabry–Perot (airspaced $n = 1$) (Note: Material dispersion is neglected.) $t_0 = \dfrac{2nd}{c}$: round-trip time of the Fabry–Perot R_t: intensity reflectivity of top reflector of Fabry–Perot (Bottom reflector is assumed to have a 100%-reflectivity.)
Dispersion: 2nd order	$\dfrac{\mathrm{d}^2\phi}{\mathrm{d}\omega^2} = \dfrac{-2t_0^2\,(1-R_\mathrm{t})\,\sqrt{R_\mathrm{t}}\sin\omega t_0}{\left(1+R_\mathrm{t}-2\sqrt{R_\mathrm{t}}\cos\omega t_0\right)^2}$
Four-grating compressor (Fig. 2.1.16b)	L_g: grating pair spacing Λ: grating period θ_i: angle of incidence at grating
Dispersion: 2nd order	$\dfrac{\mathrm{d}^2\phi}{\mathrm{d}\omega^2} = -\dfrac{\lambda^3 L_\mathrm{g}}{\pi c^2 \Lambda^2}\left[1-\left(\dfrac{\lambda}{\Lambda}-\sin\theta_\mathrm{i}\right)^2\right]^{-3/2}$
Dispersion: 3rd order	$\dfrac{\mathrm{d}^3\phi}{\mathrm{d}\omega^3} = -\dfrac{\mathrm{d}^2\phi}{\mathrm{d}\omega^2}\,\dfrac{6\pi\lambda}{c}\,\dfrac{1+\dfrac{\lambda}{\Lambda}\sin\theta_\mathrm{i}-\sin^2\theta_\mathrm{i}}{1-\left(\dfrac{\lambda}{\Lambda}-\sin\theta_\mathrm{i}\right)^2}$
Four-prism compressor (Fig. 2.1.16c)	n: refractive index of prisms θ_B: angle of incidence of prism is at Brewster angle $\theta_\mathrm{B} = \arctan\left[n\left(\lambda_0\right)\right]$ $\alpha = \pi - 2\theta_\mathrm{B}$: apex angle of prism $\theta_2\left(\lambda\right) = \arcsin\left[n\left(\lambda\right)\sin\left(\pi - 2\theta_\mathrm{B} - \arcsin\dfrac{\sin\theta_\mathrm{B}}{n\left(\lambda\right)}\right)\right]$ L: apex-to-apex prism distance h: beam insertion into second prism $\sin\beta = \dfrac{h}{L}\,\dfrac{\cos\theta_2}{\cos\left(\alpha/2\right)}$
Dispersion: 2nd order	$\dfrac{\mathrm{d}^2\phi}{\mathrm{d}\omega^2} = \dfrac{\lambda^3}{2\pi c^2}\dfrac{\mathrm{d}^2 P}{\mathrm{d}\lambda^2}$ $\dfrac{\mathrm{d}^2 P}{\mathrm{d}\lambda^2} = 2\left[\dfrac{\partial^2 n}{\partial\lambda^2}\left(\dfrac{\partial\theta_2}{\partial n}\right)+\left(\dfrac{\partial^2\theta_2}{\partial n^2}\right)\left(\dfrac{\partial n}{\partial\lambda}\right)^2\right]L\sin\beta - 2\left(\dfrac{\partial\theta_2}{\partial n}\dfrac{\partial n}{\partial\lambda}\right)^2 L\cos\beta$ $\approx 4\left[\dfrac{\partial^2 n}{\partial\lambda^2}+\left(2n-\dfrac{1}{n^3}\right)\left(\dfrac{\partial n}{\partial\lambda}\right)^2\right]L\sin\beta - 8\left(\dfrac{\partial n}{\partial\lambda}\right)^2 L\cos\beta$
Dispersion: 3rd order	$\dfrac{\mathrm{d}^3\phi}{\mathrm{d}\omega^3} = \dfrac{-\lambda^4}{4\pi^2 c^3}\left(3\dfrac{\mathrm{d}^2 P}{\mathrm{d}\lambda^2}+\lambda\dfrac{\mathrm{d}^3 P}{\mathrm{d}\lambda^3}\right)$ $\dfrac{\mathrm{d}^3 P}{\mathrm{d}\lambda^3} \approx 4\,\dfrac{\mathrm{d}^3 n}{\mathrm{d}\lambda^3}\,L\sin\beta - 24\,\dfrac{\mathrm{d}n}{\mathrm{d}\lambda}\dfrac{\mathrm{d}^2 n}{\mathrm{d}\lambda^2}\,L\cos\beta$

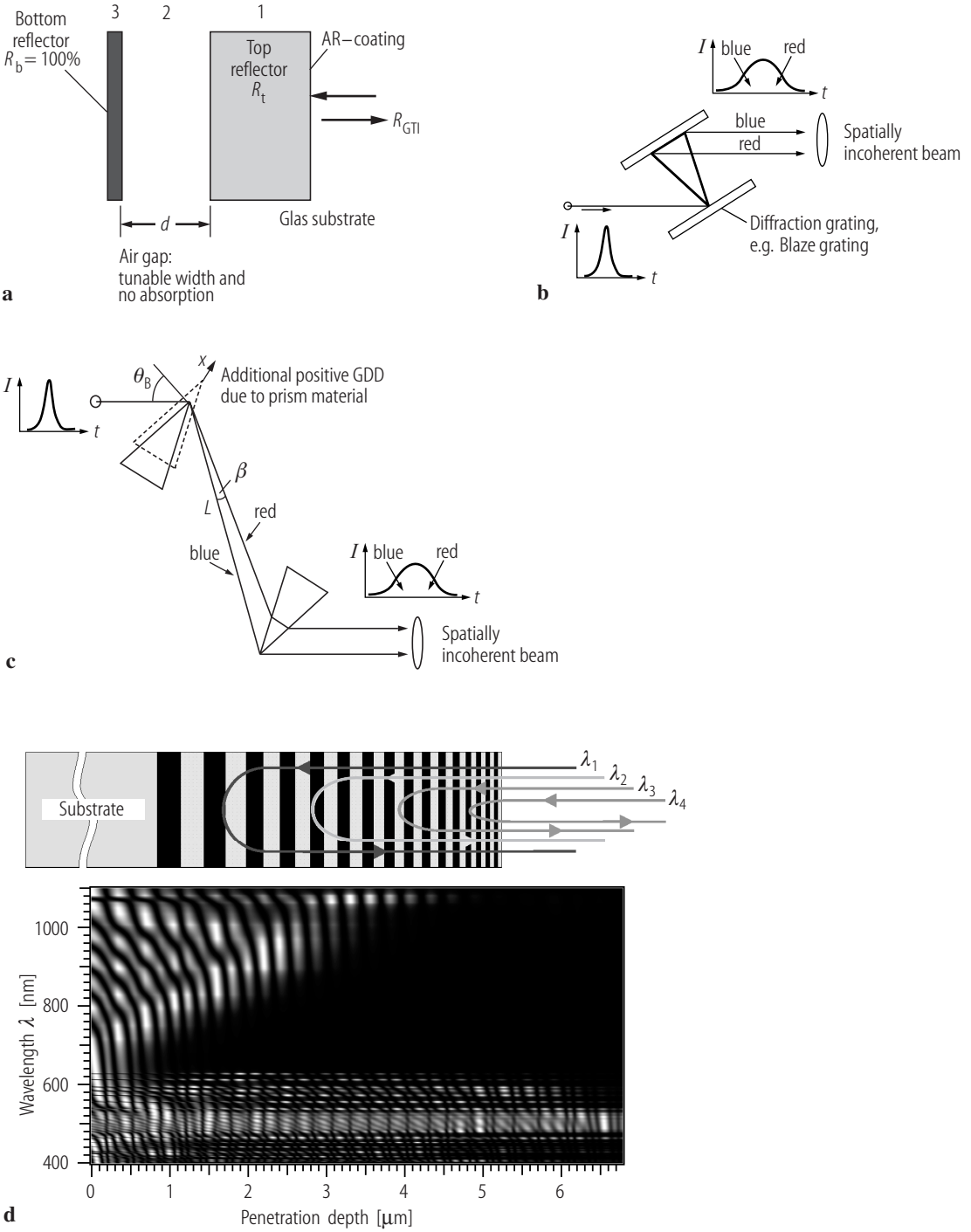

Fig. 2.1.16. Dispersion compensation techniques: (**a**) Gires–Tournois Interferometer (GTI), (**b**) grating pair, (**c**) prism pair, (**d**) chirped mirror (i.e. shown here: a double-chirped mirror).

cases with a high gain (e.g., in fiber lasers). For this reason, grating pairs are normally only used for external pulse compression [84Tom]. The grating pairs alone can only be used to compensate for second-order dispersion. Higher-order dispersion limits pulse compression in the ultrashort pulse width regime. Therefore, a combination of a grating and prism compressor was used to generate the long-standing world record of 6-fs pulses with dye lasers [87For].

There are mainly two types of gratings: ruled or holographic. Removing material from a master substrate with a precise instrument called a ruling engine produces ruled gratings. Replicas of the ruled grating are then pressed and the pressings are coated. Holographic gratings are produced by interfering two laser beams on a substrate coated with a photoresist, which is subsequently processed to reproduce the sinusoidal interference pattern. Generally, replicas cannot be produced from holographic masters, i.e. they are more expensive. Higher damage threshold can be obtained with gold-coated ruled gratings (i.e. > 500 mJ/cm^2 at 1 ps). The diffraction efficiency in this case is around 88 % to 92 % depending on the grating. Because four paths through the gratings are required for dispersion compensation and a spatially coherent beam, this amounts to at least about 30 % loss.

2.1.5.2.3 Prism pairs

Prism pairs [84For] are well established for intracavity dispersion compensation. Negative dispersion is obtained with the wavelength-dependent refraction (Fig. 2.1.16c): The different wavelength components travel in different directions after the first prism and along parallel but separated paths after the second prism. The wavelength components can be recombined simply on the way back after reflection at a plane end mirror (of a standing-wave cavity) or by a second prism pair (in a ring cavity). Spatial separation of different wavelengths occurs only in a part of the cavity. The obtained negative GDD from the geometric effect is proportional to the prism separation, and an additional (usually positive) GDD contribution results from the propagation in the prism material. Thus, to obtain a spatially coherent beam two paths through the prism pair are required. The insertion loss is very small because the angle of incidence is at Brewster angle. The prism apex angle is chosen such that the incident beam at Brewster angle is also at the minimum deviation. Prism pairs offer two advantages. First, the pulse width can be varied by simply moving one of the prisms which adjusts the prism insertion and therefore the amount of positive GDD from the propagation in the prism material (see Fig. 2.1.16c). Second, the laser can be tuned in wavelength by simply moving a knife edge at a position where the beam is spectrally broadened. Both properties are often desired for spectroscopic applications, for example. However, the prism pair suffers from higher-order dispersion, which is the main limitation in ultrashort pulse generation in the sub-10-fs regime. Different prism materials introduce different amounts of higher-order dispersion. For compact lasers with pulse durations of few tens to hundreds of femtoseconds the more dispersive SF10-prisms are better because they require a smaller prism separation than fused quartz prism for example. But the smaller prism separation comes at the expense of a larger higher-order dispersion. Fused quartz is one of the best materials for ultrashort pulse generation with minimal higher-order dispersion. The higher-order dispersion of the prism pairs is dominated by the prism spacing, which is not changed significantly when we adjust the dispersion by inserting the prisms into the laser beam.

More compact geometries for dispersion compensation make use of a single prism only [94Ram, 96Kop1]. In this case, the wavelength components are spatially separated in the whole resonator, not only in a part of it. Even without any additional prisms, refraction at a Brewster interface of the gain medium can generate negative dispersion. In certain configurations, where the cavity is operated near a stability limit, the refraction effect can be strongly increased [99Pas2], so that significant negative GDD can be generated in a compact cavity. The amount of GDD may then also strongly depend on the thermal lens in the gain medium and on certain cavity dimensions.

For example, at a fused quartz prism spacing of 40 cm, the total dispersion that is produced by a double pass through the prism pairs amounts to -862 fs^2 and a third-order dispersion of -970 fs^3 at a center wavelength of 800 nm, assuming zero prism insertion into the beam (Table 2.1.9). We can reduce the negative dispersion by moving the prisms into the laser beam: Each additional millimeter of prism insertion produces a positive dispersion of 101 fs^2 but only a third-order dispersion of 78 fs^3 per cavity round trip. Thus, the prism pairs can generally only be used to compensate for either second- or third-order dispersion. With fused quartz prisms alone pulses as short as 10 fs can be produced with a Ti:sapphire laser [93Asa, 96Flu1]. Slightly shorter pulses can be achieved if the Ti:sapphire laser is operated at a center wavelength of approximately 850 nm, where near-zero second- and third-order dispersion can be obtained for a Ti:sapphire crystal of about 2 mm thickness. In this case 8.5 fs have been generated [94Zho]. Another dispersion compensation is then required for shorter pulse generation. Therefore, the chirped mirrors were designed to show the inverse higher-order group delay dispersion of the dispersion of the prism pair plus laser crystal to eliminate the higher-order dispersion and obtain a slightly negative but constant group delay dispersion required for an ideal soliton pulse.

2.1.5.2.4 Chirped mirrors

Dielectric Bragg mirrors with regular quarter-wave layer stacks have a fairly small dispersion when operated well within their reflection bandwidth, but increasing dispersion at the edges of this range. Modified designs can be used to obtain well-controlled dispersion over a large wavelength range. One possibility already discussed is the use of a GTI structure (see Sect. 2.1.5.2.1). Another broad range of designs is based on the concept of the chirped mirrors [94Szi] (Fig. 2.1.16d): If the Bragg wavelength is appropriately varied within a Bragg mirror design, longer wavelengths can be reflected deeper in the mirror structure, thus acquire a larger phase change, which leads to negative dispersion. However, the straight-forward implementation of this idea leads to strong oscillations of the GDD (as a function of frequency) which render such simple designs useless. These oscillations can be greatly reduced by numerical optimizations which introduce complicated (and not analytically explainable) deviations from the simple chirp law. A great difficulty is that the figure of merit to optimize is a complicated function of many layer thickness variables, which typically has a large number of local maxima and minima and thus is quite difficult to optimize. Nevertheless, refined computing algorithms have lead to designs with respectable performance, which were realized with precision growth of dielectric mirrors. Such mirrors can compensate the dispersion in Ti^{3+}:sapphire lasers for operation with pulse durations well below 10 fs. Figure 2.1.16d shows a typical chirped mirror structure which schematically shows the path of a long-wavelength (i.e. 1000 nm) and short-wavelength (i.e. 650 nm) beam. This results in negative dispersion, because the long wavelengths are made to penetrate deeper into the mirror structure than short wavelengths. Figure 2.1.16d also shows the standing-wave electric field patterns in a chirped mirror structure versus wavelength. The negative dispersion of the mirrors is clearly illustrated by the dependence of penetration depth on wavelength for the range of 650 to 1050 nm. The highly transmissive region around 500 nm is used for pumping the Ti:sapphire laser through these chirped mirrors. According to [94Szi], chirping means that the Bragg wavelength λ_B is gradually increased along the mirror, producing a negative Group Delay Dispersion (GDD). However, no analytical explanation of the unwanted oscillations typically observed in the group delay and GDD of such a simple-chirped mirror was given. These oscillations were minimized purely by computer optimization.

The original chirped mirror design was further refined by the Double-Chirped Mirror (DCM) [97Kae, 99Mat] concept which takes into account the impedance matching problem which occurs at the air–mirror interface and the grating structure in the mirror. An exact coupled-mode analysis [97Mat] was used to develop a double-chirp technique. The impedance matching concept allowed a much better insight to the design limitations and allowed for the first time for an analytical design with custom-tailored dispersion characteristics which required only minor numerical optimization

[99Mat]. The strong periodic variation in the group delay of the original chirped mirrors occurs due to impedance mismatch between the incident medium (i.e. typically air) and the mirror stack and also within the mirror stack. Using the accurate analytical expressions for phase, group delay, and GDD [99Mat], DCMs could be designed and fabricated with a smooth and custom-tailored GDD suitable for generating pulses in the two-cycle regime directly from a Ti:sapphire laser [99Sut, 99Mor1, 99Mor2].

A Double-Chirped Mirror (DCM) [97Kae, 99Mat] is a multilayer interference coating that can be considered as a composition of at least two sections, each with a different task. The layer materials are typically SiO_2 and TiO_2. The first section is the AR coating, typically composed of 10 to 14 layers. It is necessary because the theory is derived assuming an ideal matching to air. The other section represents the actual DCM structure, as derived from theory. The double-chirp section is responsible for the elimination of the oscillations in the GDD from within the mirror stack. Double-chirping means that in addition to the local Bragg wavelength λ_B the local coupling of the incident wave to the reflected wave is independently chirped as well. The local coupling is adjusted by slowly increasing the high-index layer thickness in every pair so that the total optical thickness remains $\lambda_B/2$. This corresponds to an adiabatic matching of the impedance. The AR-coating, together with the rest of the mirror, is used as a starting design for a numerical optimization program. Since theoretical design is close to the desired design goal, a local optimization using a standard gradient algorithm is sufficient. At this point, only the broadband AR-coating sets a limitation on the reduction of the GDD oscillations. An AR-coating with a residual reflectivity of less than 10^{-4} is required for a DCM at a center wavelength of around 800 nm, which results in a bandwidth of only 250 nm [00Mat]. This bandwidth limitation cannot be removed with more layers in the mirror structure [96Dob].

The invention of the BAck-SIde-Coated (BASIC) mirrors [00Mat] or later the tilted front-side mirrors [01Tem] resolved this issue. In the BASIC mirror the ideal DCM structure is matched to the low-index material of the mirror which ideally matches the mirror substrate material. This DCM structure is deposited on the back of the substrate and the AR-coating is deposited on the front of the slightly wedged or curved substrate, so that the residual reflection is directed out of the beam and does not deteriorate the dispersion properties of the DCM structure on the other side of the substrate. Thus, the purpose of the AR-coating is only to reduce the insertion losses of the mirror at the air–substrate interface. For most applications it is sufficient to get this losses as low as 0.5 %. Therefore, the bandwidth of such an AR-coating can be much broader. Both the DCM and AR-coating multilayer structures can be independently designed and optimized. Based on this analysis, we designed a BAck-SIde-Coated Double-Chirped Mirror (BASIC DCM) that supports a bandwidth of 220 THz with group delay dispersion oscillations of about 2 fs^2 (rms), an order-of-magnitude improvement compared to previous designs of similar bandwidth [00Mat]. Ultrabroad BASIC DCMs with a bandwidth of 270 THz have also been used to compress supercontinuum of cascaded hollow fibers down to 4.6 fs [04San]. The trade-off is that the substrate has to be as thin as possible to minimize the overall material dispersion. In addition, the wedged mirror leads to an undesired angular dispersion of the beam.

Another possibility to overcome the AR-coating problem is given with the idea to use an ideal DCM under Brewster-angle incidence [03Ste]. In this case, the low-index layer is matched to air. However, under p-polarized incidence the index contrast and therefore the Fresnel reflectivity of a layer pair is reduced and more layer pairs are necessary to achieve high reflectivity. This increases the penetration depth into the mirror which has the advantage that these mirrors can produce more dispersion per reflection but this means that scattering and other losses and also fabrication tolerances become even more severe. In addition, this concept is difficult to apply to curved mirrors. Furthermore, the spatial chirp of the reflected beam has to be removed by back reflection or an additional reflection from another Brewster-angle mirror.

Other methods to overcome the AR-coating problem are based on using different chirped mirrors with slightly shifted GTI oscillations that partially cancel each other. Normally, these chirped mirrors are very difficult to fabricate [00Mat]. Many different growth runs normally result in strong

shifts of those GTI oscillations so that a special selection of mirrors makes it ultimately possible to obtain the right dispersion compensation. Some tuning of the oscillation peaks can be obtained by the angle of incidence [00Sut]. A specially designed pair of DCMs has been used to cancel the spurious GTI oscillation [01Kae] where an additional quarter-wave layer between the AR-coating and the DCM structure was added in one of the DCMs. Also this design has its drawbacks and limitations because it requires an extremely high precision in fabrication and restricts the range of angles of incidence.

After this overview it becomes clear that there is no perfect solution to the challenge of ultrabroadband dispersion compensation. At this point ultrabroadband chirped mirrors are the only way to compress pulses in the one- to two-optical-cycle regime and normally a larger selection of chirped mirrors are required to "match and reduce" the residual unwanted GDD oscillations from all mirrors inside the laser cavity.

2.1.6 Mode-locking techniques

2.1.6.1 Overview

Passive mode-locking mechanisms are well-explained by three fundamental models: slow saturable absorber mode-locking with dynamic gain saturation [72New, 74New] (Fig. 2.1.5a), fast saturable absorber mode-locking [75Hau1, 92Hau] (Fig. 2.1.5b) and slow saturable absorber mode-locking without dynamic gain saturation which in the femtosecond regime is described by soliton mode-locking [95Kae1, 95Jun2, 96Kae] and in the picosecond regime by Paschotta et al. [01Pas1] (Fig. 2.1.5c). The physics of most of these techniques can be well explained with Haus's master equation formalism as long as at steady state the changes in the pulse envelope during the propagation inside the cavity are small. At steady state the pulse envelope has to be unchanged after one round trip through the cavity.

Passive mode-locking, however, can only be analytically modeled in the weak saturation regime, which is typically not the case in SESAM mode-locked solid-state lasers. However, this formalism still provides a useful approach to describe mode-locking techniques in an unified fashion. Recent numerical simulations show that analytical results with fast saturable absorbers only slightly underestimate numerical solutions and correctly describe the dependence on saturated gain, gain bandwidth and absorber modulation taking into account more strongly saturated absorbers and somewhat longer saturation recovery times in SESAM mode-locked solid-state lasers [01Pas1].

A short introduction to Haus's formalism is given in Sect. 2.1.6.2 and Table 2.1.10. Afterwards we will describe all mode-locking techniques using this formalism and summarize the theoretical prediction for pulse shape and pulse duration (Table 2.1.11). For solid-state lasers self-Q-switching instabilities in passive mode-locking are a serious challenge. Simple guidelines to prevent those instabilities and obtain stable cw mode-locking are presented in Sect. 2.1.6.8.

2.1.6.2 Haus's master equations

Haus's master equation formalism [95Hau2] is based on linearized differential operators that describe the temporal evolution of a pulse envelope inside the laser cavity. At steady state we then obtain the differential equation:

Table 2.1.10. Linearized operators that model the change in the pulse envelope $A(t)$ for each element in the laser cavity and their defining equations. The pulse envelope is normalized such that $|A(z,t)|^2$ is the pulse power $P(z,t)$ (2.1.24). k_n: wave vector in the dispersive media, i.e. $k_n = kn = n2\pi/\lambda$, where λ is the vacuum wavelength. z: the relevant propagation distance for negative dispersion or SPM, respectively. c: vacuum light velocity. ω: frequency in radians/second.

Laser cavity element	Eq.	Linearized operator	New constants	Constants
Gain	(2.1.32)	$\Delta A \approx \left[g + D_\mathrm{g}\dfrac{\partial^2}{\partial t^2}\right] A$	$D_\mathrm{g} \equiv \dfrac{g}{\Omega_\mathrm{g}^2}$	D_g: gain dispersion (2.1.32) g: saturated amplitude gain coefficient Ω_g: HWHM of gain bandwidth in radians/second $\Delta\nu_\mathrm{g}$: FWHM of gain bandwidth, i.e. $\Delta\nu_\mathrm{g} = \Omega_\mathrm{g}/\pi$
Loss modulator	(2.1.34)	$\Delta A \approx -M_\mathrm{s} t^2 A$	$M_\mathrm{s} \equiv \dfrac{M\omega_\mathrm{m}^2}{2}$	ω_m: loss modulation frequency in radians/second $2M$: peak-to-peak modulation depth for amplitude loss coefficient
Constant loss		$\Delta A \approx -lA$		l: amplitude loss coefficient
Constant phase shift		$\Delta A \approx \mathrm{i}\psi A$		ψ: phase shift
Fast saturable absorber	(2.1.36)	$\Delta A \approx \gamma_\mathrm{A} \lvert A\rvert^2 A$	$\gamma_\mathrm{A} \equiv \dfrac{q_0}{I_\mathrm{sat,A} A_\mathrm{A}}$	γ_A: absorber coefficient (2.1.18) and (2.1.35) q_0: maximum saturable amplitude loss coefficient $I_\mathrm{sat,A}$: saturation intensity A_A: laser mode area in saturable absorber
Dispersion: 2nd order	(2.1.41)	$\Delta A \approx \mathrm{i}D\dfrac{\partial^2}{\partial t^2} A$	$D \equiv \dfrac{1}{2}k_n'' z$	D: dispersion parameter (half of the total group delay dispersion per cavity round trip – Table 2.1.7) (2.1.40) $k_n'' = \dfrac{\mathrm{d}^2 k_n}{\mathrm{d}\omega^2}$
SPM	(2.1.47)	$\Delta A \approx -\mathrm{i}\delta_\mathrm{L} \lvert A\rvert^2 A$	$\delta_\mathrm{L} \equiv \dfrac{kn_2 z}{A_\mathrm{L}}$	δ_L: SPM coefficient (2.1.44) n_2: nonlinear refractive index A_L: laser mode area inside laser material (Note: Here we assume that the dominant SPM occurs in the laser material. Then z is equal to 2 times the length of the laser crystal in a standing-wave cavity.)

Table 2.1.11. Predicted pulse duration for the different ModeLocking (ML) techniques. The parameters used here are summarized and defined in Table 2.1.10. The pulse is transform-limited for proper dispersion compensation and is either an unchirped Gaussian or soliton pulse.

ML technique	Eq.	Pulse shape	Pulse duration (FWHM)
Active ML: Amplitude loss modulation	(2.1.49)	Gauss	$\tau_\mathrm{p} = 1.66 \times \sqrt[4]{\frac{D_\mathrm{g}}{M_\mathrm{s}}} = 1.66 \times \sqrt[4]{\frac{2g}{M}} \sqrt{\frac{1}{\omega_\mathrm{m}\Omega_\mathrm{g}}}$
Passive ML: Slow saturable absorber and dynamic gain saturation	(2.1.62)	soliton	$\tau_\mathrm{p} \approx 1.76 \times \frac{4}{\pi} \frac{1}{\Delta\nu_\mathrm{g}}$
Slow saturable absorber for solid-state lasers and strongly saturated absorbers ($S > 3$)	(2.1.70)	numerical simulations	$\tau_{p,\mathrm{min}} \approx \frac{1.5}{\Delta\nu_\mathrm{g}} \sqrt{\frac{g}{\Delta R}}$ for $\tau_\mathrm{A} \lesssim 30\ \tau_\mathrm{p}$
Fast Saturable Absorber (FSA)	(2.1.65)	soliton	$\tau_\mathrm{p} = 1.76\ \frac{4D_\mathrm{g}}{\gamma_\mathrm{A} E_\mathrm{p}}$
			only transform-limited soliton pulses for a well-defined intracavity group delay dispersion (assuming negligible higher-order dispersion): $\lvert D\rvert/\delta_\mathrm{L} = D_\mathrm{g}/\gamma_\mathrm{A}$
Fully saturated ideal fast saturable absorber	(2.1.67)		$\tau_{p,\mathrm{min}} = \frac{1.76}{\Omega_\mathrm{g}} \sqrt{\frac{2g}{q_0}} \approx \frac{1.12}{\Delta\nu_\mathrm{g}} \sqrt{\frac{g}{\Delta R}}$ for $\frac{\lvert D\rvert}{\delta_\mathrm{L}} = \frac{D_\mathrm{g}}{\gamma_\mathrm{A}}$
Soliton mode-locking	(2.1.74)	soliton	$\tau_\mathrm{p} = 1.76\ \frac{2\,\lvert D\rvert}{\delta_\mathrm{L} E_\mathrm{p}}$
			transform-limited soliton pulses for the total intracavity group delay dispersion (assuming negligible higher-order dispersion)
	(2.1.76)		$\tau_{p,\mathrm{min}} = 1.7627 \left(\frac{1}{\sqrt{6}\,\Omega_\mathrm{g}}\right)^{3/4} \phi_\mathrm{s}^{-1/8} \left(\frac{\tau_\mathrm{A} g^{3/2}}{q_0}\right)^{1/4} \approx 0.45 \left(\frac{1}{\Delta\nu_\mathrm{g}}\right)^{3/4} \left(\frac{\tau_\mathrm{A}}{\Delta R}\right)^{1/4} \frac{g^{3/8}}{\phi_\mathrm{s}^{1/8}}$

$$T_{\mathrm{R}} \frac{\partial A(T,t)}{\partial T} = \sum_i \Delta A_i = 0 \,, \tag{2.1.23}$$

where A is the pulse envelope, T_{R} is the cavity round-trip time, T is the time that develops on a time scale of the order of T_{R}, t is the fast time of the order of the pulse duration, and ΔA_i are the changes of the pulse envelope due to different elements in the cavity (such as gain, loss modulator or saturable absorber, dispersion etc.) (Table 2.1.10). Equation (2.1.23) basically means that at steady state after one laser round trip the pulse envelope cannot change and all the small changes due to the different elements in the cavity have to sum up to zero. Each element is modeled as a linearized operator, which will be discussed in more detail below.

The pulse envelope is normalized such that $|A(z,t)|^2$ is the pulse power $P(z,t)$:

$$E(z,t) \propto A(z,t)\, \mathrm{e}^{\mathrm{i}[\omega_0 t - k_n(\omega_0) z]} \quad \text{with} \quad |A(z,t)|^2 \equiv P(z,t) \,, \tag{2.1.24}$$

where $E(z,t)$ is the electric field, ω_0 the center frequency in radians/second of the pulse spectrum and $k_n = nk$ with $k = 2\pi/\lambda$ the wave number with λ the vacuum wavelength and n the refractive index. Before we discuss the different mode-locking models we briefly discuss the linearized operators for the differential equations.

2.1.6.2.1 Gain

A homogeneously broadened gain medium is described by a Lorentzian lineshape for which the frequency-dependent gain coefficient $g(\omega)$ is given by

$$g(\omega) = \frac{g}{1 + \left(\dfrac{\omega - \omega_0}{\Omega_{\mathrm{g}}}\right)^2} \approx g\left(1 - \frac{\Delta\omega^2}{\Omega_{\mathrm{g}}^2}\right) \quad \text{for} \quad ((\omega - \omega_0)/\Omega_{\mathrm{g}})^2 \ll 1 \,, \tag{2.1.25}$$

where $\Delta\omega = \omega - \omega_0$, g is the saturated gain coefficient for a cavity round trip, and Ω_{g} is the Half Width at Half Maximum (HWHM) of the gain bandwidth in radians/seconds. In the frequency domain the pulse envelope after the gain medium is given by

$$\tilde{A}_{\mathrm{out}}(\omega) = \mathrm{e}^{\,g(\omega)} \tilde{A}_{\mathrm{in}}(\omega) \approx [1 + g(\omega)]\, \tilde{A}_{\mathrm{in}}(\omega) \quad \text{for} \quad g \ll 1 \,, \tag{2.1.26}$$

where $\tilde{A}(\omega)$ is the Fourier transformation of $A(t)$. Equations (2.1.25) and (2.1.26) then give

$$\tilde{A}_{\mathrm{out}}(\omega) = \left[1 + g - \frac{g}{\Omega_{\mathrm{g}}^2}\Delta\omega^2\right] \tilde{A}_{\mathrm{in}}(\omega) \;\Rightarrow\; A_{\mathrm{out}}(t) = \left[1 + g + \frac{g}{\Omega_{\mathrm{g}}^2}\frac{\partial^2}{\partial t^2}\right] A_{\mathrm{in}}(t) \,, \tag{2.1.27}$$

where we used the fact that a factor of $\Delta\omega$ in the frequency domain produces a time derivative in the time domain. For example for the electric field we obtain:

$$\frac{\partial}{\partial t} E(t) = \frac{\partial}{\partial t}\left\{\frac{1}{2\pi}\int \tilde{E}(\omega)\, \mathrm{e}^{\mathrm{i}\omega t}\mathrm{d}\omega\right\} = \frac{1}{2\pi}\int \tilde{E}(\omega)\, \mathrm{i}\omega\, \mathrm{e}^{\mathrm{i}\omega t}\mathrm{d}\omega \tag{2.1.28}$$

and

$$\frac{\partial^2}{\partial t^2} E(t) = \frac{\partial^2}{\partial t^2}\left\{\frac{1}{2\pi}\int \tilde{E}(\omega)\, \mathrm{e}^{\mathrm{i}\omega t}\mathrm{d}\omega\right\} = \frac{1}{2\pi}\int \tilde{E}(\omega)\left[-\omega^2\right] \mathrm{e}^{\mathrm{i}\omega t}\mathrm{d}\omega \,, \tag{2.1.29}$$

and similarly for the pulse envelope:

$$\frac{\partial}{\partial t} A(t) = \frac{\partial}{\partial t}\left\{\frac{1}{2\pi}\int \tilde{A}(\omega)\, \mathrm{e}^{\mathrm{i}\Delta\omega t}\mathrm{d}\omega\right\} = \frac{1}{2\pi}\int \tilde{A}(\omega)\, \mathrm{i}\Delta\omega\, \mathrm{e}^{\mathrm{i}\Delta\omega t}\mathrm{d}\omega \tag{2.1.30}$$

and

$$\frac{\partial^2}{\partial t^2}A(t) = \frac{\partial^2}{\partial t^2}\left\{\frac{1}{2\pi}\int \tilde{A}(\omega)\,\mathrm{e}^{\mathrm{i}\Delta\omega t}\mathrm{d}\omega\right\} = \frac{1}{2\pi}\int \tilde{A}(\omega)\left[-\Delta\omega^2\right]\mathrm{e}^{\mathrm{i}\Delta\omega t}\mathrm{d}\omega\ . \tag{2.1.31}$$

For the change in the pulse envelope $\Delta A = A_{\mathrm{out}} - A_{\mathrm{in}}$ after the gain medium we then obtain:

$$\Delta A \approx \left[g + D_{\mathrm{g}}\frac{\partial^2}{\partial t^2}\right]A\ , \quad D_{\mathrm{g}} \equiv \frac{g}{\Omega_{\mathrm{g}}^2}\ , \tag{2.1.32}$$

where D_{g} is the gain dispersion.

2.1.6.2.2 Loss modulator

A loss modulator inside a laser cavity is typically an acousto-optic modulator and produces a sinusoidal loss modulation given by a time-dependent loss coefficient:

$$l(t) = M(1-\cos\omega_{\mathrm{m}}t) \approx M_{\mathrm{s}}t^2\ , \quad M_{\mathrm{s}} \equiv \frac{M\omega_{\mathrm{m}}^2}{2}\ , \tag{2.1.33}$$

where M_{s} is the curvature of the loss modulation, $2M$ is the peak-to-peak modulation depth and ω_{m} the modulation frequency which corresponds to the axial mode spacing in fundamental mode-locking. In fundamental mode-locking we only have one pulse per cavity round trip. The change in the pulse envelope is then given by

$$A_{\mathrm{out}}(t) = \mathrm{e}^{-l(t)}A_{\mathrm{in}}(t) \approx [1-l(t)]\,A_{\mathrm{in}}(t) \ \Rightarrow\ \Delta A \approx -M_{\mathrm{s}}t^2A\ . \tag{2.1.34}$$

2.1.6.2.3 Fast saturable absorber

In case of an ideal fast saturable absorber we assume that the loss recovers instantaneously and therefore shows the same time dependence as the pulse envelope, (2.1.17) and (2.1.18):

$$q(t) = \frac{q_0}{1+I_{\mathrm{A}}(t)/I_{\mathrm{sat,A}}} \approx q_0 - \gamma_{\mathrm{A}}P(t)\ , \quad \gamma_{\mathrm{A}} \equiv \frac{q_0}{I_{\mathrm{sat,A}}A_{\mathrm{A}}}\ . \tag{2.1.35}$$

The change in the pulse envelope is then given by

$$A_{\mathrm{out}}(t) = \mathrm{e}^{-q(t)}A_{\mathrm{in}}(t) \approx [1-q(t)]\,A_{\mathrm{in}}(t) \ \Rightarrow\ \Delta A \approx \gamma_{\mathrm{A}}|A|^2A\ . \tag{2.1.36}$$

2.1.6.2.4 Group velocity dispersion (GVD)

The wave number $k_n(\omega)$ in a dispersive material depends on the frequency and can be approximately written as:

$$k_n(\omega) \approx k_n(\omega_0) + k_n'\Delta\omega + \frac{1}{2}k_n''\Delta\omega^2 + \dots\ , \tag{2.1.37}$$

where $\Delta\omega = \omega - \omega_0$, $k_n' = \left.\dfrac{\partial k_n}{\partial\omega}\right|_{\omega=\omega_0}$ and $k_n'' = \left.\dfrac{\partial^2 k_n}{\partial\omega^2}\right|_{\omega=\omega_0}$. In the frequency domain the pulse envelope in a dispersive medium after a propagation distance of z is given by

$$\tilde{A}(z,\omega) = \mathrm{e}^{-\mathrm{i}[k_n(\omega)-k_n(\omega_0)]z}\tilde{A}(0,\omega) \approx \{1-\mathrm{i}[k_n(\omega)-k_n(\omega_0)]\,z\}\,\tilde{A}(0,\omega)\ , \tag{2.1.38}$$

where we used the slowly-varying-envelope approximation (which is applicable for pulse durations of more than 10 fs in the near infrared wavelength regime). Taking into account only the first-order and second-order dispersion terms we then obtain:

$$\tilde{A}(z,\omega) \approx \left[1 - \mathrm{i}k_n' \Delta\omega z - \mathrm{i}\frac{1}{2}k_n'' \Delta\omega^2 z\right] \tilde{A}(0,\omega) \ . \tag{2.1.39}$$

The linear term in $\Delta\omega$ determines the propagation velocity of the pulse envelope (i.e. the group velocity v_g) and the quadratic term in $\Delta\omega$ determines how the pulse envelope gets deformed due to second-order dispersion. The influence of higher-order dispersion can be considered with more terms in the expansion of $k_n(\omega)$ (2.1.37). However, higher-order dispersion only becomes important for ultrashort pulse generation with pulse durations below approximately 30 fs depending how much material is inside the cavity. Normally we are only interested in the changes of the pulse envelope and therefore it is useful to restrict our observation to a reference system that is moving with the pulse envelope. In this reference system we only need to consider second- and higher-order dispersion. In the time domain we then obtain for second-order dispersion:

$$A(z,t) \approx \left[1 + \mathrm{i}D\frac{\partial^2}{\partial t^2}\right] A(0,t) \ , \quad D \equiv \frac{1}{2}k_n'' z = \frac{1}{2}\frac{\mathrm{d}^2\phi}{\mathrm{d}\,\omega^2} \ , \tag{2.1.40}$$

where D is the dispersion parameter which is half of the total group delay dispersion per cavity round trip. Therefore we obtain for the change in the pulse envelope:

$$\Delta A \approx \mathrm{i}D\frac{\partial^2}{\partial t^2}A \ . \tag{2.1.41}$$

2.1.6.2.5 Self-phase modulation (SPM)

The Kerr effect introduces a space- and time-dependent refractive index:

$$n(r,t) = n + n_2 I(r,t) \ , \tag{2.1.42}$$

where n is the linear refractive index, n_2 the nonlinear refractive index and $I(r,t)$ the intensity of the laser beam, typically a Gaussian beam profile. For laser host materials, n_2 is typically of the order of 10^{-16} cm^2/W and does not change very much for different materials. For example, for sapphire $n_2 = 3 \times 10^{-16}$ cm^2/W, fused quartz $n_2 = 2.46 \times 10^{-16}$ cm^2/W, Schott glass LG-760 $n_2 = 2.9 \times 10^{-16}$ cm^2/W, YAG $n_2 = 6.2 \times 10^{-16}$ cm^2/W, and YLF $n_2 = 1.72 \times 10^{-16}$ cm^2/W. The nonlinear refractive index produces a nonlinear phase shift during pulse propagation:

$$\phi(z,r,t) = -k\,n(r,t)\,z = -k\left[n + n_2 I(r,t)\right]z = -knz - \delta_\mathrm{L}\left|A(r,t)\right|^2 \ , \tag{2.1.43}$$

where δ_L is the Self-Phase Modulation coefficient (SPM coefficient):

$$\delta_\mathrm{L} \equiv kn_2 z/A_\mathrm{L} \ , \tag{2.1.44}$$

where A_L is the laser mode area inside the laser medium. Here we assume that the dominant SPM inside the laser occurs in the gain medium. In this case, z is equal to twice the laser material length. Of course the mode area can be also very small in other materials. In this case, we will have to add up all the SPM contributions inside the laser resonator. The laser mode area A_L is an "averaged value" in case the mode is changing within the gain medium.

The electric field during propagation is changing due to SPM:

$$E(z,t) = \mathrm{e}^{\mathrm{i}\phi}E(0,t) \propto \mathrm{e}^{-\mathrm{i}\delta_\mathrm{L}|A(t)|^2}A(0,t)\,\mathrm{e}^{\mathrm{i}\omega_0 t - \mathrm{i}k_n(\omega_0)z} \ . \tag{2.1.45}$$

For $\delta_\mathrm{L}|A|^2 \ll 1$ we obtain:

$$A(z,t) = \mathrm{e}^{-\mathrm{i}\delta_\mathrm{L}|A(t)|^2} A(0,t)\,\mathrm{e}^{-\mathrm{i}k_n(\omega_0)z} \approx \left(1 - \mathrm{i}\delta_\mathrm{L}\,|A(t)|^2\right) A(0,t)\,\mathrm{e}^{-\mathrm{i}k_n(\omega_0)z}\ . \tag{2.1.46}$$

After one cavity round trip we then obtain

$$\Delta A \approx -\mathrm{i}\delta_\mathrm{L}\,|A|^2\,A\ . \tag{2.1.47}$$

2.1.6.3 Active mode-locking

Short pulses from a laser can be generated with a loss or phase modulator inside the resonator. For example, the laser beam is amplitude-modulated when it passes through an acousto-optic modulator. Such a modulator can modulate the loss of the resonator at a period equal to the round-trip time T_R of the resonator (i.e. fundamental mode-locking). The pulse evolution in an actively mode-locked laser without Self-Phase Modulation (SPM) and Group-Velocity Dispersion (GVD) can be described by the master equation of Haus [75Hau2]. Taking into account gain dispersion and loss modulation we obtain with (2.1.32) and (2.1.34) (Table 2.1.10) the following differential equation:

$$\sum_i \Delta A_i = \left[g\left(1 + \frac{1}{\Omega_\mathrm{g}^2}\frac{\partial^2}{\partial t^2}\right) - l - M\,\frac{\omega_\mathrm{m} t^2}{2}\right] A(T,t) = 0\ . \tag{2.1.48}$$

Typically we obtain pulses which are much shorter than the round-trip time in the cavity and which are placed in time at the position where the modulator introduces the least amount of loss. Therefore, we were able to approximate the cosine modulation by a parabola (2.1.33). The only stable solution to this differential equation is a Gaussian pulse shape with a pulse duration:

$$\tau_\mathrm{p} = 1.66 \times \sqrt[4]{D_\mathrm{g}/M_\mathrm{s}}\ , \tag{2.1.49}$$

where D_g is the gain dispersion ((2.1.32) and Table 2.1.10) and M_s is the curvature of the loss modulation ((2.1.33) and Table 2.1.10). Therefore, in active mode-locking the pulse duration becomes shorter until the pulse shortening of the loss modulator balances the pulse broadening of the gain filter. Basically, the curvature of the gain is given by the gain dispersion D_g and the curvature of the loss modulation is given by M_s. The pulse duration is only scaling with the fourth root of the saturated gain (i.e. $\tau_\mathrm{p} \propto \sqrt[4]{g}$) and the modulation depth (i.e. $\tau_\mathrm{p} \propto \sqrt[4]{1/M}$) and with the square root of the modulation frequency (i.e. $\tau_\mathrm{p} \propto \sqrt{1/\omega_\mathrm{m}}$) and the gain bandwidth (i.e. $\tau_\mathrm{p} \propto \sqrt{1/\Delta\,\omega_\mathrm{g}}$). A higher modulation frequency or a higher modulation depth increases the curvature of the loss modulation and a larger gain bandwidth decreases gain dispersion. Therefore, we obtain shorter pulse durations in all cases. At steady state the saturated gain is equal to the total cavity losses, therefore, a larger output coupler will result in longer pulses. Thus, higher average output power is generally obtained at the expense of longer pulses (Table 2.1.2).

The results that have been obtained in actively mode-locked flashlamp-pumped Nd:YAG and Nd:YLF lasers can be very well explained by this result. For example, with Nd:YAG at a lasing wavelength of 1.064 μm we have a gain bandwidth of $\Delta\lambda_\mathrm{g} = 0.45$ nm. With a modulation frequency of 100 MHz (i.e. $\omega_\mathrm{m} = 2\,\pi{\cdot}100$ MHz), a 10 % output coupler (i.e. $2g \approx T_\mathrm{out} = 0.1$) and a modulation depth $M = 0.2$, we obtain a FWHM pulse duration of 93 ps (2.1.49). For example, with Nd:YLF at a lasing wavelength of 1.047 μm and a gain bandwidth of $\Delta\lambda_\mathrm{g} = 1.3$ nm we obtain with the same mode-locking parameters a pulse duration of 53 ps (2.1.49).

The same result for the pulse duration (2.1.49) has been previously derived by Kuizenga and Siegman [70Kui1, 70Kui2] where they assumed a Gaussian pulse shape and then followed the pulse once around the laser cavity, through the gain and the modulator. They then obtained a self-consistent solution when no net change occurs in the complete round trip. The advantage of

Haus's theory is that no prior assumption has to be made for the pulse shape. His theory then predicts a Gaussian pulse shape for actively mode-locked lasers, which then in principle justifies Kuizenga and Siegman's assumption.

Equation (2.1.49) shows that increasing the modulation frequency is an effective method to shorten the pulses. Harmonic mode-locking is a technique in which the cavity is modulated at a frequency that is some integer multiple of the fundamental pulse repetition rate with a period given by the cavity round-trip time. This technique was first introduced and analyzed by Becker et al. [72Bec] in a phase mode-locked Nd:YAG laser. Second-harmonic mode-locking of a flashlamp-pumped Nd:YAG laser at 1.06 μm resulted in less than 50 ps [83Joh, 85Joh] and at 1.32 μm in 53 ps [88Kel].

It has been well known for quite some time that the addition of a nonlinear index medium to a passively [84Mar, 85Mar] or actively [86Hau] mode-locked laser system can lead to shorter pulses. The bandwidth limitation that results from gain dispersion can be partially overcome by the spectral broadening caused by the nonlinearity. We can extend the differential equation (2.1.48) with the additional terms for SPM ((2.1.47) and Table 2.1.10):

$$\sum_i \Delta A_i = \left[g\left(1 + \frac{1}{\Omega_g^2}\frac{\partial^2}{\partial t^2}\right) - l - M\,\frac{\omega_m t^2}{2} - \mathrm{i}\delta_L\,|A|^2 + \mathrm{i}\psi \right] A\,(T,t) = 0\ . \tag{2.1.50}$$

In this case, however, we have to include an additional phase shift ψ to obtain a self-consistent solution. So far, we always assumed $\psi = 0$. This phase shift is an additional degree of freedom because the boundary condition for intracavity pulses only requires that the pulse envelope is unchanged after one cavity round trip. The electric field, however, can have an arbitrary phase shift ψ after one round trip. This is normally the case because the phase and the group velocity are not the same. It is important to note, that for ultrashort pulses in the one- to two-cycle regime this becomes important and stabilization of the electric field with respect to the peak of the pulse envelope is required [99Tel].

We can obtain an analytic solution of (2.1.50) if we assume a parabolic approximation for $|A|^2$:

$$|A|^2 = |A_0|^2\,\mathrm{e}^{-t^2/\tau^2} \approx P_0\left(1 - \frac{t^2}{\tau^2}\right)\ . \tag{2.1.51}$$

The solution of (2.1.50) is then a chirped Gaussian pulse

$$A\,(t) = A_0 \exp\left[-\frac{1}{2}\frac{t^2}{\tau^2}\,(1 - \mathrm{i}x)\right] \tag{2.1.52}$$

with the chirp parameter

$$x = \frac{\tau^2\phi_{nl}}{2D_g} \tag{2.1.53}$$

and the FWHM pulse duration

$$\tau_p = 1.66 \cdot \tau = 1.66 \cdot \sqrt[4]{\frac{D_g}{M_s + \phi_{nl}^2/4D_g}}\ , \tag{2.1.54}$$

where ϕ_{nl} is the nonlinear phase shift per cavity round trip at peak intensity. Typically, the beam diameter is very small in the laser gain material, thus the dominant SPM contribution comes from propagation through the gain material:

$$\phi_{nl} = 2kL_g n_2 I_{0,L}\ , \tag{2.1.55}$$

where L_g is the length of the laser gain material (assuming a standing-wave cavity) and $I_{0,L}$ the peak intensity inside the SPM medium, i.e. the laser gain medium.

This analytical result can explain the much shorter 7–12 ps pulses in actively mode-locked diode-pumped Nd:YAG [89Mak1] and Nd:YLF [89Mak2, 90Kel1, 90Wei, 90Juh] lasers because the laser mode area in those diode-pumped lasers is very small which results in significant SPM pulse shortening (2.1.54). For example, our experiments with an actively mode-locked diode-pumped Nd:YLF laser [95Bra2] are very well explained with (2.1.54). In this case the lasing wavelength is 1.047 μm, the gain bandwidth is $\Delta\lambda_g = 1.3$ nm, the pulse repetition rate is 250 MHz, the output coupler is 2.5 %, the average output power is 620 mW, the mode radius inside the 5 mm long Nd:YLF crystal is 127 μm × 87 μm and the loss modulation of the acousto-optic mode-locker is about 20 %. We then obtain a FWHM pulse duration of 17.8 ps (2.1.54) which agrees well with the experimentally observed pulse duration of 17 ps. Without SPM we would predict a pulse duration of 33 ps (2.1.49).

Equation (2.1.54) would predict that more SPM continues to reduce the pulse duration. However, too much SPM will ultimately drive the laser unstable. This has been shown by the numerical simulations of Haus and Silberberg [86Hau] which predict that pulse shortening in an actively mode-locked system is limited by roughly a factor of 2 in the case of SPM only. They also showed that the addition of negative GVD can undo the chirp introduced by SPM, and therefore both effects together may lead to stable pulse shortening by a factor of 2.5.

However, experimental results with fiber lasers and solid-state lasers indicate that soliton shaping in the negative GVD regime can lead to pulse stabilization and considerable more pulse shortening. We have extended the analysis of Haus and Silberberg by investigating the possible reduction in pulse width of an actively mode-locked laser as a result of soliton-like pulse formation, i.e., the presence of SPM and an excessive amount of negative GVD [95Kae2]. We show, by means of soliton perturbation theory, that beyond a critical amount of negative GVD a soliton-like pulse is formed and kept stable by an active mode-locker. If the bandwidth of the gain is large enough, the width of this solitary pulse can be much less than the width of a Gaussian pulse generated by the active mode-locker and gain dispersion alone. We established analytically that the pulse shortening possible by addition of SPM and GVD does not have a firm limit of 2.5. Numerical simulations and experiments with a regeneratively actively mode-locked Nd:glass laser [94Kop2] confirm these analytical results. The pulse-width reduction achievable depends on the amount of negative GVD available. For an actively mode-locked Nd:glass laser a pulse shortening up to a factor of 6 may result, until instabilities arise.

2.1.6.4 Passive mode-locking with a slow saturable absorber and dynamic gain saturation

Dynamic gain saturation can strongly support pulse formation in passive mode-locking and has allowed pulses with duration much shorter than the absorber recovery time. Dynamic gain saturation means that the gain undergoes a fast pulse-induced saturation that recovers between consecutive pulses. This technique has been used to produce sub-100-fs pulses with dye lasers and dye saturable absorbers even though the absorber recovery time was in the nanosecond regime. Dynamic gain saturation can only help if the following conditions are fulfilled (Fig. 2.1.5a):

1. The loss needs to be larger than the gain before the pulse:

$$q_0 > g_0 \ , \tag{2.1.56}$$

   where q_0 is the unsaturated loss coefficient (2.1.6) and g_0 is the small signal gain coefficient in the laser.
2. The absorber needs to saturate faster than the gain. From (2.1.14) (i.e. slow saturable absorber and gain) then follows that

Table 2.1.12. Femtosecond Rhodamin 6G dye laser with its saturable absorber DODCI at a wavelength of 620 nm. σ_L gain and σ_A absorber cross-section, τ_L upper-state lifetime, τ_A absorber recovery time.

Dye material	Cross-section	Time
Rhodamin 6G	$\sigma_L = 1.36 \times 10^{-16}$ cm^2	$\tau_L = 4$ ns
DODCI	$\sigma_A = 0.52 \times 10^{-16}$ cm^2	$\tau_A = 2.2$ ns
Photoisomer	$\tilde{\sigma}_A = 1.08 \times 10^{-16}$ cm^2	$\tilde{\tau}_L = 1$ ns

$$E_{sat,A} < E_{sat,L} \Leftrightarrow \frac{A_A}{\sigma_A} < \frac{A_L}{\sigma_L} , \tag{2.1.57}$$

where $E_{sat,A}$ and $E_{sat,L}$ are the saturation energy of the absorber and the gain, σ_A and σ_L the absorber and gain cross section, and A_A and A_L the laser mode area in the absorber and gain.

3. The absorber has to recover faster than the gain:

$$\tau_A < \tau_L , \tag{2.1.58}$$

where τ_A is the absorber recovery time and τ_L the upper-state lifetime of the gain medium (Table 2.1.1).

Passively mode-locked dye lasers are based on this mode-locking technique and a more extensive review of ultrashort pulse generation with dye lasers is given in [88Sha, 90Die]. The most important dye laser for sub-100-fs pulse generation is the Colliding Pulse Mode-locked (CPM) laser [81For]. The design considerations of such a laser are very well described in [86Val]. This laser is based on Rhodamin 6G as the gain medium and on DODCI as the absorber [72Ipp]. From Table 2.1.12 follows that the conditions (2.1.56)–(2.1.58) are only fulfilled if the mode area in the absorber jet is smaller than in the gain jet. In addition, a six-mirror ring cavity design where the absorber and the gain jet are separated by 1/4 of the resonator round trip gives the two counter-propagating pulses the same gain and the absorber is more strongly saturated because of the two pulses colliding inside the saturable absorber jet (i.e. Colliding Pulse Mode-locking – CPM). This effectively shortens the pulses and increases the stability. The best performance of this laser was only obtained after both the gain and the absorber dyes have been freshly prepared, because both photodegrade within a relatively short time (i.e. 1–3 weeks). The best result was 27 fs pulses at a center wavelength of 620 nm with an average output power of 20 mW each in two output beams at a pulse repetition rate of 100 MHz [85Val, 86Val]. More typically, this laser produced slightly below 100 fs pulses. This laser was the "work horse" for all the pioneering work on sub-100-fs spectroscopy for nearly 10 years in the 1980's. However, the rather large maintenance of this laser explains the success of the Ti:sapphire laser at the beginning of the 1990's. Today, solid-state lasers with much shorter pulses, higher output powers and better stability have replaced practically all ultrafast dye laser systems.

Another important application of this mode-locking technique are semiconductor lasers, which also have an upper-state lifetime in the nanosecond regime and a large gain cross section in the range of 10^{-14} cm^2. A more extensive recent review of ultrashort pulse generation with semiconductor lasers is given in [95Jia, 95Vai]. The CPM technique, as developed for dye lasers, has been also used for passively mode-locked semiconductor lasers [81Zie, 86Vas]. Wu and Chen et al. [90Wu, 92Che] monolithically incorporated the CPM technique in quantum-well lasers. Pulses of 0.64 ps at a repetition rate of 710 MHz were generated [91Che].

The master equation for this mode-locking mechanism (Fig. 2.1.5a) is given by [75Hau3, 94Ipp]:

$$\sum_i \Delta A_i = \left[g(t) - q(t) + \frac{g_0}{\Omega_g^2} \frac{d^2}{dt^2} + t_D \frac{d}{dt} \right] A(T,t) = 0 . \tag{2.1.59}$$

For a self-consistent solution we will have to include a time shift t_D of the pulse envelope due to the saturation of the absorber. $g(t)$ and $q(t)$ are given by the slow-saturation approximation (2.1.14).

For an analytical solution we have to expand the exponential function up to the second order, i.e. $e^x \approx 1 + x + \frac{x^2}{2}$:

$$q(t) = q_0 \exp\left[-\frac{\sigma_A}{A_A h\nu}\int_{-\infty}^{t} |A(t')|^2 \,dt'\right]$$
$$\approx q_0\left[1 - \frac{\sigma_A}{A_A h\nu}\int_{-\infty}^{t} |A(t')|^2 \,dt' + \frac{\sigma_A^2}{2(A_A h\nu)^2}\left(\int_{-\infty}^{t} |A(t')|^2 \,dt'\right)^2\right] \quad (2.1.60)$$

and analogous for $g(t)$. In this case we can obtain an analytical solution with a sech^2-pulse shape:

$$A(t) = A_0 \,\mathrm{sech}\left(\frac{t}{\tau}\right) \quad (2.1.61)$$

and a FWHM pulse duration

$$\tau_p \approx 1.76 \times \frac{4}{\pi}\frac{1}{\Delta\nu_g}\,, \quad (2.1.62)$$

where $\Delta\nu_g$ is the FWHM gain bandwidth of the laser. In (2.1.62) the conditions (2.1.56)–(2.1.58) are assumed and in addition $E_{sat,L} \gg E_{sat,A}$ and $E_p \gg E_{sat,A}$ (i.e. a fully saturated absorber).

For the example of Rhodamin 6G and DODCI (Table 2.1.12) we then obtain for a gain bandwidth of $\Delta\nu_g \approx 4 \times 10^{13}$ Hz a pulse duration of about 56 fs (2.1.62). Pulses as short as 27 fs have been demonstrated [85Val]. However, it was recognized early on that SPM together with negative dispersion results in soliton formation and further reduces pulse duration by about a factor of 2 in dye lasers [84Mar, 85Mar]. This would explain the difference in the theoretical prediction of (2.1.62) from the experimentally demonstrated 27 fs. However, at that time an analytic solution for the pulse-shortening effect was not presented.

For semiconductor lasers we typically observe strongly chirped pulses [95Jia]. Therefore, we would have to include dispersion and self-phase modulation in the rate equation. This is not so easy because we would have to also include the refractive-index change that occurs during gain saturation.

2.1.6.5 Passive mode-locking with a fast saturable absorber

In passive mode-locking the loss modulation is obtained by Self-Amplitude Modulation (SAM), where the pulse saturates an absorber, for example. In the ideal case, the SAM follows the intensity profile of the pulse. This is the case of an ideal fast saturable absorber. In this case, SAM produces a much larger curvature of loss modulation than in the sinusoidal loss modulation of active mode-locking, because the mode-locked pulse duration is much shorter than the cavity round-trip time. Therefore, we would expect from the previous discussion of active mode-locking, that we obtain much shorter pulses with passive mode-locking. This is indeed observed.

In the fast saturable absorber model no dynamic gain saturation is required and the short net-gain window is formed by a fast recovering saturable absorber alone (Fig. 2.1.5b). This was initially believed to be the only stable approach to passively mode-lock solid-state lasers with long upper-state lifetimes. Additive Pulse Mode-locking (APM) was the first fast saturable absorber for such solid-state lasers (Sect. 2.1.4.4.2). However, APM required interferometric cavity-length stabilization. Kerr-Lens Mode-locking (KLM) [91Spe] (Sect. 2.1.4.4.3) was the first useful demonstration of an intracavity fast saturable absorber for a solid-state laser and because of its simplicity replaced

coupled cavity mode-locking techniques. KLM is very close to an ideal fast saturable absorber, where the modulation depth is produced either by the decreased losses because of self-focusing through a hard aperture [91Kel, 91Sal1, 91Neg] or by increased gain in the laser as a result of an increased overlap of the laser mode with the pump mode in the laser crystal [93Pic]. Only in the ultrashort pulse regime of a few optical cycles more complicated space–time coupling occurs and wavelength-dependent effects start to limit further pulse reduction.

Besides the tremendous success of KLM, there are some significant limitations for practical or "real-world" ultrafast lasers. First, the cavity is typically operated near one end of its stability range, where the Kerr-lens-induced change of the beam diameter is large enough to sustain mode-locking. This results in a requirement for critical cavity alignment where mirrors and the laser crystal have to be positioned to an accuracy of several hundred microns typically. Once the cavity is correctly aligned, KLM can be very stable and under certain conditions even self-starting. However, self-starting KLM lasers in the sub-50-fs regime have not yet been demonstrated without any additional starting mechanisms. This is not surprising, since in a 10-fs Ti:sapphire laser with a 100 MHz repetition rate, the peak power changes by 6 orders of magnitude when the laser switches from cw to pulsed operation. Therefore, nonlinear effects that are still effective in the sub-10-fs regime are typically too small to initiate mode-locking in the cw-operation regime. In contrast, if self-starting is optimized, KLM tends to saturate in the ultrashort pulse regime or the large Self-Phase Modulation (SPM) will drive the laser unstable.

For an ideal fast saturable absorber, Haus et al. [92Hau] developed an analytic solution for the pulse width starting with the following master equation:

$$\sum_i \Delta A_i = \left[g\left(1 + \frac{1}{\Omega_g^2}\frac{\partial^2}{\partial t^2}\right) - l + \gamma_A |A|^2 \right] A(T,t) = 0 \tag{2.1.63}$$

not taking into account GVD and SPM. The solution is an unchirped sech^2-pulse shape

$$P(t) = P_0 \,\mathrm{sech}^2\left(\frac{t}{\tau}\right) \tag{2.1.64}$$

with a FWHM pulse width:

$$\tau_p = 1.7627 \cdot \tau = 1.7627 \,\frac{4D_g}{\gamma_A E_p}\,, \tag{2.1.65}$$

where P_0 is the peak power of the pulse, E_p is the intracavity pulse energy and D_g is the gain dispersion of the laser medium (2.1.32).

The shortest possible pulses can be obtained when we use the full modulation depth of the fast saturable absorber. We only obtain an analytic solution if we assume an ideal fast absorber that saturates linearly with the pulse intensity (2.1.18) over the full modulation depth. This is clearly a strong approximation because (2.1.18) only holds for weak absorber saturation. For a maximum modulation depth and this linear approximation we then can assume that $\gamma_A P_0 = q_0$. For a sech^2-shaped pulse (2.1.64), the pulse energy is given by

$$E_p = \int I(t)\mathrm{d}t = 2\tau P_0\,. \tag{2.1.66}$$

The minimal pulse width for a fully saturated ideal fast absorber then follows from (2.1.65):

$$\tau_{p,\min} = \frac{1.7627}{\Omega_g}\sqrt{\frac{2g}{q_0}}\,. \tag{2.1.67}$$

This occurs right at the stability limit when the filter loss due to gain dispersion is equal to the residual loss a soliton undergoes in an ideal fast saturable absorber (2.1.19):

$$\text{Filter loss } = \frac{D_\mathrm{g}}{3\tau^2} = \frac{q_0}{3} = q_\mathrm{s} = \text{residual saturable absorber loss .} \tag{2.1.68}$$

The residual saturable absorber loss q_s results from the fact that the soliton pulse initially experiences loss to fully saturate the absorber (see Sect. 2.1.4.2.2). This residual loss is exactly $q_0/3$ for a sech^2-pulse shape and a fully saturated ideal fast saturable absorber. This condition results in a minimal FWHM pulse duration given by (2.1.67).

Including GVD and SPM, i.e. soliton formation, in the fast saturable absorber model, an additional pulse shortening of a factor of 2 was predicted. However, unchirped soliton pulses (i.e. ideal sech^2-shaped pulses) are only obtained for a certain negative dispersion value given by

$$\frac{|D|}{\delta_\mathrm{L}} = \frac{D_\mathrm{g}}{\gamma_\mathrm{A}} \,. \tag{2.1.69}$$

This is also where we obtain the shortest pulses with a fast saturable absorber. Here we assume that higher-order dispersion is fully compensated or negligibly small. In addition, computer simulations show that too much self-phase modulation drives the laser unstable.

KLM is well described by the fast absorber mode-locking model discussed above even though it is not so easy to determine the exact saturable absorber parameters such as the effective saturation fluence. However, the linearized model does not describe the pulse generation with Ti:sapphire lasers in the sub-10-fs regime very well. Pulse-shaping processes in these lasers are more complex [91Bra, 92Kra2]. Under the influence of the different linear and nonlinear pulse shaping mechanisms, the pulse is significantly broadened and recompressed, giving rise to a "breathing" of the pulse width. The order of the pulse shaping elements in the laser cavity becomes relevant and the spectrum of the mode-locked pulses becomes more complex. In this case, an analytical solution can no longer be obtained. As a rough approximation, the pulses still behave like solitons and consequently these lasers are also called solitary lasers [91Bra].

2.1.6.6 Passive mode-locking with a slow saturable absorber without gain saturation and soliton formation

Over many years we consistently observed in experiments that even without soliton effects the pulse duration can be much shorter than the absorber recovery time in SESAM mode-locked solid-state lasers. It has always been postulated that without soliton pulse shaping, we need to have a fast saturable absorber for stable mode-locking, which is in disagreement with our experimental observations. More recently, we therefore performed some more detailed numerical investigations [01Pas1]. For a strongly saturated slow absorber with a saturation parameter $S > 3$ and an absorber recovery time smaller than 10 to 30 times the pulse duration, we found a useful guideline for the predicted pulse duration

$$\tau_{p,\min} \approx \frac{1.5}{\Delta\nu_\mathrm{g}} \sqrt{\frac{g}{\Delta R}} \,. \tag{2.1.70}$$

We neglected similar to the ideal fast saturable absorber mode-locking model, the effects of Kerr nonlinearity and dispersion in the cavity, phase changes on the absorber and spatial hole burning in the gain medium. Compared to the analytical solution of a fully saturated absorber (2.1.67) we would predict a slightly longer pulse duration given by a factor of about 1.3. Otherwise, the dependence with regards to gain saturation, gain bandwidth and absorber modulation depth has been explained very well with the analytical solution.

Numerical simulations show that the pulse duration in (2.1.70) can be significantly shorter than the absorber recovery time and has little influence on the pulse duration as long as $\tau_\mathrm{A} < 10\,\tau_\mathrm{p}$

to $30\,\tau_p$. Numerical simulations show that this is a reasonable estimate and that with too long recovery time, the pulse does not simply become longer but unstable.

At first this long recovery time might be surprising, because on the trailing edge of the pulse there is no shaping action of the absorber. There is even net gain, because the loss caused by the absorber is very small for the trailing edge (always assuming a fully saturated absorber), while the total loss for the pulse is larger and is balanced by the saturated gain in steady state. Thus, one might expect that this net gain after the pulse would destabilize the pulse – but this is not the case. The reason is that the pulses experience a temporal shift by the absorber, which limits the time in which noise behind the pulse can be amplified. The absorber attenuates mostly the leading wing of the pulse, thus shifting the pulse center backwards in each cavity round trip. This means that the pulse is constantly moving backward and swallows any noise growing behind itself. An upper limit on the recovery time than follows from the condition that this noise cannot grow too much. Note that weak reflections in the laser cavity could generate weak satellite pulses behind the main pulse. These satellite pulses could be stronger than the noise level and thus significantly reduce maximum tolerable recovery time of the absorber.

So far we have not included any additional pulse-shaping effects such as SPM or solitons. Further simulations show that SPM alone in the positive dispersion regime should always be kept small because it always makes pulses longer and even destabilizes them, particularly for absorbers with small modulation depth [01Pas1]. This result might be surprising at first – but again the temporal delay caused by the absorber gives a simple explanation. SPM (with positive n_2, as is the usual case) decreases the instantaneous frequency in the leading wing and increases the frequency in the trailing wing. The absorber always attenuates the leading wing, thus removing the lower frequency components, which results in an increased center frequency and broader pulses due to the decrease in pulse bandwidth. For strong SPM the pulses become unstable. A rule of thumb is that the nonlinear phase shift for the peak should be at most a few mrad per 1 % of modulation depth. It is clear that SPM could hardly be made weak enough in the sub-picosecond regime. For this reason, soliton mode-locking is usually required in the sub-picosecond domain, because there the nonlinear phase changes can be much larger.

2.1.6.7 Soliton mode-locking

In soliton mode-locking, the pulse shaping is done solely by soliton formation, i.e. the balance of Group-Velocity Dispersion (GVD) and Self-Phase Modulation (SPM) at steady state, with no additional requirements on the cavity stability regime as for example for KLM. In contrast to KLM we use only the time-dependent part of the Kerr effect at the peak intensity (i.e. $n\,(t) = n + n_2\,I_0\,(t)$, (2.1.42)) and not the radially dependent part as well (i.e. $n\,(r,t) = n + n_2\,I\,(r,t)$, (2.1.42)). The radially dependent part of the Kerr effect is responsible for KLM because it forms the nonlinear lens that reduces the beam diameter at an intracavity aperture inside the gain medium. Thus, this nonlinear lens forms an effective fast saturable absorber because the intensity-dependent beam-diameter reduction at an aperture introduces less loss at high intensity and more loss at low intensity. Such a radially dependent effective saturable however couples the mode-locking mechanism with the cavity mode. In contrast, soliton mode-locking does not depend on the transverse Kerr effect and has therefore the advantage that the mode-locking mechanism is decoupled from the cavity design and no critical cavity stability regime is required – it basically works over the full cavity stability range.

In soliton mode-locking, an additional loss mechanism, such as a saturable absorber [95Kae1], or an acousto-optic modulator [95Kae2], is necessary to start the mode-locking process and to stabilize the soliton pulse-forming process. In soliton mode-locking, we have shown that the net-gain window (Fig. 2.1.5c) can remain open for significantly more than 10 times longer than the ultrashort pulse, depending on the specific laser parameters [95Jun2, 96Kae]. This strongly relaxes

the requirements on the saturable absorber and we can obtain ultrashort pulses even in the 10-fs regime with semiconductor saturable absorbers that have much longer recovery times. With the same modulation depth, one can obtain almost the same minimal pulse duration as with a fast saturable absorber, as long as the absorber recovery time is roughly less than ten times longer than the final pulse width. In addition, high dynamic range autocorrelation measurements showed excellent pulse pedestal suppression over more than seven orders of magnitude in 130-fs pulses of a Nd:glass laser [95Kop1] and very similar to or even better than KLM pulses in the 10-fs pulse width regime [97Jun2]. Even better performance can be expected if the saturable absorber also shows a negative refractive-index change coupled with the absorption change as is the case for semiconductor materials [96Kae].

With a slow saturable absorber as a starting and stabilizing mechanism for soliton mode-locking, there remains a time window with net round-trip gain behind the pulse, where the loss of the still saturated absorber is smaller than the total loss for the pulse that is balancing the saturated gain. At a first glance it may seem that the discussion in the last section, Sect. 2.1.6.6, with slow saturable absorbers would apply here as well. However, there is another limiting effect which usually becomes more effective in soliton mode-locked lasers: The dispersion causes the background to temporally broaden and thus permanently loosing the energy in those parts which drift into the time regions with net loss.

We can describe soliton mode-locking by the Haus's master equation formalism, where we take into account GVD, SPM and a slow saturable absorber $q(T,t)$ that recovers slower than the pulse duration (see Fig. 2.1.5c) [95Kae1, 96Kae]:

$$\sum_i \Delta A_i = \left[-\mathrm{i}D\frac{\partial^2}{\partial t^2} + \mathrm{i}\delta_\mathrm{L}\left|A(T,t)\right|^2\right] A(T,t) + \left[g - l + D_\mathrm{g}\frac{\partial^2}{\partial t^2} - q(T,t)\right] A(T,t) = 0\ . \tag{2.1.71}$$

This differential equation can be solved analytically using soliton perturbation theory. The first bracket term of this differential equation determines the nonlinear Schrödinger equation for which the soliton pulse is a stable solution for negative GVD (i.e. $D<0$) and positive SPM (i.e. $n_2>0$):

$$A(z,t) = A_0\ \mathrm{sech}\left(\frac{t}{\tau}\right)\mathrm{e}^{-\mathrm{i}\phi_\mathrm{s}(z)}\ . \tag{2.1.72}$$

This soliton pulse propagates without distortion through a medium with negative GVD and positive SPM because the effect of SPM exactly cancels that due to dispersion. The FWHM soliton pulse duration is given by $\tau_\mathrm{p} = 1.7627\cdot\tau$ and the time–bandwidth product by $\Delta\nu_\mathrm{p}\tau_\mathrm{p} = 0.3148$. $\phi_\mathrm{s}(z)$ is the phase shift of the soliton during propagation along the z-axis

$$\phi_\mathrm{s}(z) = \frac{1}{2}kn_2I_0z \equiv \frac{1}{2}\phi_\mathrm{nl}(z)\ , \tag{2.1.73}$$

where I_0 is the peak intensity inside the SPM medium (i.e. typically the gain medium). Thus, the soliton pulse experiences during propagation a constant phase shift over the full beam profile. For a given negative dispersion and an intracavity pulse energy E_p we obtain a pulse duration

$$\tau_\mathrm{p} = 1.7627\ \frac{2\left|D\right|}{\delta_\mathrm{L}E_\mathrm{p}}\ , \tag{2.1.74}$$

for which the effects of SPM and GVD are balanced with a stable soliton pulse.

This soliton pulse looses energy due to gain dispersion and losses in the cavity. Gain dispersion and losses can be treated as perturbation to the nonlinear Schrödinger equation for which a soliton is a stable solution (i.e. second bracket term in (2.1.71)). This lost energy, called continuum in soliton perturbation theory, is initially contained in a low-intensity background pulse, which experiences negligible SPM, but spreads in time due to GDD (Fig. 2.1.17a). In soliton mode-locking a stable

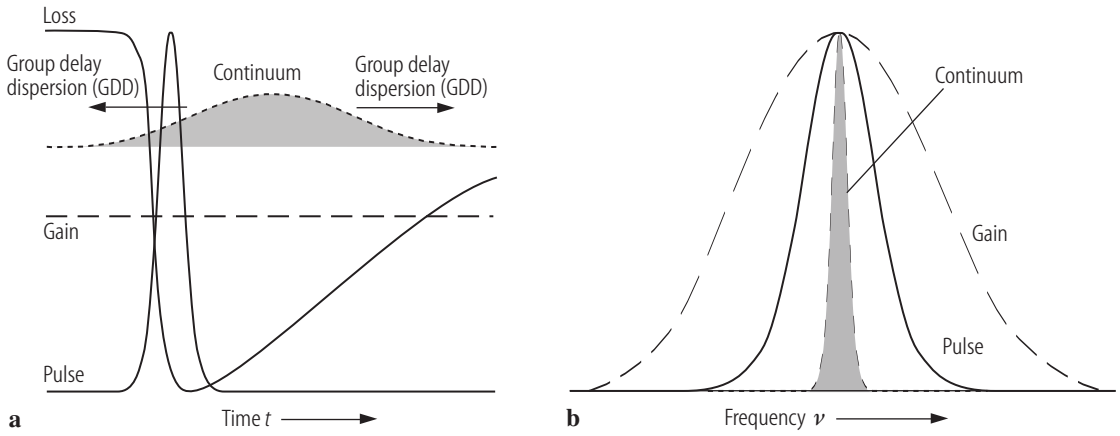

Fig. 2.1.17. Soliton mode-locking in (**a**) time and (**b**) frequency domain. The continuum pulse spreads in time due to group velocity dispersion and thus undergoes more loss in the relatively slow absorber, which is saturated by the shorter soliton pulse. However, the longer continuum pulse has a narrower spectrum and thus undergoes more gain than the spectrally broader soliton pulse.

soliton pulse is formed for all group delay dispersion values as long as the continuum loss is larger than the soliton loss [96Kae] or the pulses break up in two or more pulses [97Aus]. Thus, for smaller negative dispersion the pulse duration becomes shorter (2.1.74) until minimal pulse duration is reached. With no pulse-break-up, the minimal pulse duration is given when the loss for the continuum pulse becomes equal to the loss of the soliton pulse. When the soliton pulse is stable, then the saturated gain is equal to the loss:

$$g = l + l_\mathrm{s} \quad \text{with} \quad l_\mathrm{s} = \frac{D_\mathrm{g}}{3\tau^2} + q_0 \frac{E_\mathrm{sat,A}}{E_\mathrm{p}} \left[1 - \exp\left(-\frac{E_\mathrm{p}}{E_\mathrm{sat,A}}\right)\right] , \tag{2.1.75}$$

where l is the total saturated amplitude loss coefficient per cavity round trip (i.e. output coupler, residual cavity losses and nonsaturable absorber loss of the saturable absorber) and l_s the additional loss experienced by the soliton as a result of gain filtering (2.1.68) and the amplitude loss coefficient for saturation of the slow absorber (2.1.15). Soliton perturbation theory then determines the round-trip loss of the continuum pulse [96Kae]. The continuum is spread in time because of dispersion and therefore experiences enhanced loss in the recovering absorber that has been saturated by the much shorter soliton pulse.

We then predict a minimum pulse duration for a soliton pulse [95Kae1, 96Kae]:

$$\tau_\mathrm{p,min} = 1.7627 \left(\frac{1}{\sqrt{6}\,\Omega_\mathrm{g}}\right)^{3/4} \phi_\mathrm{s}^{-1/8} \left(\frac{\tau_\mathrm{A}\, g^{3/2}}{q_0}\right)^{1/4} \approx 0.45 \left(\frac{1}{\Delta\,\nu_\mathrm{g}}\right)^{3/4} \left(\frac{\tau_\mathrm{A}}{\Delta R}\right)^{1/4} \frac{g^{3/8}}{\phi_\mathrm{s}^{1/8}} , \tag{2.1.76}$$

where ϕ_s is the phase shift of the soliton per cavity round trip (assuming that the dominant SPM occurs in the laser gain medium), $\Delta\,\nu_\mathrm{g}$ the FWHM gain bandwidth and $\Delta R \approx 2q_0$ (2.1.6). With (2.1.73) then follows $\phi_\mathrm{s} = \phi_\mathrm{s}\,(z = 2L_\mathrm{g}) = k n_2 L_\mathrm{g} I_\mathrm{0,L} = \frac{1}{2}\delta_\mathrm{L} P_0$, where δ_L is the SPM coefficient (2.1.47) and P_0 the peak power inside the laser cavity. In (2.1.76) we assume a fully saturated slow saturable absorber and a linear approximation for the exponential decay of the slow saturable absorber. The analytical solution for soliton mode-locking (2.1.76) has been experimentally confirmed with a Ti:sapphire laser where a Fabry–Perot filter has been inserted to give a well-defined gain bandwidth [95Jun2]. However, this equation still does not tell us what soliton phase shift would be ideal. Equation (2.1.76) would suggest that very high values are preferred, which actually leads to instabilities. Also this equation is not taking into account that the soliton pulse may break up into two solitons which occurs more easily if the absorber is too strongly saturated. Numerical simulations can give better estimates for these open questions [01Pas1].

In soliton mode-locking, the dominant pulse-formation process is assumed to be soliton formation. Therefore, the pulse has to be a soliton for which the negative GVD is balanced with the SPM inside the laser cavity. The pulse duration is then given by the simple soliton solution (2.1.74). This means that the pulse duration scales linearly with the negative group delay dispersion inside the laser cavity (i.e. $\tau_p \propto |D|$). In the case of an ideal fast saturable absorber, an unchirped soliton pulse is only obtained at a very specific dispersion setting (2.1.69), whereas for soliton mode-locking an unchirped transform-limited soliton is obtained for all dispersion levels as long as the stability requirement against the continuum is fulfilled. This fact has been also used to experimentally confirm that soliton mode-locking is the dominant pulse-formation process and not a fast saturable absorber such as KLM [97Aus]. Higher-order dispersion only increases the pulse duration, therefore it is undesirable and is assumed to be compensated.

Solitons alone in the cavity are not stable. The continuum pulse is much longer and therefore experiences only the gain at line center, while the soliton exhibits an effectively lower average gain due to its larger bandwidth. Thus, the continuum exhibits a higher gain than the soliton. After a sufficient build-up time, the continuum would actually grow until it reaches lasing threshold, destabilizing the soliton. However, we can stabilize the soliton by introducing a relatively slow saturable absorber into the cavity. This absorber is fast enough to add sufficient additional loss for the growing continuum that spreads in time during its build-up phase so that it no longer reaches lasing threshold.

The break-up into two or even three pulses can be explained as follows: Beyond a certain pulse energy, two soliton pulses with lower power, longer duration, and narrower spectrum will be preferred, since their loss introduced by the limited gain bandwidth decreases so much that the slightly increased residual loss of the less saturated saturable absorber cannot compensate for it. This results in a lower total round-trip loss and thus a reduced saturated or average gain for two pulses compared to one pulse. The threshold for multiple pulsing is lower for shorter pulses, i.e. with spectra which are broad compared to the gain bandwidth of the laser. A more detailed description of multiple pulsing is given elsewhere [98Kae]. Numerical simulations show, however, that the tendency for pulse break-up in cases with strong absorber saturation is found to be significantly weaker than expected from simple gain/loss arguments [01Pas1].

To conclude, soliton shaping effects can allow for the generation of significantly shorter pulses, compared to cases without SPM and dispersion. The improvement is particularly large for absorbers with a relatively low modulation depth and when the absorber recovery is not too slow. In this regime, the pulse shaping is mainly done by the soliton effects, and the absorber is only needed to stabilize the solitons against growth of the continuum. The absorber parameters are generally not very critical. It is important not only to adjust the ratio of dispersion and SPM to obtain the desired soliton pulse duration (2.1.74), but also to keep their absolute values in a reasonable range where the nonlinear phase change is in the order of a few hundred mrad per round trip (i.e. significantly larger than acceptable in cases without negative dispersion). Soliton formation is generally very important in femtosecond lasers, which has been already recognized in colliding pulse mode-locked dye lasers. However, no analytic solution was presented for the soliton pulse shortening. It was always assumed that for a stable solution the mode-locking mechanism without soliton effects has to generate a net gain window as short as the pulse (Fig. 2.1.5a and b). In contrast to these cases, in soliton mode-locking we present an analytic solution based on soliton perturbation theory, where soliton pulse shaping is clearly assumed to be the dominant pulse formation process, and the saturable absorber required for a stable solution is treated as a perturbation. Then, the net gain window can be much longer than the pulse (Fig. 2.1.5c). Stability of the soliton against the continuum then determines the shortest possible pulse duration. This is a fundamentally different mode-locking model than previously described. We therefore refer to it as soliton mode-locking, emphasizing the fact that soliton pulse shaping is the dominant factor.

2.1.6.8 Design guidelines to prevent Q-switching instabilities

For picosecond solid-state lasers the self-amplitude modulation of a saturable absorber with a picosecond or tens of picoseconds recovery time is sufficient for stable pulse generation. A picosecond recovery time can be achieved with low-temperature grown semiconductor saturable absorbers where mid-gap defect states form very efficient traps for the photoexcited electrons in the conduction band (Sect. 2.1.4.3) . In the picosecond regime, we developed a very simple stability criterion for stable passive mode-locking without Q-switching instabilities [99Hoe1]:

$$E_\mathrm{p}^2 > E_\mathrm{p,c}^2 = E_\mathrm{sat,L} E_\mathrm{sat,A} \Delta R \,. \tag{2.1.77}$$

The critical intracavity pulse energy $E_\mathrm{p,c}$ is the minimum intracavity pulse energy, which is required to obtain stable cw mode-locking, that is, for $E_\mathrm{p} > E_\mathrm{p,c}$ we obtain stable cw mode-locking and for $E_\mathrm{p} < E_\mathrm{p,c}$ we obtain Q-switched mode-locking. For good stability of a mode-locked laser against unwanted fluctuations of pulse energy, operation close to the stability limit is not recommended. Thus, a large modulation depth supports shorter pulses (Table 2.1.11), but an upper limit is given by the onset of self-Q-switching instabilities (2.1.77).

In the femtosecond regime, we observe a significant reduction of the tendency of Q-switching instabilities compared to pure saturable absorber mode-locked picosecond lasers (2.1.77). This can be explained as follows: If the energy of an ultrashort pulse rises slightly due to relaxation oscillations, SPM and/or SAM broadens the pulse spectrum. A broader pulse spectrum, however, increases the loss due to the finite gain bandwidth, (2.1.68) and (2.1.74), which provides some negative feedback, thus decreasing the critical pulse energy which is necessary for stable cw mode-locking. The simple stability requirement of (2.1.77) then has to be modified as follows [99Hoe1]:

$$E_\mathrm{sat,L}\, g K^2 E_\mathrm{p}^2 + E_\mathrm{p}^2 > E_\mathrm{sat,L} E_\mathrm{sat,A} \Delta R \,, \tag{2.1.78}$$

where K is given by

$$K \equiv \frac{0.315}{1.76} \frac{2\pi\, n_2 L_\mathrm{g}}{D A_\mathrm{L} \lambda_0\, \Delta\, \nu_\mathrm{g}} \,. \tag{2.1.79}$$

Here we assume a standing-wave cavity and that the dominant SPM is produced in the laser medium. In other cases we have to add all other contributions as well.

Theoretical results for the QML threshold, (2.1.77)–(2.1.79), have generally been found to be in good agreement with experimental values. However, inverse saturable absorption can show some significant improvement of the QML threshold. Two-Photon Absorption (TPA) has been widely used for optical power limiter [86Wal] and a roll-over which lowers the Q-switching threshold [99Tho]. In addition, for some recent high-repetition-rate lasers [04Pas] the QML threshold was found to be significantly lower than expected even taking into account TPA. It was shown that for some Er:Yb:glass lasers this could be explained with modified saturation characteristics of the used SESAMs, namely with a roll-over of the nonlinear reflectivity for higher pulse fluences [04Sch1]. However, for picosecond pulse durations TPA cannot explain the observed significant roll-over (Fig. 2.1.18). The reflectivity of a SESAM is generally expected to increase with increasing pulse energy. However, for higher pulse energies the reflectivity can decrease again; we call this a "roll-over" of the nonlinear reflectivity curve caused by inverse saturable absorption (Fig. 2.1.18). We showed for several SESAMs that the measured roll-over is consistent with TPA only for short (femtosecond) pulses, while a stronger kind of nonlinear absorption is dominant for longer (picosecond) pulses [05Gra2]. The QML threshold criteria of (2.1.77) then have to be modified to [05Gra2]

$$E_\mathrm{p}^2 > \frac{E_\mathrm{sat,A}\, \Delta R}{\dfrac{1}{E_\mathrm{sat,L}} + \dfrac{1}{A_\mathrm{A} F_2}} \,. \tag{2.1.80}$$

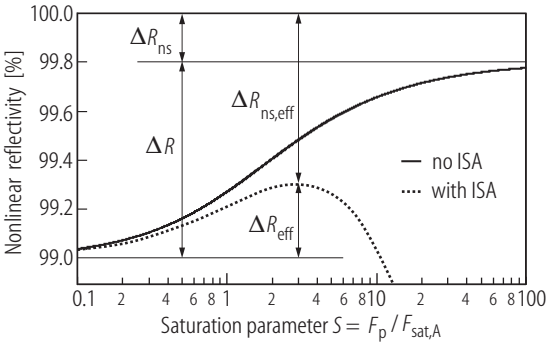

Fig. 2.1.18. Nonlinear reflectivity as function of saturation parameter S which is equal to $F_\mathrm{p}/F_\mathrm{sat,A}$. F_p is the pulse fluence incident on the absorber mirror (i.e. pulse energy density) and $F_\mathrm{sat,A}$ is the saturation fluence of the absorber mirror. Inverse saturable absorption decreases the reflectivity at higher pulse energies such that a "roll-over" is observed. This decreases the effective modulation depth and increases the effective nonsaturable absorption. However, it improves the Q-switching mode-locking threshold.

For $F_2 \to \infty$ (i.e. without induced nonlinear losses) we retrieve the simpler equation (2.1.77). F_2 is the inverse slope of the induced absorption effect and can be determined from nonlinear SESAM reflectivity measurements (Fig. 2.1.18) [05Gra2, 04Hai]:

$$R_\mathrm{ISA}(F_\mathrm{p}) = R(F_\mathrm{p}) - \frac{F_\mathrm{p}}{F_2}\,, \tag{2.1.81}$$

where F_p is the pulse fluence incident on the SESAM (i.e. pulse energy density), $R(F_\mathrm{p})$ the measured nonlinear reflectivity without Inverse Saturable Absorption (ISA) and $R_\mathrm{ISA}(F_\mathrm{p})$ the measured reflectivity with inverse saturable absorption. The smaller the inverse slope of the roll-over F_2, the stronger is the roll-over. The stronger the roll-over, the smaller the maximum modulation depth of the SESAM.

2.1.6.9 External pulse compression

SPM generates extra frequency components. The superposition with the other frequency components in the pulse can spectrally broaden the pulse (i.e. for positively chirped pulses assuming $n_2 > 0$). SPM alone does not modify the pulse width, but with proper dispersion compensation a much shorter pulse can be generated with the extra bandwidth [80Mol]. The positively chirped spectrally broadened pulse then can be compressed with appropriate negative dispersion compensation, where the "blue" spectral components have to be advanced relative to the "red" ones. A careful balance between a nonlinear spectral broadening process and negative dispersion is needed for efficient compression of a pulse. Typically, self-phase modulation in a single-mode fiber with optimized length was used to linearly chirp the pulse, which is then compressed with a grating pair compressor [84Tom].

Ultimately, uncompensated higher-order dispersion and higher-order nonlinearities limit compression schemes. For pulses shorter than 100 fs, compression is typically limited to factors of less than 10. Compression of amplified CPM dye laser pulses with 50 fs duration produced the long-standing world record of 6 fs [87For]. Similar concepts have been used for external pulse compression of 13-fs pulses from a cavity-dumped Ti:sapphire laser [97Bal] and of 20-fs pulses from a Ti:sapphire laser amplifier [97Nis] resulting, in both cases, in approximately 4.5-fs pulses. In the latter case, the use of a noble-gas-filled hollow fiber instead of a normal fiber allows for much higher pulse energies. For example, pulse energies of about 0.5 mJ with 5.2-fs pulses and a peak power of 0.1 TW [97Sar]. More recently, adaptive pulse compression of a super-continuum produced in two cascaded hollow fibers generated 3.8-fs pulses with energies of up to 15 μJ [03Sch]. Further improvements resulted in 3.4-fs pulses but with only 500 nJ pulse energies [03Yam]. The pulse duration was fully characterized by Spectral-Phase Interferometry for Direct Electric-field Reconstruction (SPIDER) (Sect. 2.1.7.3). This is currently the world record in the visible and near-infrared spectral regime.

The extra bandwidth obtained with SPM can be extremely large producing a white-light continuum [83For], which can be used as a seed for broadband parametric amplification. Parametric processes can provide amplification with an even broader bandwidth than can typically be achieved in laser amplifiers. Noncollinear phase-matching at a crossing angle of 3.8 ° in beta barium borate (BBO) provides more than 150 THz amplification bandwidth [95Gal]. With this type of set-up, parametric amplification has been successfully demonstrated with pulse durations of less than 5 fs [99Shi, 02Zav].

2.1.7 Pulse characterization

2.1.7.1 Electronic techniques

Electronic techniques for pulse-width measurements are typically limited to the picosecond regime. Photodetectors and sampling heads with bandwidths up to 60 GHz are commercially available. This means that the measured pulse duration is limited to about 7 ps. This follows from simple linear system analysis for which the impulse response of a photodetector or a sampling head can be approximated by a Gauss-function. The impulse response for a given system bandwidth B has a FWHM τ_{FWHM} in units of ps:

$$\tau_{\mathrm{FWHM}}\ [\mathrm{ps}] \approx \frac{312\ \mathrm{GHz}}{B\ [\mathrm{GHz}]}\ . \tag{2.1.82}$$

The impulse response of a measurement system can be determined from the impulse response of each element in the detection chain:

$$\tau^2_{\mathrm{FWHM}} = \sqrt{\tau_1^2 + \tau_2^2 + \tau_3^2 + \dots}\ , \tag{2.1.83}$$

where for example τ_1 is the FWHM of the impulse response of the photodetector, τ_2 of the sampling head and so on. Thus, with a 40 GHz sampling head and a 60 GHz photodetector we only measure a impulse response with FWHM of 9.4 ps.

2.1.7.2 Optical autocorrelation

Optical autocorrelation techniques with second-harmonic generation of two identical pulses that are delayed with respect to each other are typically used to measure shorter pulses [80Sal, 83Wei]. We distinguish between collinear and non-collinear intensity autocorrelation measurements for which the two pulse beams in the nonlinear crystal are either collinear or non-collinear. In the non-collinear case the second-harmonic signal only depends on the pulse overlap and is given by

$$I_{2\omega}\left(\Delta t\right) \propto \int I\left(t\right) I\left(t - \Delta t\right) \mathrm{d}t\ . \tag{2.1.84}$$

The FWHM of the autocorrelation signal $I_{2\omega}\left(\Delta t\right)$ is given by τ_{Au} and determines the FWHM pulse duration τ_{p} of the incoming pulse $I\left(t\right)$. However, τ_{Au} depends on the specific pulse shape (Table 2.1.13) and any phase information is lost in this measurement. So normally, transform-limited pulses are assumed. This assumption is only justified as long as the measured spectrum also agrees with the assumption of pulse shape and constant phase (i.e. the time–bandwidth product corresponds to a transform-limited pulse, Table 2.1.13). For passively mode-locked lasers, for

Table 2.1.13. Optical pulses: defining equations for Gaussian and soliton pulse shapes, FWHM (full-width-half-maximum) intensity pulse duration τ_p, time–bandwidth products $\Delta\nu_\mathrm{p}\tau_\mathrm{p}$ for which $\Delta\nu_\mathrm{p}$ is the FWHM of the spectral intensity, FWHM intensity autocorrelation pulse duration τ_Au.

Pulse shape	τ_p/τ	$\Delta\nu_\mathrm{p}\tau_\mathrm{p}$	$\tau_\mathrm{p}/\tau_\mathrm{Au}$
Gauss: $I(t) \propto \exp\left(\frac{t^2}{\tau^2}\right)$	$2\sqrt{\ln 2}$	0.4413	0.7071
Soliton: $I(t) \propto \mathrm{sech}^2\left(\frac{t}{\tau}\right)$	1.7627	0.3148	0.6482

example, that allow for parabolic approximation of pulse-formation mechanisms one expects a sech^2 temporal and spectral pulse shape (Sects. 2.1.6.4–2.1.6.7). Passively mode-locked solid-state lasers with pulse durations well above 10 fs normally generate pulses close to this ideal sech^2-shape. Therefore, this non-collinear autocorrelation technique is a good standard diagnostic for such laser sources. For ultrashort pulse generation in the sub-10-fs regime this is generally not the case anymore. Experimentally, this is clearly indicated by more complex pulse spectra.

Interferometric AutoCorrelation (IAC) techniques [83Min] have been used to get more information. In IAC a collinear intensity autocorrelation is fringe-resolved and gives some indication how well the pulse is transform-limited. However, we still do not obtain full phase information about the pulse. The temporal parameters have usually been obtained by fitting an analytical pulse shape with constant phase to the autocorrelation measurement. Theoretical models of the pulse-formation process motivate the particular fitting function. For lasers obeying such a model the a-priori assumption of a theoretically predicted pulse shape is well-motivated and leads to good estimates of the pulse duration as long as the measured spectrum also agrees with the theoretical prediction. However, we have seen that fits to an IAC trace with a more complex pulse spectrum tend to underestimate the true duration of the pulses. Problems with IAC measurement for ultrashort pulses are also discussed in the two-optical-cycle regime [04Yam].

For few-cycle pulses, a limitation in a noncollinear beam geometry arises because of the finite crossing angle of two beams. In this case the temporal delay between two beams is different in the center and in the wings of the spatial beam profile. This geometrical artifact results in a measured pulse duration that is longer than the actual pulse duration τ_p:

$$\tau_\mathrm{p,meas}^2 = \tau_\mathrm{p}^2 + \delta\tau^2 \,. \tag{2.1.85}$$

For a beam diameter d and a crossing angle θ between the two beams this results in an $\delta\tau$ of

$$\delta\tau = \sqrt{2}\,\frac{d}{c}\tan\frac{\theta}{2} \approx \frac{\theta\, d}{\sqrt{2}\, c} \tag{2.1.86}$$

with the speed of light c and the additional approximation for a small crossing angle θ. For example a crossing angle of 1.7° and a beam diameter of 30 µm results in $\delta\tau = 2.1$ fs. For an actual pulse duration of 10 fs (resp. 5 fs) this gives a measured pulse duration of 10.2 fs (resp. 5.4 fs) which corresponds to an error of 2 % (resp. 8 %). This means this becomes more severe for pulse durations in the few-cycle regime. However, if the crossing angle is significantly increased this can become also more important for longer pulses. For this reason, in the few-cycle-pulse-width regime collinear geometries have always been preferred to avoid geometrical blurring artifacts and to prevent temporal resolution from being reduced.

2.1.7.3 New techniques: FROG, FROG-CRAB, SPIDER, ...

For a more precise measurement, a variety of methods have been proposed to fully reconstruct both pulse amplitude and phase from measured data only [91Chi, 93Kan, 95Chu2, 96Rhe, 98Iac]. Initially, especially Frequency-Resolved Optical Gating (FROG, [93Kan, 97Tre]) and Spectral Phase Interferometry for Direct Electric-field Reconstruction (SPIDER, [98Iac, 99Iac]) have found widespread use.

2.1.7.3.1 FROG, SHG-FROG, FROG-CRAB

Frequency-Resolved Optical Gating (FROG) [93Kan, 97Tre] is a characterization method based on the measurement of a spectrally resolved autocorrelation signal followed by an iterative phase-retrieval algorithm to extract the intensity and phase of the laser pulse. In a general sense the FROG technique uses a gate $G(t)$ that is being used to measure the spectrum $S(\omega,\tau)$ of a series of temporal slices:

$$S(\omega,\tau) = \left| \int G(t-\tau)\, E(t)\, \mathrm{e}^{\mathrm{i}\omega t} \mathrm{d}t \right|^2 , \tag{2.1.87}$$

where $E(t)$ is the electric field of the pulse that needs to be characterized and τ the time delay between the gate and the pulse. The gate can either be an amplitude or phase gate [93Bec, 03Kan]. The most commonly used FROG is based on an amplitude gate using Second-Harmonic Generation (SHG) and the pulse that needs to be characterized (i.e. "blind FROG" because the gate is unknown):

$$G(t) = \chi^{(2)} E(t) \ . \tag{2.1.88}$$

This is generally referred to as SHG-FROG. Collinear SHG-FROG has been demonstrated using type II phase matching in the 20-fs [99Fit] and sub-10-fs [00Gal1] pulse-width regime. An example for a phase gate would be cross phase modulation using again the same pulse for the gate:

$$G(t) = \exp\left(-\mathrm{i}kn_2 \left|E(t)\right|^2\right) \ . \tag{2.1.89}$$

The iterative retrieval algorithm is not very intuitive and rather complex and is based on a Principal Component Generalized Projections Algorithm (PCGPA) which starts in an initial guess for $G(t)$ and $E(t)$ that is than being compared to the measured $S(\omega,\tau)$ [99Kan]. For femtosecond pulses in the visible to infrared regime nonlinear optics can be used to obtain very good FROG traces.

In the XUV and attosecond-pulse-width regime this becomes more complicated. We basically need a non-stationary filter in the XUV with a response time on the order of the attosecond-pulse duration. A phase gate can be obtained using photoionization of an atom in the presence of a weak InfraRed (IR) pulse that has been used to generate the attosecond pulses and therefore is precisely synchronized. As long as the XUV pulse is shorter than the IR period the temporal information of the XUV pulse is mapped into the electron energy distribution in the linear part of the optical IR field. This technique is referred to as Frequency-Resolved Optical Gating for Complete Reconstruction of Attosecond Burst (FROG-CRAB) where the linear phase modulation is obtained through the photoionization of atoms by the short XUV pulse in the presence of a weak linear part of the IR field and the spectrometer is being replaced by the electron energy detection [05Mai]. The XUV pulse is then converted in a modulated electron wave packet.

2.1.7.3.2 SPIDER

Spectral Phase Interferometry for Direct Electric-field Reconstruction (SPIDER) measures the spectral interference of a pulse with a frequency-shifted replica [98Iac, 99Iac]:

$$S(\omega,\tau) = \left|\tilde{E}(\omega-\omega_0) + \tilde{E}(\omega-\omega_0-\delta\omega)\,\mathrm{e}^{\mathrm{i}\omega\tau}\right|^2 , \tag{2.1.90}$$

where $\tilde{E}(\omega)$ is the Fourier-transformation of the electric field $E(t)$. To access the spectral phase it is necessary to produce two time-delayed replicas by a predetermined delay τ of the pulse and with a spectral shear $\delta\omega$ between their carrier frequencies. The spectral shear between the central frequencies of the two replicas is generated by upconversion of the two replicas with a strongly chirped pulse using sum-frequency generation in a nonlinear optical crystal. The strongly chirped pulse is generated by propagating another copy of the original pulse through a thick glass block. The spectral shear arises because the time delay between the replicas assures that each replica is upconverted with a different portion of the chirped pulse containing a different instantaneous frequency [99Gal]. The time delay τ between the replica is kept constant during the measurements and therefore only a 1D trace needs to be measured for the resulting SPIDER interferogram

$$\begin{aligned} I_{\mathrm{SPIDER}}(\omega) = {} & \left|\tilde{E}(\omega)\right|^2 + \left|\tilde{E}(\omega+\delta\omega)\right|^2 \\ & +2\left|\tilde{E}(\omega)\tilde{E}(\omega+\delta\omega)\right| \cos\left[\varphi(\omega+\delta\omega)-\varphi(\omega)+\omega\tau\right] . \end{aligned} \tag{2.1.91}$$

The phase information can be extracted from the cosine term by the following, purely algebraic, method: The Fourier transform to the time domain of the SPIDER interferogram consists of a peak at zero time and two side peaks located near τ and $-\tau$. The two side peaks contain equivalent phase information and are equal. One of the peaks is isolated by applying a suitable filter function and an inverse Fourier transform back to the frequency domain yields a complex function $z(\omega)$, whose complex phase gives access to the pulse spectral phase: $\arg(z(\omega)) = \varphi(\omega+\delta\omega)-\varphi(\omega)+\omega\tau$. A separate measurement of the linear phase term $\omega\tau$ by spectral interferometry of the short unsheared pulse replicas is subtracted from the previous expression to yield the spectral phase difference $\Delta\varphi(\omega) = \varphi(\omega+\delta\omega)-\varphi(\omega)$. From an arbitrarily chosen starting frequency ω_0 one obtains the spectral phase $\varphi(\omega)$ at evenly spaced frequencies $\omega_i = \omega_0 + i\cdot\delta\omega$ by the following concatenation procedure:

$$\begin{aligned} &\varphi(\omega_0) = \varphi_0 , \\ &\varphi(\omega_1) = \Delta\varphi(\omega_0)+\varphi(\omega_0) = \varphi(\omega_0+\delta\omega)-\varphi(\omega_0)+\varphi(\omega_0) = \varphi(\omega_0+1\cdot\delta\omega) , \\ &\vdots \\ &\varphi(\omega_{i+1}) = \Delta\varphi(\omega_i)+\varphi(\omega_i) . \end{aligned} \tag{2.1.92}$$

The constant φ_0 remains undetermined but is only an offset to the spectral phase, which does not affect the temporal pulse shape and we may thus set it equal to zero. The spectral phase is written as:

$$\varphi(\omega_{i+1}) = \sum_{k=0}^{i} \Delta\varphi(\omega_k) . \tag{2.1.93}$$

If $\delta\omega$ is small relative to features in the spectral phase, $\Delta\varphi(\omega)$ corresponds in first order to the first derivative of the spectral phase and we can approximate the spectral phase by:

$$\varphi(\omega) \simeq \frac{1}{\delta\omega}\int_{\omega_0}^{\omega} \Delta\varphi(\omega')\,\mathrm{d}\omega' . \tag{2.1.94}$$

The integral expression for the spectral phase has the advantage that all the measured sampling points of the interferogram can be used instead of only using a subset with sampling according

to the spectral shear as with the concatenation method. The phase information of the resulting interferogram allows the direct reconstruction of the spectral phase of the input pulse. Combined with the measured spectrum of the pulse the actual pulse can be calculated without any prior assumptions.

Three design parameters determine the range of pulse durations that can be measured by a certain SPIDER apparatus: the delay τ, the spectral shear $\delta\omega$ and the group-delay dispersion $\mathrm{GDD_{up}}$ used to generate the strongly linearly chirped upconverter pulse. These three parameters are related as:

$$\delta\omega = \frac{\tau}{\mathrm{GDD_{up}}} \,. \tag{2.1.95}$$

The delay τ, which determines the positions of the two side peaks of the Fourier transform of the interferogram, is chosen in such a way as to assure that the side peaks are well-separated from the center peak. On the other hand, the fringe spacing of the interferogram is proportional to $2\pi/\tau$ and thus τ must be sufficiently small such that the spectrometer is able to fully resolve the fringes. The stretching factor $\mathrm{GDD_{up}}$ is then chosen such that the spectral shear $\delta\omega$, which determines the sampling interval of the reconstructed spectral phase, is small enough to assure correct reconstruction of the electric field in the time domain according to the Whittaker–Shannon sampling theorem [00Dor]. The constrained relationship for τ and $\delta\omega$ expressed by (2.1.95) means that with a particular SPIDER setup, only pulses with a limited range of pulse durations can be measured. A set-up for the sub-10-femtosecond regime in described in [99Gal].

2.1.7.3.3 Comparison between FROG and SPIDER techniques

The highest acquisition rates for single-shot pulse characterization reported so far were 1 kHz using SPIDER [03Kor] and 30 Hz using FROG [03Gar]. FROG is not well suited for high acquisition rates for two reasons: FROG requires the measurement of a 2D trace which makes the acquisition itself inherently slow and moreover the FROG algorithm uses an iterative process which requires a minimum number of steps for convergence depending on the complexity of the measured pulse. SPIDER however only requires the acquisition of two 1D spectra: the so-called SPIDER interferogram and the optical spectrum of the pulse. Furthermore, the SPIDER algorithm is deterministic since it is based on two Fourier transforms with intermittent spectral filtering to reconstruct the spectral phase of the pulse. An additional Fourier transform is then required to calculate the electric field in the time domain and therefore the pulse reconstruction is fast. SPIDER is thus well suited for high acquisition rates and real-time operation. SPIDER has been shown to achieve high accuracy, i.e. the reconstructed electric field matches well with the physical field of the pulse [02Dor1], and high precision [02Dor2], implying a small spread between several reconstructions of the field obtained from the same data. In particular the SPIDER technique is reliable in the presence of limited experimental noise [00And, 04Jen]. SPIDER offers more bandwidth than any other technique and we even can measure pulses in the single-cycle regime [03Sch]. In addition, SPIDER still gives valid results even if the beam profile is not spatially coherent anymore because we can spatially resolve these measurements [01Gal]. A direct comparison between FROG and SPIDER techniques in the sub-10-femtosecond regime is given in [00Gal2].

Only fully characterized pulses in phase and amplitude will provide reliable information about pulse shape and pulse duration – this becomes even more important for pulses with very broad and complex spectra. In such a situation any other technique, such as fitting attempts to IAC traces, is very erroneous and generally underestimates the pulse duration.

2.1.8 Carrier envelope offset (CEO)

Progress in ultrashort pulse generation [99Ste] has reached a level where the slowly-varying-envelope approximation starts to fail. Pulse durations of Ti:sapphire laser oscillators have reached around 5 fs which is so short that only about two optical cycles of the underlying electric field fit into the full-width half maximum of the pulse envelope. For such short pulses the maximum electric-field strength depends strongly on the exact position of the electric field with regards to the pulse envelope, i.e. the Carrier Envelope Offset (CEO) [99Tel]. In passively mode-locked lasers this carrier envelope offset is a freely varying parameter because the steady-state boundary condition only requires that the pulse envelope is the same after one round trip (Fig. 2.1.19). Therefore the CEO phase may exhibit large fluctuations, even when all other laser parameters are stabilized. We have discussed the physical origin of these fluctuations before [02Hel2, 02Hel1]. Because nonlinear laser–matter interaction depends strongly on the strength of the electric field, this CEO fluctuations cause strong signal fluctuations in nonlinear experiments such as high-harmonic generation [00Bra], attosecond pulse generation [01Dre], photoelectron emission [01Pau1] etc.

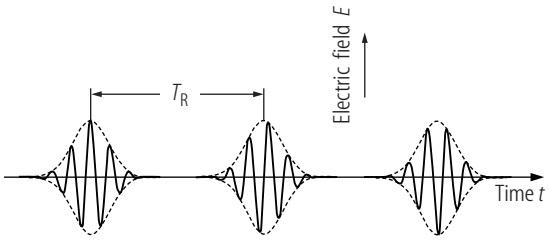

Fig. 2.1.19. Electric field $E(t)$ of three subsequent pulses from a mode-locked laser with a pulse repetition rate of $T_R = 1/f_{rep}$. The envelope $\pm A(t)$ is shown as dashed lines. The electric-field patterns of the pulses experience large pulse-to-pulse fluctuations.

Different techniques have been proposed to stabilize these CEO fluctuations in the time domain [96Xu1] and in the frequency domain [99Tel]. The frequency-domain technique is based on the frequency comb generated from mode-locked lasers (Sect. 2.1.2.2) and is much more sensitive and is the technique that is being used today. Optical frequency comb techniques recently received a lot of attention and were also an important part of the 2005 Nobel Prize in Physics for Theodor W. Hänsch and John L. Hall in the area of laser-based precision spectroscopy [05Nob].

In the following we follow the notation and derivation of Helbing et al. [03Hel]. A very stable frequency comb is generated with a mode-locked laser which follows directly from the time domain:

$$E_{\text{train}}(t) = A(t)\exp\left(\mathrm{i}\omega_c t + \mathrm{i}\varphi_0(t)\right) \otimes \sum_{m=-\infty}^{+\infty} \delta\left(t - mT_R\right) , \tag{2.1.96}$$

where $E_{\text{train}}(t)$ is the electric field of a pulse train (Fig. 2.1.19), ω_c is the (angular) carrier frequency which is the center of gravity of the mode-locked spectrum, $A(t)$ the pulse envelope, and $\varphi_0(t)$ the absolute phase of the pulse. The *change* of the carrier-envelope offset phase φ_0 in (2.1.96) *per round trip* is given by:

$$\Delta\varphi_0 = \Delta\varphi_{\,\text{GPO}} \mod 2\pi . \tag{2.1.97}$$

The Group-Phase Offset (GPO) only arises from the first-order dispersion of the material along the beam path:

$$\Delta\varphi_{\,\text{GPO}} = -\omega \int_0^L \left(\frac{1}{v_g} - \frac{1}{v_p}\right) \mathrm{d}x = \int_0^L \frac{\omega^2}{c} \frac{\mathrm{d}n(\omega, x)}{\mathrm{d}\omega} \mathrm{d}x , \tag{2.1.98}$$

where v_g is the group velocity and v_p is the phase velocity (Table 2.1.7).

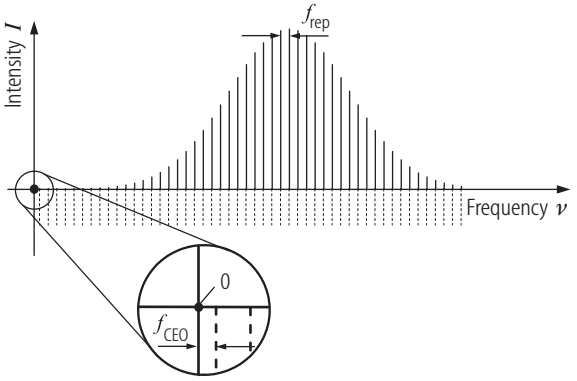

Fig. 2.1.20. Equidistant frequency comb of a mode-locked laser. The comb lines are spaced by the repetition rate f_{rep} and exhibit a non-vanishing offset frequency f_{CEO} at zero frequency unless the electric field pattern exactly reproduces from pulse to pulse.

We define the (angular) carrier-envelope offset frequency as

$$2\pi\, f_{\mathrm{CEO}} = \omega_{\mathrm{CEO}} = \Delta\varphi_0 f_{\mathrm{rep}} = \frac{\Delta\varphi_0}{T_{\mathrm{R}}} \equiv \frac{\Delta\varphi_{\mathrm{GPO}}}{T_{\mathrm{R}}} \mod 2\pi \equiv \left(\frac{\partial}{\partial t}\,\varphi_{\mathrm{GPO}}\right) \mod 2\pi\,. \tag{2.1.99}$$

Taking into account the varying carrier-envelope offset phase the electric field of the pulse train becomes:

$$E_{\mathrm{train}}(t) = A(t)\exp\left(\mathrm{i}\omega_{\mathrm{c}}t + \mathrm{i}\,\omega_{\mathrm{CEO}}\,t\right) \otimes \sum_{m=-\infty}^{+\infty} \delta\left(t - mT_{\mathrm{R}}\right)\,. \tag{2.1.100}$$

The Fourier-transformation of (2.1.100) then results in the frequency comb as shown in Fig. 2.1.20:

$$\tilde{E}_{\mathrm{train}}(f) = \tilde{A}\left(f - f_{\mathrm{c}}\right) \cdot \sum_{m=-\infty}^{+\infty} \delta\left(f - mf_{\mathrm{rep}} - f_{\mathrm{CEO}}\right)\,. \tag{2.1.101}$$

The whole equidistant frequency comb is shifted by f_{CEO} due to the per round trip carrier-envelope offset phase shift of $\Delta\varphi_0$. Therefore, a mode-locked laser generates an equidistant frequency comb with a frequency step given by the pulse repetition frequency f_{rep} which can be measured and stabilized with very high precision [86Lin, 86Rod, 89Rod, 89Kel]. The uniformity of the mode-locked frequency comb has been demonstrated to a relative uncertainty below 10^{-15} [99Ude]. The timing jitter in the arrival time of the pulses (i.e. variations in f_{rep}) produces a "breathing" of the fully equidistant frequency comb. The additional freedom of the frequency offset to DC of this frequency comb is given by the CEO frequency f_{CEO} (Fig. 2.1.20) and every "tick of the frequency ruler" then can be described by [99Tel]

$$f_m = mf_{\mathrm{rep}} + f_{\mathrm{CEO}} \tag{2.1.102}$$

with m being an integer number. The timing jitter of the CEO results in a translation of the full frequency comb. Note that the equidistant frequency-comb spacing is given by the round-trip propagation time of the pulse envelope (i.e. by the group velocity and not the phase velocity). This means that the axial modes of a mode-locked laser are not the same as the ones from a cw laser for which the phase velocity determines the axial mode spacing.

Even though a measurement of the repetition rate is straightforward, it is virtually impossible to access the CEO-frequency directly, as the laser spectrum contains no energy close to zero frequency. One therefore has to use an indirect way to measure the second comb parameter. Depending on the available optical bandwidth different techniques have been proposed by Telle et al. [99Tel] such as f-to-$2f$, $2f$-to-$3f$ heterodyne techniques and others. Selecting some low-frequency portion of the comb and frequency doubling it gives rise to the comb

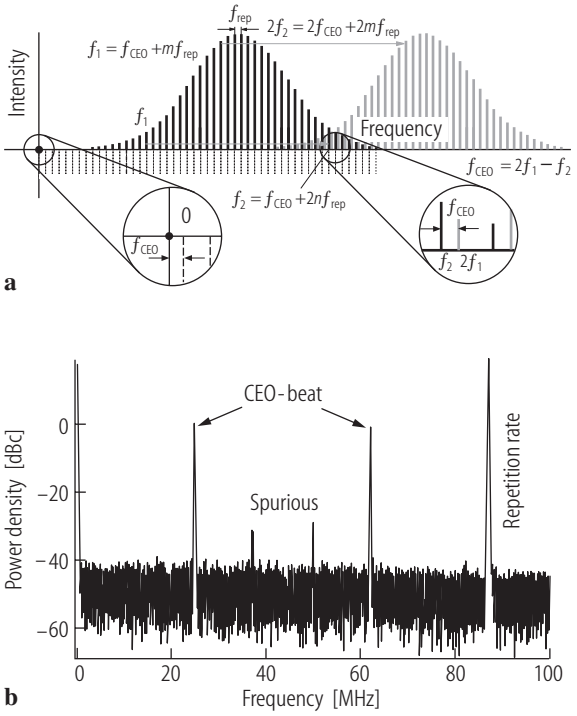

Fig. 2.1.21. f-to-$2f$ interference technique to measure the CEO frequency according to [99Tel]: (**a**) Mode beating of fundamental and second harmonic frequency comb results in the carrier envelope offset frequency $f_{\mathrm{CEO}} = 2f_1 - f_2$, where f_{rep} is the pulse repetition rate frequency, f_{CEO} is the carrier envelope offset frequency and m is an integer number. (**b**) Mode beating signal measurement with a microwave spectrum analyzer which shows a strong peak at the pulse repetition rate and the two CEO beats at f_{CEO} and $f_{\mathrm{rep}} - f_{\mathrm{CEO}}$ with a signal-to-noise ratio of more than 40 dB. This is ideal for a stabilizing feedback loop using a weak modulation of the pump laser power to compensate for the CEO fluctuations.

$$2f_m = 2f_{\mathrm{CEO}} + 2mf_{\mathrm{rep}} \; . \tag{2.1.103}$$

If the fundamental comb spectrum covers more than an optical octave it will also contain modes at

$$f_{2m} = f_{\mathrm{CEO}} + 2mf_{\mathrm{rep}} \; . \tag{2.1.104}$$

Beating the combs of (2.1.103) and (2.1.104), therefore extracts the CEO-frequency from the comb spectrum [99Tel]:

$$f_{\mathrm{CEO}} = 2f_m - f_{2m} = (2f_{\mathrm{CEO}} + 2mf_{\mathrm{rep}}) - (f_{\mathrm{CEO}} + 2mf_{\mathrm{rep}}) \; , \tag{2.1.105}$$

see Fig. 2.1.21. Today the most common technique is based on this f-to-$2f$ heterodyne technique because of its simplicity and because an octave-spanning spectrum can be generated with external spectral broadening in a microstructure fiber for example [00Jon, 00Apo]. With this technique we achieved a long-term CEO stabilization with residual 10 attosecond timing jitter which corresponds to 0.025 rad rms CEO phase noise in a (0.01 Hz–100 kHz) bandwidth [02Hel1]. The f-to-$2f$ interference technique requires an octave-spanning spectrum. So far, all attempts to generate this spectrum directly from a laser source have only reached unsatisfactory control of the CEO frequency, which was mainly caused by poor signal strength. Therefore most experiments required additional spectral broadening, e.g. in an external microstructure fiber. The continuum generation process with its strong nonlinearity, however, introduces additional CEO noise. It is important to note that the CEO stabilization is achieved for the pulses *after* the microstructure fiber, which means that the pulses directly from the Ti:sapphire laser will exhibit excess CEO phase noise even with a perfectly working CEO stabilization.

The relative phase between the carrier and the envelope of an optical pulse is the key parameter linking the fields of precision frequency metrology and ultrafast laser physics. As we have discussed, the spectrum of a mode-locked laser consists of a comb of precisely equally spaced frequencies. The uniformity of this frequency comb has been demonstrated to a relative uncertainty below 10^{-15}

[99Ude]. Knowledge of only two parameters, the comb spacing and a common offset frequency of all modes, provides one with a set of reference frequencies, similar to the tick marks on a ruler. The beat (difference-frequency) signal of this unknown frequency with the closest frequency in the ruler always gives a beat signal smaller than the comb period. Thus, an optical frequency in the 100 THz regime can be translated down to a microwave frequency in the range of 100 MHz, which can then be measured very accurately. This can be used for an all-optical atomic clock that is expected to outperform today's state-of-the-art cesium clocks [02Ude]. The mode-locked laser provides a phase-locked clockwork mediating between radio frequencies and the Terahertz frequencies of the lines in the optical comb, effectively rendering optical frequencies countable. Details on precision frequency measurements with mode-locked laser combs can be found in [99Rei, 01Hol, 01Cun, 02Bau].

2.1.9 Conclusion and outlook

We have shown that the technology of ultrafast lasers has become very refined and is now suitable for application in many areas. Points of particular importance in this respect are:

- The transition from dye lasers to solid-state lasers, which can be compact, powerful, efficient and long-lived. It has been shown that solid-state lasers can generate pulses which are even shorter pulses than those generated in dye lasers with much more average output power.
- The development of high-power and high-brightness diode lasers for direct pumping of solid-state lasers. This has lead not only to very efficient and compact lasers, but also to lasers with more than 1000 W of average output power.
- The development of novel saturable absorbers such as KLM which has pushed the frontier in ultrashort pulse duration into the two-optical-cycle regime using novel chirped mirrors for dispersion compensation. New parameters such as the Carrier Envelope Offset (CEO) of the electric field underneath the pulse envelope have become important for many different applications.
- The development of SEmiconductor Saturable Absorber Mirrors (SESAMs) which passively mode-lock many different diode-pumped solid-state lasers without Q-switching instabilities and can be optimized for operation in very different parameter regimes such as laser wavelength, pulse duration, pulse repetition rate and power levels. SESAMs can be optimized independently of the cavity design. This allowed for pushing the frontier in ultrafast solid-state lasers by several orders of magnitude: femtosecond mode-locked lasers with close to 100 W of average output power and more than 1 μJ of pulse energies and different lasers with high pulse repetition rates up to 160 GHz have been demonstrated so far.

For the next few years we expect many new exciting developments in the field of diode-pumped solid-state lasers:

- Very high power levels ($>$ 100 W of average power) should become possible with passively mode-locked thin-disk lasers. Pulse durations just below 1 ps are feasible and with new materials the regime of 200 fs or even below should become accessible with similarly high powers.
- Nonlinear frequency conversion stages (based on second-harmonic generation, sum frequency mixing, or parametric oscillation) will be pumped with high-power mode-locked lasers to generate short and powerful pulses at other wavelengths. The high power makes the nonlinear conversion efficiencies very high with very simple arrangements [01Sue, 05Mar]. This will be of interest for application in large-screen RGB display systems, for example [04Bru, 06Inn].
- Simple external pulse compression combined with novel high-average-power solid-state lasers now allows for peak intensities as high as 12 MW with 33-fs pulses at the full pulse repetition rate of the laser oscillator [03Sue]. This could be focused to a peak intensity of 10^{14} W/cm^2, a

regime where high-field laser physics such as high-harmonic generation [88Fer, 94Lew, 98Sal] and laser-plasma-generated X-rays [91Mur] are possible at more than 10 MHz pulse repetition rate. This improves signal-to-noise ratios in measurements by 4 orders of magnitude compared to the standard sources at kHz repetition rates. This would be important for low-power applications such as X-ray imaging and microscopy [02Sch1], femtosecond EUV and soft-X-ray photoelectron spectroscopy [01Bau] and ultrafast X-ray diffraction [99Sid, 01Rou].

- Very high pulse repetition rates with $\gtrsim 100$ GHz should be possible from passively mode-locked diode-pumped solid-state lasers at different wavelengths, even in the wavelength range around 1.5 μm and 1.3 μm for telecom applications.
- As an alternative to ion-doped gain media at high pulse-repetition rates (i.e. > 1 GHz) optically pumped VECSELs and even hopefully electrically pumped VECSELs will become very interesting alternatives [06Kel]. The integration of the SESAM into the VECSEL structure will provide even more compact ultrafast lasers [07Maa].
- So far octave-spanning frequency combs have been mostly generated with KLM Ti:sapphire lasers and supercontinuum generation in a microstructured fiber. However, many applications need more compact sources. The progress in femtosecond diode-pumped solid-state lasers and VECSELs reported here will make this possible in the near future.

Thus, all these examples show that the development of ultrafast diode-pumped sources has not come to its end but will continue to deliver superior performances for many established and new applications.

In addition, research to produce pulses of even shorter duration is underway. Currently, the most promising path to attosecond pulse generation and attosecond spectroscopy is high-harmonic generation (recent reviews are given with [98Sal, 95DiM, 04Ago]). High-order-Harmonic Generation (HHG), being an up-conversion process, provides a laser-like source of temporally and spatially coherent radiation consisting of odd multiples of the laser driving frequency down to the XUV region of the spectrum. Since its discovery in 1987 in Chicago and Saclay [88Fer, 87McP], it has been speculated early on that pulses from existing sources of high-harmonic generation exhibit attosecond time signature [95Cor, 96Ant]. Meanwhile much progress has been made and by controlling its properties, Attosecond Pulse Trains (APT) [01Pau2] and isolated attosecond pulses [02Dre] have been successfully produced and applied in first proof-of-principle experiments. The higher orders are produced simultaneously and fully phase-coherent with the driving IR field, which makes this source ideally suited for two-color or even multi-color pump probe experiments. Furthermore, it is important to note, that much of this progress is directly related to advancements in laser science.

Isolated attosecond pulse generation depends on the maximum amplitude of the driving pulse's electric field, i.e. the exact position of the electric field with regard to the pulse envelope (Carrier Envelope Offset: CEO) [99Tel]. Generally in mode-locked lasers, the CEO phase exhibits large fluctuations, which have to be measured and be corrected for. Until recently the only successful demonstration of CEO-phase-locked intense pulses was based on a CEO-stabilized Ti:sapphire laser, chirped-pulse amplification and pulse compression in a hollow fiber (Sect. 2.1.6.9). Meanwhile, there are some new promising ways to achieve this goal. One is based on Chirped-Pulse Optical Parametric Amplification (CPOPA) [92Dub] and the other on pulse compression through filamentation [04Hau1]. We have demonstrated CEO-phase-stabilized CPOPA for the first time with near-transform-limited 17.3-fs pulses [04Hau2]. But even more amazing was that even though filamentation is a highly nonlinear process involving plasma generation, the CEO stabilization was maintained and intense CEO-stabilized pulses as short as 5.1 fs with 180 μJ pulse energy have been generated [05Hau]. It is expected that both pulse duration and energies will be further improved in the near future. For example just recently CPOPA resulted in 9.8 fs pulses with 10.5 mJ at 30 Hz pulse repetition rate [05Wit].

We would expect that with attosecond time resolution we open up a new world of physics with as much impact as has been demonstrated in the 70's and 80's with the transition from picosecond to femtosecond time resolution. First time-resolved measurements have been done [02Dre]. At this

point, however, we still have some significant challenges to tackle before we demonstrate standard attosecond pulse generation and attosecond spectroscopy. Solving all of these challenges will make the research in ultrashort pulse generation very exciting and rewarding for many years to come.

2.1.10 Glossary

A	pulse envelope (2.1.23)
A_A	laser mode area on saturable absorber (Table 2.1.5)
A_L	laser mode area in laser gain media
A_p	pump mode area
B	system bandwidth (2.1.82)
b	depth of focus or confocal parameter of a Gaussian beam
D	dispersion parameter (2.1.40), i.e. half of the total group delay dispersion per cavity round trip
D_g	gain dispersion ((2.1.32) and Table 2.1.10)
D_p	width of the pump source (i.e. approximately the stripe width of a diode array or bar or more accurately given in Sect. 2.1.3.2)
$DR(t)$	differential impulse response of a saturable absorber mirror measured with standard pump probe (Sect. 2.1.4.2)
d	thickness of Fabry–Perot (Table 2.1.9)
E	electric field of the electromagnetic wave
E_p	intracavity pulse energy
$E_\mathrm{p,c}$	critical E_p (2.1.77)
$E_\mathrm{p,out}$	output pulse energy
$E_\mathrm{sat,A}$	absorber saturation energy (Table 2.1.5)
$E_\mathrm{sat,L}$	laser saturation energy
E_train	electric field of a pulse train (2.1.96)
F_2	inverse slope of roll-over (2.1.81)
F_in	incident saturation fluence on SESAM (2.1.9)
F_out	reflected saturation fluence on SESAM (2.1.9)
$F_\mathrm{p,A}$	incident pulse fluence on saturable absorber (Table 2.1.5)
$F_\mathrm{sat,A}$	absorber saturation fluence (Table 2.1.5)
$F_\mathrm{sat,L}$	laser saturation fluence (2.1.1) and (2.1.2)
f_CEO	carrier envelope offset (CEO) frequency (2.1.99)
f_rep	pulse repetition frequency
$G(t)$	gate (see Sect. 2.1.7.3.1)
g	saturated amplitude laser gain coefficient
g_0	small signal amplitude laser gain
h	beam insertion into second prism (Table 2.1.9)
I	intensity
I_A	incident intensity on saturable absorber (Table 2.1.5)
$I_\mathrm{in}(t)$	incident intensity onto the saturable absorber (2.1.8)
$I_\mathrm{out}(t)$	reflected intensity from the saturable absorber (2.1.8)
$I_\mathrm{sat,A}$	absorber saturation intensity (Table 2.1.5)
k	vacuum wave number, i.e. $k = 2\pi/\lambda$
k_n	wave number in a dispersive medium, i.e. $k_n = nk$ (2.1.24)
L	apex-to-apex prism distance (Table 2.1.9)
L_a	absorption length

L_g	length of laser gain material or grating pair spacing (Table 2.1.9)
l	total saturated amplitude loss coefficient (Table 2.1.10). l includes the output coupler, all the residual cavity losses and the unsaturated loss of the saturable absorber.
l_{out}	amplitude loss coefficient of output coupler
l_s	amplitude loss coefficient of soliton due to gain filtering and absorber saturation (2.1.75)
M	modulation depth of loss modulator (2.1.33)
M_1, M_2, M_3, ...	different mirrors in laser cavity
M^2	M^2 factor defining the laser beam quality (2.1.3)
M^2_{fast}	M^2 factor in the "fast" axis, perpendicular to the pn-junction of the diode laser
M^2_{slow}	M^2 factor in the "slow" axis, parallel to the pn-junction of the diode laser
M_s	curvature of loss modulation ((2.1.33) and Table 2.1.10)
n	refractive index of a dispersive medium
n_2	nonlinear refractive index (Fig. 2.1.13, (2.1.42))
P	power
$P(z,t)$	pulse power (2.1.24)
P_{abs}	absorbed pump power
$P_{av,out}$	average output power
q	saturable amplitude loss coefficient (i.e. nonsaturable losses not included) (2.1.7)
q_0	unsaturated amplitude loss coefficient or maximal saturable amplitude loss coefficient (2.1.6)
q_p	total absorber loss coefficient which results from the fact that part of the excitation pulse needs to be absorbed to saturate the absorber ((2.1.11) and (2.1.15))
q_s	residual saturable absorber amplitude loss coefficient for a fully saturated ideal fast absorber with soliton pulses
$R(F_{p,A})$	measured nonlinear reflectivity of a SESAM (Fig. 2.1.9)
$R(t)$	impulse response of a saturable absorber mirror (Sect. 2.1.4.2)
R_{ISA}	measured nonlinear reflectivity with inverse saturable absorption (ISA) (2.1.81)
R_t	top intensity reflectivity (Table 2.1.9)
R_{tot}	total net reflectivity (2.1.9)
$S(\omega,\tau)$	spectral interference of a pulse with a frequency-shifted replica (2.1.90)
T	time that develops on a time scale of the order of T_R (2.1.23)
T_g	group delay (Table 2.1.7)
T_{out}	intensity transmission of the laser output coupler
T_R	cavity round-trip time
t	fast time of the order of the pulse duration (2.1.23)
t_0	round-trip time of Fabry–Perot (Table 2.1.9)
t_D	time shift (2.1.59)
V_p	pump volume
v_g	group velocity (Table 2.1.7)
v_p	phase velocity (Table 2.1.7)
W_0	beam waist
$W_{0,G}$	beam waist of a Gaussian beam
$W_{0,opt}$	optimized beam waist for efficient diode pumping (2.1.5)
z	pulse propagation distance
z_0	Rayleigh range of a Gaussian beam, i.e. $z_0 = \pi W_0^2/\lambda$
α	apex angle of prism (Table 2.1.9)
β	angle in prism compressor (Fig. 2.1.16c and Table 2.1.9)
γ_A	absorber coefficient ((2.1.18), (2.1.35) and Table 2.1.10)
ΔA	change in the pulse envelope

ΔR	modulation depth of a saturable absorber mirror (Fig. 2.1.9 and Table 2.1.5)
ΔR_{ns}	nonsaturable reflection loss of a saturable absorber mirror (Fig. 2.1.9 and Table 2.1.5)
ΔT	modulation depth of saturable absorber in transmission
ΔT_{ns}	nonsaturable transmission loss of saturable absorber
$\Delta\lambda_{\mathrm{g}}$	FWHM gain bandwidth
$\Delta\nu_{\mathrm{g}}$	FWHM gain bandwidth, i.e. $\dfrac{\Delta\nu_{\mathrm{g}}}{\nu_0} = \dfrac{\Delta\lambda_{\mathrm{g}}}{\lambda_0}$
$\Delta\nu_{\mathrm{p}}$	FWHM of pulse intensity spectrum
$\Delta\varphi_{\mathrm{GPO}}$	group phase offset ((2.1.97) and (2.1.98))
δ_{L}	SPM coefficient (2.1.44)
$\delta\tau$	temporal delay between two beams (2.1.86)
θ	divergence angle of a pump source (i.e. the beam radius increases approximately linearly with propagation distance, defining a cone with half-angle θ)
θ_{B}	Brewster angle (Table 2.1.9)
θ_{G}	divergence angle of a Gaussian beam, i.e. $\theta_{\mathrm{G}} = \lambda/(\pi W_{0,\mathrm{G}})$ (2.1.3)
θ_{i}	angle of incidence (Table 2.1.9)
Λ	grating period (Table 2.1.9)
λ	vacuum wavelength of light
λ_0	center vacuum wavelength
λ_{eff}	effective wavelength (2.1.4)
λ_n	wavelength in a dispersive medium with refractive index n, i.e. $\lambda_n = \lambda/n$
ν	frequency
ν_{pump}	pump photon frequency
σ_{A}	absorber cross section
σ_{L}	gain cross section
$\sigma_{\mathrm{L}}^{\mathrm{abs}}$	absorption cross section of the three-level gain medium
τ_0	initial transform-limited pulse duration (2.1.20)
τ_{A}	recovery time of saturable absorber (Table 2.1.5)
τ_{Au}	FWHM of intensity autocorrelation pulse
τ_{c}	photon cavity lifetime
τ_{L}	upper-state lifetime of laser gain material
τ_{p}	FWHM intensity pulse duration
$\tau_{\mathrm{p,min}}$	minimal τ_{p}
$\Phi(\omega)$	frequency-dependent phase shift (Sect. 2.1.5.1)
Φ_0	phase shift at center angular frequency ω_0
$\varphi_0(t)$	absolute phase of pulse (2.1.96)
ϕ_{nl}	nonlinear phase shift per cavity round trip (2.1.73)
$\phi_{\mathrm{nl}}(z)$	nonlinear phase shift of a pulse with peak intensity I_0 during propagation through a Kerr medium along the z-axis, i.e. $\phi_{\mathrm{nl}}(z) = kn_2I_0z$ (2.1.73)
ϕ_{s}	phase shift of the soliton per cavity round trip
$\phi_{\mathrm{s}}(z)$	phase shift of the soliton during propagation along the z-axis (2.1.73)
ψ	phase shift (Table 2.1.10)
Ω_{g}	Half-Width-Half-Maximum (HWHM) gain bandwidth of laser in radians/second, i.e. $\Omega_{\mathrm{g}} = \pi\Delta\nu_{\mathrm{g}}$
ω	radian frequency
ω_0	center radian frequency
ω_{c}	carrier radian frequency (2.1.96)
ω_{CEO}	carrier envelope offset (CEO) frequency in radians/second (2.1.99)
ω_{m}	modulation frequency in radians/second

References for 2.1

61Hel Hellwarth, R.W. (ed.): Advances in Quantum Electronics, New York: Columbia Univ. Press, 1961.

62Col Collins, R.J., Kisliuk, P.: Control of population inversion in pulsed optical masers by feedback modulation; J. Appl. Phys. **33** (1962) 2009–2011.

62McC McClung, F.J., Hellwarth, R.W.: Giant optical pulsations from ruby; J. Appl. Phys. **33** (1962) 828–829.

64Geu Geusic, J.E., Marcos, H.M., Uitert, L.G.V.: Laser oscillations in Nd-doped yttrium aluminum, yttrium gallium, and gadolinium garnets; Appl. Phys. Lett. **4** (1964) 182–184.

64Gir Gires, F., Tournois, P.: Interféromètre utilisable pour la compression d'impulsions lumineuses modulées en fréquence; C. R. Acad. Sci. Paris **258** (1964) 6112–6115.

64Har Hargrove, L.E., Fork, R.L., Pollack, M.A.: Locking of HeNe laser modes induced by synchronous intracavity modulation; Appl. Phys. Lett. **5** (1964) 4.

64Her Herriott, D., Kogelnik, H., Kompfner, R.: Off-axis paths in spherical mirror interferometers; Appl. Opt. **3** (1964) 523–526.

65Moc Mocker, H.W., Collins, R.J.: Mode competition and self-locking effects in a Q-switched ruby laser; Appl. Phys. Lett. **7** (1965) 270–273.

66DeM De Maria, A.J., Stetser, D.A., Heynau, H.: Self mode-locking of lasers with saturable absorbers; Appl. Phys. Lett. **8** (1966) 174–176.

66Eri Erickson, L.E., Szabo, A.: Effects of saturable absorber lifetime on the performance of giant-pulse lasers; J. Appl. Phys. **37** (1966) 4953–4961.

67Eri Erickson, L.E., Szabo, A.: Behavior of saturable-absorber giant-pulse lasers in the limit of large absorber cross section; J. Appl. Phys. **38** (1967) 2540–2542.

69Har Harmer, A.L., Linz, A., Gabbe, D.R.: Fluorescence of Nd^{3+} in lithium yttrium fluoride; J. Phys. Chem. Solids **30** (1969) 1483–1491.

69Tre Treacy, E.B.: Optical pulse compression with diffraction gratings; IEEE J. Quantum Electron. **5** (1969) 454–458.

70Kui1 Kuizenga, D.J., Siegman, A.E.: FM und AM mode locking of the homogeneous laser – Part I: Theory; Part II: Experimental results; IEEE J. Quantum Electron. **6** (1970) 694–708.

70Kui2 Kuizenga, D.J., Siegman, A.E.: FM and AM mode locking of the homogeneous laser – Part II: Experimental results in a Nd:YAG laser with internal FM modulation; IEEE J. Quantum Electron. **6** (1970) 709–715.

72Bec Becker, M.F., Kuizenga, K.J., Siegman, A.E.: Harmonic mode locking of the Nd:YAG laser; IEEE J. Quantum Electron. **8** (1972) 687–693.

72Ipp Ippen, E.P., Shank, C.V., Dienes, A.: Passive modelocking of the cw dye laser; Appl. Phys. Lett. **21** (1972) 348–350.

72New New, G.H.C.: Modelocking of quasi-continuous lasers; Opt. Commun. **6** (1972) 188–192.

74Gib Gibson, A.F., Kimmitt, M.F., Norris, B.: Generation of bandwidth-limited pulses from a TEA CO_2 laser using p-type germanium; Appl. Phys. Lett. **24** (1974) 306–307.

74New New, G.H.C.: Pulse evolution in mode-locked quasi-continuous lasers; IEEE J. Quantum Electron. **10** (1974) 115–124.
74Sha Shank, C.V., Ippen, E.P.: Subpicosecond kilowatt pulses from a modelocked cw dye laser; Appl. Phys. Lett. **24** (1974) 373–375.

75All Allen, L., Eberly, J.H.: Optical Resonance and Two-Level Atoms, New York: Dover, 1975.
75Hau1 Haus, H.A.: Theory of modelocking with a fast saturable absorber; J. Appl. Phys **46** (1975) 3049–3058.
75Hau2 Haus, H.A.: A theory of forced mode locking; IEEE J. Quantum Electron. **11** (1975) 323–330.
75Hau3 Haus, H.A.: Theory of mode locking with a slow saturable absorber; IEEE J. Quantum Electron. **11** (1975) 736–746.

76Rud Ruddock, I.S., Bradley, D.J.: Bandwidth-limited subpicosecond pulse generation in modelocked cw dye lasers; Appl. Phys. Lett. **29** (1976) 296–297.

78Die Diels, J.C., Stryland, E.W.V., Benedict, G.: Generation and measurement of pulses of 0.2 ps duration; Opt. Commun. **25** (1978) 93.
78Sch Schott Glass Technologies: Glass for Laser Applications, Data Sheets, 1978.

79Wal Walling, J.C., Jenssen, H.P., Morris, R.C., O'Dell, E.W., Peterson, O.G.: Tunable laser performance in $BeAl_2O_4Cr^{3+}$; Opt. Lett. **4** (1979) 182–183.

80Ipp Ippen, E.P., Eichenberger, D.J., Dixon, R.W.: Picosecond pulse generation by passive modelocking of diode lasers; Appl. Phys. Lett. **37** (1980) 267–269.
80Mol Mollenauer, L.F., Stolen, R.H., Gordon, J.P.: Experimental observation of picosecond pulse narrowing and solitons in optical fibers; Phys. Rev. Lett. **45** (1980) 1095–1098.
80Sal Sala, K.L., Kenney-Wallace, G.A., Hall, G.E.: CW autocorrelation measurements of picosecond laser pulses; IEEE J. Quantum Electron. **16** (1980) 990–996.

81For Fork, R.L., Greene, B.I., Shank, C.V.: Generation of optical pulses shorter than 0.1 ps by colliding pulse modelocking; Appl. Phys. Lett. **38** (1981) 617–619.
81Zie van der Ziel, J.P., Logan, R.A., Mikulyak, R.M.: Generation of subpicosecond pulses from an actively modelocked GaAs laser in an external ring cavity; Appl. Phys. Lett. **39** (1981) 867–869.

83For Fork, R.L., Shank, C.V., Hirlimann, C., Yen, R., Tomlinson, W.J.: Femtosecond white-light continuum pulses; Opt. Lett. **8** (1983) 1–3.
83Joh Johnson, A.M., Simpson, W.M.: Continuous-wave modelocked Nd:YAG-pumped subpicosecond dye lasers; Opt. Lett. **8** (1983) 554–556.
83Min Mindl, T., Hefferle, P., Schneider, S., Dörr, F.: Characterization of a train of subpicosecond laser pulses by fringe resolved autocorrelation measurements; Appl. Phys. B **31** (1983) 201–207.
83Wei Weiner, A.M.: Effect of group velocity mismatch on the measurement of ultrashort optical pulses via second harmonic generation; IEEE J. Quantum Electron. **19** (1983) 1276–1283.

84For Fork, R.L., Martinez, O.E., Gordon, J.P.: Negative dispersion using pairs of prisms; Opt. Lett. **9** (1984) 150–152.
84Mar Martinez, O.E., Fork, R.L., Gordon, J.P.: Theory of passively modelocked lasers including self-phase modulation and group-velocity dispersion; Opt. Lett. **9** (1984) 156–158.

84Mol Mollenauer, L.F., Stolen, R.H.: The soliton laser; Opt. Lett. **9** (1984) 13–15.
84Pes Pestryakov, E.V., Trunov, V.I., Matrosov, V.N., Razvalyaev, V.N.: Generation of ultrashort pulses that are tunable in the 0.7–0.8 μm range in a laser based on alexandrite; Bull. Acad. Sci. USSR **48** (1984) 94–98.
84Tom Tomlinson, W.J., Stolen, R.H., Shank, C.V.: Compression of optical pulses chirped by self-phase modulation in fibers; J. Opt. Soc. Am. B **1** (1984) 139–149.
84Yar Yariv, A., Yeh, P.: Optical Waves in Crystals, New York: John Wiley & Sons, 1984.

85Joh Johnson, A.M., Simpson, W.M.: Tunable femtosecond dye laser synchronously pumped by the compressed second harmonic of Nd:YAG; J. Opt. Soc. Am. B **2** (1985) 619–625.
85Mar Martinez, O.E., Fork, R.L., Gordon, J.P.: Theory of passively modelocked lasers for the case of a nonlinear complex propagation coefficient; J. Opt. Soc. Am. B **2** (1985) 753.
85Oud Oudar, J.L., Hulin, D., Migus, A., Antonetti, A., Alexandre, F.: Subpicosecond spectral hole burning due to nonthermalized photoexcited carriers in GaAs; Phys. Rev. Lett. **55** (1985) 2074–2077.
85Val Valdmanis, J.A., Fork, R.L., Gordon, J.P.: Generation of optical pulses as short as 27 fs directly from a laser balancing self-phase modulation, group-velocity dispersion, saturable absorption, and saturable gain; Opt. Lett. **10** (1985) 131–133.

86Hau Haus, H.A., Silberberg, Y.: Laser mode locking with addition of nonlinear index; IEEE J. Quantum Electron. **22** (1986) 325–331.
86Kno Knox, W.H., Hirlimann, C., Miller, D.A.B., Shah, J., Chemla, D.S., Shank, C.V.: Femtosecond excitation of nonthermal carrier populations in GaAs quantum wells; Phys. Rev. Lett. **56** (1986) 1191–1193.
86Lin Linde, D. v. d.: Characterization of the noise in continuously operating mode-locked lasers; Appl. Phys. B **39** (1986) 201–217.
86Mou Moulton, P.F.: Spectroscopic and laser characteristics of Ti:Al_2O_3; J. Opt. Soc. Am. B **3** (1986) 125–132.
86Rod Rodwell, M.J.W., Weingarten, K.J., Bloom, D.M., Baer, T., Kolner, B.H.: Reduction in the timing fluctuations in a modelocked Nd:YAG laser by electronic feedback; Opt. Lett. **11** (1986) 638–640.
86Ros Roskos, H., Robl, T., Seilmeier, A.: Pulse shortening to 25 ps in a cw mode-locked Nd:YAG laser by introducing an intracavity etalon; Appl. Phys. B **40** (1986) 59–65.
86Sie Siegman, A.E.: Lasers, Mill Valley, California: University Science Books, 1986.
86Val Valdmanis, J.A., Fork, R.L.: Design considerations for a femtosecond pulse laser balancing self phase modulation, group velocity dispersion, saturable absorption, and saturable gain; IEEE J. Quantum Electron. **22** (1986) 112–118.
86Vas Vasil'ev, P.P., Morzov, V.N., Popov, Y.M., Sergeev, A.B.: Subpicosecond pulse generation by tandem-type AlGaAs DH laser with colliding pulse modelocking; IEEE J. Quantum Electron. **22** (1986) 149–151.
86Wal Walker, A.C., Kar, A.K., Wei Ji, Keller, U., Smith, S.D.: All-optical power limiting of CO_2 laser pulses using cascaded optical bistable elements; Appl. Phys. Lett. **48** (1986) 683–685.
86Yan Yan, L., Ling, J.D., Ho, P.-T., Lee, C.H.: Picosecond-pulse generation from a continuous-wave neodymium:phosphate glass laser; Opt. Lett. **11** (1986) 502–503.

87Ada Adachi, S.: Band gaps and refractive indices of AlGaAsSb, GaInAsSb, and InPAsSb: Key properties for a variety of the 2–4-μm optoelectronic device applications; J. Appl. Phys. **61** (1987) 4869–4876.
87Bad Bado, P., Bouvier, M., Coe, J.S.: Nd:YLF mode-locked oscillator and regenerative amplifier; Opt. Lett. **12** (1987) 319–321.

87Fan Fan, T.Y., Byer, R.L.: Modelling and cw operation of a quasi-three-level 946 nm Nd:YAG Laser; IEEE J. Quantum Electron. **23** (1987) 605–612.

87For Fork, R.L., Cruz, C.H.B., Becker, P.C., Shank, C.V.: Compression of optical pulses to six femtoseconds by using cubic phase compensation; Opt. Lett. **12** (1987) 483–485.

87McP McPherson, A., Gibson, G., Jara, H., Johann, U., Luk, T.S., McIntyre, I., Boyer, K., Rhodes, C.K.: Studies of multiphoton production of vacuum-ultraviolet radiation in the rare gases; J. Opt. Soc. Am. B **4** (1987) 595.

87Mit Mitschke, F.M., Mollenauer, L.F.: Ultrashort pulses from the soliton laser; Opt. Lett. **12** (1987) 407–409.

87Sch Schoenlein, R.W., Lin, W.Z., Ippen, E.P., Fujimoto, J.G.: Femtosecond hot-carrier energy relaxation in GaAs; Appl. Phys. Lett. **51** (1987) 1442–1444.

88Ang Angert, N.B., Borodin, N.I., Garmash, V.M., Zhitnyuk, V.A., Okhrimchuk, V.G., Siyuchenko, O.G., Shestakov, A.V.: Lasing due to impurity color centers in yttrium aluminum garnet crystals at wavelengths in the range 1.35–1.45 μm; Sov. J. Quantum Electron. (English Transl.) **18** (1988) 73–74.

88Bas Basu, S., Byer, R.L.: Continuous-wave mode-locked Nd:glass laser pumped by a laser diode; Opt. Lett. **13** (1988) 458–460.

88Fer Ferray, M., L'Huillier, A., Li, X.F., Lompré, L.A., Mainfray, G., Manus, C.: Multiple-harmonic conversion of 1064 nm radiation in rare gases; J. Phys. B **21** (1988) L31–L35.

88Kel Keller, U., Valdmanis, J.A., Nuss, M.C., Johnson, A.M.: 53 ps pulses at 1.32 μm from a harmonic mode-locked Nd:YAG laser; IEEE J. Quantum Electron. **24** (1988) 427–430.

88Pay Payne, S.A., Chase, L.L., Newkirk, H.W., Smith, L.K., Krupke, W.F.: Cr:LiCAF: a promising new solid-state laser material; IEEE J. Quantum Electron. **24** (1988) 2243–2252.

88Pet Petricevic, V., Gayen, S.K., Alfano, R.R.: Laser action in chromium-doped forsterite; Appl. Phys. Lett. **52** (1988) 1040–1042.

88Ris Risk, W.P.: Modeling of longitudinally pumped solid-state lasers exhibiting reabsorption losses; J. Opt. Soc. Am. B **5** (1988) 1412–1423.

88Sha Shank, C.V.: Generation of Ultrashort Optical Pulses, in: Ultrashort Laser Pulses and Applications, Kaiser, W. (ed.), Heidelberg: Springer-Verlag, 1988, Chap. 2.

88Smi Smith, F.W., Calawa, A.R., Chen, C.-L., Manfra, M.J., Mahoney, L.J.: New MBE buffer used to eliminated backgating in GaAs MESFET's; IEEE Electron Device Lett. **9** (1988) 77–80.

88Sta Stankov, K.A.: A mirror with an intensity-dependent reflection coefficient; Appl. Phys. B **45** (1988) 191.

89Agr Agrawal, G.P., Olsson, N.A.: Self-phase modulation and spectral broadening of optical pulses in semiconductor laser amplifiers; IEEE J. Quantum Electron. **25** (1989) 2297–2306.

89Goo Goodberlet, J., Wang, J., Fujimoto, J.G., Schulz, P.A.: Femtosecond passively mode-locked Ti:Sapphire laser with a nonlinear external cavity; Opt. Lett. **14** (1989) 1125–1127.

89Ipp Ippen, E.P., Haus, H.A., Liu, L.Y.: Additive pulse modelocking; J. Opt. Soc. Am. B **6** (1989) 1736–1745.

89Isl Islam, M.N., Sunderman, E.R., Soccolich, C.E., Bar-Joseph, I., Sauer, N., Chang, T.Y., Miller, B.I.: Color center lasers passively mode locked by quantum wells; IEEE J. Quantum Electron. **25** (1989) 2454–2463.

89Kea Kean, P.N., Zhu, X., Crust, D.W., Grant, R.S., Landford, N., Sibbett, W.: Enhanced modelocking of color center lasers; Opt. Lett. **14** (1989) 39–41.

89Kel Keller, U., Li, K.D., Rodwell, M.J.W., Bloom, D.M.: Noise characterization of femtosecond fiber Raman soliton lasers; IEEE J. Quantum Electron. **25** (1989) 280–288.

89Kim Kim, B.G., Garmire, E., Hummel, S.G., Dapkus, P.D.: Nonlinear Bragg reflector based on saturable absorption; Appl. Phys. Lett. **54** (1989) 1095–1097.

89Mak1 Maker, G.T., Ferguson, A.I.: Frequency-modulation mode locking of diode-pumped Nd:YAG laser; Opt. Lett. **14** (1989) 788–790.

89Mak2 Maker, G.T., Ferguson, A.I.: Modelocking and Q-switching of a diode laser pumped neodymium-doped yttrium lithium fluoride laser; Appl. Phys. Lett. **54** (1989) 403–405.

89Pay Payne, S.A., Chase, L.L., Smith, L.K., Kway, W.L., Newkirk, H.: Laser performance of $LiSrAlF_6$:Cr^{3+}; J. Appl. Phys. **66** (1989) 1051–1056.

89Rod Rodwell, M.J.W., Bloom, D.M., Weingarten, K.J.: Subpicosecond laser timing stabilization; IEEE J. Quantum Electron. **25** (1989) 817–827.

89Sam Sam, R.C.: Alexandrite Lasers, in: Handbook of Solid-State Lasers, Cheo, P.K. (ed.), New York: Marcel Dekker, 1989, p. 349–455.

89Sas Sasnett, M.W.: Propagation of Multimode Laser Beams – The M^2 Factor, in: The Physics and Technology of Laser Resonators, Hall, D.R., Jackson, P.E. (eds), New York: Adam Hilger, 1989, p. 132–142.

89Vas Vasilev, P.P., Sergeev, A.B.: Generation of bandwidth-limited 2 ps pulses with 100 Ghz repetition rate from multisegmented injection-laser; Electron. Lett. **25** (1989) 1049–1050.

89Zay Zayhowski, J.J., Mooradian, A.: Single-frequency microchip Nd lasers; Opt. Lett. **14** (1989) 24–26.

89Zie Ziegler, J.F., Biersack, J.P., Littmark, U.: The Stopping and Range of Ions in Solids, Vol. 1, New York: Pergamon, 1989.

90Die Diels, J.-C.: Femtosecond Dye Lasers, in: Dye Lasers Principles: With Applications, Hillman, F.D.a.L. (ed), Boston: Academic Press, 1990, p. 41–132.

90Fan Fan, T.Y., Sanchez, A.: Pump source requirements for end-pumped lasers; IEEE J.Quantum Electron. **26** (1990) 311–316.

90Goe Göbel, E.O.: Ultrafast Spectroscopy of Semiconductors, in: Advances in Solid State Physics, Vol. 30, Rössler, U. (ed.), Braunschweig/Wiesbaden: Friedrich Vieweg & Sohn, 1990, p. 269–294.

90Goo Goodberlet, J., Jacobson, J., Fujimoto, J.G., Schulz, P.A., Fan, T.Y.: Self-starting additive pulse modelocked diode-pumped Nd:YAG laser; Opt. Lett. **15** (1990) 504–506.

90Juh Juhasz, T., Lai, S.T., Pessot, M.A.: Efficient short-pulse generation from a diode-pumped Nd:YLF laser with a piezoelectrically induced diffraction modulator; Opt. Lett. **15** (1990) 1458–1460.

90Kel1 Keller, U., Weingarten, K.J., Li, K.D., Gerstenberger, D.C., Khuri-Yakub, P.T., Bloom, D.M.: High-frequency acousto-optic modelocker for picosecond pulse generation; Opt. Lett. **15** (1990) 45–47.

90Kel2 Keller, U., Knox, W.H., Roskos, H.: Coupled-cavity resonant passive modelocked Ti:Sapphire Laser; Opt. Lett. **15** (1990) 1377–1379.

90Liu1 Liu, L.Y., Huxley, J.M., Ippen, E.P., Haus, H.A.: Self-starting additive pulse modelocking of a Nd:YAG laser; Opt. Lett. **15** (1990) 553–555.

90Liu2 Liu, J.M., Chee, J.K.: Passive modelocking of a cw Nd:YLF laser with a nonlinear external coupled cavity; Opt. Lett. **15** (1990) 685–687.

90Mal Malcom, G.P.A., Curley, P.F., Ferguson, A.I.: Additive pulse modelocking of a diode-pumped Nd:YLF laser; Opt. Lett. **15** (1990) 1303–1305.

90Wal Walker, S.J., Avramopoulos, H., Sizer II, T.: Compact mode-locked solid-state lasers at 0.5- and 1-GHz repetition rates; Opt. Lett. **15** (1990) 1070–1072.

90Wei Weingarten, K.J., Shannon, D.C., Wallace, R.W., Keller, U.: Two gigahertz repetition rate, diode-pumped, mode-locked, Nd:yttrium lithium fluoride (YLF) laser; Opt. Lett. **15** (1990) 962–964.

90Wu Wu, M.C., Chen, Y.K., Tanbun-Ek, T., Logan, R.A., Chin, M.A., Raybon, G.: Transform-limited 1.4 ps optical pulses from a monolithic colliding-pulse modelocked quantum well laser; Appl. Phys. Lett. **57** (1990) 759–761.

91Bra Brabec, T., Spielmann, C., Krausz, F.: Mode locking in solitary lasers; Opt. Lett. **16** (1991) 1961–1963.

91Che Chen, Y.K., Wu, M.C., Tanbun-Ek, T., Logan, R.A., Chin, M.A.: Subpicosecond monolithic colliding-pulse modelocked multiple quantum well lasers; Appl. Phys. Lett. **58** (1991) 1253–1255.

91Chi Chilla, J.L.A., Martinez, O.E.: Direct determination of the amplitude and the phase of femtosecond light pulses; Opt. Lett. **16** (1991) 39–41.

91Cur Curley, P.F., Ferguson, A.I.: Actively modelocked Ti:Sapphire laser producing transform-limited pulses of 150 fs duration; Opt. Lett. **16** (1991) 1016–1018.

91God Godil, A.A., Hou, A.S., Auld, B.A., Bloom, D.M.: Harmonic mode locking of a Nd:BEL laser using a 20-GHz dielectric resonator/optical modulator; Opt. Lett. **16** (1991) 1765–1767.

91Hau Haus, H.A., Fujimoto, J.G., Ippen, E.P.: Structures for additive pulse modelocking; J. Opt. Soc. Am. B **8** (1991) 2068–2076.

91Hug Hughes, D.W., Barr, J.R.M., Hanna, D.C.: Mode locking of a diode-laser-pumped Nd:glass laser by frequency modulation; Opt. Lett. **16** (1991) 147–149.

91Kel Keller, U., 'tHooft, G.W., Knox, W.H., Cunningham, J.E.: Femtosecond pulses from a continuously self-starting passively mode-locked Ti:sapphire Laser; Opt. Lett. **16** (1991) 1022–1024.

91Kut Kutovoi, S.A., Laptev, V.V., Matsnev, S.Y.: Lanthanum scandoborate as a new highly efficient active medium of solid state lasers; Sov. J. Quantum Electron. (English Transl.) **21** (1991) 131–132.

91Lap Laporta, P., Silvestri, S.D., Magni, V., Svelto, O.: Diode-pumped cw bulk Er:Yb:glass laser; Opt. Lett. **16** (1991) 1952–1954.

91Li Li, K.D., Sheridan, J.A., Bloom, D.M.: Picosecond pulse generation in Nd:BEL with a high-frequency acousto-optic mode locker; Opt. Lett. **16** (1991) 1505–1507.

91McC McCarthy, M.J., Maker, G.T., Hanna, D.C.: Efficient frequency doubling of a self-starting additive-pulse mode-locked diode-pumped Nd:YAG laser; Opt. Commun. **82** (1991) 327–332.

91Mur Murnane, M.M., Kapteyn, H.C., Rosen, M.D., Falcone, R.W.: Ultrafast X-ray pulses from laser-produced plasmas; Science **251** (1991) 531–536.

91Neg Negus, D.K., Spinelli, L., Goldblatt, N., Feugnet, G.: Sub-100 femtosecond pulse generation by Kerr lens modelocking in Ti:Sapphire, in: Advanced Solid-State Lasers, Dubé, G., Chase, L. (eds), Washington, D.C.: Optical Society of America, 1991, Vol. 10, p. 120–124.

91Sal1 Salin, F., Squier, J., Piché, M.: Modelocking of Ti:Sapphire lasers and self-focusing: a Gaussian approximation; Opt. Lett. **16** (1991) 1674–1676.

91Sal2 Saleh, B.E.A., Teich, M.C.: Fundamentals of Photonics, New York: John Wiley & Sons, Inc., 1991.

91Sar Sarukura, N., Ishida, Y., Nakano, H.: Generation of 50 fs pulses from a pulse compressed, cw, passively modelocked Ti:sapphire laser; Opt. Lett. **16** (1991) 153–155.

91Sch1 Scheps, R., Myers, J.F., Serreze, H.B., Rosenberg, A., Morris, R.C., Long, M.: Diode-pumped Cr:$LiSrAlF_6$ laser; Opt. Lett. **16** (1991) 820–822.

91Sch2 Schulz, P.A., Henion, S.R.: 5-GHz mode locking of a Nd:YLF laser; Opt. Lett. **16** (1991) 1502–1504

91Spe Spence, D.E., Kean, P.N., Sibbett, W.: 60-fsec pulse generation from a self-mode-locked Ti:sapphire laser; Opt. Lett. **16** (1991) 42–44.

91Spi Spielmann, C., Krausz, F., Brabec, T., Wintner, E., Schmidt, A.J.: Femtosecond passive modelocking of a solid-state laser by dispersively balanced nonlinear interferometer; Appl. Phys. Lett. **58** (1991) 2470–2472.

91Sta Stankov, K.A., Kubecek, V., Hamal, K.: Mode-locking of a Nd-$YAlO_3$-laser at 1.08 and 1.34 μ-m wavelengths using a single $LiIO_3$ crystal; IEEE J. Quantum Electron. **27** (1991) 2135–2141.

91Zho Zhou, F., Malcolm, G.P.A., Ferguson, A.I.: 1-GHz repetition-rate frequency-modulation mode-locked neodymium lasers at 1.3 μm; Opt. Lett. **16** (1991) 1101–1103.

91Zir Zirngibl, M., Stulz, L.W., Stone, J., Hugi, J., DiGiovanni, D., Hansen, P.B.: 1.2 ps pulses from passively modelocked laser diode pumped Er-doped fiber ring lasers; Electron. Lett. **27** (1991) 1734–1735.

92Bea Beaudoin, Y., Chien, C.Y., Coe, J.S., Tapié, J.L., Mourou, G.: Ultrahigh-contrast Ti:sapphire/Nd:glass terawatt laser system; Opt. Lett. **17** (1992) 865–867.

92Cha Chai, B.H.T., Lefaucheur, J.-L., Stalder, M., Bass, M.: Cr:$LiSr_{0.8}Ca_{0.2}AlF_6$ tunable laser; Opt. Lett. **17** (1992) 1584–1586.

92Che Chen, Y.-K., Wu, M.C.: Monolithic colliding pulse modelocked quantum well lasers; IEEE J. Quantum Electron. **28** (1992) 2176–2185.

92Del Delfyett, P.J., Florez, L.T., Stoffel, N., Gmitter, T., Andreadakis, N.C., Silberberg, Y., Heritage, J.P., Alphonse, G.A.: High-power ultrafast laser diodes; IEEE J. Quantum Electron. **28** (1992) 2203–2219.

92Dub Dubietis, A., Jonusauskas, G., Piskarskas, A.: Powerful femtosecond pulse generation by chirped and stretched pulse parametric amplification in BBO crystal; Opt. Commun. **88** (1992) 437–440.

92Eva Evans, J.M., Spence, D.E., Sibbett, W., Chai, B.H.T., Miller, A.: 50-fs pulse generation from a self-mode-locked Cr:$LiSrAlF_6$ laser; Opt. Lett. **17** (1992) 1447–1449.

92Hau Haus, H.A., Fujimoto, J.G., Ippen, E.P.: Analytic theory of additive pulse and Kerr lens mode locking; IEEE J. Quantum Electron. **28** (1992) 2086–2096.

92Hof Hofer, M., Ober, M.H., Haberl, F., Fermann, M.E.: Characterization of ultrashort pulse formation in passively mode-locked fiber lasers; IEEE J. Quantum Electron. **28** (1992) 720–728.

92Hua1 Huang, C.-P., Kapteyn, H.C., McIntosh, J.W., Murnane, M.M.: Generation of transform-limited 32-fs pulses from a self-mode-locked Ti:sapphire laser; Opt. Lett. **17** (1992) 139–141.

92Hua2 Huang, C.-P., Asaki, M.T., Backus, S., Murnane, M.M., Kapteyn, H.C., Nathel, H.: 17-fs pulses from a self-mode-locked Ti:sapphire laser; Opt. Lett. **17** (1992) 1289–1291.

92Hug Hughes, D.W., Phillips, M.W., Barr, J.R.M., Hanna, D.C.: A laser-diode-pumped Nd:glass laser: Mode-locked, high power, and single frequency performance; IEEE J. Quantum Electron. **28** (1992) 1010–1017.

92Kaf Kafka, J.D., Watts, M.L., Pieterse, J.-W.J.: Picosecond and femtosecond pulse generation in a regeneratively modelocked Ti:sapphire laser; IEEE J. Quantum Electron. **28** (1992) 2151–2162.

92Kel1 Keller, U., Chiu, T.H.: Resonant passive modelocked Nd:YLF laser; IEEE J. Quantum Electron. **28** (1992) 1710–1721.

92Kel2 Keller, U., Miller, D.A.B., Boyd, G.D., Chiu, T.H., Ferguson, J.F., Asom, M.T.: Solid-state low-loss intracavity saturable absorber for Nd:YLF lasers: an antiresonant semiconductor Fabry–Perot saturable absorber; Opt. Lett. **17** (1992) 505–507.

92Kra1 Krausz, F., Spielmann, C., Brabec, T., Wintner, E., Schmidt, A.J.: Generation of 33 fs optical pulses from a solid-state laser; Opt. Lett. **17** (1992) 204–206.

92Kra2 Krausz, F., Fermann, M.E., Brabec, T., Curley, P.F., Hofer, M., Ober, M.H., Spielmann, C., Wintner, E., Schmidt, A.J.: Femtosecond solid-state lasers; IEEE J. Quantum Electron. **28** (1992) 2097–2122

92Lem Lemoff, B.E., Barty, C.P.J.: Generation of high-peak-power 20-fs pulses from a regeneratively initiated, self-mode-locked Ti:sapphire laser; Opt. Lett. **17** (1992) 1367–1369.

92LiK LiKamWa, P., Chai, B.H.T., Miller, A.: Self-mode-locked Cr^{3+}:$LiCaAlF_6$ laser; Opt. Lett. **17** (1992) 1438–1440

92Liu Liu, K.X., Flood, C.J., Walker, D.R., Driel, H.M. v.: Kerr lens mode locking of a diode-pumped Nd:YAG laser; Opt. Lett. **17** (1992) 1361–1363.

92Mil Miller, A., LiKamWa, P., Chai, B.H.T., Stryland, E.W.V.: Generation of 150-fs tunable pulses in Cr:LiSAF; Opt. Lett. **17** (1992) 195–197.

92Riz1 Rizvi, N.H., French, P.M.W., Taylor, J.R.: Continuously self-mode-locked Ti:Sapphire laser that produces sub-50-fs pulses; Opt. Lett. **17** (1992) 279–281.

92Riz2 Rizvi, N.H., French, P.M.W., Taylor, J.R.: 50-fs pulse generation from a self-starting cw passively mode-locked Cr:$LiSrAlF_6$ laser; Opt. Lett. **17** (1992) 877–879.

92Riz3 Rizvi, N.H., French, P.M.W., Taylor, J.R.: Generation of 33-fs pulses from a passively mode-locked Cr^{3+}:$LiSrAlF_6$ laser; Opt. Lett. **17** (1992) 1605–1607.

92Smi Smith, L.K., Payne, S.A., Kway, W.L., Chase, L.L., Chai, B.H.T.: Investigation of the laser properties of Cr^{3+}:$LiSrGaF_6$; IEEE J. Quantum Electron. **28** (1992) 2612–2618.

92Tap Tapié, J.-L., Mourou, G.: Shaping of clean, femtosecond pulses at 1.053 μm for chirped-pulse amplification; Opt. Lett. **17** (1992) 136–138.

92Wei Weingarten, K.J., Godil, A.A., Gifford, M.: FM modelocking at 2.85 GHz using a microwave resonant optical modulator; IEEE Photonics Technol. Lett. **4** (1992) 1106–1109.

92Zay Zayhowski, J.J., Dill III, C.: Diode-pumped microchip lasers electro-optically Q-switched at high pulse repetition rates; Opt. Lett. **17** (1992) 1201–1203.

93Asa Asaki, M.T., Huang, C.-P., Garvey, D., Zhou, J., Kapteyn, H.C., Murnane, M.N.: Generation of 11-fs pulses from a self-mode-locked Ti:sapphire laser; Opt. Lett. **18** (1993) 977–979.

93Bec Beck, M., Raymer, M.G., Walmsley, I.A., Wong, V.: Chronocyclic tomography for measuring the amplitude and phase structure of optical pulses; Opt. Lett. **18** (1993) 2041–2043.

93Car Carrig, T.J., Pollock, C.R.: Performance of a cw forsterite laser with krypton ion, Ti:sapphire, and Nd:YAG pump lasers; IEEE J. Quantum Electron. **29** (1993) 2835–2844.

93Cur Curley, P.F., Spielmann, C., Brabec, T., Krausz, F., Wintner, E., Schmidt, A.J.: Operation of a femtosecond Ti:sapphire solitary laser in the vicinity of zero group-delay dispersion; Opt. Lett. **18** (1993) 54–56.

93Fan Fan, T.Y.: Heat generation in Nd:YAG and Yb:YAG; IEEE J. Quantum Electron. **29** (1993) 1457–1459.

93Fer Fermann, M.E., Andrejco, M.J., Stock, M.L., Silberberg, Y., Weiner, A.M.: Passive modelocking in erbium fiber lasers with negative group delay; Appl. Phys. Lett. **62** (1993) 910–912.

93Fre French, P.M.W., Mellish, R., Taylor, J.R., Delfyett, P.J., Florez, L.T.: Modelocked all-solid-state diode-pumped Cr:LiSAF laser; Opt. Lett. **18** (1993) 1934–1936.

93Jia Jiang, W., Shimizu, M., Mirin, R.P., Reynolds, T.E., Bowers, J.E.: Electrically pumped mode-locked vertical-cavity semiconductor lasers; Opt. Lett. **18** (1993) 1937–1939.

93Kan Kane, D.J., Trebino, R.: Characterization of arbitrary femtosecond pulses using frequency-resolved optical gating; IEEE J. Quantum Electron. **29** (1993) 571–578.

93Obe Ober, M.H., Hofer, M., Keller, U., Chiu, T.H.: Self-starting, diode-pumped femtosecond Nd:fiber laser; Opt. Lett. **18** (1993) 1532–1534.

93Pic Piché, M., Salin, F.: Self-mode locking of solid-state lasers without apertures; Opt. Lett. **18** (1993) 1041–1043.

93Ram1 Ramaswamy, M., Gouveia-Neto, A.S., Negus, D.K., Izatt, J.A., Fujimoto, J.G.: 2.3-ps pulses from a Kerr-lens mode-locked lamp-pumped Nd:YLF laser with a microdot mirror; Opt. Lett. **18** (1993) 1825–1827.

93Ram2 Ramaswamy, M., Ulman, M., Paye, J., Fujimoto, J.G.: Cavity-dumped femtosecond Kerr-lens mode-locked Ti:Al_2O_3 laser; Opt. Lett. **18** (1993) 1822–1824.

93Riz Rizvi, N.H., French, P.M.W., Taylor, J.R., Delfyett, P.J., Florez, L.T.: Generation of pulses as short as 93 fs from a self-starting femtosecond Cr:$LiSrAlF_6$ laser by exploiting multiple-quantum-well absorbers; Opt. Lett. **18** (1993) 983–985.

93Sea Seas, A., Petricevic, V., Alfano, R.R.: Self-mode-locked chromium-doped forsterite laser generates 50 fs pulses; Opt. Lett. **18** (1993) 891–893.

93Sen Sennaroglu, A., Pollock, C.R., Nathel, H.: Generation of 48-fs pulses and measurement of crystal dispersion by using a regeneratively initiated self-mode-locked chromium-doped forsterite laser; Opt. Lett. **18** (1993) 826–828.

93Wit Witt, G.L.: LTMBE GaAs: present status and perspectives; Mater. Sci. Eng. B **22** (1993) 9.

93Yan Yanovsky, V., Pang, Y., Wise, F., Minkov, B.I.: Generation of 25-fs from a self-modelocked Cr:forsterite laser with optimized group-delay dispersion; Opt. Lett. **18** (1993) 1541–1543.

93Wei Weingarten, K.J., Keller, U., Chiu, T.H., Ferguson, J.F.: Passively mode-locked diode-pumped solid-state lasers using an antiresonant Fabry–Perot saturable absorber; Opt. Lett. **18** (1993) 640–642.

94Cer Cerullo, G., De Silvestri, S., Laporta, P., Longhi, S., Magni, V., Taccheo, S., Svelto, O.: Continuous-wave mode locking of a bulk erbium-ytterbium glass laser; Opt. Lett. **19** (1994) 272–274.

94Con Conlon, P.J., Tong,, Y.P., French, P.M.W., Taylor, J.R., Shestakov, A.V.: Passive modelocking and dispersion measurement of a sub-100-fs Cr^{4+}:YAG laser; Opt. Lett. **19** (1994) 1468–1470.

94DeL DeLoach, L.D., Payne, S.A., Smith, L.K., Kway, W.L., Krupke, W.F.: Laser and spectroscopic properties of $Sr_5(PO_4)_3F$:Yb; J. Opt. Soc. Am. B **11** (1994) 269–276.

94Dym Dymott, M.J.P., Ferguson, A.I.: Self-mode-locked diode-pumped Cr:LiSAF laser; Opt. Lett. **19** (1994) 1988–1990.

94Fer Fermann, M.E.: Ultrashort-pulse sources based on single-mode rare-earth-doped fibers; Appl. Phys. B **58** (1994) 197–209.

94Gie Giesen, A., Hügel, H., Voss, A., Wittig, K., Brauch, U., Opower, H.: Scalable concept for diode-pumped high-power solid-state lasers; Appl. Phys. B **58** (1994) 363–372.

94Ipp Ippen, E.P.: Principles of passive mode locking; Appl. Phys. B **58** (1994) 159–170.

94Ish Ishida, Y., Naganuma, K.: Characteristics of femtosecond pulses near 1.5 μm in a self-mode-locked Cr^{4+}:YAG laser Opt. Lett. **19** (1994) 2003–2005.

94Jen Jensen, T., Ostroumov, V.G., Meyn, J.P., Huber, G., Zagumennyi, A.I., Shcherbakov, I.A.: Spectroscopic characterization and laser performance of diode-laser-pumped Nd-$GdVO_4$; Appl. Phys. B **58** (1994) 373–379.

94Kel Keller, U.: Ultrafast all-solid-state laser technology; Appl. Phys. B **58** (1994) 347–363.

94Kop1 Kopf, D., Weingarten, K.J., Brovelli, L.R., Kamp, M., Keller, U.: Diode-pumped 100-fs passively mode-locked Cr:LiSAF laser with an antiresonant Fabry–Perot saturable absorber; Opt. Lett. **19** (1994) 2143–2145.

94Kop2 Kopf, D., Kärtner, F.X., Weingarten, K.J., Keller, U.: Pulse shortening in a Nd:glass laser by gain reshaping and soliton formation; Opt. Lett. **19** (1994) 2146–2148.

94Lew Lewenstein, M., Balcou, P., Ivanov, M.Y., L'Huillier, A., Corkum, P.B.: Theory of high-harmonic generation by low-frequency laser fields; Phys. Rev. A **49** (1994) 2117–2132.

94Lin1 Lincoln, J.R., Dymott, M.J.P., Ferguson, A.I.: Femtosecond pulses from an all-solid-state Kerr-lens mode-locked Cr:LiSAF laser; Opt. Lett. **19** (1994) 1210–1212.

94Lin2 Lincoln, J.R., Ferguson, A.I.: All-solid-state self-mode locking of a Nd:YLF laser; Opt. Lett. **19** (1994) 2119–2121.

94Liu Liu, X., Prasad, A., Chen, W.M., Kurpiewski, A., Stoschek, A., Liliental-Weber, Z., Weber, E.R.: Mechanism responsible for the semi-insulating properties of low-temperature-grown GaAs; Appl. Phys. Lett. **65** (1994) 3002–3004.

94Lon Longhi, S., Laporta, P., Taccheo, S., Svelto, O.: Third-order-harmonic mode locking of a bulk erbium:ytterbium:glass at a 2.5-GHz repetition rate; Opt. Lett. **19** (1994) 1985–1987.

94Mel Mellish, P.M., French, P.M.W., Taylor, J.R., Delfyett, P.J., Florez, L.T.: All-solid-state femtosecond diode-pumped Cr:LiSAF laser; Electron. Lett. **30** (1994) 223–224.

94Mey Meyn, J.-P., Jensen, T., Huber, G.: Spectroscopic properties and efficient diode-pumped laser operation of neodymium doped lanthanum scandium borate; IEEE J. Quantum Electron. **30** (1994) 913–917.

94Psh Pshenichnikov, M.S., de Boeij, W.P., Wiersma, D.A.: Generation of 13-fs, 5-MW pulses from a cavity-dumped Ti:sapphire laser; Opt. Lett. **19** (1994) 572–574.

94Ram Ramaswamy-Paye, M., Fujimoto, J.G.: Compact dispersion-compensating geometry for Kerr-lens mode-locked femtosecond lasers; Opt. Lett. **19** (1994) 1756–1758.

94Sen Sennaroglu, A., Pollock, C.R., Nathel, H.: Continuous-wave self-mode-locked operation of a femtosecond Cr^{4+}:YAG laser; Opt. Lett. **19** (1994) 390–392.

94Sti Stingl, A., Spielmann, C., Krausz, F.: Generation of 11-fs pulses from a Ti:sapphire laser without the use of prisms; Opt. Lett. **19** (1994) 204–206

94Szi Szipöcs, R., Ferencz, K., Spielmann, C., Krausz, F.: Chirped multilayer coatings for broadband dispersion control in femtosecond lasers; Opt. Lett. **19** (1994) 201–203.

94Wan Wang, H.S., Wa, P.L.K., Lefaucheur, J.L., Chai, B.H.T., Miller, A.: Cw and self-mode-locking performance of a red pumped Cr:LiSCAF laser; Opt. Commun. **110** (1994) 679–688.

94Wei Weingarten, K.J., Braun, B., Keller, U.: In-situ small-signal gain of solid-state lasers determined from relaxation oscillation frequency measurements; Opt. Lett. **19** (1994) 1140–1142.

94Zay Zayhowski, J.J., Dill III, C.: Diode-pumped passively Q-switched picosecond microchip lasers; Opt. Lett. **19** (1994) 1427–1429.

94Zho Zhou, J., Taft, G., Huang, C.-P., Murnane, M.M., Kapteyn, H.C., Christov, I.P.: Pulse evolution in a broad-bandwidth Ti:sapphire laser; Opt. Lett. **19** (1994) 1149–1151.

95Bra1 Braun, B., Keller, U.: Single frequency Q-switched ring laser with an A-FPSA; Opt. Lett. **20** (1995) 1020–1022.

95Bra2 Braun, B., Weingarten, K.J., Kärtner, F.X., Keller, U.: Continuous-wave mode-locked solid-state lasers with enhanced spatial hole-burning; Part I: Experiments; Appl. Phys. B **61** (1995) 429–437.

95Bro1 Brovelli, L.R., Keller, U., Chiu, T.H.: Design and operation of antiresonant Fabry–Perot saturable semiconductor absorbers for mode-locked solid-state lasers; J. Opt. Soc. Am. B **12** (1995) 311–322.

95Bro2 Brovelli, L.R., Jung, I.D., Kopf, D., Kamp, M., Moser, M., Kärtner, F.X., Keller, U.: Self-starting soliton modelocked Ti:Sapphire laser using a thin semiconductor saturable absorber; Electron. Lett. **31** (1995) 287–289.

95Bro3 Brovelli, L.R., Lanker, M., Keller, U., Goossen, K.W., Walker, J.A., Cunningham, J.E.: Antiresonant Fabry–Perot quantum well modulator to actively modelock and synchronize solid-state lasers; Electron. Lett. **31** (1995) 381–382.

95Chu1 Chung, J., Siegman, A.E.: Optical-Kerr-enhanced mode locking of a lamp-pumped Nd:YAG Laser; IEEE J. Quantum Electron. **31** (1995) 582–590.

95Chu2 Chu, K.C., Heritage, J.P., Grant, R.S., Liu, K.X., Dienes, A., White, W.E., Sullivan, A.: Direct measurement of the spectral phase of femtosecond pulses; Opt. Lett. **20** (1995) 904–906.

95Cor Corkum, P.: Breaking the attosecond barrier, Optics and Photonics, p. 18–22, May 1995.

95Deg Degnan, J.J.: Optimization of passively Q-switched lasers; IEEE J. Quantum Electron. **31** (1995) 1890–1901.

95Del Delfyett, P.J.: High power ultrafast semiconductor injection diode lasers, in: Compact Sources of Ultrashort Pulses, Duling, I.I.N. (ed.), New York: Cambridge University Press, 1995, p. 274–328.

95DiM DiMauro, L.F., Agostini, P.: Ionization dynamics in strong laser fields; in: Advances in Atomic, Molecular, and Optical Physics, Vol. 35, Bederson, B., Walther, H. (eds.), San Diego: Academic Press, 1995, p. 79–120.

95Dul Duling III, I.N.: Modelocking of all-fiber lasers, in: Compact Sources of Ultrashort Pulses Duling III, I.N. (ed.), New York: Cambridge University Press, 1995, p. 140–178.

95Dym Dymott, M.J.P., Ferguson, A.I.: Self-mode-locked diode-pumped Cr:LiSAF laser producing 34-fs pulses at 42 mW average output power; Opt. Lett. **20** (1995) 1157–1159.

95Fal Falcoz, F., Balembois, F., Georges, P., Brun, A.: Self-starting self-mode-locked femtosecond diode-pumped Cr:LiSAF laser; Opt. Lett. **20** (1995) 1874–1876.

95Fer Fermann, M.E.: Nonlinear polarization evolution in passively modelocked fiber lasers, in: Compact Sources of Ultrashort Pulses, New York: Cambridge University Press, 1995, p. 179–207.

95Flo Flood, C.J., Walker, D.R., van Driel, H.M.: CW diode-pumped and FM modelocking of a Nd:KGW laser; Appl. Phys. B **60** (1995) 309–312.

95Gal Gale, G.M., Cavallari, M., Driscoll, T.J., Hache, F.: Sub-20 fs tunable pulses in the visible from an 82 MHz optical parametric oscillator; Opt. Lett. **20** (1995) 1562–1564.

95Hau1 Haus, H.A., Tamura, K., Nelson, L.E., Ippen, E.P.: Stretched-pulse additive pulse modelocking in fiber ring lasers: Theory and experiment; IEEE J. Quantum Electron. **31** (1995) 591–598.

95Hau2 Haus, H.A.: Short pulse generation, in: Compact Sources of Ultrashort Pulses, Duling, I.I.N. (ed.), New York: Cambridge University Press, 1995, p. 1–56.

95Hoe Hönninger, C., Zhang, G., Keller, U., Giesen, A.: Femtosecond Yb:YAG laser using semiconductor saturable absorbers; Opt. Lett. **20** (1995) 2402–2404.

95Jac Jacquemet, M., Jacquemet, C., Janel, N., Druon, F., Balembois, F., Georges, P., Petit, J., Viana, B., Vivien, D., Ferrand, B.: Efficient laser action of Yb:LSO and Yb:YSO oxyorthosilicates crystals under high-power diode-pumping; Appl. Phys. B **80** (2005) 171–176.

95Jia Jiang, W., Bowers, J.: Ultrafast vertical cavity semiconductor lasers, in: Compact Sources of Ultrashort Pulses, Duling, I.I.N. (ed.), New York: Cambridge University Press, 1995, p. 208–273.

95Jun1 Jung, I.D., Brovelli, L.R., Kamp, M., Keller, U., Moser, M.: Scaling of the A-FPSA design toward a thin saturable absorber; Opt. Lett. **20** (1995) 1559–1561.

95Jun2 Jung, I.D., Kärtner, F.X., Brovelli, L.R., Kamp, M., Keller, U.: Experimental verification of soliton modelocking using only a slow saturable absorber; Opt. Lett. **20** (1995) 1892–1894.

95Kae1 Kärtner, F.X., Keller, U.: Stabilization of soliton-like pulses with a slow saturable absorber; Opt. Lett. **20** (1995) 16–18.

95Kae2 Kärtner, F.X., Kopf, D., Keller, U.: Solitary pulse stabilization and shortening in actively mode-locked lasers; J. Opt. Soc. Am. B **12** (1995) 486–496.

95Kae3 Kärtner, F.X., Braun, B., Keller, U.: Continuous-wave-mode-locked solid-state lasers with enhanced spatial hole-burning, Part II: Theory; Appl. Phys. B **61** (1995) 569–579.

95Kel Keller, U., Kopf, D.: Optical component for generating pulsed laser radiation, European Patent No. EP 0 826 164 B1, priority date 19. May 1995.

95Kno Knox, W.H.: Saturable Bragg Reflector, US Patent No. 5,627,854, priority date 15. March 1995.

95Kop1 Kopf, D., Kärtner, F.X., Weingarten, K.J., Keller, U.: Diode-pumped modelocked Nd:glass lasers using an A-FPSA; Opt. Lett. **20** (1995) 1169–1171.

95Kop2 Kopf, D., Weingarten, K.J., Brovelli, L.R., Kamp, M., Keller, U.: Sub-50-fs diode-pumped mode-locked Cr:LiSAF with an A-FPSA, Conference on Lasers and Electro-Optics (CLEO), 1995, paper CWM2.

95Kop3 Kopf, D., Aus der Au, J., Keller, U., Bona, G.L., Roentgen, P.: 400-mW continuous-wave diode-pumped Cr:LiSAF laser based on a power-scalable concept; Opt. Lett. **20** (1995) 1782–1784.

95Kue Kück, S., Petermann, K., Pohlmann, U., Huber, G.: Near-infrared emission of Cr^{4+}-doped garnets: Lifetimes, quantum efficiencies, and emission cross sections; Phys. Rev. B **51** (1995) 17323–17331.

95Lap Laporta, P., Longhi, S., Marchesi, M., Taccheo, S., Svelto, O.: 2.5 GHz and 5 GHz harmonic mode-locking of a diode-pumped bulk erbium-ytterbium glass laser at 1.5 microns; IEEE Photon. Technol. Lett. **7** (1995) 155–157.

95Mag Magni, V., Cerullo, G., Silvestri, S. d., Monguzzi, A.: Astigmatism in Gaussian-beam self-focussing and in resonators for Kerr-lens mode-locking; J. Opt. Soc. Am. B **12** (1995) 476–485.

95Mel Mellish, R., Barry, N.P., Hyde, S.C.W., Jones, R., French, P.M.W., Taylor, J.R., Poel, C.J. v. d., Valster, A.: Diode-pumped Cr:LiSAF all-solid-state femtosecond oscillator and regenerative amplifier; Opt. Lett. **20** (1995) 2312–2314.

95Ski Skidmore, J.A., Emanuel, M.A., Beach, R.J., Benett, W.J., Freitas, B.L., Carlson, N.W., Solarz, R.W.: High-power continous wave 690 nm AlGaInP laser-diode arrays; Appl. Phys. Lett. **66** (1995) 1163–1165.

95Sti Stingl, A., Lenzner, M., Spielmann, Ch., Krausz, F., Szipöcs, R.: Sub-10-fs mirror-dispersion-controlled Ti:sapphire laser; Opt. Lett. **20** (1995) 602–604.

95Tam Tamura, K., Ippen, E.P., Haus, H.A.: Pulse dynamics in stretched-pulse fiber lasers; Appl. Phys. Lett. **67** (1995) 158–160.

95Tsu Tsuda, S., Knox, W.H., Souza, E.A. d., Jan, W.Y., Cunningham, J.E.: Low-loss intracavity AlAs/AlGaAs saturable Bragg reflector for femtosecond mode locking in solid-state lasers; Opt. Lett. **20** (1995) 1406–1408.

95Vai Vail'ev, P.: Ultrafast diode lasers, Boston: Artech House, Inc., 1995.

95Yan Yanovsky, V.P., Wise, F.W., Cassanho, A., Jenssen, H.P.: Kerr-lens mode-locked diode-pumped Cr:LiSGAF laser; Opt. Lett. **20** (1995) 1304–1306.

95Zay Zayhowski, J.J., Dill III, C.: Coupled cavity electro-optically Q-switched Nd:YVO_4 microchip lasers; Opt. Lett. **20** (1995) 716–718.

96Ant Antoine, P., L'Huillier, A., Lewenstein, M.: Attosecond pulse trains using high-order harmonics; Phys. Rev. Lett. **77** (1996) 1234–1237.

96Bra1 Braun, B., Kärtner, F.X., Keller, U., Meyn, J.-P., Huber, G.: Passively Q-switched 180 ps Nd:LSB microchip laser; Opt. Lett. **21** (1996) 405–407.

96Bra2 Braun, B., Hönninger, C., Zhang, G., Keller, U., Heine, F., Kellner, T., Huber, G.: Efficient intracavity frequency doubling of a passively modelocked diode-pumped Nd:LSB laser; Opt. Lett. **21** (1996) 1567–1569.

96Col Collings, B.C., Stark, J.B., Tsuda, S., Knox, W.H., Cunningham, J.E., Jan, W.Y., Pathak, R., Bergman, K.: Saturable Bragg reflector self-starting passive mode locking of a Cr^{4+}:YAG laser pumped with a diode-pumped Nd:YVO_4 laser; Opt. Lett. **21** (1996) 1171–1173.

96Dob Dobrowolski, J.A., Tikhonravov, A.V., Trubetskov, M.K., Sullivan, B.T., Verly, P.G.: Optimal single-band normal-incidence antireflection coatings; Appl. Opt. **35** (1996) 644–658.

96Flu1 Fluck, R., Jung, I.D., Zhang, G., Kärtner, F.X., Keller, U.: Broadband saturable absorber for 10-fs pulse generation; Opt. Lett. **21** (1996) 743–745.

96Flu2 Fluck, R., Zhang, G., Keller, U., Weingarten, K.J., Moser, M.: Diode-pumped passively mode-locked 1.3 μm Nd:YVO_4 and Nd:YLF lasers by use of semiconductor saturable absorbers; Opt. Lett. **21** (1996) 1378–1380.

96Gib Gibson, G.N., Klank, R., Gibson, F., Bouma, B.E.: Electro-optically cavity-dumped ultrashort-pulse Ti:sapphire oscillator; Opt. Lett. **21** (1996) 1055–1057.

96Guy Guy, O., Kubecek, V., Barthelemy, A.: Mode-locked diode-pumped Nd:YAP laser; Opt. Commun. **130** (1996) 41–43.

96Kae Kärtner, F.X., Jung, I.D., Keller, U.: Soliton modelocking with saturable absorbers," special issue on ultrafast electronics, photonics and optoelectronics; IEEE J. Sel. Topics Quantum Electron. **2** (1996) 540–556.

96Kel Keller, U., Weingarten, K.J., Kärtner, F.X., Kopf, D., Braun, B., Jung, I.D., Fluck, R., Hönninger, C., Matuschek, N., Aus der Au, J.: Semiconductor saturable absorber mirrors (SESAMs) for femtosecond to nanosecond pulse generation in solid-state lasers; IEEE J. Sel. Topics Quantum Electron. **2** (1996) 435–453.

96Kig Kigre Inc.: QX Laser Glasses, Data Sheet (1996).

96Koe Koechner, W.: Solid-State Laser Engineering, Schawlow, A.L., Siegman, A.E., Tamir, T., Lotsch, H.K.V. (eds.), Springer Series in Optical Sciences, Heidelberg, Germany: Springer-Verlag, 1996, Vol. 1.

96Kop1 Kopf, D., Spühler, G.J., Weingarten, K.J., Keller, U.: Mode-locked laser cavities with a single prism for dispersion compensation; Appl. Opt. **35** (1996) 912–915.

96Kop2 Kopf, D., Zhang, G., Fluck, R., Moser, M., Keller, U.: All-in-one dispersion-compensating saturable absorber mirror for compact femtosecond laser sources; Opt. Lett. **21** (1996) 486–488.

96Let Lettenberger, M., Wolfrum, K.: Optimized Kerr lens mode-locking of a pulsed Nd:KGW laser; Opt. Commun. **131** (1996) 295–300.

96Nel Nelson, L.E., Fleischer, S.B., Lenz, G., Ippen, E.P.: Efficient frequency doubling of a femtosecond fiber laser; Opt. Lett. **21** (1996) 1759–1761.

96Rhe Rhee, J.-K., Sosnowski, T.S., Tien, A.-C., Norris, T.B.: Real-time dispersion analyzer of femtosecond laser pulses with use of a spectrally and temporally resolved upconversion technique; J. Opt. Soc. Am. B **13** (1996) 1780–1785.

96Sch Schaffers, K.I., DeLoach, L.D., Payne, S.A.: Crystal growth, frequency doubling, and infrared laser performance of Yb^{3+}:$BaCaBO_3F$; IEEE J. Quantum Electron. **32** (1996) 741–748.

96Sha Sharp, R.C., Spock, D.E., Pan, N., Elliot, J.: 190-fs passively modelocked thulium fiber laser with a low threshold; Opt. Lett. **21** (1996) 881.

96Sie Siegner, U., Fluck, R., Zhang, G., Keller, U.: Ultrafast high-intensity nonlinear absorption dynamics in low-temperature grown gallium arsenide; Appl. Phys. Lett. **69** (1996) 2566–2568.

96Sor1 Sorokina, I.T., Sorokin, E., Wintner, E., Cassanho, A., Jenssen, H.P., Noginov, M.A.: Efficient cw TEM00 and femtosecond Kerr-lens modelocked Cr:LiSrGaF laser; Opt. Lett. **21** (1996) 204–206.

96Sor2 Sorokina, I.T., Sorokin, E., Wintner, E., Cassanho, A., Jenssen, H.P., Szipöcs, R.: Prismless passively mode-locked femtosecond Cr:LiSGaF laser; Opt. Lett. **21** (1996) 1165–1167.

96Ton Tong, Y.P., Sutherland, J.M., French, P.M.W., Taylor, J.R., Shestakov, A.V., Chai, B.H.T.: Self-starting Kerr-lens mode-locked femtosecond Cr^{4+}:YAG and picosecond Pr^{3+}:YLF solid-state lasers; Opt. Lett. **21** (1996) 644–646.

96Tsu Tsuda, S., Knox, W.H., Cundiff, S.T.: High efficiency diode pumping of a saturable Bragg reflector-mode-locked Cr:LiSAF femtosecond laser; Appl. Phys. Lett. **69** (1996) 1538–1540.

96Xu1 Xu, L., Spielmann, C., Poppe, A., Brabec, T., Krausz, F., Haensch, T.W.: Route to phase control of ultrashort light pulses; Opt. Lett. **21** (1996) 2008–2010.

96Xu2 Xu, L., Spielmann, C., Krausz, F., Szipöcs, R.: Ultrabroadband ring oscillator for sub-10-fs pulse generation; Opt. Lett. **21** (1996) 1259–1261.

97Agn Agnesi, A., Pennacchio, C., Reali, G.C., Kubecek, V.: High-power diode-pumped picosecond Nd:YVO_4 laser; Opt. Lett. **22** (1997) 1645–1647.

97Aus Aus der Au, J., Kopf, D., Morier-Genoud, F., Moser, M., Keller, U.: 60-fs pulses from a diode-pumped Nd:glass laser; Opt. Lett. **22** (1997) 307–309.

97Bal Baltuska, A., Wei, Z., Pshenichnikov, M.S., Wiersma, D.A., Szipöcs, R.: All-solid-state cavity dumped sub-5-fs laser; Appl. Phys. B **65** (1997) 175–188.

97Bra Braun, B., Kärtner, F.X., Moser, M., Zhang, G., Keller, U.: 56 ps passively Q-switched diode-pumped microchip laser; Opt. Lett. **22** (1997) 381–383.

97Col Collings, B.C., Bergman, K., Knox, W.H.: True fundamental solitons in a passively mode-locked short cavity Cr^{4+}:YAG laser; Opt. Lett. **22** (1997) 1098–1100.

97Dym Dymott, M.J.P., Ferguson, A.I.: Pulse duration limitations in a diode-pumped femtosecond Kerr-lens modelocked Cr:LiSAF laser; Appl. Phys. B **65** (1997) 227–234.

97Fer Fermann, M.E., Galvanauskas, A., Sucha, G., Harter, D.: Fiber-lasers for ultrafast optics; Appl. Phys. B **65** (1997) 259–275.

97Flu Fluck, R., Braun, B., Gini, E., Melchior, H., Keller, U.: Passively Q-switched 1.34 μm Nd:YVO_4 microchip laser using semiconductor saturable-absorber mirrors; Opt. Lett. **22** (1997) 991–993.

97Hen Henrich, B., Beigang, R.: Self-starting Kerr-lens mode locking of a Nd:YAG-laser; Opt. Commun. **135** (1997) 300–304.

97Jun1 Jung, I.D., Kärtner, F.X., Matuschek, N., Sutter, D.H., Morier-Genoud, F., Shi, Z., Scheuer, V., Tilsch, M., Tschudi, T., Keller, U.: Semiconductor saturable absorber mirrors supporting sub-10 fs pulses; Appl. Phys. B **65** (1997) 137–150.

97Jun2 Jung, I.D., Kärtner, F.X., Henkmann, J., Zhang, G., Keller, U.: High-dynamic-range characterization of ultrashort pulses; Appl. Phys. B **65** (1997) 307–310.

97Jun3 Jung, I.D., Kärtner, F.X., Matuschek, N., Sutter, D.H., Morier-Genoud, F., Zhang, G., Keller, U., Scheuer, V., Tilsch, M., Tschudi, T.: Self-starting 6.5 fs pulses from a Ti:sapphire laser; Opt. Lett. **22** (1997) 1009–1011.

97Kae Kärtner, F.X., Matuschek, N., Schibli, T., Keller, U., Haus, H.A., Heine, C., Morf, R., Scheuer, V., Tilsch, M., Tschudi, T.: Design and fabrication of double-chirped mirrors; Opt. Lett. **22** (1997) 831–833.

97Kop1 Kopf, D., Keller, U., Emanuel, M.A., Beach, R.J., Skidmore, J.A.: 1.1-W cw Cr:LiSAF laser pumped by a 1-cm diode-array; Opt. Lett. **22** (1997) 99–101.

97Kop2 Kopf, D., Prasad, A., Zhang, G., Moser, M., Keller, U.: Broadly tunable femtosecond Cr:LiSAF laser; Opt. Lett. **22** (1997) 621–623.

97Kop3 Kopf, D., Weingarten, K.J., Zhang, G., Moser, M., Emanuel, M.A., Beach, R.J., Skidmore, J.A., Keller, U.: High-average-power diode-pumped femtosecond Cr:LiSAF lasers; Appl. Phys. B **65** (1997) 235–243.

97Kul1 Kuleshov, N.V., Lagatsky, A.A., Podlipensky, A.V., Mikhailov, V.P., Huber, G.: Pulsed laser operation of Yb-doped $KY(WO_4)_2$ and $KGd(WO_4)_2$; Opt. Lett. **22** (1997) 1317–1319.

97Kul2 Kuleshov, N.V., Lagatsky, A.A., Shcherbitsky, V.G., Mikhailov, V.P., Heumann, E., Jensen, T., Diening, A., Huber, G.: CW laser performance of Yb and Er,Yb doped tungstates; Appl. Phys. B **64** (1997) 409–413.

97Loe Loesel, F.H., Horvath, C., Grasbon, F., Jost, M., Niemz, M.H.: Selfstarting femtosecond operation and transient dynamics of a diode-pumped Cr:LiSGaF laser with a semiconductor saturable absorber mirror; Appl. Phys. B **65** (1997) 783–787.

97Mat Matuschek, N., Kärtner, F.X., Keller, U.: Exact coupled-mode theories for multilayer interference coatings with arbitrary strong index modulations; IEEE J. Quantum Electron. **33** (1997) 295–302.

97Nis Nisoli, M., Stagira, S., Silvestri, S.D., Svelto, O., Sartania, S., Cheng, Z., Lenzner, M., Spielmann, C., Krausz, F.: A novel high-energy pulse compression system: generation of multigigawatt sub-5-fs pulses; Appl. Phys. B **65** (1997) 189–196.

97Pag Page, R.H., Schaffers, K.I., DeLoach, L.D., Wilke, G.D., Patel, F.D., Tassano, J.B., Payne, S.A., Krupke, W.F., Chen, K.-T., Burger, A.: Cr^{2+}-doped zinc chalcogenides as efficient, widely tunable mid-infrared lasers; IEEE J. Quantum Electron. **33** (1997) 609–619.

97Ruf Ruffing, B., Nebel, A., Wallenstein, R.: A 20-W KTA-OPO synchronously pumped by a cw modelocked Nd:YVO_4 oscillator-amplifier system, Conference on Lasers and Electro-Optics 1997, paper CWB2, p. 199.

97Sar Sartania, S., Cheng, Z., Lenzner, M., Tempea, G., Spielmann, C., Krausz, F., Ferencz, K.: Generation of 0.1-TW 5-fs optical pulses at a 1-kHz repetition rate; Opt. Lett. **22** (1997) 1562–1564.

97Sor Sorokina, I.T., Sorokin, E., Wintner, E., Cassanho, A., Jenssen, H.P., Szipöcs, R.: 14-fs pulse generation in Kerr-lens modelocked prismless Cr:LiSGaF and Cr:LiSAF lasers observation of pulse self-frequency shift; Opt. Lett. **22** (1997) 1716–1718.

97Spa Spälter, S., Böhm, M., Burk, M., Mikulla, B., Fluck, R., Jung, I.D., Zhang, G., Keller, U., Sizmann, A., Leuchs, G.: Self-starting soliton-modelocked femtosecond Cr^{4+}:YAG laser using an antiresonant Fabry–Perot saturable absorber; Appl. Phys. B **65** (1997) 335–338.

97Ton Tong, Y.P., French, P.M.W., Taylor, J.R., Fujimoto, J.O.: All-solid-state femtosecond sources in the near infrared; Opt. Commun. **136** (1997) 235–238.

97Tre Trebino, R., DeLong, K.W., Fittinghoff, D.N., Sweetser, J., Krumbügel, M.A., Richman, B.: Measuring ultrashort laser pulses in the time-frequency domain using frequency-resolved optical gating; Rev. Sci. Instrum. **68** (1997) 1–19.

97Zay Zayhowski, J.J., Harrison, J.: Miniature Solid-State Lasers, in: Handbook of Photonics Gupta, M.C. (ed.), New York: CRC Press, 1997, p. 326–392.

97Zha1 Zhang, Z., Torizuka, K., Itatani, T., Kobayashi, K., Sugaya, T., Nakagawa, T.: Self-starting mode-locked femtosecond forsterite laser with a semiconductor saturable-absorber mirror; Opt. Lett. **22** (1997) 1006–1008.

97Zha2 Zhang, Z., Torizuka, K., Itatani, T., Kobayashi, K., Sugaya, T., Nakagawa, T.: Femtosecond Cr:forsterite laser with modelocking initiated by a quantum well saturable absorber; IEEE J. Quantum Electron. **33** (1997) 1975–1981.

98Aus Aus der Au, J., Loesel, F.H., Morier-Genoud, F., Moser, M., Keller, U.: Femtosecond diode-pumped Nd:glass laser with more than 1-W average output power; Opt. Lett. **23** (1998) 271–273.

98Bal Baltuska, A., Pshenichnikov, M.S., Wiersma, D.A.: Amplitude and phase characterization of 4.5-fs pulses by frequency-resolved optical gating; Opt. Lett. **23** (1998) 1474–1476.

98Cha Chang, Y., Maciejko, R., Leonelli, R., Thorpe, A.: Self-starting passively mode-locked tunable Cr^{4+}:yttrium-aluminium-garnet laser with a single prism for dispersion compensation; Appl. Phys. Lett. **73** (1998) 2098–2100.

98Flu Fluck, R., Häring, R., Paschotta, R., Gini, E., Melchior, H., Keller, U.: Eyesafe pulsed microchip laser using semiconductor saturable absorber mirrors; Appl. Phys. Lett. **72** (1998) 3273–3275.

98For Fornasiero, L., Kück, S., Jensen, T., Huber, G., Chai, B.H.T.: Excited state absorption and stimulated emission of Nd^{3+} in crystals. Part2: YVO_4, $GdVO_4$, and $Sr_5(PO_4)_3F$; Appl. Phys. B **67** (1998) 549–553.

98Gab Gabel, K.M., Russbuldt, P., Lebert, R., Valster, A.: Diode-pumped Cr^{3+}:LiCAF fs-laser; Opt. Commun. **157** (1998) 327–334.

98Hoe Hönninger, C., Morier-Genoud, F., Moser, M., Keller, U., Brovelli, L.R., Harder, C.: Efficient and tunable diode-pumped femtosecond Yb:glass lasers; Opt. Lett. **23** (1998) 126–128.

98Hop Hopkins, J.M., Valentine, G.J., Sibbett, W., Aus der Au, J., Morier-Genoud, F., Keller, U., Valster, A.: Efficient, low-noise, SESAM-based femtosecond Cr^{3+}:$LiSrAlF_6$ laser; Opt. Commun. **154** (1998) 54–58.

98Iac Iaconis, C., Walmsley, I.A.: Spectral phase interferometry for direct electric field reconstruction of ultrashort optical pulses; Opt. Lett. **23** (1998) 792–794.

98Kae Kärtner, F.X., Aus der Au, J., Keller, U.: Modelocking with slow and fast saturable absorbers – What's the difference?; IEEE J. Sel. Topics Quantum Electron. **4** (1998) 159–168.

98Kel Kellner, T., Heine, F., Huber, G., Hönninger, C., Braun, B., Morier-Genoud, F., Keller, U.: Soliton mode-locked Nd:$YAlO_3$ laser at 930 nm; J. Opt. Soc. Am. B **15** (1998) 1663–1666.

98Liu Liu, X., Qian, L., Wise, F., Zhang, Z., Itatani, T., Sugaya, T., Nakagawa, T., Torizuka, K.: Femtosecond Cr:forsterite laser diode pumped by a double-clad fiber; Opt. Lett. **23** (1998) 129–131.

98Lon Longhi, S., Sorbello, G., Taccheo, S., Laporta, P.: 5-GHz repetition-rate dual-wavelength pulse-train generation from an intracavity frequency-modulated Er-Yb:glass laser; Opt. Lett. **23** (1998) 1547–1549.

98Mel Mellish, R., Chernikov, S.V., French, P.M.W., Taylor, J.R.: All-solid-state compact high repetition rate modelocked Cr^{4+}:YAG laser; Electron. Lett. **34** (1998) 552–553.

98Pet Petrov, V., Shcheslavskiy, V., Mirtchev, T., Noack, F., Itatani, T., Sugaya, T., Nakagawa, T.: High-power self-starting femtosecond Cr:forsterite laser; Electron. Lett. **34** (1998) 559–561.

98Sal Salieres, P., L'Huillier, A., Antoine, P., Lewenstein, M.: Study of the spatial and temporal coherence of high-order harmonics, in: Advances in Atomic, Molecular, and Optical Physics, Vol. 41, Bederson, B., Walther, H. (eds.), New York: Academic Press, 1998, p. 83.

98Sor Sorokina, I.T., Sorokin, E., Wintner, E.: On the way towards the pulse-duration limits in prismless KLM Cr:LiSGaF and Cr:LiSAF lasers; Laser Physics **8** (1998) 607–611.

98Sut Sutter, D.H., Jung, I.D., Kärtner, F.X., Matuschek, N., Morier-Genoud, F., Scheuer, V., Tilsch, M., Tschudi, T., Keller, U.: Self-starting 6.5-fs pulses from a Ti:sapphire laser using a semiconductor saturable absorber and double-chirped mirrors; IEEE J. Sel. Topics Quantum Electron. **4** (1998) 169–178.

98Sve Svelto, O.: Principles of Lasers (4th Ed.), New York: Plenum Press, 1998.

98Xu Xu, L., Tempea, G., Spielmann, C., Krausz, F.: Continuous-wave mode-locked Ti:sapphire laser focusable to 5×10^{13} W/cm^2; Opt. Lett. **23** (1998) 789–791.

99Agn Agnesi, A., Dell'Acqua, S., Reali, G.: Nonlinear mirror mode-locking of efficiently diode-pumped pulsed neodymium lasers; J. Opt. Soc. Am. B **16** (1999) 1236–1242.

99Aus Aus der Au, J., Schaer, S.F., Paschotta, R., Hönninger, C., Keller, U., Moser, M.: High-power diode-pumped passively modelocked Yb:YAG lasers; Opt. Lett. **24** (1999) 1281–1283.

99Bar Bartels, A., Dekorsky, T., Kurz, H.: Femtosecond Ti:sapphire ring laser with 2-GHz repetition rate and its application in time-resolved spectroscopy; Opt. Lett. **24** (1999) 996–998.

99Bed Beddard, T., Sibbett, W., Reid, D.T., Garduno-Mejia, J., Jamasbi, N., Mohebi, M.: High-average-power, 1-MW peak-power self-mode-locked Ti:sapphire oscillator; Opt. Lett. **24** (1999) 163–165.

99Bil Bilinsky, I.P., Fujimoto, J.G., Walpole, J.N., Missaggia, L.J.: InAs-doped silica films for saturable absorber applications; Appl. Phys. Lett. **74** (1999) 2411–2413.

99Che Cheng, Z., Fürbach, A., Sartania, S., Lenzner, M., Spielmann, C., Krausz, F.: Amplitude and chirp characterization of high-power laser pulses in the 5-fs regime; Opt. Lett. **24** (1999) 247–249.

99Cho Cho, S.H., Bouma, B.E., Ippen, E.P., Fujimoto, J.G.: Low-repetition-rate high-peak-power Kerr-lens mode-locked Ti:Al_2O_3 laser with a multiple-pass cell; Opt. Lett. **24** (1999) 417–419.

99Cou Couderc, V., Louradour, F., Barthelemy, A.: 2.8 ps pulses from a modelocked diode pumped Nd:YVO_4 laser using quadratic polarization switching; Opt. Commun. **166** (1999) 103–111.

99Dur Durfee III, C.G., Backus, S., Kapteyn, H.C., Murnane, M.M.: Intense 8-fs pulse generation in the deep ultraviolet; Opt. Lett. **24** (1999) 697–699.

99Fit Fittinghoff, D.N., Millard, A.C., Squier, J.A., Müller, M.: Frequency-resolved optical gating measurement of ultrashort pulses passing through a high numerical aperture objective; IEEE J. Quantum Electron. **35** (1999) 479–486.

99Gal Gallmann, L., Sutter, D.H., Matuschek, N., Steinmeyer, G., Keller, U., Iaconis, C., Walmsley, I.A.: Characterization of sub-6-fs optical pulses with spectral phase interferometry for direct electric-field reconstruction; Opt. Lett. **24** (1999) 1314–1316.

99Gra Graf, Th., Ferguson, A.I., Bente, E., Burns, D., Dawson, M.D.: Multi-Watt Nd:YVO_4 laser, mode locked by a semiconductor saturable absorber mirror and side-pumped by a diode-laser bar; Opt. Commun. **159** (1999) 84–87.

99Hai1 Haiml, M., Siegner, U., Morier-Genoud, F., Keller, U., Luysberg, M., Specht, P., Weber, E.R.: Femtosecond response times and high optical nonlinearity in Beryllium doped low-temperature grown GaAs; Appl. Phys. Lett. **74** (1999) 1269–1271.

99Hai2 Haiml, M., Siegner, U., Morier-Genoud, F., Keller, U., Luysberg, M., Lutz, R.C., Specht, P., Weber, E.R.: Optical nonlinearity in low-temperature grown GaAs: microscopic limitations and optimization strategies; Appl. Phys. Lett. **74** (1999) 3134–3136.

99Hol Holm, M.A., Cusumano, P., Burns, D., Ferguson, A.I., Dawson, M.D.: Mode-locked operation of a diode-pumped, external-cavity GaAs/AlGaAs surface emitting laser, Conference on Lasers and Electro-Optics, CLEO'99, 1999, paper CTuK63.

99Hoe1 Hönninger, C., Paschotta, R., Morier-Genoud, F., Moser, M., Keller, U.: Q-switching stability limits of cw passive modelocking; J. Opt. Soc. Am. B **16** (1999) 46–56.

99Hoe2 Hönninger, C., Paschotta, R., Graf, M., Morier-Genoud, F., Zhang, G., Moser, M., Biswal, S., Nees, J., Braun, A., Mourou, G.A., Johannsen, I., Giesen, A., Seeber, W., Keller, U.: Ultrafast ytterbium-doped bulk lasers and laser amplifiers; Appl. Phys. B **69** (1999) 3–17.

99Iac Iaconis, C., Walmsley, I.A.: Self-referencing spectral interferometry for measuring ultrashort optical pulses; IEEE J. Quantum Electron. **35** (1999) 501–509.

99Jeo Jeong, T.M., Kang, E.C., Nam, C.H.: Temporal and spectral characteristics of an additive-pulse mode-locked Nd:YLF laser with Michelson-type configuration; Opt. Commun. **166** (1999) 95–102.

99Kan Kane, D.J.: Recent progress toward real-time measurement of ultrashort laser pulses; IEEE J. Quantum Electron. **35** (1999) 421–431.

99Kel Keller, U.: Semiconductor nonlinearities for solid-state laser modelocking and Q-switching, in: Nonlinear Optics in Semiconductors, Vol. 59, Chap. 4, Garmire, E., Kost, A. (eds.), Boston: Academic Press Inc., 1999, p. 211–286.

99Kra1 Krainer, L., Paschotta, R., Aus der Au, J., Hönninger, C., Keller, U., Moser, M., Kopf, D., Weingarten, K.J.: Passively mode-locked Nd:YVO_4 laser with up to 13 GHz repetition rate; Appl. Phys. B **69** (1999) 245–247.

99Kra2 Krainer, L., Paschotta, R., Spühler, G., Moser, M., Keller, U.: 29 GHz modelocked miniature Nd:YVO_4 laser; Electron. Lett. **35** (1999) 1160–1161.

99Kub Kubecek, V., Couderc, V., Bourliaguet, B., Louradour, F., Barthelemy, A.: 4-W and 23-ps pulses from a lamp-pumped Nd:YAG laser passively mode-locked by polarization switching in a KTP crystal; Appl. Phys. B **69** (1999) 99–102.

99Kuz Kuznetsov, M., Hakimi, F., Sprague, R., Mooradian, A.: Design and characteristics of high-power (> 0.5-W CW) diode-pumped vertical-external-cavity surface-emitting semiconductor lasers with circular TEM_{00} Beams; IEEE J. Sel. Topics Quantum Electron. **5** (1999) 561–573.

99Lap Laporta, P., Taccheo, S., Longhi, S., Svelto, O., Svelto, C.: Erbium-ytterbium microlasers: optical properties and lasing characteristics; Opt. Mater. **11** (1999) 269–288.

99Led Lederer, M.J., Luther-Davies, B., Tan, H.H., Jagadish, C., Haiml, M., Siegner, U., Keller, U.: Nonlinear optical absorption and temporal response of arsenic- and oxygen-implanted GaAs; Appl. Phys. Lett. **74** (1999) 1993–1995.

99Lef Lefort, L., Puech, K., Butterworth, S.D., Svirko, Y.P., Hanna, D.C.: Generation of femtosecond pulses from order-of-magnitude pulse compression in a synchronously pumped optical parametric oscillator based on periodically poled lithium niobate; Opt. Lett. **24** (1999) 28–30.

99Mat Matuschek, N., Kärtner, F.X., Keller, U.: Analytical design of double-chirped mirrors with custom-tailored dispersion characteristics; IEEE J. Quantum Electron. **35** (1999) 129–137.

99Mor1 Morgner, U., Kärtner, F.X., Cho, S.H., Chen, Y., Haus, H.A., Fujimoto, J.G., Ippen, E.P., Scheuer, V., Angelow, G., Tschudi, T.: Sub-two-cycle pulses from a Kerr-lens mode-locked Ti:sapphire laser; Opt. Lett. **24** (1999) 411–413.

99Mor2 Morgner, U., Kärtner, F.X., Cho, S.H., Chen, Y., Haus, H.A., Fujimoto, J.G., Ippen, E.P., Scheuer, V., Angelow, G., Tschudi, T.: Sub-two-cycle pulses from a Kerr-lens mode-locked Ti:sapphire laser: addenda; Opt. Lett. **24** (1999) 920.

99Mou Mougel, F., Dardenne, K., Aka, G., Kahn-Harari, A., Vivien, D.: Ytterbium-doped $Ca_4GdO(BO_3)_3$: an efficient infrared laser and self-frequency doubling crystal; J. Opt. Soc. Am. B **16** (1999) 164–172.

99Pas1 Paschotta, R., Spühler, G.J., Sutter, D.H., Matuschek, N., Keller, U., Moser, M., Hövel, R., Scheuer, V., Angelow, G., Tschudi, T.: Double-chirped semiconductor mirror for dispersion compensation in femtosecond lasers; Appl. Phys. Lett. **75** (1999) 2166–2168.

99Pas2 Paschotta, R., Aus der Au, J., Keller, U.: Strongly enhanced negative dispersion from thermal lensing or other focussing elements in femtosecond laser cavities; J. Opt. Soc. Am. B **17** (1999) 646–651.

99Rei Reichert, J., Holzwarth, R., Udem, T., Hänsch, T.W.: Measuring the frequency of light with mode-locked lasers; Opt. Commun. **172** (1999) 59–68.

99Rob Robertson, A., Ernst, U., Knappe, R., Wallenstein, R., Scheuer, V., Tschudi, T., Burns, D., Dawson, M.D., Ferguson, A.I.: Prismless diode-pumped mode-locked femtosecond Cr:LiSAF laser; Opt. Commun. **163** (1999) 38–43.

99Sch Schott Glass Technologies: Glass for Laser Applications, Data Sheets 1999.

99Sha Shah, J.: Ultrafast spectroscopy of semiconductors and semiconductor nanostructures, 2nd ed., Berlin: Springer-Verlag, 1999.

99Shi Shirakawa, A., Sakane, I., Takasaka, M., Kobayashi, T.: Sub-5-fs visible pulse generation by pulse-front-matched noncollinear optical parametric amplification; Appl. Phys. Lett. **74** (1999) 2268–2270.

99Sid Siders, C.W., Cavalleri, A., Sokolowski-Tinten, K., Toth, C., Guo, T., Kammler, M., Hoegen, M.H. v., Wilson, K.R., Linde, D. v. d., Barty, C.P.J.: Detection of nonthermal melting by ultrafast X-ray diffraction; Science **286** (1999) 1340–1342.

99Spu1 Spühler, G.J., Paschotta, R., Fluck, R., Braun, B., Moser, M., Zhang, G., Gini, E., Keller, U.: Experimentally confirmed design guidelines for passively Q-switched microchip lasers using semiconductor saturable absorbers; J. Opt. Soc. Am. B **16** (1999) 376–388.

99Spu2 Spühler, G.J., Gallmann, L., Fluck, R., Zhang, G., Brovelli, L.R., Harder, C., Laporta, P., Keller, U.: Passively modelocked diode-pumped erbium-ytterbium glass laser using a semiconductor saturable absorber mirror; Electron. Lett. **35** (1999) 567–568.

99Spu3 Spühler, G.J., Paschotta, R., Keller, U., Moser, M., Dymott, M.J.P., Kopf, D., Meyer, J., Weingarten, K.J., Kmetec, J.D., Alexander, J., Truong, G.: Diode-pumped passively mode-locked Nd:YAG laser with 10-W average power in diffraction-limited beam; Opt. Lett. **24** (1999) 528–530.

99Ste Steinmeyer, G., Sutter, D.H., Gallmann, L., Matuschek, N., Keller, U.: Frontiers in ultrashort pulse generation: Pushing the limits in linear and nonlinear optics; Science **286** (1999) 1507–1512.

99Sut Sutter, D.H., Steinmeyer, G., Gallmann, L., Matuschek, N., Morier-Genoud, F., Keller, U., Scheuer, V., Angelow, G., Tschudi, T.: Semiconductor saturable-absorber mirror-assisted Kerr-lens mode-locked Ti:sapphire laser producing pulses in the two-cycle regime; Opt. Lett. **24** (1999) 631–633.

99Tel Telle, H.R., Steinmeyer, G., Dunlop, A.E., Stenger, J., Sutter, D.H., Keller, U.: Carrier-envelope offset phase control: A novel concept for asolute optical frequency measurement and ultrashort pulse generation; Appl. Phys. B **69** (1999) 327–332.

99Tho Thoen, E.R., Koontz, E.M., Joschko, M., Langlois, P., Schibli, T.R., Kärtner, F.X., Ippen, E.P., Kolodziejski, L.A.: Two-photon absorption in semiconductor saturable absorber mirrors; Appl. Phys. Lett. **74** (1999) 3927–3929.

99Tsu Tsuchida, H.: Pulse timing stabilization of a mode-locked Cr:LiSAF laser; Opt. Lett. **24** (1999) 1641–1643.

99Ude Udem, T., Reichert, J., Holzwarth, R., Hänsch, T.W.: Accurate measurement of large optical frequency differences with a mode-locked laser; Opt. Lett. **24** (1999) 881–883.

99Uem Uemura, S., Torizuka, K.: Generation of 12-fs pulses from a diode-pumped Kerr-lens mode-locked Cr:LiSAF laser; Opt. Lett. **24** (1999) 780–782.

99Zha Zhang, Z., Nakagawa, T., Torizuka, K., Sugaya, T., Kobayashi, K.: Self-starting modelocked Cr^{4+}:YAG laser with a low-loss broadband semiconductor saturable-absorber mirror; Opt. Lett. **24** (1999) 1768–1770.

00And Anderson, M.E., de Araujo, L.E.E., Kosik, E.M., Walmsley, I.A.: The effects of noise on ultrashort-optical-pulse measurement using SPIDER; Appl. Phys. B **70**, Supplement 1 (2000) S85–S93.

00Apo Apolonski, A., Poppe, A., Tempea, G., Spielmann, C., Udem, T., Holzwarth, R., Hänsch, T.W., Krausz, F.: Controlling the phase evolution of few-cycle light pulses; Phys. Rev. Lett. **85** (2000) 740.

00Aus Aus der Au, J., Spühler, G.J., Südmeyer, T., Paschotta, R., Hövel, R., Moser, M., Erhard, S., Karszewski, M., Giesen, A., Keller, U.: 16.2 W average power from a diode-pumped femtosecond Yb:YAG thin disk laser; Opt. Lett. **25** (2000) 859.

00Avr Avrutin, E.A., Marsh, J.H., Portnoi, E.L.: Monolithic and multi-GigaHertz mode-locked semiconductor lasers: Constructions, experiments, models and applications; IEE Proc. Part J Optoelectron. **147** (2000) 251–278.

00Bra Brabec, T., Krausz, F.: Intense few-cycle laser fields: Frontiers of nonlinear optics; Rev. Mod. Phys. **72** (2000) 545–591.

00Bru Brunner, F., Spühler, G.J., Aus der Au, J., Krainer, L., Morier-Genoud, F., Paschotta, R., Lichtenstein, N., Weiss, S., Harder, C., Lagatsky, A.A., Abdolvand, A., Kuleshov, N.V., Keller, U.: Diode-pumped femtosecond Yb:$KGd(WO_4)_2$ laser with 1.1-W average power; Opt. Lett. **25** (2000) 1119–1121.

00Bur Burns, D., Hetterich, M., Ferguson, A.I., Bente, E., Dawson, M.D., Davies, J.I., Bland, S.W.: High-average-power (> 20 W) Nd:YVO_4 lasers mode locked by strain-compensated saturable Bragg reflectors; J. Opt. Soc. Am. B **17** (2000) 919–926.

00Car Carrig, T.J., Wagner, G.J., Sennaroglu, A., Jeong, J.Y., Pollock, C.R.: Mode-locked Cr^{2+}:ZnSe laser; Opt. Lett. **25** (2000) 168–170.

00Dem Demidovich, A.A., Kuzmin, A.N., Ryabtsev, G.I., Danailov, M.B., Strek, W., Titov, A.N.: Influence of Yb concentration on Yb:KYW laser properties; J. Alloys Compounds **300–301** (2000) 238–241

00Dor Dorrer, C., Belabas, N., Likforman, J.P., Joffre, M.: Spectral resolution and sampling issues in Fourier-transform spectral interferometry; J. Opt. Soc. Am. B **17** (2000) 1795–1802.

00Dru Druon, F., Balembois, F., Georges, P., Brun, A., Courjaud, A., Hönninger, C., Salin, F., Aron, A., Mougel, F., Aka, G., Vivien, D.: Generation of 90-fs pulses from a modelocked diode-pumped Yb:$Ca_4GdO(BO_3)_3$ laser; Opt. Lett. **25** (2000) 423–425.

00Gal1 Gallmann, L., Steinmeyer, G., Sutter, D.H., Matuschek, N., Keller, U.: Collinear type-II second-harmonic-generation frequency-resolved optical gating for the characterization of sub-10-fs optical pulses; Opt. Lett. **25** (2000) 269–271.

00Gal2 Gallmann, L., Sutter, D.H., Matuschek, N., Steinmeyer, G., Keller, U.: Techniques for the characterization of sub-10-fs optical pulses: A comparison; Appl. Phys. B **70** (2000) S67–S75.

00Hau Haus, H.A.: Mode-locking of lasers; IEEE J. Sel. Topics Quantum Electron. **6** (2000) 1173–1185.

00Hoo Hoogland, S., Dhanjal, S., Roberts, J.S., Tropper, A.C., Häring, R., Paschotta, R., Morier-Genoud, F., Keller, U.: Passively modelocked diode-pumped surface-emitting semiconductor laser; IEEE Photon. Technol. Lett. **12** (2000) 1135–1137.

00Jon Jones, D.J., Diddams, S.A., Ranka, J.K., Stentz, A., Windeler, R.S., Hall, J.L., Cundiff, S.T.: Carrier-envelope phase control of femtosecond mode-locked lasers and direct optical frequency synthesis; Science **288** (2000) 635–639.

00Kra1 Krainer, L., Paschotta, R., Moser, M., Keller, U.: Passively modelocked picosecond lasers with up to 59 GHz repetition rate; Appl. Phys. Lett. **77** (2000) 2104–2105.

00Kra2 Krainer, L., Paschotta, R., Moser, M., Keller, U.: 77 GHz soliton modelocked Nd:YVO_4 laser; Electron. Lett. **36** (2000) 1846–1848.

00Lar Larotonda, M.A., Hnilo, A.A., Diodati, F.P.: Diode-pumped self-starting Kerr-lens mode locking Nd:YAG laser; Opt. Commun. **183** (2000) 485–491.

00Li Li, C., Song, J., Shen, D., Kim, N.S., Lu, J., Ueda, K.: Diode-pumped passively Q-switched Nd:$GdVO_4$ lasers operating at 1.06 μm wavelength; Appl. Phys. B **70** (2000) 471–474.

00Mat Matuschek, N., Gallmann, L., Sutter, D.H., Steinmeyer, G., Keller, U.: Back-side coated chirped mirror with ultra-smooth broadband dispersion characteristics; Appl. Phys. B **71** (2000) 509–522.

00Pas1 Paschotta, R., Aus der Au, J., Spühler, G.J., Morier-Genoud, F., Hövel, R., Moser, M., Erhard, S., Karszewski, M., Giesen, A., Keller, U.: Diode-pumped passively mode-locked lasers with high average power; Appl. Phys. B **70** (2000) S25–S31.

00Pas2 Paschotta, R., Aus der Au, J., Keller, U.: Thermal effects in high power end-pumped lasers with elliptical mode geometry; J. Sel. Topics Quantum Electron. **6** (2000) 636–642.

00Sch Schön, S., Haiml, M., Keller, U.: Ultrabroadband AlGaAs/CaF_2 semiconductor saturable absorber mirrors; Appl. Phys. Lett. **77** (2000) 782.

00Sie Siegner, U., Keller, U.: Nonlinear optical processes for ultrashort pulse generation, in: Handbook of Optics, Vol. III, Bass, M., Stryland, E.W., Williams, D.R., Wolfe, W.L. (eds.), New York: McGraw-Hill, Inc., 2000.

00Spu Spühler, G.J., Südmeyer, T., Paschotta, R., Moser, M., Weingarten, K.J., Keller, U.: Passively mode-locked high-power Nd:YAG lasers with multiple laser heads; Appl. Phys. B **71** (2000) 19–25.

00Sut Sutter, D.H., Gallmann, L., Matuschek, N., Morier-Genoud, F., Scheuer, V., Angelow, G., Tschudi, T., Steinmeyer, G., Keller, U.: Sub-6-fs pulses from a SESAM-assisted

Kerr-lens modelocked Ti:sapphire laser: At the frontiers of ultrashort pulse generation; Appl. Phys. B **71** (2000) S5–S12.

00Tom Tomaru, T., Petek, H.: Femtosecond Cr^{4+}:YAG laser with an L-fold cavity operating at a 1.2 GHz repetition rate; Opt. Lett. **25** (2000) 584–586.

00Wan Wang, P., Dawes, J.M., Dekker, P., Piper, J.A.: Highly efficient diode-pumped ytterbium-doped yttrium aluminum berate laser; Opt. Commun. **174** (2000) 467–470.

01Bau Bauer, M., Lei, C., Read, K., Tobey, R., Gland, J., Murnane, M.M., Kapteyn, H.C.: Direct observation of surface chemistry using ultrafast soft-X-ray pulses; Phys. Rev. Lett. **87** (2001) 025501.

01Bru Brunner, F., Paschotta, R., Aus der Au, J., Spühler, G.J., Morier-Genoud, F., Hövel, R., Moser, M., Erhard, S., Karszewski, M., Giesen, A., Keller, U.: Widely tunable pulse durations from a passively mode-locked thin-disk Yb:YAG laser; Opt. Lett. **26** (2001) 379–381.

01Che1 Chen, Y.F., Tsai, S.W., Lan, Y.P., Wang, S.C., Huang, K.F.: Diode-end-pumped passively mode-locked high-power Nd:YVO_4 laser with a relaxed saturable Bragg reflector; Opt. Lett. **26** (2001) 199–201.

01Che2 Chen, Y.F., Huang, K.F., Tsai, S.W., Lan, Y.P., Wang, S.C., Chen, J.: Simultaneous modelocking in a diode-pumped passively Q-switched Nd:YVO_4 laser with a GaAs saturable absorber; Appl. Opt. **40** (2001) 6038–6041.

01Chu Chudoba, C., Fujimoto, J.G., Ippen, E.P., Haus, H.A., Morgner, U., Kärtner, F.X., Scheuer, V., Angelow, G., Tschudi, T.: All-solid-state Cr:forsterite laser generating 14-fs pulses at 1.3 μm; Opt. Lett. **26** (2001) 292–294.

01Cun Cundiff, S.T., Ye, J., Hall, J.L.: Optical frequency synthesis based on mode-locked lasers; Rev. Sci. Instrum. **27** (2001) 3750–3771.

01Dai Dai, J.M., Zhang, W.L., Zhang, L.Z., Chai, L., Wang, Y., Zhang, Z.G., Xing, Q.R., Wang, C.Y., Torizuka, K., Nakagawa, T., Sugaya, T.: A diode-pumped, self-starting, all-solid-state self-mode-locked Cr:LiSGAF laser; Opt. Laser Technol. **33** (2001) 71–73.

01Dre Drescher, M., Hentschel, M., Kienberger, R., Tempea, G., Spielmann, C., Reider, G.A., Corkum, P.B., Krausz, F.: X-ray pulses approaching the attosecond frontier; Science **291** (2001) 1923–1927.

01Ell Ell, R., Morgner, U., Kärtner, F.X., Fujimoto, J.G., Ippen, E.P., Scheuer, V., Angelow, G., Tschudi, T., Lederer, M.J., Boiko, A., Luther-Davis, B.: Generation of 5-fs pulses and octave-spanning spectra directly from a Ti:sapphire laser; Opt. Lett. **26** (2001) 373–375.

01Gal Gallmann, L., Steinmeyer, G., Sutter, D.H., Rupp, T., Iaconis, C., Walmsley, I.A., Keller, U.: Spatially resolved amplitude and phase characterization of femtosecond optical pulses; Opt. Lett. **26** (2001) 96–98.

01Gar Garnache, A., Hoogland, S., Tropper, A.C., Gerard, J.M., Thierry-Mieg, V., Roberts, J.S.: CLEO/Europe-EQEC, Postdeadline Paper C-PSL 163, 2001.

01Han Hansson, B.T., Friberg, A.T.: Eye-safe Q-switched microchip laser with an electro-absoring semiconductor modulator; Opt. Lett. **26** (2001) 1057–1059.

01Hae1 Häring, R., Paschotta, R., Fluck, R., Gini, E., Melchior, H., Keller, U.: Passively Q-switched microchip laser at 1.5 μm; J. Opt. Soc. Am. B **18** (2001) 1805–1812.

01Hae2 Häring, R., Paschotta, R., Gini, E., Morier-Genoud, F., Melchior, H., Martin, D., Keller, U.: Picosecond surface-emitting semiconductor laser with > 200 mW average power; Electron. Lett. **37** (2001) 766–767.

01Hae3 Häring, R., Paschotta, R., Fluck, R., Gini, E., Melchior, H., Keller, U.: Passively Q-switched Microchip Laser at 1.5 μm; J. Opt. Soc. Am. B **18** (2001) 1805–1812.

01Hen Hentschel, M., Kienberger, R., Spielmann, Ch., Reider, G.A., Milosevic, N., Brabec, T., Corkum, P., Heinzmann, U., Drescher, M., Krausz, F.: Attosecond metrology; Nature (London) **414** (2001) 511–515.

01Hol Holzwarth, R., Zimmermann, M., Udem, T., Hänsch, T.W.: Optical clockworks and the measurement of laser frequencies with a mode-locked frequency comb; IEEE J. Quantum Electron. **37** (2001) 1493–1501.

01Kae Kärtner, F.X., Morgner, U., Ell, R., Schibli, T., Fujimoto, J.G., Ippen, E.P., Scheuer, V., Angelow, G., Tschudi, T.: Ultrabroadband double-chirped mirror pairs for generation of octave spectra; J. Opt. Soc. Am. B **18** (2001) 882–885.

01Kem Kemp, A.J., Stormont, B., Agate, B., Brown, C.T.A., Keller, U., Sibbett, W.: Gigahertz repetition-rates from a directly diode-pumped femtosecond Cr:LiSAF laser; Electron. Lett. **37** (2001) 1457–1458.

01Led Lederer, M.J., Kolev, V., Luther-Davies, B., Tan, H.H., Jagadish, C.: Ion-implanted InGaAs single quantum well semiconductor saturable absorber mirrors for passive mode-locking; J. Phys. D **34** (2001) 2455–2464.

01Liu Liu, H., Nees, J., Mourou, G.: Diode-pumped Kerr-lens mode-locked Yb:$KY(WO_4)_2$ laser; Opt. Lett. **26** (2001) 1723–1725.

01Lu Lu, W., Yan, L., Menyuk, C.R.: Kerr-lens mode-locking of Nd:glass laser; Opt. Commun. **200** (2001) 159–163.

01Pas1 Paschotta, R., Keller, U.: Passive mode locking with slow saturable absorbers; Appl. Phys. B **73** (2001) 653–662.

01Pas2 Paschotta, R., Aus der Au, J., Spühler, G.J., Erhard, S., Giesen, A., Keller, U.: Passive mode locking of thin disk lasers: effects of spatial hole burning; Appl. Phys. B **72** (2001) 267–278.

01Pau1 Paulus, G.G., Grasborn, F., Walther, H., Villoresi, P., Nisoli, M., Stagira, S., Priori, E., Silvestri, S.D.: Absolute-phase phenomena in photoionization with few-cycle laser pulses; Nature (London) **414** (2001) 182–184.

01Pau2 Paul, P.M., Toma, E.S., Breger, P., Mullot, G., Augé, F., Balcou, P., Muller, H.G., Agostini, P.: Observation of a train of attosecond pulses from high harmonic generation; Science **292** (2001) 1689–1692.

01Rou Rousse, A., Rischel, C., Fourmaux, S., Uschmann, I., Sebban, S., Grillon, G., Balcou, P., Förster, E., Geindre, J.P., Audebert, P., Gauthier, J.C., Hulin, D.: Non-termal melting in semiconductors measured at femtosecond resolution; Nature (London) **410** (2001) 65–68.

01Sch Schibli, T.R., Kremp, T., Morgner, U., Kärtner, F.X., Butendeich, R., Schwarz, J., Schweizer, H., Scholz, F., Hetzler, J., Wegener, M.: Continuous-wave operation and Q-switched mode locking of Cr^{4+}:YAG microchip lasers; Opt. Lett. **26** (2001) 941–943.

01Spu1 Spühler, G.J., Reffert, S., Haiml, M., Moser, M., Keller, U.: Output-coupling semiconductor saturable absorber mirror; Appl. Phys. Lett. **78** (2001) 2733–2735.

01Spu2 Spühler, G.J., Paschotta, R., Kullberg, M.P., Graf, M., Moser, M., Mix, E., Huber, G., Harder, C., Keller, U.: A passively Q-switched Yb:YAG microchip laser; Appl. Phys. B **72** (2001) 285–287.

01Spu3 Spühler, G.J., Paschotta, R., Fluck, R., Braun, B., Moser, M., Zhang, G., Gini, E., Keller, U.: Errata to [99Spu1]: J. Opt. Soc. Am. B **18** (2001) 886.

01Sue Südmeyer, T., Aus der Au, J., Paschotta, R., Keller, U., Smith, P.G.R., Ross, G.W., Hanna, D.C.: Novel ultrafast parametric systems: high repetition rate single-pass OPG and fiber-feedback OPO; J. Phys. D **34** (2001) 2433–2439.

01Tem Tempea, G.: Tilted-front-interface chirped mirrors; J. Opt. Soc. Am. B **18** (2001) 1747–1750.

01Tom Tomaru, T.: Two-element-cavity femtosecond Cr:YAG laser operating at a 2.6-GHz repetition rate; Opt. Lett. **26** (2001) 1439–1441.

01Was Wasik, G., Helbing, F.W., König, F., Sizmann, A., Leuchs, G.: Bulk Er:Yb:glass soliton femtosecond laser, Conference on Lasers and Electro-Optics (CLEO) 2001, paper CMA4.

02Aga Agate, B., Stormont, B., Kemp, A.J., Brown, C.T.A., Keller, U., Sibbett, W.: Simplified cavity designs for efficient and compact femtosecond Cr:LiSAF lasers; Opt. Commun. **205** (2002) 207–213.

02Bar Bartels, A., Kurz, H.: Generation of a broadband continuum by a Ti:sapphire femtosecond oscillator with a 1-GHz repetition rate; Opt. Lett. **27** (2002) 1839–1841.

02Bau Bauch, A., Telle, H.R.: Frequency standards and frequency measurement; Rep. Prog. Phys. **65** (2002) 789–843.

02Bru Brunner, F., Südmeyer, T., Innerhofer, E., Morier-Genoud, F., Paschotta, R., Kisel, V.E., Shcherbitsky, V.G., Kuleshov, N.V., Gao, J., Contag, K., Giesen, A., Keller, U.: 240-fs pulses with 22-W average power from a mode-locked thin-disk Yb:$KY(WO_4)_2$ laser; Opt. Lett. **27** (2002) 1162–1164.

02Dor1 Dorrer, C., Walmsley, I.A.: Accuracy criterion for ultrashort pulse characterization techniques: application to spectral phase interferometry for direct electric field reconstruction,; J. Opt. Soc. Am. B **19** (2002) 1019–1029.

02Dor2 Dorrer, C., Walmsley, I.A.: Precision and consistency criteria in spectral phase interferometry for direct electric-field reconstruction; J. Opt. Soc. Am. B **19** (2002) 1030–1038.

02Dre Drescher, M., Hentschel, M., Kienberger, R., Uiberacker, M., Yakovlev, V., Scrinzi, A., Westerwalbesloh, Th., Kleineberg, U., Heinzmann, U., Krausz, F.: Time-resolved atomic inner-shell spectroscopy; Nature (London) **419** (2002) 803–807.

02Dru1 Druon, F., Chenais, S., Raybaut, P., Balembois, F., Georges, P., Gaume, R., Aka, G., Viana, B., Mohr, S., Kopf, D.: Diode-pumped Yb:$Sr_3Y(BO_3)_3$ femtosecond laser; Opt. Lett. **27** (2002) 197–199.

02Dru2 Druon, F., Chenais, S., Balembois, F., Georges, P., Brun, A., Courjaud, A., Honninger, C., Salin, F., Zavelani-Rossi, M., Auge, F., Chambaret, J.P., Aron, A., Mougel, F., Aka, G., Vivien, D.: High-power diode-pumped Yb: GdCOB laser: from continuous-wave to femtosecond regime; Opt. Mater. **19** (2002) 73–80.

02Gal Gallmann, L., Steinmeyer, G., Imeshev, G., Meyn, J.-P., Fejer, M.M., Keller, U.: Sub-6-fs blue pulses generated by quasi phase-matching second-harmonic generation pulse compression; Appl. Phys. B **74** (2002) S237–S243.

02Gar Garnache, A., Hoogland, S., Tropper, A.C., Sagnes, I., Saint-Girons, G., Roberts, J.S.: $<$ 500-fs soliton pulse in a passively mode-locked broadband surface-emitting laser with 100-mW average power; Appl. Phys. Lett. **80** (2002) 3892–3894.

02Hae Häring. R., Paschotta, R., Aschwanden, A., Gini, E., Morier-Genoud, F., Keller, U.: High power passively modelocked semiconductor laser; IEEE J. Quantum Electron. **38** (2002) 1268–1275.

02Han Han, S., Lu, W., Sheh, B.Y., Yan, L., Wraback, M., Shen, H., Pamulapati, J., Newman, P.G.: Generation of sub-40 fs pulses from a mode-locked dual-gain-media Nd:glass laser; Appl. Phys. B **74** (2002) S177–S179.

02Har Harris jr., J.S.: GaInNAs long-wavelength lasers: progress and challenges; Semicond. Sci. Technol. **17** (2002) 880–891.

02Hel1 Helbing, F.W., Steinmeyer, G., Stenger, J., Telle, H.R., Keller, U.: Carrier-envelope offset dynamics and stabilization of femtosecond pulses; Appl. Phys. B **74** (2002) S35–S42.

02Hel2 Helbing, F.W., Steinmeyer, G., Keller, U., Windeler, R.S., Stenger, J., Telle, H.R.: Carrier-envelope offset dynamics of mode-locked lasers; Opt. Lett. **27** (2002) 194–196.

02Hop Hopkins, J.M., Valentine, G.J., Agate, B., Kemp, A.J., Keller, U., Sibbett, W.: Highly compact and efficient femtosecond Cr:LiSAF lasers; IEEE J. Quantum Electron. **38** (2002) 360–368.

02Klo Klopp, P., Petrov, V., Griebner, U., Erbert, G.: Passively mode-locked Yb:KYW laser pumped by a tapered diode laser; Opt. Express **10** (2002) 108–113.

02Kra1 Krainer, L., Paschotta, R., Spühler, G.J., Klimov, I., Teisset, C., Weingarten, K.J., Keller, U.: Tunable picosecond pulse-generating laser with a repetition rate exceeding 10 GHz; Electron. Lett. **38** (2002) 225–226.

02Kra2 Krainer, L., Paschotta, R., Lecomte, S., Moser, M., Weingarten, K.J., Keller, U.: Compact Nd:YVO_4 lasers with pulse repetition rates up to 160 GHz; IEEE J. Quantum Electron. **38** (2002) 1331–1338.

02Lec Lecomte, S., Krainer, L., Paschotta, R., Dymott, M.J.P., Weingarten, K.J., Keller, U.: Optical parametric oscillator with 10 GHz repetition rate and 100 mW average output power in the 1.5-μm spectral region; Opt. Lett. **27** (2002) 1714–1717.

02Led Lederer, M.J., Hildebrandt, M., Kolev, V.Z., Luther-Davies, B., Taylor, B., Dawes, J., Dekker, P., Piper, J., Tan, H.H., Jagadish, C.: Passive mode locking of a self-frequency-doubling Yb:$YAl_3(BO_3)_4$ laser; Opt. Lett. **27** (2002) 436–438.

02Maj1 Major, A., Langford, N., Graf, T., Ferguson, A.I.: Additive-pulse mode locking of a diode-pumped Nd:$KGd(WO_4)_2$ laser; Appl. Phys. B **75** (2002) 467–469.

02Maj2 Major, A., Langford, N., Graf, T., Burns, D., Ferguson, A.I.: Diode-pumped passively mode-locked Nd:$KGd(WO_4)_2$ laser with 1-W average output power; Opt. Lett. **27** (2002) 1478–1480.

02Maj3 Major, A., Giniunas, L., Langford, N., Ferguson, A.I., Burns, D., Bente, E., Danielius, R.: Saturable Bragg reflector-based continuous-wave mode locking of Yb: $KGd(WO_4)_2$ laser; J. Mod. Opt. **49** (2002) 787–793.

02Pas Paschotta, R., Häring, R., Keller, U., Garnache, A., Hoogland, S., Tropper, A.C.: Soliton-like pulse formation mechanism in passively mode-locked surface-emitting semiconductor lasers; Appl. Phys. B **75** (2002) 445–451.

02Pra Prasankumar, R.P., Chudoba, C., Fujimoto, J.G., Mak, P., Ruane, M.F.: Self-starting mode locking in a Cr:forsterite laser by use of non-epitaxially-grown semiconductor-doped silica films; Opt. Lett. **27** (2002) 1564–1566.

02Puj Pujol, M.C., Bursukova, M.A., Güell, F., Mateos, X., Solé, R., Gavaldà, Jna., Aguiló, M., Massons, J., Diaz, F., Klopp, P., Griebner, U., Petrov, V.: Growth, optical characterization, and laser operation of a stoichiometric crystal KYb $(WO_4)_2$; Phys. Rev. B **65** (2002) 165121–165131.

02Rie Riechert, H., Ramakrishnan, A., Steinle, G.: Development of InGaAsN-based 1.3 μm VCSELs; Semicond. Sci. Technol. **17** (2002) 892–897.

02Rip1 Ripin, D.J., Chudoba, C., Gopinath, J.T., Fujimoto, J.G., Ippen, E.P., Morgner, U., Kärtner, F.X., Scheuer, V., Angelow, G., Tschudi, T.: Generation of 20-fs pulses by a prismless Cr:YAG laser; Opt. Lett. **27** (2002) 61–63.

02Rip2 Ripin, D.J., Gopinath, J.T., Shen, H.M., Erchak, A.A., Petrich, G.S., Kolodziejski, L.A., Kärtner, F.X., Ippen, E.P.: Oxidized GaAs/AlAs mirror with a quantum-well saturable absorber for ultrashort-pulse Cr^{4+}:YAG laser; Opt. Commun. **214** (2002) 285–289.

02Rot Roth U., Balmer, J.E.: Neodymium: YLF lasers at 1053 nm passively mode locked with a saturable Bragg reflector; Appl. Opt. **41** (2002) 459–463.

02Sch1 Schmidt, O., Bauer, M., Wiemann, C., Porath, R., Scharte, M., Andreyev, O., Schönhense, G., Aeschlimann, M.: Time-resolved two-photon photoemission electron microscopy; Appl. Phys. B **74** (2002) 223–227.

02Sch2 Schön, S., Haiml, M., Gallmann, L., Keller, U.: Fluoride semiconductor saturable-absorber mirror for ultrashort pulse generation; Opt. Lett. **27** (2002) 1845–1847.

02She Shen, D.Y., Tang, D.Y., Ueda, K.: Continuous wave and Q-Switched mode-locking of a Nd:YVO_4 laser with a single crystal GaAs wafer; Jpn. J. Appl. Phys. Part 2 **41** (2002) L1224–L1227.

02Spu Spühler, G.J., Dymott, M., Klimov, I., Luntz, G., Baraldi, L., Kilburn, I., Crosby, P., Thomas, S., Zehnder, O., Teisset, C.Y., Brownell, M., Weingarten, K.J., Dangel, R., Offrein, B.J., Bona, G.L., Buccafusca, O., Kaneko, Y., Krainer, L., Paschotta, R.,

Keller, U.: 40 GHz pulse generating source with sub-picosecond timing jitter; Electron. Lett. **38** (2002) 1031–1033.

02Sun Sun, H.D., Valentine, G.J., Macaluso, R., Calvez, S., Burns, D., Dawson, M.D., Jouhti, T., Pessa, M.: Low-loss 1.3 μm GaInNAs saturable Bragg reflector for high-power picosecond neodymium lasers; Opt. Lett. **27** (2002) 2124–2126.

02Ude Udem, T., Holzwarth, R., Hänsch, T.W.: Optical frequency metrology; Nature (London) **416** (2002) 233–237.

02Wag Wagenblast, P.C., Morgner, U., Grawert, F., Schibli, T.R., Kärtner, F.X., Scheuer, V., Angelow, G., Lederer, M.J.: Generation of sub-10-fs pulses from a Kerr-lens mode-locked Cr:LiCAF laser oscillator by use of third-order dispersion-compensating double-chirped mirrors; Opt. Lett. **27** (2002) 1726–1728.

02Zav Zavelani-Rossi, M., Polli, D., Cerullo, G., De Silvestri, S., Gallmann, L., Steinmeyer, G. Keller, U.: Few-optical-cycle laser pulses by OPA: broadband chirped mirror compression and SPIDER characterization; Appl. Phys. B **74** (2002) S245–S251.

03Del Delfyett, P.J.: Ultrafast single- and multiwavelength modelocked semiconductor lasers: physics and applications, in: Ultrafast Lasers: Technology and Applications, Fermann, M.E., Galvanauskas, A., Sucha, G. (eds.), New York: Marcel Dekker Inc., 2003, p. 219–321.

03Dru Druon, F., Balembois, F., Georges, P.: Laser crystals for the production of ultra-short laser pulses; Ann. Chim. (Paris) **28** (2003) 47–72.

03Fer Fermann, M.E.: Ultrafast fiber oscillators, in: Ultrafast Lasers: Technology and Applications, Fermann, M.E., Galvanauskas, A., Sucha, G. (eds.), New York: Marcel Dekker Inc., 2003, p. 89–154.

03Gal Galvanauskas, A.: Ultrashort-pulse fiber amplifiers, in: Ultrafast Lasers: Technology and Applications, Fermann, M.E., Galvanauskas, A., Sucha, G. (eds.), New York: Marcel Dekker Inc., 2003, p. 155–217.

03Gar Garduno-Mejia, J., Ramsay, E., Greenaway, A., Reid, D.T.: Real time femtosecond optical pulse measurement using a video-rate frequency-resolved optical gating system.; Rev. Sci. Instrum. **74** (2003) 3624–3627.

03He He, J.L., Lee, C.K., Huang, J.Y.J., Wang, S.C., Pan, C.L., Huang, K.F.: Diode-pumped passively mode-locked multiwatt Nd:$GdVO_4$ laser with a saturable Bragg reflector; Appl. Opt. **42** (2003) 5496–5499.

03Hel Helbing, F.W., Steinmeyer, G., Keller, U.: Carrier-envelope offset phase-locking with attosecond timing jitter; IEEE J. Sel. Topics Quantum Electron. **9** (2003) 1030–1040.

03Hoo Hoogland, S., Garnache, A., Sagnes, I., Paldus, B., Weingarten, K.J., Grange, R., Haiml, M., Paschotta, R., Keller, U., Tropper, A.C.: Picosecond pulse generation with a 1.5-μm passively mode-locked surface-emitting semiconductor laser; Electron. Lett. **39** (11) (2003) 846–847.

03Inn Innerhofer, E., Südmeyer, T., Brunner, F., Häring, R., Aschwanden, A., Paschotta, R., Hönninger, C., Kumkar, M., Keller, U.: 60-W average power in 810-fs pulses from a thin-disk Yb:YAG laser; Opt. Lett. **28** (2003) 367–369.

03Jas Jasim, K., Zhang, Q., Nurmikko, A.V., Mooradian, A., Carey, G., Ha, W., Ippen, E.: Passively modelocked vertical extended cavity surface emitting diode laser; Electron. Lett. **39** (2003) 373–375.

03Kan Kang, I., Dorrer, C., Quochi, F.: Implementation of electro-optic spectral shearing interferometry for ultrashort pulse characterization; Opt. Lett. **28** (2003) 2264–2266.

03Kel Keller, U.: Recent developments in compact ultrafast lasers; Nature (London) **424** (2003) 831–838.

03Kol Kolev, V.Z., Lederer, M.J., Luther-Davies, B., Rode, A.V.: Passive mode locking of a Nd:YVO_4 laser with an extra-long optical resonator; Opt. Lett. **28** (2003) 1275–1277.

03Kor Kornelis, W., Biegert, J., Tisch, J.W.G., Nisoli, M., Sansone, G., De Silvestri, S., Keller, U.: Single-shot kilohertz characterization of ultrashort pulses by spectral phase interferometry for direct electric-field reconstruction; Opt. Lett. **28** (2003) 281–283.

03Kow Kowalevicz, A.M., Zare, A.T., Kärtner, F.X., Fujimoto, J.G., Dewald, S., Morgner, U., Scheuer, V., Angelow, G.: Generation of 150-nJ pulses from a multiple-pass cavity Kerr-lens mode-locked Ti: Al_2O_3 oscillator; Opt. Lett. **28** (2003) 1597–1599.

03Kul Kuleshov, N.V.: Private communication.

03Lag1 Lagatsky, A.A., Rafailov, E.U., Leburn, C.G., Brown, C.T.A., Xiang, N., Okhotnikov, O.G., Sibbett, W.: Highly efficient femtosecond Yb:KYW laser pumped by single narrow-stripe laser diode; Electron. Lett. **39** (2003) 1108–1110.

03Lag2 Lagatsky, A.A., Leburn, C.G., Brown, C.T.A., Sibbett, W., Knox, W.H.: Compact self-starting femtosecond Cr^{4+}:YAG laser diode pumped by a Yb-fiber laser; Opt. Commun. **217** (2003) 363–367.

03Lim Limpert, J., Clausnitzer, T., Liem, A., Schreiber, T., Fuchs, H.-J., Zellmer, H., Kley, E.-B., Tünnermann, A.: High-average-power femtosecond fiber chirped-pulse amplification system; Opt. Lett. **28** (2003) 1984–1986.

03Maj Major, A., Langford, N., Lee, S.T., Ferguson, A.I.: Additive-pulse mode locking of a thin-disk Yb:YAG laser: Appl. Phys. B **76** (2003) 505–508.

03McI McInerney, J.G., Mooradian, A., Lewis, A., Shchegrov, A.V., Strzelecka, E.M., Lee, D., Watson, J.P., Liebman, M., Carey, G.P., Cantos, B.D., Hitchens, W.R., Heald, D.: High-power surface emitting semiconductor laser with extended vertical compound cavity; Electron. Lett. **39** (2003) 523–525.

03Nau Naumov, S., Sorokin, E., Kalashnikov, V.L., Tempea, G., Sorokina, I.T.: Self-starting five optical cycle pulse generation in Cr^{4+}:YAG laser; Appl. Phys. B **76** (2003) 1–11.

03Okh Okhotnikov, O.G., Jouhti, T., Konttinen, J., Karirinne, S., Pessa, M.: 1.5 μm monolithic GaInNAs semiconductor saturable-absorber mode locking of an erbium fiber laser; Opt. Lett. **28** (2003) 364–366.

03Pap Papadopoulos, D.N., Forget, S., Delaigue, M., Druon, F., Balembois, F., Georges, P.: Passively mode-locked diode-pumped Nd:YVO_4 oscillator operating at an ultralow repetition rate; Opt. Lett. **28** (2003) 1838–1840.

03Pas Paschotta, R., Keller, U.: Ultrafast solid-state lasers, in: Ultrafast Lasers: Technology and Applications, Fermann, M.E., Galvanauskas, A., Sucha, G. (eds.), New York: Marcel Dekker Inc., 2003, p. 1–60.

03Pra Prasankumar, R.P., Hirakawa, Y., Kowalevicz, A.M., Kärtner, F.X., Fujimoto, J.G., Knox, W.H.: An extended cavity femtosecond Cr: LiSAF laser pumped by low cost diode lasers; Opt. Express **11** (2003) 1265–1269.

03Qin Qin, L., Meng, X., Du, C., Zhu, L., Xu, B., Shao, Z., Liu, Z., Fang, Q., Cheng, R.: Growth and porperties of mixed crystal Nd:$YGdVO_4$; J. Alloys Compounds **354** (2003) 259–262.

03Saa Saadallah, F., Yacoubi, N., Genty, F., Alibert, C.: Photothermal investigations of thermal and optical properties of GaAlAsSb and AlAsSb thin layers; J. Appl. Phys. **94** (2003) 5041–5048.

03Sch Schenkel, B., Biegert, J., Keller, U., Vozzi, C., Nisoli, M., Sansone, G., Stagira, S., Silvestri, S.D., Svelto, O.: Generation of 3.8-fs pulses from adaptive compression of a cascaded hollow fiber supercontinuum; Opt. Lett. **28** (2003) 1987–1989.

03Sei Seitz, W., Ell, R., Morgner, U., Kärtner, F.X.: All-optical synchronization and mode locking of solid-state lasers with nonlinear semiconductor Fabry–Perot mirrors; IEEE J. Sel. Topics Quantum Electron. **9** (2003) 1093–1101.

03Spu Spühler, G.J., Golding, P.S., Krainer, L., Kilburn, I.J., Crosby, P.A., Brownell, M., Weingarten, K.J., Paschotta, R., Haiml, M., Grange, R., Keller, U.: Novel multi-wavelength source with 25-GHz channel spacing tunable over the C-band; Electron. Lett. **39** (2003) 778–780.

03Ste Steinmeyer, G.: Brewster-angled chirped mirrors for high-fidelity dispersion compensation and bandwidths exceeding one optical octave; Opt. Express **11** (2003) 2385–2396.

03Sto Stormont, B., Cormack, I.G., Mazilu, M., Brown, C.T.A., Burns, D., Sibbett, W.: Low-threshold, multi-gigahertz repetition-rate femtosecond Ti:sapphire laser; Electron. Lett. **39** (2003) 1820–1822.

03Sue Südmeyer, T., Brunner, F., Innerhofer, E., Paschotta, R., Furusawa, K., Baggett, J.C., Monro, T.M., Richardson, D.J., Keller, U.: Nonlinear femtosecond pulse compression at high average power levels using a large mode area holey fiber; Opt. Lett. **28** (2003) 951–953.

03Tom Tomaru, T.: Mode-locking operating points of a three-element-cavity ferntosecond Cr^{4+}:YAG laser; Opt. Commun. **225** (2003) 163–175.

03Uem Uemura, S., Torizuka, K.: Development of a diode-pumped Kerr-lens mode-locked Cr:LiSAF laser; IEEE J. Quantum Electron. **39** (2003) 68–73.

03Wag Wagenblast, P., Ell, R., Morgner, U., Grawert, F., Kärtner, F.X.: Diode-pumped 10-fs Cr^{3+}:LiCAF laser; Opt. Lett. **28** (2003) 1713–1715.

03Wei1 Weingarten, K.J., Spühler, G.J., Keller, U., Krainer, L.: Semiconductor saturable absorber mirror, US Patent No. 6,53,296 B1. U.S.A., 2003.

03Wei2 Weingarten, K.J., Spühler, G.J., Keller, U., Thomas, S.: Semiconductor saturable absorber device, and laser, US Patent No. 6,826,219 B2. U.S.A., 2003.

03Yam Yamane, K., Zhang, Z., Oka, K., Morita, R., Yamashita, M.: Optical pulse compression to 3.4 fs in the monocycle region by feedback phase compensation; Opt. Lett. **28** (2003) 2258–2260.

03Zay Zayhowski, J.J., Wilson, A.L.: Pump-induced bleaching of the saturable absorber in short-pulse Nd:YAG/Cr^{4+}:YAG passively Q-switched microchip lasers; IEEE J. Quantum Electron. **39** (2003) 1588–1593.

03Zel Zeller, S.C., Krainer, L., Spühler, G.J., Weingarten, K.J., Paschotta, R., Keller, U.: Passively modelocked 40-GHz Er:Yb:glass laser; Appl. Phys. B **76** (2003) 1181–1182.

03Zha Zhang, B., Gang, L., Chen, M., Zhang, Z., Wang, Y.: Passive mode locking of a diode-end-pumped Nd:$GdVO_4$ laser with a semiconductor saturable absorber mirror; Opt. Lett. **28** (2003) 1829–1831.

04Ago Agostini, P., DiMauro, L.F.: The physics of attosecond light pulses; Rep. Prog. Phys. **67** (2004) 813–855.

04Bru Brunner, F., Innerhofer, E., Marchese, S.V., Südmeyer, T., Paschotta, R., Usami, T., Ito, H., Kurimura, S., Kitamura, K., Arisholm, G., Keller, U.: Powerful red-green-blue laser source pumped with a mode-locked thin disk laser; Opt. Lett. **29** (2004) 1921–1923.

04Bur Buryy, O.A., Ubiszkii, S.B., Melnyk, S.S., Matkovskii, A.O.: The Q-switched Nd:YAG and Yb:YAG microchip lasers optimization and comparative analysis; Appl. Phys. B **78** (2004) 291–297.

04Chi Chilla, J.L.A., Butterworth, S.D., Zeitschel, A., Charles, J.P., Caprara, A.L., Reed, M.K., Spinelli, L.: High Power Optically Pumped Semiconductor Lasers, presented at Photonics West 2004, Solid State Lasers XIII: Technology and Devices; Proc. SPIE **5332** (2004) 143–150.

04Dru Druon, F., Balembois, F., Georges, P.: Ultra-short-pulsed and highly-efficient diode-pumped Yb:SYS mode-locked oscillators; Opt. Express **12** (2004) 5005–5012.

04Ern Erny, C., Spühler, G.J., Krainer, L., Paschotta, R., Weingarten, K.J., Keller, U.: Simple repetition rate tunable picosecond pulse-generating 10 GHz laser; Electron. Lett. **40** (2004) 877–878.

04Fer Fernandez, A., Fuji, T., Poppe, A., Fürbach, A., Krausz, F., Apolonski, A.: Chirped-pulse oscillators: a route to high-power femtosecond pulses without external amplification; Opt. Lett. **29** (2004) 1366–1368.

04Gra Grange, R., Ostinelli, O., Haiml, M., Krainer, L., Spühler, G.J., Schön, S., Ebnöther, M., Gini, E., Keller, U.: Antimonide semiconductor saturable absorber for 1.5-μm; Electron. Lett. **40** (2004) 1414–1415.

04Gri Griebner, U., Petrov, V., Petermann, K., Peters, V.: Passively mode-locked Yb:Lu_2O_3 laser; Opt. Express **12** (2004) 3125–3130.

04Hai Haiml, M., Grange, R., Keller, U.: Optical characterization of semiconductor saturable absorbers; Appl. Phys. B **79** (2004) 331–339.

04Hau1 Hauri, C.P., Kornelis, W., Helbing, F.W., Heinrich, A., Courairon, A., Mysyrowicz, A., Biegert, J., Keller, U.: Generation of intense, carrier-envelope phase-locked few-cycle laser pulses through filamentation; Appl. Phys. B **79** (2004) 673–677.

04Hau2 Hauri, C.P., Schlup, P., Arisholm, G., Biegert, J., Keller, U.: Phase-preserving chirped-pulse optical parametric amplification to 17.3 fs directly from a Ti:sapphire oscillator; Opt. Lett. **29** (2004) 1369–1371.

04He He, J.-L., Fan, Y.-X., Du, J., Wang, Y.-G., Liu, S., Wang, H.-T., Zhang, L.-H., Hang, Y.: 4-ps passively mode-locked Nd:$Gd_{0.5}Y_{0.5}YVO_4$ laser with a semiconductor saturable-absorber mirror; Opt. Lett. **29** (2004) 2803–2805.

04Jac Jacquemet, M., Balembois, F., Chenais, S., Druon, F., Georges, P., Gaume, R., Ferrand, B.: First diode-pumped Yb-doped solid-state laser continuously tunable between 1000 and 1010 nm; Appl. Phys. B **78** (2004) 13–18.

04Jas Jasim, K., Zhang, Q., Nurmikko, A.V., Ippen, E., Mooradian, A., Carey, G., Ha, W.: Picosecond pulse generation from passively modelocked vertical cavity diode laser at up to 15 GHz pulse repetition rate; Electron. Lett. **40** (2004) 34–35.

04Jen Jensen S., Anderson, M.E.: Measuring ultrashort optical pulses in the presence of noise: an empirical study of the performance of spectral phase interferometry for direct electric field reconstruction; Appl. Opt. **43** (2004) 883–893.

04Kel Keller, U.: Ultrafast solid-state lasers, in: Progress in Optics, Vol. 46, Wolf, E. (ed), Amsterdam: Elsevier, 2004, p. 1–115 (ISBN 0 444 51468 6).

04Kil Killi, A., Morgner, U., Lederer, M.J., Kopf, D.: Diode-pumped femtosecond laser oscillator with cavity dumping; Opt. Lett. **29** (2004) 1288–1290.

04Kis Kisel, V.E., Troshin, A.E., Tolstik, N.A., Shcherbitsky, V.G., Kuleshov, N.V., Matrosov, V.N., Matrosova, T.A., Kupchenko, M.I.: Spectroscopy and continuous-wave diode-pumped laser action of Yb^{3+}:YVO_4; Opt. Lett. **29** (2004) 2491–2493.

04Kon Kong, J., Tang, D.Y., Ng, S.P., Zhao, B., Qin, L.J., Meng, X.L.: Diode-pumped passively mode-locked Nd:$GdVO_4$ laser with a GaAs saturable absorber mirror; Appl. Phys. B **79** (2004) 203–206.

04Kra1 Kränkel, C., Fagundes-Peters, D., Friedrich, S.T., Johannsen, J., Mond, M., Huber, G., Bernhagen, M., Uecker, R.: Continuous wave laser operation of Yb^{3+}:YVO_4; Appl. Phys. B **79** (2004) 543–546.

04Kra2 Krainer, L., Nodop, D., Spühler, G.J., Lecomte, S., Golling, M., Paschotta, R., Ebling, D., Ohgoh, T., Hayakawa, T., Weingarten, K.J., Keller, U.: Compact 10-GHz Nd:$GdVO_4$ laser with 0.5-W average output power and low timing jitter; Opt. Lett. **29** (2004) 2629–2631.

04Lag1 Lagatsky, A.A., Brown, C.T.A., Sibbett, W.: Highly efficient and low threshold diode-pumped Kerr-lens mode-locked Yb:KYW laser; Opt. Express **12** (2004) 3928–3933.

04Lag2 Lagatsky, A.A., Leburn, C.G., Brown, C.T.A., Sibbett, W., Malyarevich, A.M., Savitski, V.G., Yumashev, K.V., Raaben, E.L., Zhilin, A.A.: Passive mode locking of a Cr^{4+}:YAG laser by PbS quantum-dot-doped glass saturable absorber; Opt. Commun. **241** (2004) 449–454.

04Lec Lecomte, S., Paschotta, R., Golling, M., Ebling, D., Keller, U.: Synchronously pumped optical parametric oscillators in the 1.5-μm spectral region with a repetition rate of 10 GHz; J. Opt. Soc. Am. B **21** (2004) 844–850.

04Liv Liverini, V., Schön, S., Grange, R., Haiml, M., Zeller, S.C., Keller, U.: A low-loss GaInNAs SESAM mode-locking a 1.3-μm solid-state laser; Appl. Phys. Lett. **84** (2004) 4002–4004.

04Lor Lorenser, D., Unold, H.J., Maas, D.J.H.C., Aschwanden, A., Grange, R., Paschotta, R., Ebling, D., Gini, E., Keller, U.: Towards wafer-scale integration of high repetition rate passively mode-locked surface-emitting semiconductor lasers; Appl. Phys. B **79** (2004) 927–932.

04Luc Lucca, A., Jacquemet, M., Druon, F., Balembois, F., Georges, P., Camy, P., Doualan, J.L., Moncorge, R.: High-power tunable diode-pumped Yb^{3+}:CaF_2 laser; Opt. Lett. **29** (2004) 1879–1881.

04Lut Luther-Davies, B., Kolev, V.Z., Lederer, M.J., Madsen, N.R., Rode, A.V., Giesekus, J., Du, K.M., Duering, M.: Table-top 50-W laser system for ultra-fast laser ablation; Appl. Phys. A **79** (2004) 1051–1055.

04Nau Naumov, S., Sorokin, E., Sorokina, I.T.: Directly diode-pumped Kerr-lens mode-locked Cr^{4+}:YAG laser; Opt. Lett. **29** (2004) 1276–1278.

04Ost Ostinelli, O., Almuneau, G., Ebnöther, M., Gini, E., Haiml, M., Bächtold, W.: MOVPE growth of long wavelength AlGaAsSb/InP Bragg mirrors; Electron. Lett. **40** (2004) 940–942.

04Pas Paschotta, R., Krainer, L., Lecomte, S., Spühler, G.J., Zeller, S.C., Aschwanden, A., Lorenser, D., Unold, H.J., Weingarten, K.J., Keller, U.: Picosecond pulse sources with multi-GHz repetition rates and high output power; New J. Phys. **6** (2004) 174.

04Pau Paunescu, G., Hein, J., Sauerbrey, R.: 100-fs diode-pumped Yb: KGW mode-locked laser; Appl. Phys. B **79** (2004) 555–558.

04Pet Petit, V., Doualan, J.L., Camy, P., Menard, V., Moncorge, R.: CW and tunable laser operation of Yb^{3+} doped CaF_2; Appl. Phys. B **78** (2004) 681–684.

04Pra Prasankumar, R.P., Hartl, I., Gopinath, J.T., Ippen, E.P., Fujimoto, J.G., Mak, P., Ruane, M.E.: Design and characterization of semiconductor-doped silica film saturable absorbers; J. Opt. Soc. Am. **21** (2004) 851–857.

04San Sansone, G., Stagira, S., Nisoli, M., DeSilvestri, S., Vozzi, C., Schenkel, B., Biegert, J., Gosteva, A., Starke, K., Ristau, D., Steinmeyer, G., Keller, U.: Mirror dispersion control of a hollow fiber supercontinuum; Appl. Phys. B **78** (2004) 551–555.

04Sch1 Schlatter, A., Zeller, S.C., Grange, R., Paschotta, R., Keller, U.: Pulse energy dynamics of passively mode-locked solid-state lasers above the Q-switching threshold; J. Opt. Soc. Am. B **21** (2004) 1469–1478.

04Sch2 Schön, S., Rutz, A., Liverini, V., Grange, R., Haiml, M., Zeller, S.C., Keller, U.: Dilute nitride absorbers in passive devices for mode locking of solid-state lasers; J. Cryst. Growth **278** (2004) 239–243.

04Sor Sorokina, I.T.: Cr^{2+}-doped II–VI materials for lasers and nonlinear optics; Opt. Materials **26** (2004) 395–412.

04Tan Tandon, S.N., Gopinath, J.T., Shen, H.M., Petrich, G.S., Kolodziejski, L.A., Kärtner, F.X., Ippen, E.P.: Large-area broadband saturable Bragg reflectors by use of oxidized AlAs; Opt. Lett. **29** (2004) 2551–2553.

04Yam Yamane, K., Kito, T., Morita, R., Yamashita, M.: Experimental and theoretical demonstration of validity and limitations in fringe-resolved autocorrelation measurements for pulses of few optical cycles; Opt. Express **12** (2004) 2762–2773.

04Zel Zeller, S.C., Krainer, L., Spühler, G.J., Paschotta, R., Golling, M., Ebling, D., Weingarten, K.J., Keller, U.: Passively mode-locked 50-GHz Er:Yb:glass laser; Electron. Lett. **40** (2004) 875–876.

04Zha1 Zhang, S., Wu, E., Pan, H.F., Zeng, H.P.: Passive mode locking in a diode-pumped Nd:$GdVO_4$ laser with a semiconductor saturable absorber mirror; IEEE J. Quantum Electron. **40** (2004) 505–508.

04Zha2 Zhang, Q.A., Jasim, K., Nurmikko, A.V., Mooradian, A., Carey, G., Ha, W., Ippen, E.: Operation of a passively mode-locked extended-cavity surface-emitting diode laser in multi-GHz regime; IEEE Photon. Technol. Lett. **16** (2004) 885–887.

05Agn Agnesi, A., Pirzio, F., Tomaselli, A., Reali, G., Braggio, C.: Multi-GHz tunable-repetition-rate mode-locked Nd:$GdVO_4$ laser; Opt. Express **13** (2005) 5302–5307.

05Asc1 Aschwanden, A., Lorenser, D., Unold, H.J., Paschotta, R., Gini, E., Keller, U.: 2.1-W picosecond passively mode-locked external-cavity semiconductor laser; Opt. Lett. **30** (2005) 272–274.

05Asc2 Aschwanden, A., Lorenser, D., Unold, H.J., Paschotta, R., Gini, E., Keller, U.: 10-GHz passively mode-locked surface emitting semiconductor laser with 1.4-W average output power; Appl. Phys. Lett. **86** (2005) 131102.

05Cas Casel, O., Woll, D., Tremont, M.A., Fuchs, H., Wallenstein, R., Gerster, E., Unger, P., Zorn, M., Weyers, M.: Blue 489-nm picosecond pulses generated by intracavity frequency doubling in a passively mode-locked optically pumped semiconductor disk laser; Appl. Phys. B **81** (2005) 443–446.

05Dat Datta, P.K., Mukhopadhyay, S., Samanta, G.K., Das, S.K., Agnesi, A.: Realization of inverse saturable absorption by intracavity third-harmonic generation for efficient nonlinear mirror mode-locking; Appl. Phys. Lett. **86** (2005) 151105.

05Fan Fan, Y.X., He, J.L., Wang, Y.G., Liu, S., Wang, H.T., Ma, X.Y.: 2-ps passively mode-locked Nd:YVO_4 laser using an output-coupling-type semiconductor saturable absorber mirror; Appl. Phys. Lett. **86** (2005) 101103.

05Gra1 Grawert, F.J., Gopinath, J.T., Ilday, F.O., Shen, H.M., Ippen, E.P., Kärtner, F.X., Akiyama, S., Liu, J., Wada, K., Kimerling, L.C.: 220-fs erbium-ytterbium:glass laser mode locked by a broadband low-loss silicon/germanium saturable absorber; Opt. Lett. **30** (2005) 329–331.

05Gra2 Grange, R., Haiml, M., Paschotta, R., Spühler, G.J., Krainer, L., Ostinelli, O., Golling, M., Keller, U.: New regime of inverse saturable absorption for self-stabilizing passively mode-locked lasers; Appl. Phys. B **80** (2005) 151–158.

05Gra3 Grange, R., Rutz, A., Liverini, V., Haiml, M., Schön, S., Keller, U.: Nonlinear absorption edge properties of 1.3 μm GaInNAs saturable absorbers; Appl. Phys. Lett. **87** (2005) 132103.

05Guo Guo, L., Hou, W., Zhang, H.B., Sun, Z.P., Cui, D.F., Xu, Z.Y., Wang, Y.G., Ma, X.Y.: Diode-end-pumped passively mode-locked ceramic Nd:YAG Laser with a semiconductor saturable mirror; Opt. Express **13** (2005) 4085–4089.

05Hau Hauri, C.P., Guandalini, A., Eckle, P., Kornelis, W., Biegert, J., Keller, U.: Generation of intense few-cycle laser pulses through filamentation – parameter dependence; Opt. Express **13** (19) (2005) 7541–7547.

05Hoo Hoogland, S., Garnache, A., Sagnes, I., Roberts, J.S., Tropper, A.C.: 10-GHz train of sub-500-fs optical soliton-like pulses from a surface-emitting semiconductor laser; IEEE Photon. Technol. Lett. **17** (2005) 267–269.

05Jac Jacquemet, M., Jacquemet, C., Janel, N., Druon, F., Balembois, F., Georges, P., Petit, J., Viana, B., Vivien, D., Ferrand, B.: Efficient laser action of Yb:LSO and Yb:YSO oxyorthosilicates crystals under high-power diode-pumping; Appl. Phys. B **80** (2005) 171–176.

05Kil1 Killi, A., Steinmann, A., Dörring, J., Morgner, U., Lederer, M.J., Kopf, D., Fallnich, C.: High-peak-power pulses from a cavity-dumped Yb:$KY(WO_4)_2$ oscillator; Opt. Lett. **30** (2005) 1891–1893.

05Kil2 Killi, A., Dörring, J., Morgner, U., Lederer, M.J., Frei, J., Kopf, D.: High speed electro-optical cavity dumping of mode-locked laser oscillators; Opt. Express **13** (2005) 1916–1922.

05Kim Kim, K., Lee, S., Delfyett, P.J.: 1.4 kW high peak power generation from an all semiconductor mode-locked master oscillator power amplifier system based on eXtreme Chirped Pulse Amplification(X-CPA); Opt. Express **13** (2005) 4600–4606.

05Kis Kisel, V.E., Troshin, A.E., Shcherbitsky, V.G., Kuleshov, N.V., Matrosov, V.N., Matrosova, T.A., Kupchenko, M.I., Brunner, F., Paschotta, R., Morier-Genoud, F., Keller, U.: Femtosecond pulse generation with a diode-pumped Yb^{3+}:YVO_4 laser; Opt. Lett. **30** (2005) 1150–1152.

05Lag Lagatsky, A.A., Rafailov, E.U., Sibbett, W., Livshits, D.A., Zhukov, A.E., Ustinov, V.M.: Quantum-dot-based saturable absorber with p-n junction for mode-locking of solid-state lasers; IEEE Photon. Technol. Lett. **17** (2005) 294–296.

05Lec1 Lecomte, S., Kalisch, M., Krainer, L., Spühler, G.J., Paschotta, R., Krainer, L., Golling, M., Ebling, D., Ohgoh, T., Hayakawa, T., Pawlik, S., Schmidt, B., Keller, U.: Diode-pumped passively mode-locked Nd:YVO_4 lasers with 40-GHz repetition rate; IEEE J. Quantum Electron. **41** (2005) 45–52.

05Lec2 Lecomte, S., Paschotta, R., Pawlik, S., Schmidt, B., Furusawa, K., Malinowski, A., Richardson, D.J., Keller, U.: Synchronously pumped optical parametric oscillator with a repetition rate of 81.8 GHz; IEEE Photon. Technol. Lett. **17** (2005) 483–485.

05Lin1 Lin, J.H., Yang, W.H., Hsieh, W.F., Lin, K.H.: Low threshold and high power output of a diode-pumped nonlinear mirror mode-locked Nd:$GdVO_4$ laser; Opt. Express **13** (2005) 6323–6329.

05Lin2 Lindberg, H., Sadeghi, M., Westlund, M., Wang, S., Larsson, A., Strassner, M., Marcinkevicius, S.: Mode locking a 1550 nm semiconductor disk laser by using a GaInNAs saturable absorber; Opt. Lett. **30** (2005) 2793–2795.

05Liu Liu, J., Mateos, X., Zhang, H., Wang, J., Jiang, M., Griebner, U., Petrov, V.: Continuous-wave laser operation of Yb:$LuVO_4$; Opt. Lett. **30** (2005) 3162–3164.

05Mai Mairesse, Y., Quere, F.: Frequency-resolved optical gating for complete reconstruction of attosecond bursts; Phys. Rev. A **71** (2005) 011401.

05Man Mandrik, A.V., Troshin, A.E., Kisel, V.E., Yasukevich, A.S., Klavsut, G.N., Kuleshov, N.V., Pavlyuk, A.A.: CW and Q-switched diode-pumped laser operation of Yb^{3+}:$NaLa(MoO_4)_2$; Appl. Phys. B **81** (2005) 1119–1121.

05Mar Marchese, S.V., Innerhofer, E., Paschotta, R., Kurimura, S., Kitamura, K., Arisholm, G., Keller, U.: Room temperature femtosecond optical parametric generation in MgO-doped stoichiometric $LiTaO_3$; Appl. Phys. B **81** (2005) 1049–1052.

05Nau Naumov, S., Fernandez, A., Graf, R., Dombi, P., Krausz, F., Apolonski, A.: Approaching the microjoule frontier with femtosecond laser oscillators; New J. Phys. **7** (2005) 216.

05Nob `http://nobelprize.org/physics/laureates/2005/adv.html` – load down text with advanced information.

05Pet Petit, J., Goldner, P., Viana, B.: Laser emission with low quantum defect in Yb:$CaGdAlO_4$; Opt. Lett. **30** (2005) 1345–1347.

05Riv Rivier, S., Mateos, X., Petrov, V., Griebner, U., Aznar, A., Silvestre, O., Sole, R., Aguilo, M., Diaz, F., Zorn, M., Weyers, M.: Mode-locked laser operation of epitaxially grown Yb:$KLu(WOO_4)_2$ composites; Opt. Lett. **30** (2005) 2484–2486.

05Rom Romero, J.J., Johannsen, J., Mond, M., Petermann, K., Huber, G., Heumann, E.: Continuous-wave laser action of Yb^{3+}-doped lanthanum scandium borate; Appl. Phys. B **80** (2005) 159–163.

05Ros Roser, F., Rothhard, J., Ortac, B., Liem, A., Schmidt, O., Schreiber, T., Limpert, J., Tünnermann, A.: 131 W 220 fs fiber laser system; Opt. Lett. **30** (2005) 2754–2756.

05Rut Rutz, A., Grange, R., Liverini, V., Haiml, M., Schön, S., Keller, U.: 1.5 μm GaInNAs semiconductor saturable absorber for passively modelocked solid-state lasers; Electron. Lett. **41** (2005) 321–323.

05Sch1 Schlatter, A., Krainer, L., Golling, M., Paschotta, R., Ebling, D., Keller, U.: Passively mode-locked 914-nm Nd:YVO_4 laser; Opt. Lett. **30** (2005) 44–46.

05Sch2 Schlatter, A., Rudin, B., Zeller, S.C., Paschotta, R., Spühler, G.J., Krainer, L., Haverkamp, N., Telle, H.R., Keller, U.: Nearly quantum-noise-limited timing jitter from miniature Er:Yb:glass lasers: Opt. Lett. **30** (2005) 1536–1538.

05Sch3 Schibli, T.R., Minoshima, K., Kataura, H., Itoga, E., Minami, N., Kazaoui, S., Miyashita, K., Tokumoto, M., Sakakibara, Y.: Ultrashort pulse-generation by saturable absorber mirrors based on polymer-embedded carbon nanotubes; Opt. Express **13** (2005) 8025–8031.

05Sor Sorokin, E., Naumov, S., Sorokina, I.T.: Ultrabroadband infrared solid-state lasers; IEEE J. Sel. Topics Quantum Electron. **11** (2005) 690–712.

05Spu1 Spühler, G.J., Krainer, L., Innerhofer, E., Paschotta, R., Weingarten, K.J., Keller, U.: Soliton mode-locked Er:Yb:glass laser; Opt. Lett. **30** (2005) 263–265.

05Spu2 Spühler, G.J., Krainer, L., Liverini, V., Schön, S., Grange, R., Haiml, M., Schlatter, A., Pawlik, S., Schmidt, B., Keller, U.: Passively mode-locked multi-GHz 1.3-μm Nd:vanadate lasers with low timing jitter; IEEE Photon. Technol. Lett. **17** (2005) 1319–1321.

05Spu3 Spühler, G.J., Weingarten, K.J., Grange, R., Krainer, L., Haiml, M., Liverini, V., Golling, M., Schon, S., Keller, U.: Semiconductor saturable absorber mirror structures with low saturation fluence; Appl. Phys. B **81** (2005) 27–32.

05Su Su, K.W., Lai, H.C., Li, A., Chen, Y.F., Huang, K.E.: InAs/GaAs quantum-dot saturable absorber for a diode-pumped passively mode-locked Nd:YVO_4 laser at 1342 nm; Opt. Lett. **30** (2005) 1482–1484.

05Uem Uemura, S., Torizuka, K.: Center-wavelength-shifted passively mode-locked diode-pumped ytterbium(Yb): Yttrium aluminum garnet(YAG) laser; Jpn. J. Appl. Phys. Part 2 **44** (2005) L361–L363.

05Voi Voitikov, S.V., Demidovich, A.A., Batay, L.E., Kuzmin, A.N., Danailov, M.B.: Sub-nanosecond pulse dynamics of Nd:LSB microchip laser passively Q-switched by Cr:YAG saturable absorber; Opt. Commun. **251** (2005) 154–164.

05Wan Wang, Y.G., Ma, X.Y., Fan, Y.X., Wang, H.T.: Passively mode-locking Nd:$Gd_{0.5}Y_{0.5}VO_4$ laser with an $In_{0.25}Ga_{0.75}As$ absorber grown at low temperature; Appl. Opt. **44** (2005) 4384–4387.

05Wit Witte, S., Zinkstok, R.T., Hogervorst, W., Eikema, K.W.E.: Generation of few-cycle terawatt light pulses using optical parametric chirped pulse amplification; Opt. Express **13** (2005) 4903–4908.

05Zha1 Zhang, B.Y., Li, G., Chen, M., Yu, H.J., Wang, Y.G., Ma, X.Y.: Passive mode locking of diode-end-pumped Nd:$GdVO_4$ laser with an $In_{0.25}Ga_{0.75}As$ output coupler; Opt. Commun. **244** (2005) 311–314.

05Zha2 Zhang, Q., Jasim, K., Nurmikko, A.V., Ippen, E., Mooradian, A., Carey, G., Ha, W.: Characteristics of a high-speed passively mode-locked surface-emitting semiconductor InGaAs laser diode; IEEE Photon. Technol. Lett. **17** (2005) 525–527.

06Cas Cascales, C., Serrano, M.D., Esteban-Betegón, F., Zaldo, C., Peters, R., Petermann, K., Huber, G., Ackermann, L., Rytz, D., Dupré, C., Rico, M., Liu, J., Griebner, U., Petrov, V.: Structural, spectroscopic, and tunable laser properties of Yb^{3+}-doped $NaGd(WO_4)_2$; Phys. Rev. B **74** (2006) 174114–174128.

06Dew Dewald, S., Lang, T., Schröter, C.D., Moshammer, R., Ullrich, J., Siegel, M., Morgner, U.: Ionization of noble gases with pulses directly from a laser oscillator; Opt. Lett. **31** (2006) 2072–2074.

06Gra Grange, R., Zeller, S.C., Schön, S., Haiml, M., Ostinelli, O., Ebnöther, M., Gini, E., Keller, U.: Antimonide semiconductor saturable absorber for passive mode locking of a 1.5-μm Er:Yb:glass laser at 10 GHz; IEEE Phot. Tech. Lett. **18** (2006) 805–807.

06Hol Holtom, G.R.: Mode-locked Yb:KGW laser longitudinally pumped by polarization-coupled diode bars; Opt. Lett. **31** (2006) 2719–2721.

06Inn Innerhofer, E., Brunner, F., Marchese, S.V., Paschotta, R., Arisholm, G., Kurimura, S., Kitamura, K., Usami, T., Ito, H., Keller, U.: Analysis of nonlinear wavelength conversion system for a red-green-blue laser projection source; J. Opt. Soc. Am. B **23** (2006) 265–275.

06Kel Keller, U., Tropper, A.C.: Passively modelocked surface emitting semiconductor lasers; Physics Report **429** (2006) 67–120.

06Li Li, G., Zhao, S., Yang, K., Li, D.: Control of the pulse width in a diode-pumped passively Q-switched Nd:$GdVO_4$ laser with GaAs saturable absorber; Opt. Materials, to be published.

06Lor Lorenser, D., Maas, D.J.H.C., Unold, H.J., Bellancourt, A.R., Rudin, B., Gini, E., Ebling, D., Keller, U.: 50-GHz passively mode-locked surface emitting semiconductor laser with 100 mW average output power; IEEE J. Quantum Electron. **42** (2006) 838–847.

06Maj Major, A., Cisek, R., Barzda, V.: Femtosecond Yb:$KGd(WO_4)_2$ laser oscillator pumped by a high power fiber-coupled diode laser module; Opt. Express **14** (2006) 12163–12168.

06Mar Marchese, S.V., Südmeyer, T., Golling, M., Grange, R., Keller, U.: Pulse energy scaling to 5 μJ from a femtosecond thin disk laser; Opt. Lett. **31** (2006) 2728–2730.

06Ost Ostinelli, O., Haiml, M., Grange, R., Almuneau, G., Ebnöther, M., Gini, E., Müller, E., Keller, U., Bächtold, W.: Highly reflective AlGaAsSb/InP Bragg reflector at 1.55 μm grown by MOVPE; J. Cryst. Growth **286** (2006) 247–254.

06Pla Plant, J.J., Gopinath, J.T., Chann, B., Ripin, D.J., Huang, R.K., Juodawlkis, P.W.: 250 mW, 1.5 μm monolithic passively mode-locked slab-coupled optical waveguide laser; Opt. Lett. **31** (2006) 223–225.

06Riv Rivier, S., Mateos, X., Liu, J., Petrov, V., Griebner, U., Zorn, M., Weyers, M., Zhang, H., Wang, J., Jiang, M.: Passively mode-locked Yb:$LuVO_4$ oscillator; Opt. Express **14** (2006) 11668–11671.

06Thi Thibault, F., Pelenc, D., Druon, F., Zaouter, Y., Jacquemet, M., Georges, P.: Efficient diode-pumped Yb^{3+}:Y_2SiO_5 and Yb^{3+}:Lu_2SiO_5 high-power femtosecond laser operation; Opt. Lett. **31** (2006) 1555–1557.

06Xue Xue, Y., Wang, C., Liu, Q., Li, Y., Chai, L., Yan, C., Zhao, G., Su, L., Xu, X., Xu, J.: Characterization of diode-pumped laser operation of a novel Yb:GSO crystal; IEEE J. Quantum Electron. **42** (2006) 517–521.

06Zao Zaouter, Y., Didierjean, J., Balembois, F., Leclin, G.L., Druon, F., Georges, P., Petit, J., Goldner, P., Viana, B.: 47-fs diode-pumped Yb^{3+}:$CaGdAlO_4$ laser; Opt. Lett. **31** (2006) 119–121.

06Zel Zeller, S.C., Grange, R., Liverini, V., Rutz, A., Schön, S., Haiml, M., Pawlik, S., Schmidt, B., Keller, U.: A low-loss buried resonant GaInNAs SESAM for 1.3-μm Nd:YLF laser at 1.4 GHz; Appl. Phys. Lett., submitted.

06Zho Zhou, X., Kapteyn, H., Murnane, M.: Positive-dispersion cavity-dumped Ti:sapphire laser oscillator and its application to white light generation; Opt. Express **14** (2006) 9750–9757.

07Bel Bellancourt, A.R., Rudin, B., Maas, D.J.H.C., Golling, M., Unold, H.J., Südmeyer, T., Keller, U.: First demonstration of a modelocked integrated external-cavity surface emitting laser (MIXSEL); Conference on Lasers and Electro-Optics (CLEO '07), Baltimore, USA, May 8–10 (2007) upgraded to invited talk CWI1.

07Fon Fong, K.H., Kikuchi, K., Goh, C.S., Set, S.Y., Grange, R., Haiml, M., Schlatter, A., Keller, U.: Solid-state Er:Yb:glass laser mode-locked by using single-wall carbon nanotube thin film; Opt. Lett. **32** (2007) 38–40.

07Gar García-Cortés, A., Cano-Torres, J.M., Serrano, M.D., Cascales, C., Zaldo, C., Rivier, S., Mateos, X., Griebner, U., Petrov, V.: Spectroscopy and Lasing of Yb-Doped

$NaY(WO_4)_2$: Tunable and Femtosecond Mode-Locked Laser Operation; IEEE J. Quantum Electron. **43** (2007) 758–764.

07Li Li, W., Hao, Q., Zhai, H., Zeng, H., Lu, W., Zhao, G., Zheng, L., Su, L., Xu, J.: Diode-pumped Yb:GSO femtosecond laser; Opt. Express **15** (2007) 2354–2359.

07Maa Maas, D.J.H.C., Bellancourt, A.R., Rudin, B., Golling, M., Unold, H.J., Südmeyer, T., Keller, U.: Vertical integration of ultrafast semiconductor lasers; Appl. Phys. B **88** (2007) 493–497.

07Mar Marchese, S.V., Hashimoto, S., Bär, C.R.E., Ruosch, M.S., Grange, R., Golling, M., Südmeyer, T., Keller, U., Lépine, G., Gingras, G., Witzel, B.: Passively mode-locked thin disk lasers reach 10 μJ pulse energy at megahertz repetition rate and drive high field physics experiments; CLEO Europe 2007, Munich, Germany, June 17–22 (2007) Talk CF3-2-MON.

07Pal Palmer, G., Siegel, M., Steinmann, A., Morgner, U.: Microjoule pulses from a passively mode-locked Yb:$KY(WO_4)_2$ thin-disk oscillator with cavity dumping; Opt. Lett. **32** (2007) 1593–1595.

07Riv Rivier, S., Schmidt, A., Petrov, V., Griebner, U., Kränkel, C., Peters, R., Petermann, K., Huber, G., Zorn, M., Weyers, M., Klehr, A., Ebert, G.: Ultrashort pulse Yb:$LaSc_3(BO_3)_4$ mode-locked oscillator; Opt. Express, submitted.

07Saa Saarinen, E.J., Harkonen, A., Herda, R., Suomalainen, S., Orsila, L., Hakulinen, T., Guina, M., Okhotnikov, O.G.: Harmonically mode-locked VECSELs for multi-GHz pulse train generation; Opt. Express **15** (2007) 955–964.

07Sor Sorokina, I.T., Sorokin, E.: Chirped-mirror dispersion controlled femtosecond Cr:ZnSe laser; Advanced Solid-State Photonics OSA Technical Digest, Vancouver, Canada, Jan. 28–31 (2007) WA7.

07Zel Zeller, S.C., Südmeyer, T., Weingarten, K.J., Keller, U.: Passively modelocked 77 GHz Er:Yb:glass laser; Electron. Lett. **43** (2007) 32–33.